Organometallic Iridium Anticancer Complexes

A Thesis Submitted for the Degree of

Doctor of Philosophy

by

Zhe Liu

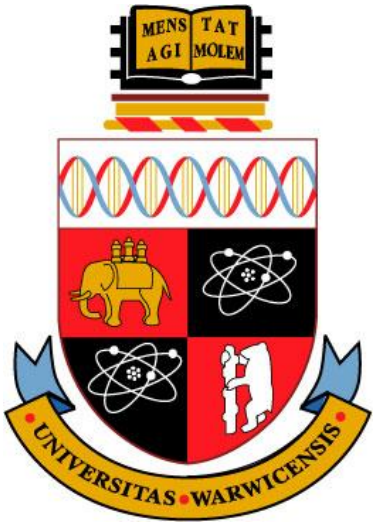

University of Warwick, Department of Chemistry

September 2011

Contents

Acknowledgements i

Declaration iii

Abstract iv

Abbreviations v

Chapter 1 Introduction **1**

1.1 Metal-Based Anticancer Agents 2

1.2 Organometallic Anticancer Complexes 7

1.2.1 Cyclopentadienyl Anticancer Complexes 8

1.2.2 Ruthenium and Osmium Arene Anticancer Complexes 10

1.3 Iridium Anticancer Agents 15

1.3.1 Iridium(I) Anticancer Complexes 16

1.3.2 Iridium(III) Anticancer Complexes 16

1.4 Ir^{III} Pentamethylcyclopentadienyl Complexes as Catalytic Agents 21

1.5 Aims 25

1.6 References 26

Chapter 2 Experimental Methods and Materials **34**

2.1 Instrumentation and Methods 35

2.1.1 Nuclear Magnetic Resonance Spectroscopy (NMR) 35

2.1.1.1 Experimental 37

2.1.1.2 Water Suppression 37

2.1.2 pH Measurements 38

2.1.3 Determination of pK_a Values 38

2.1.4 X-ray Crystallography 39

2.1.5 Elemental Analysis 39

2.1.6 Electrospray Ionisation Mass Spectrometry (ESI-MS) 40

2.1.7 Inductively Coupled Plasma Mass Spectroscopy (ICP-MS) 40

2.1.8 UV-Vis Absorption Spectroscopy 41

2.1.9 Computational Methods 42

2.1.10 Determination of Partition Coefficient, Log *P* 42

2.1.11 Cancer Cell Growth Inhibition 43

2.1.11.1 Cytotoxicity against A2780 Human Ovarian Cancer Cells 43

2.1.11.1.1 Materials and Maintenance 44

2.1.11.1.2 In Vitro Growth Inhibition Assay 44

2.1.11.2 NCI/DTP Cytotoxicity 46

2.2 Synthesis and Characterisation of Starting Materials 47

2.2.1 Materials 48

2.2.2 Syntheses 48

2.2.3 X-ray Crystal Structure 49

2.3 References 54

Chapter 3 Cyclopentadienyl Iridium Complexes Containing N,N- or N,O-Chelating Ligands 56

3.1 Introduction 57

3.2 Experimental Section 59

3.2.1 Materials 59

3.2.2 Syntheses 60

3.2.3 Methods 70

3.2.3.1 X-ray Crystallography 70

3.2.3.2 Kinetics of Hydrolysis 71

3.2.3.3 Determination of pK_a Values 71

3.2.3.4 Computation 71

3.2.3.5 Interactions with Nucleobases 72

3.2.3.6 Cytotoxicity 72

3.2.3.7 log *P* Determination 73

3.2.3.8 Cellular Accumulation, Cellular Distribution, and DNA Binding in A2780 Human Ovarian Cancer Cells 73

3.2.3.9 Sequence Preference of DNA Adducts 74

3.2.3.10 Fluorescence Measurements 75

3.2.3.11 Viscometry 75

3.2.3.12 ICP-MS Analysis 76

3.3 Results 76

3.3.1 Synthesis and Characterisation 76

3.3.2 Hydrolysis Studies 88

3.3.3 pK_a Determination 94

3.3.4 Interactions with Nucleobases 96

3.3.5 Cytotoxicity 102

3.3.6 Hydrophobicity (log *P*) 109

3.3.7 Cell Accumulation and DNA Binding 110

3.3.8 Distribution of Iridium in Cell Fractions 111

3.3.9 Replication Mapping of Ir−DNA Adducts 113

3.3.10 Ethidium Bromide (EtBr) Displacement 115

3.3.11 Viscometry 116

3.4 Discussion 117

3.4.1 X-ray Crystal Structures 117

3.4.2 Hydrolysis and pK_a of Aqua Adducts 118

3.4.3 Interactions with Nucleobases 121

3.4.4 Hydrophobicity (log *P*) and Cell Accumulation 123

3.4.5 Distribution of Iridium in Cells 124

3.4.6 DNA Binding in A2780 Human Ovarian Cancer Cells 125

3.4.7 EtBr Displacement and Viscometry 125

3.4.8 Cytotoxicity 126

3.5 Conclusions 129

3.6 References 133

Chapter 4 Cyclopentadienyl Iridium Complexes Containing C^N-Chelating Ligands 142

4.1 Introduction 143

4.2 Experimental Section 146

4.2.1 Materials 146

4.2.2 Syntheses 147

4.2.3 Methods 152

4.2.3.1 X-ray Crystallography 152

4.2.3.2 Determination of pK_a Values 152

4.2.3.3 Computation 153

4.2.3.4 Interactions with Nucleobases 153

4.2.3.5 log *P* Determination 154

4.2.3.6 Cytotoxicity 154

4.2.3.7 ICP-MS Analysis 154

4.3 Results 155

4.3.1 Synthesis and Characterisation 155

4.3.2 Structural and Electronic Differences between Complexes **32** and **7** 158

4.3.3 Hydrolysis Studies 161

4.3.4 pK_a Determination 162

4.3.5 Interactions with Nucleobases 165

4.3.6 Cytotoxicity 175

4.3.7 Hydrophobicity (log *P*) 179

4.4 Discussion 180

4.4.1 X-ray Crystal Structures 180

4.4.2 Hydrolysis and pK_a of Aqua Adducts 181

4.4.3 Interaction with Nucleobases 184

4.4.4 Hydrophobicity (log *P*) 187

4.4.5 Cytotoxicity 188

4.5 Conclusions 190

4.6 References 192

Chapter 5 Hydride-Transfer Reactions of Cyclopentadienyl Iridium Aqua Complexes 198

5.1 Introduction 199

5.2 Experimental Section 201

5.2.1 Materials 201

5.2.2 Methods 202

5.2.2.1 NMR Spectroscopy 202

5.2.2.2 UV-Vis Absorption Spectroscopy 202

5.2.2.3 pH Measurements 202

5.2.2.4 Reduction of NAD^+ by **4A** Using Formate as a Hydride Source 203

5.2.2.5 NMR Spectroscopy Studied Reactions with 1,4-NADH 203

5.2.2.6 Detection of H_2 by Gas Chromatography 203

5.2.2.7 Hydrogenation of Pyruvate 204

5.2.2.8 Catalytic Conversion of 1,4-NADH to NAD^+ by **5A** 204

5.3 Results 205

5.3.1 Reduction of NAD^+ Using Formate as a Hydride Source 205

5.3.2 NMR Spectroscopy of Reactions with 1,4-NADH 208

5.3.3 Hydrogenation of Pyruvate 211

5.3.4 Reaction with Enzymatically Produced 1,4-NADH 212

5.3.5 Detection of H_2 214

5.3.6 Catalytic Studies on Reactions with 1,4-NADH 216

5.3.6.1 Effect of 1,4-NADH on the Catalytic Reaction 216

5.3.6.2 Effect of **5A** and Temperature on the Catalytic Reaction 219

5.4 Discussion 220

5.4.1 Reduction of NAD^+ Using Formate as a Hydride Source 220

5.4.2 Hydride-Transfer from 1,4-NADH 223

5.5 Conclusions 226

5.6 References 228

Chapter 6 Future Work **231**

6.1 Cyclopentadienyl Ligand, Chelating Ligand and Leaving Group 232

6.2 Intercalation into DNA 233

6.3 Enantiomer Separation 234

6.4 Other Biological Targets 236

6.5 Bio-inspired Hydride-Transfer Reactions 236

6.6 References 238

Chemical Structures of Iridium Complexes Studied in This Thesis 240

Courses Attended 242

Conferences and Meetings Attended 242

Acknowledgements

I would like to thank Professor Peter John Sadler for his supervision and encouragement throughout the project. I am very grateful for everything that he has taught me and for all help and opportunities he has given me to explore different areas of research. Without him, I would not have come this far. The help he gave me are too much to be detailed here, but they are all in my heart. I have thoroughly enjoyed working in the PJS group and the BBQ every year at his home.

A big and special thanks goes to my dearest friend Dr. Abraha Habtemariam for sharing his knowledge, professional supervision, and all the help he gave me. Thanks a lot for your infinite patience, guidance, and advice throughout the three years. Cannot forget your help to get into the 'iridium world', and to set up and deal with every dangerous experiment. I will miss our chats in the lab and in the office.

A big and special thanks goes to Dr. Ana M. Pizarro and Captain Dr. Luca Salassa. Thanks Ana for all the perfect biological works and infinite patience in helping me accessing the cell-testing data. Her serious attitude to research impressed me deeply. Thanks captain Luca for his awesome calculations, graphics for TOC in our publications and helpful discussions. Without you our office is quiet. With you, our office is full of smiles. You are No.1, Captain!

A big and special thanks goes to all PJS members, both past and present, with whom I formed many friendships. Thanks to Dr. Pieter C. A. Bruijnincx for his help and assistance in getting this project started. Thanks for Ying Fu, Yao Zhao, Khatija

Bhayat, Claire Booyjzsen, Hui-chung Tai, Dr. Jun Du, and Dr. Maria J. Romero-Castro for spending a happy time with me at Warwick. I am so very grateful of having had the chance to have you as a friend. I am going to miss you guys a lot. Thanks also to Sally A. Fletcher for her help with log P and cell accumulation studies.

Thanks to Professor Viktor Brabec, Dr. Anna Kisova and Dr. Oldrich Vrana of the Institute of Biophysics at Academy of Sciences of the Czech Republic for their collaboration on the phenanthroline complexes. Thanks to Dr. Guy Clarkson for solving the X-ray crystal structures. Thanks to Philip Aston and Dr. Lijiang Song for their help with mass spectrometry, and Dr. Ivan Prokes for NMR training. Thanks to Professor Colin Murrell and Dr. Andrew Crombie for assistance with gas chromatography. I would also like to thank National Cancer Institute Developmental Therapeutics Program (NCI/DTP, U.S.A.) for in vitro cytotoxic test.

I would like to thank the University of Warwick Research Scholarship for financial support. Thanks to EU COST Action D39 for giving me the opportunity to attend and present at their meeting.

Finally I would like to thank my parents and my friends for their support and encouragement. In particular a very big special thank to my dearest wife and my mother-in-law for their dedication, patience, supports and staying with me over the past three years. I hope this thesis is one of the best gifts for my wife.

Declaration

I hereby declare that except where specific reference is made to other sources, the work contained in this thesis is the original work of the author. It has been composed by myself and has not been submitted, in whole or in part, for any other degree, diploma, or other qualification.

Some of the work presented in this thesis has been published:

1. Liu, Z.; Habtemariam, A.; Pizarro, A. M.; Fletcher, S. A.; Kisova, A.; Vrana, O.; Salassa, L.; Bruijnincx, P. C. A.; Clarkson, G. J.; Brabec, V.; Sadler, P. J. Organometallic Half-Sandwich Iridium Anticancer Complexes. *J. Med. Chem.* **2011**, *54*, 3011-3026.

2. Liu, Z.; Salassa, L.; Habtemariam, A.; Pizarro, A. M.; Clarkson, G. J.; Sadler, P. J. Contrasting Reactivity and Cancer Cell Cytotoxicity of Isoelectronic Organometallic Iridium(III) Complexes. *Inorg. Chem.* **2011**, *50*, 5777-5783.

3. Liu, Z.; Habtemariam, A.; Pizarro, A. M.; Clarkson, G. J.; Sadler, P. J. Organometallic Iridium(III) Cyclopentadienyl Anticancer Complexes Containing C,N-Chelating Ligands. *Organometallics* **2011**, *30*, 4702-4710.

4. Liu, Z.; Habtemariam, A.; Sadler, P. J.; Soldevila, J. Novel Iridium/Rhodium Anti-Cancer Compounds. **2010**, International Patent Application No. PCT/GB2011/ 000776.

Zhe Liu

September 2011

Abstract

Cisplatin has been used to treat various types of cancers for over 30 years, however, a number of serious side-effects of cisplatin have stimulated the quest for other metal-based anticancer agents. Iridium complexes are generally thought to be too inert to possess high reactivity, and therefore, there are only a few previous reports of the antitumour activity of iridium complexes.

In this thesis a wide range of organometallic Ir^{III} cyclopentadienyl complexes of the type $[(\eta^5\text{-}Cp^x)Ir(XY)Cl]^{0/+}$ (where Cp^x = pentamethylcyclopentadienyl (Cp*), tetramethyl(phenyl)cyclopentadienyl (Cp^{xph}) or tetramethyl(biphenyl)cyclopentadienyl (Cp^{xbiph}), XY = N,N-, N,O- or C^N-chelating ligand) has been synthesised and characterised. All the complexes hydrolyse rapidly in aqueous solution. Complexes with N,N-chelating ligands readily form adducts with 9-ethylguanine but not 9-ethyladenine; C^N- or N,O-chelated complexes bind to both purines. Guanine residues are preferential binding sites for 1,10-phenanthroline complexes on plasmid DNA. Replacement of the neutral N,N-bound chelating ligand by the negatively-charged C,N-bound analogues can improve biological activity. In addition, cytotoxic potency towards A2780 human ovarian cancer cells increases with phenyl substitution on Cp*: $Cp^{xbiph} > Cp^{xph} > Cp^*$. This can be rationalised by increased hydrophobicity with more extended phenyl ring, resulting in increased cellular uptake and increased intercalative ability. Notably, several complexes exhibited submicromolar anticancer activity.

The interconversion of 1,4-NADH and NAD^+ through hydride-transfer reactions in the presence of cyclopentadienyl Ir^{III} aqua complexes was studied. It is shown that the Ir^{III} aqua complexes not only converts NAD^+ to 1,4-NADH using formate as the hydride source, but can also catalyse the reverse reaction with hydride donation from 1,4-NADH to a iridium centre, recovered by protonation of bound hydride with generation of H_2.

This work demonstrates how the aqueous chemistry, nucleobase binding and anticancer activity of the Ir^{III} cyclopentadienyl complexes can be controlled and fine-tuned by the modification of the chelating and cyclopentadienyl ligands. The results suggest that this new class of organometalic Ir(III) complexes is well suited for development as anticancer agents.

Abbreviations

A	adenine
A	absorbance
acac	acetylacetonate
ADH	alcohol dehydrogenase
azpy-NMe_2	4-(2-pyridylazo)-*N*,*N*-dimethylaniline
bip	biphenyl
bpy	2,2'-bipyridine
bpy-Me_2	4,4′-dimethyl-2,2′-bipyridine
bpy$(OH)_2$	bipyridine-3,3′-diol
bq	benzo[*h*]quinoline
CCDC	Cambridge Crystallographic Data Centre
CDDP	*cis*-$[PtCl_2(NH_3)_2]$
COD	*cis*,*cis*-1,5-cyclo-octadiene
Cp	cyclopentadienyl
Cp*	pentamethylcyclopentadienyl
Cp^{xph}	tetramethyl(phenyl)cyclopentadienyl
Cp^{xbiph}	tetramethyl(biphenyl)cyclopentadienyl
CT	calf thymus
DDW	double deionised water
dfphpy	2-(2,4-difluorophenyl)pyridine

dha	dihydroanthracene
dpq	dipyrido[3,2-f:2′,3′-h]quinoxaline
dppz	dipyrido[3,2-a:2′,3′-c]phenazine
en	ethylenediamine
EPS	electrostatic potential surface
9-EtA	9-ethyladenine
9-EtG	9-ethylguanine
G	guanine
GI_{50}	50% growth inhibition concentration
hmb	hexamethylbenzene
IC_{50}	50% growth inhibition concentration
impy-NMe_2	*p*-dimethylaminophenyliminopyridine
KP1019	[*trans*-$RuCl_4(Ind)_2$][IndH]
LC_{50}	50% cell number decrease concentration
LDH	lactate dehydrogenase
9-MeA	9-methyladenine
MG-MID	mean graph midpoint
NAD^+	*β*-nicotinamide adenine dinucleotide
NADH	reduced *β*-nicotinamide adenine dinucleotide
NAMI-A	[*trans*-$RuCl_4$(DMSO)(Im)][ImH]
NCI/DTP	National Cancer Institute Developmental Therapeutics Program
OSW	octanol-saturated water

PBS	phosphate buffered saline
p-cym	*para*-cymene
phen	1,10-phenanthroline
phpy	2-phenylpyridine
phq	2-phenylquinoline
pico	picolinate
SD	standard deviation
SRB	sulforhodamine B
TGI	100% growth inhibition concentration
tha	tetrahydroanthracene
TOF	turnover frequency
TON	turnover number
tpy	2-(*p*-tolyl)pyridine
transPt	*trans*-$[PtCl_2(NH_3)_2]$
WSO	water-saturated octanol

Chapter 1

Introduction

This Chapter introduces metallodrugs as anticancer agents, especially focusing on the previous studies on ruthenium, osmium and iridium organometallic anticancer complexes. Finally, the involvement of Ir^{III} complexes in biologically relevant hydride-transfer reactions is described.

1.1 Metal-Based Anticancer Agents

Cancer is caused when genetic damage to cells prevents them from being responsive to normal tissue controls. Each year, approximately 12.7 million people worldwide are diagnosed with cancer. In 2008 it caused about 13% of all human deaths worldwide (7.6 million), and is becoming the leading cause of death.[1] Different therapies, such as chemotherapy, radiotherapy and surgery, can be used to treat cancer, depending on the type of cancer and the extent of the disease.[2,3] Most commonly, chemotherapy is an effective way to kill cancer cells.

Metal complexes have played key roles in the development of pharmacy and modern chemotherapy.[4,5] Medicinal applications of metal complexes as therapeutic agents can be traced back almost 5000 years.[6] In modern medicinal inorganic chemistry, the most successful metal-based anticancer drug is cisplatin, *cis*-$[PtCl_2(NH_3)_2]$ (Figure 1.1), discovered about 40 years ago.[7,8] Today, cisplatin is still one of the world's best selling anticancer drugs. It is mainly used in the treatment of ovarian, head and neck, bladder, cervical and lymphomas cancers. Over the past decades, more than 3000 platinum complexes have been synthesised and tested for their biological activity and less than 30 compounds have entered clinical trials.[9,10]

At present, four platinum drugs have entered world-wide clinical use: cisplatin, carboplatin, oxaliplatin and nedaplatin (Figure 1.1). It is estimated that 50%–70% of cancer patients are treated with a platinum drug.[11]

Nuclear DNA is now widely accepted to be the ultimate target of cisplatin and related platinum therapeutics. The main mechanism of action of cisplatin is that it becomes activated by aquation to form $[Pt(NH_3)_2Cl(H_2O)]^+$ and $[Pt(NH_3)_2(H_2O)_2]^{2+}$ once inside the cell, and subsequently coordinatively bind to DNA via N7 positions of purines bases to afford primarily 1,2- or 1,3-intrastrand crosslinks and a lower number of interstrand crossslinks, Figure 1.2.[12] Although the activated (aquated) cisplatin can interact with other biomolecules, its antitumour activity derives from its capability to form bifunctional DNA cross-links.[13] The coordination of platinum to two adjacent bases causes the DNA to bend (kink) by around 45 °, Figure 1.3.[14] The cisplatin–DNA adducts cause various cellular responses, such as replication arrest, transcription inhibition, cell-cycle arrest, DNA repair and apoptosis.[12]

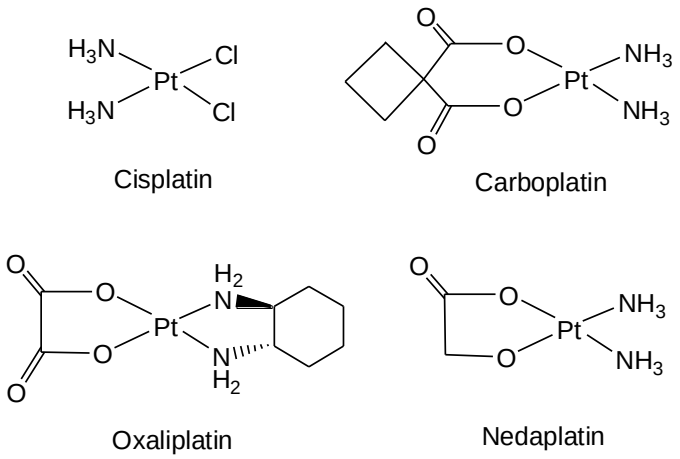

Figure 1.1. The chemical structures of currently marketed platinum anticancer drugs.

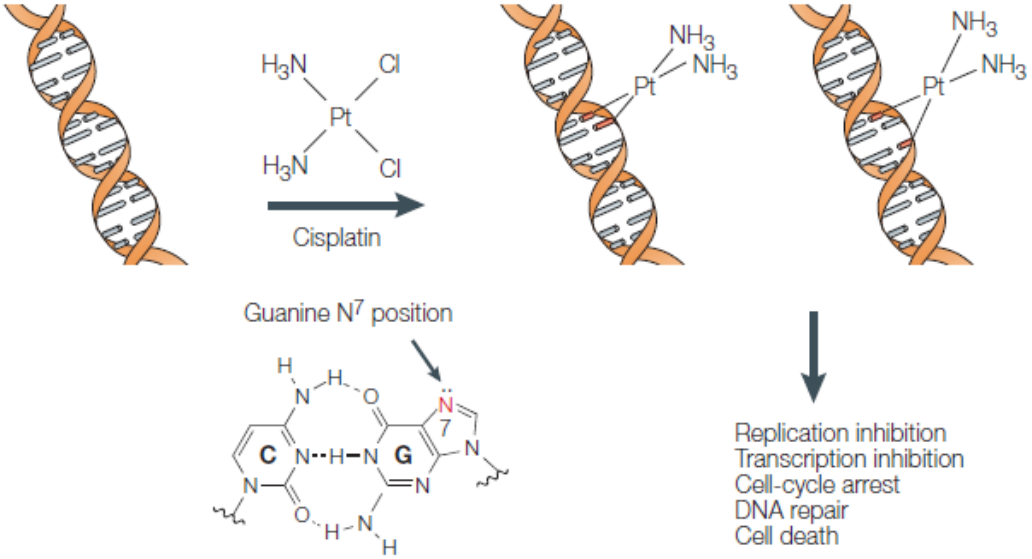

Figure 1.2. Formation and effects of cisplatin adducts.[12]

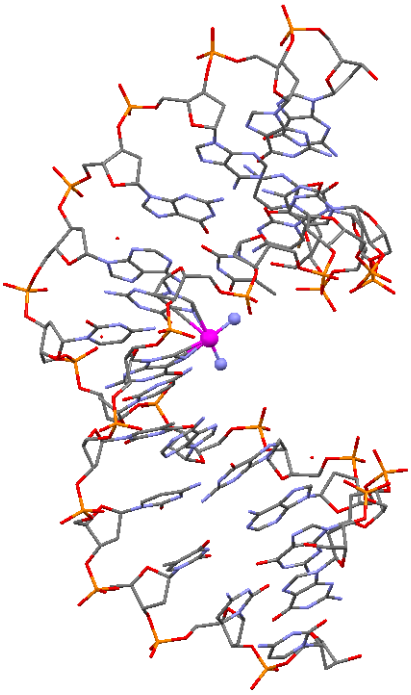

Figure 1.3. X-ray structure of *cis*-[Pt(NH_3)$_2$(d(pGpG))] showing the kinking of DNA by cisplatin.[14]

Regardless of the achievements of current platinum drugs, there are some major drawbacks which are restricting their clinical use: they are efficient only in a limited range of cancers, some tumours can have acquired or intrinsic resistance and they often cause severe side-effects like nausea, bone marrow suppression and kidney toxicity. The clinical success and drawbacks of platinum-based anticancer drugs, therefore, have stimulated the exploration for other metal-based anticancer complexes (circled metals in Figure 1.4),[15] which may address the problems associated with platinum drugs, produce significantly different lesions on DNA, and exhibit more potent cytotoxicity towards tumours which are non-responsive to current chemotherapy.

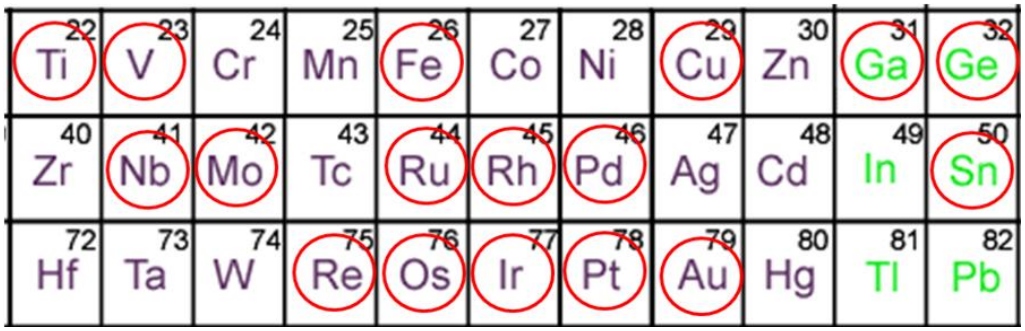

Figure 1.4. Metals (red circled) with known anticancer compounds.

In this frame, ruthenium compounds are considered to be suitable candidates for anticancer drug design since they have a rich redox chemistry (Ru^{II} and Ru^{III}), and exhibit a similar spectrum of kinetics to platinum(II).[16] A number of ruthenium compounds have been shown to display promising anticancer activity and two

ruthenium(III) complexes have entered clinical trials, [*trans*-$RuCl_4(Ind)_2$][IndH] (KP1019, Ind = indazole) and [*trans*-$RuCl_4$(DMSO)(Im)][ImH] (NAMI-A, DMSO = dimethylsulfoxide, Im = imidazole), Figure 1.5. NAMI-A showed marked efficacy against metastases,[17,18] whereas the structurally-similar KP1019 exhibited activity against colon carcinoma and some primary explanted human tumours.[19,20] Previous work has shown that Ru^{III} complexes are activated by reduction *in vivo* to more reactive Ru^{II} due to the reduced stability of Ru^{II}–Cl bonds.[21,22] This has resulted in increased interest in the anticancer Ru^{II} complexes, especially organometallic Ru^{II} arene complexes. These complexes are discussed in section 1.2.2.

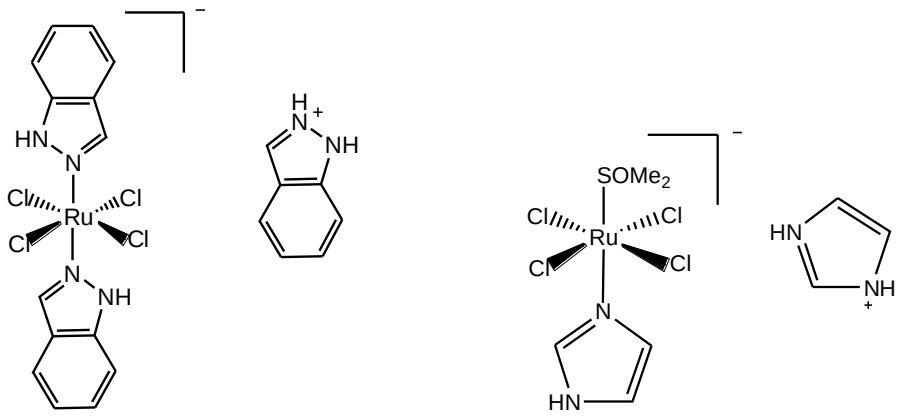

Figure 1.5. Chemical structures of KP1019 (left) and NAMI-A (right).

An anticancer gold phosphine compound has been reported (Figure 1.6), which shows a different mechanism of action compared to cisplatin and targets mitochondria; it destroys membrane potentials.[23] Gallium salts are also known to

exhibit anticancer activity, and Ga(III) maltolate (Figure 1.6) has recently entered clinical trials for the treatment of bone disease and related conditions.[24]

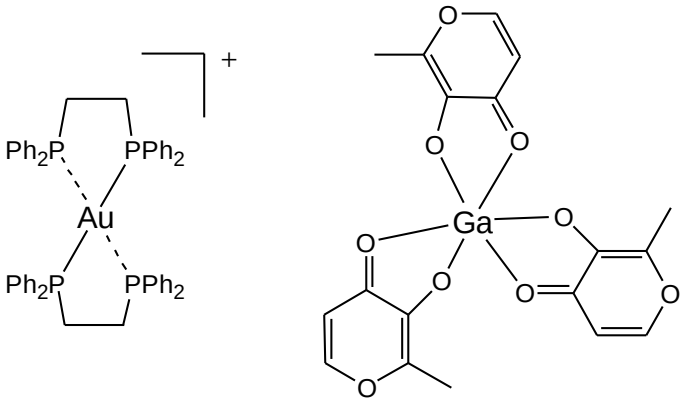

Figure 1.6. Chemical structures of the gold(I) phosphine and gallium(III) maltolate anticancer compounds.

1.2 Organometallic Anticancer Complexes

Organometallic chemistry evolved rapidly during the second half of the 20th century.[25] Organometallic complexes have at least one metal−carbon bond, according to most definitions. Organometallics have a wide choice of metals and ligands, varying oxidation states and coordination numbers, great structural variety (linear, octahedral, etc.), and kinetic stability. Therefore, organometallic complexes provide a platform for the development of anticancer agents.[26]

1.2.1 Cyclopentadienyl Anticancer Complexes

A range of organometallic complexes, containing one or more six-electron-donor η^5-cyclopentadienyl ligand ($C_5H_5^-$, abbreviated as Cp), exhibit promising anticancer activity. The Cp ligands are generally bound via all 5 carbon atoms to a metal centre (π-bonded, η^5-coordination).

Sandwich ferrocenium salts $[(C_5H_5)_2Fe^{III}]^+$ were the first antineoplastic iron complexes,[27] which sparked the development of organometallic anticancer complexes.[28,29] Ferrocene $[(C_5H_5)_2Fe^{II}]$ does not possess anticancer activity, however, large number of modified ferrocene complexes showed promising anticancer activity owing to their redox activity. A notable example is ferrocifen, Figure 1.7, which consists of ferrocene modified tamoxifen (an organic drug for breast cancer treatment). Ferrocifen has a very significant effect on breast cancers which are not treatable by tamoxifen. This appears benefit from oxidative damage to DNA after oxidation of the ferrocenyl group to ferrocenium in the cells.[30]

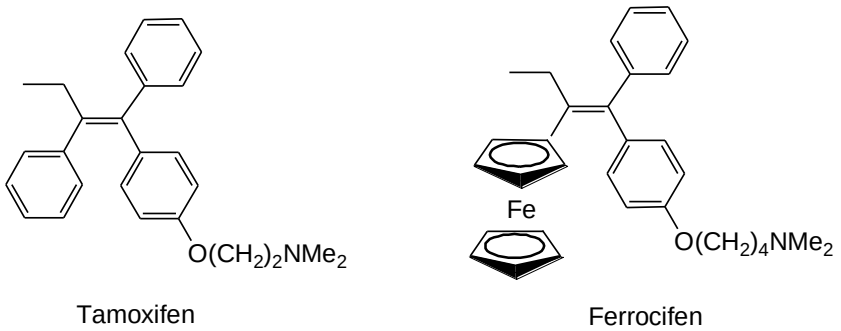

Figure 1.7. Tamoxifen and ferrocifen: active against breast cancer cells.

Titanocene dichloride Cp_2TiCl_2, Figure 1.8 A, entered clinical trials as an anticancer agent in the 1990s. It was designed because of the possibility of forming bifunctional cross-links on DNA in a similar manner to cisplatin, which might induce apoptosis and cancer cell death. However, the complex binds more strongly to phosphate backbone than to DNA.[31] Also it is difficult to identify the active species and formulate for administration due to complicated hydrolysis, loss of the Cp ligand and formation of hydroxo species. Clinical results for titanocene dichloride were not satisfactory and the trials have now been abandoned.[32,33] Nonetheless, there is continuing interest in substituted titanocenes which might offer greater aqueous stability or cytotoxicity (Figure 1.8 B and C).[34-36] For example, titanocene Y (Figure 1.8C) containing methoxyphenyl substitutions on Cp rings showed more potent cytotoxicity.[35] Some other metallocenes, like Cp_2VCl_2 and Cp_2NbCl_2, also possess anticancer activity.[37]

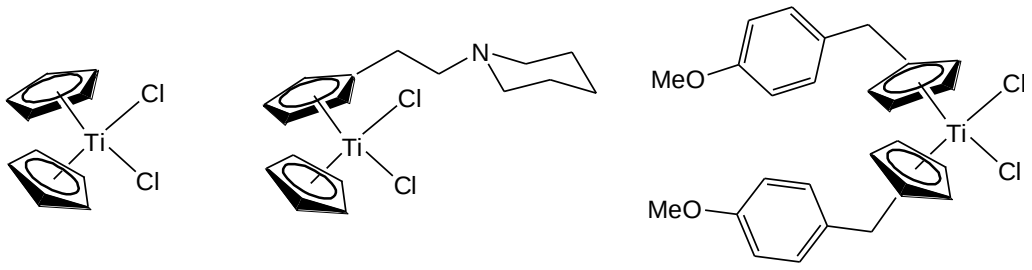

(A) (B) (C)

Figure 1.8. Examples of titanocene anticancer complexes.

The increasing use of pentamethylcyclopentadienyl (Cp*) compounds in recent years is a significant development of organometallic chemistry. Not only are such compounds usually more soluble and more readily crystallised than their unsubstituted cyclopentadienyl (Cp) analogs, but they are generally more stable as a result of the steric and electron-donation effects of the five methyl groups. This is particularly so for the Cp* iridium complexes, where the η^5-C_5Me_5 acts as an excellent stabilising ligand toward Ir(III).[38] The [Cp*Ir] fragment is often used to stabilise the elusive molecule 1,4-dithiobenzoquinone.[39,40] In addition, the formed iridium complexes showed promising anticancer activity against A2780 human ovarian cancer cell line. The pentamethylcyclopentadienyl iridium anticancer complexes are discussed in section 1.3.2.

1.2.2 Ruthenium and Osmium Arene Anticancer Complexes

This section is focused on recent data concerned with the chemistry and anticancer activity of Ru^{II} and Os^{II} arene complexes. It is believed that the activity of the Ru^{III} compounds is dependent on *in vivo* reduction to the more reactive Ru^{II}.[21,22] Neutral η^6-coordinated (π-bound) arenes can stabilise ruthenium and osmium in their +2 oxidation state. With these in mind, work in the Sadler laboratory has focused on the anticancer potential of half-sandwich Ru^{II} and Os^{II} arene complexes of the type, [(η^6-arene)(Ru/Os)(YZ)(X)], where YZ is a bidentate chelating ligand and X is a good leaving group (e. g. Cl), Figure 1.9. The structure of Ru^{II}/Os^{II} half-sandwich complexes allows for variations of the three main

building blocks, the monodentate ligand X, the bidentate ligand YZ and the arene, to design and tune the kinetic parameters and pharmacological properties of these complexes.

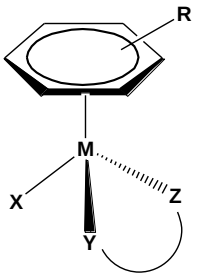

M = Ru/Os

Figure 1.9. General structure of Ru^{II}/Os^{II} arene compounds.

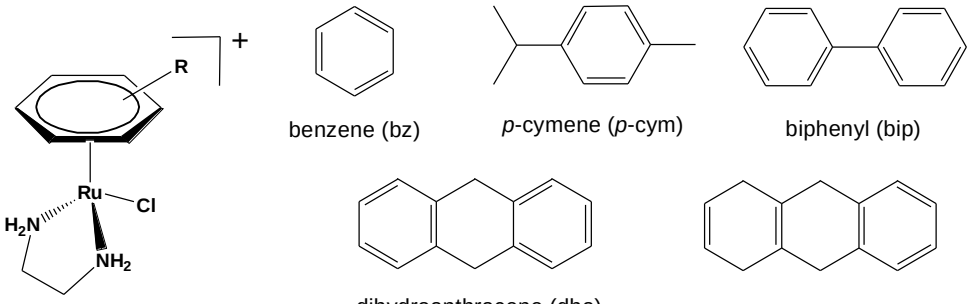

Figure 1.10. $[(\eta^6\text{-arene})Ru(en)Cl]^+$ anticancer complexes (arene shown in right).

Ruthenium arene complexes containing the chelating ligand ethylenediamine, (en), $[(\eta^6\text{-arene})Ru(en)Cl]^+$, showed promising anticancer activity both *in vitro* and *in vivo*, Figure 1.10.[41,42] The mechanism of action for this type of complexes first involves hydrolysis of the Ru–Cl bond (replacement of Cl^- by a water molecule).

Importantly, this step is suppressed in the blood because of the high chloride concentration (ca. 100 mM). Once the complexes cross the cell and nuclear membranes, the complexes are largely hydrolysed to give the reactive species [(η^6-arene)Ru(en)(H_2O)]$^{2+}$ because of the much lower chloride concentration (4 mM).[43] The aqua species are then thought to bind to nuclear DNA with a high affinity to the N7 position of guanine bases.[44-46] Despite these similarities with cisplatin, [(η^6-arene)Ru(en)Cl]$^+$ complexes also showed some obviously different mechanism of action with cisplatin. For example, the Ru arene complexes only form monofunctional adducts while cisplatin form bifunctional adducts. In addition, the [(η^6-arene)Ru(en)Cl]$^+$ complexes is active against cisplatin-resistant cancer cell lines.[42]

For this type of complex, it also has been found that the cytotoxicity against human ovarian A2780 cancer cell line increases with the size of the coordinated arene in the order benzene (IC_{50} = 17 μM, where IC_{50} is the concentration that inhibits cell growth by 50%) < *p*-cymene (IC_{50} = 10 μM) < biphenyl (IC_{50} = 5 μM) < dihydroanthracene (IC_{50} = 2 μM) < tetrahydroanthracene (IC_{50} = 0.5 μM).[42] This might indicate that the hydrophobic arene can be involved in increased cellular uptake, and in addition might be involved in the increased ability of intercalation into the main target DNA. Indeed, the X-ray crystal structure of 9-ethylguanine (9-EtG) adduct [(η^6-dha)Ru(en)(9EtG-*N7*)]$^{2+}$ has shown the base-stacks between the extended dha arene and the coordinated 9-EtG, Figure 1.11.[46]

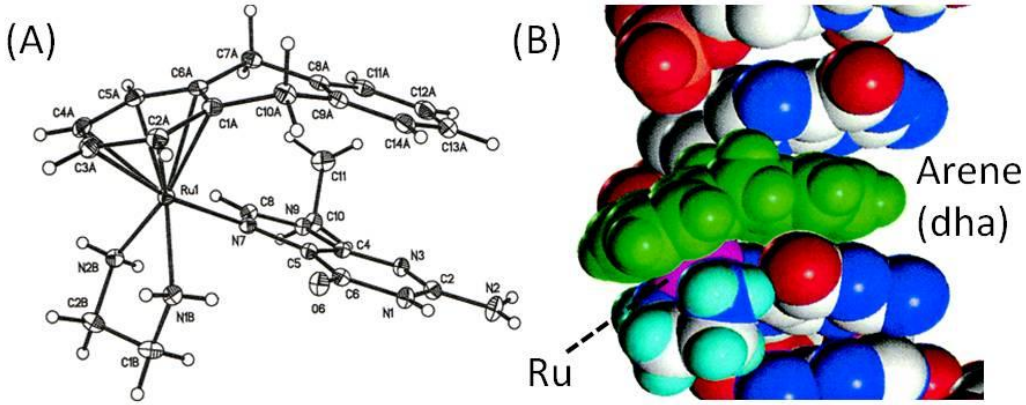

Figure 1.11. (A) X-ray structure for [(η^6-dha)Ru(en)(9EtG-*N7*)]$^{2+}$; (B) A space-filling model of the ruthenium complex bound to B-DNA, illustrating how the extended dha arene can intercalate between guanine base pairs.[46]

Compared with the lighter congener ruthenium, osmium organometallics have been little explored as therapeutic agents, probably due to its reputation of being relatively substitution inert and highly toxic. However the Sadler group have recently explored a new class of potential osmium(II) arene anticancer agents.

The osmium analogue of the active ethylenediamine (en) Ru^{II} complex, [(η^6-bip)Os(en)Cl]$^+$, Figure 1.12A, also exhibited promising activity against the human ovarian cancer A2780 cell line (IC_{50} = 9 μM). However, the hydrolysis rate of the osmium en compound is *ca.* 40 times slower than that of the Ru^{II} analogue, highlighting the lower reactivity of Os^{II}.[47] In addition, aqua adducts of osmium complexes were significantly more acidic by 1−2 units than their ruthenium analogues.[47,48]

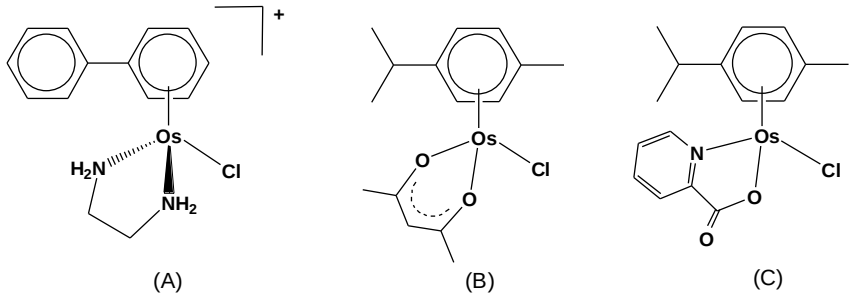

Figure 1.12. Osmium (II) arene complexes with N,N-, O,O- and N,O-chelating ligands. (A) $[(\eta^6\text{-bip})Os(en)Cl]^+$; (B) $[(\eta^6\text{-}p\text{-cym})Os(acac)Cl]$; (C) $[(\eta^6\text{-}p\text{-cym})Os(pico)Cl]$.

Changing the chelating ligand from the neutral N,N-bound en to the anionic O,O-chelator acetylacetonate (acac) (Figure 1.12B), significantly increases the extent and rate of hydrolysis (too fast to monitor by NMR at 298 K). Density functional theory (DFT) calculations have shown that the hydrolysis barrier of the Os^{II} acac complex is significantly lower than that of the en complex by nearly 30 $kJ{\cdot}mol^{-1}$.[49] However, hydrolysis of the acac compounds is complicated by the formation of the hydroxo-bridged dimer $\{[(\eta^6\text{-arene})Os]_2(\mu\text{-}OH)_3\}^+$, with loss of the acac ligand. This hydroxo-bridged dimer is the only observed species at micromolar concentrations in solutions similar to those used in biological cell culture tests,[47] which resulted in the inactivity toward the human ovarian (A2780) and human lung (A549) cancer cell lines.

Intermediate behaviour to that of the N,N- and O,O-chelated osmium arene complexes is observed for complexes containing anionic N,O-chelators. The representative is the complex containing picolinate (pico) as the N,O-chelating

ligand (Figure 1.12C). This complex hydrolyses at an intermediate rate, is stable in aqueous solutions at micromolar concentrations, and is active towards both A549 and A2780 cell lines.[50] A series of osmium(II) arene anticancer complexes containing picolinate derivatives have also been studied.[51]

The organometallic osmium arene azopyridine complex [(η^6-*p*-cym)Os(4-(2-pyridylazo)-N,N-dimethylaniline)I]PF_6, shows nanomolar activity *in vitro* in a few of human cancer cell lines,[52] and exhibits activity *in vivo* against HCT116 human colon cancer xenografts in mice.[53] Its activity may involve redox mechanisms.

1.3 Iridium Anticancer Agents

Iridium is a transition metal of the platinum-group family, which is located in the middle of osmium and platinum in the periodic table. Like osmium, iridium complexes are also generally thought to be too inert to possess high reactivity. This tenet seems to be proved by the fact that [Ir(acac)(COD)] (COD = *cis*,*cis*-1,5-cyclo-octadiene) showed much less antitumour activity than the rhodium analogue,[54,55] and that *trans*-[$IrCl_4$(DMSO)(Im)][ImH][56] and *trans*-[$IrCl_4(Im)_2$][ImH] (ImH = imidazole),[57] (analogues of NAMI-A and the imidazole analogue of indazole complex KP1019, respectively) have all been found to be biologically inactive. In comparison with ruthenium and platinum complexes, the group 9 iridium complexes have attracted only little interest as potential anticancer agents.

1.3.1 Iridium(I) Anticancer Complexes

The majority of the complexes of iridium(I) are 4-coordinate and have square-planar geometry.

[Ir(acac)(COD)] (COD = *cis*,*cis*-1,5-cyclo-octadiene) is one of the earliest iridium anticancer complexes (Figure 1.13). It was found to give 100% cures in mice bearing Ehrlich ascites carcinoma without toxic deaths at dose levels of 50 and 100 mg/kg/day in 1978.[55] In contrast to [Rh(acac)(COD)], the iridium(I) analogue had no effect on lung metastases.[54]

Interestingly, the dinuclear iridium(I) compound, $[IrCl(COD)]_2$, Figure 1.13, was found to have antimetastatic activity in the Lewis lung model, although it did not inhibit primary tumours.[58]

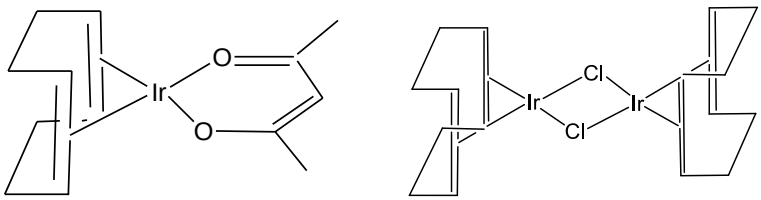

Figure 1.13. Early Ir^I anticancer complexes [Ir(acac)(COD)] and $[IrCl(COD)]_2$.

1.3.2 Iridium(III) Anticancer Complexes

Iridium complexes with a d^6 (Ir^{III}) electron configuration are coordinatively-saturated when the coordination number is 6. Iridium(III) complexes generally have an octahedral geometry.

In one of the earliest studies, no activity was found for several iridium(III) ammine complexes when tested against the solid Sarcoma 180 tumour.[59] Compound *mer*-$[Ir(NH_3)_3Cl_3]$ also showed inactivity against the Sarcoma 180 and the ADJ/PC6A systems while its rhodium(III) analogue, *mer*-$[Rh(NH_3)_3Cl_3]$, inhibited both tumours.

Although the anticancer properties of iridium compounds have been explored almost 40 years, Ir^{III} anticancer agents started to attract attentions just a few years ago. From 2007, Sheldrick and coworkers reported a series of cytotoxic pentamethylcyclopentadienyl and trichlorido Ir^{III} complexes containing N,N-chelating polypyridyl ligands, Figure 1.14.[60-63]

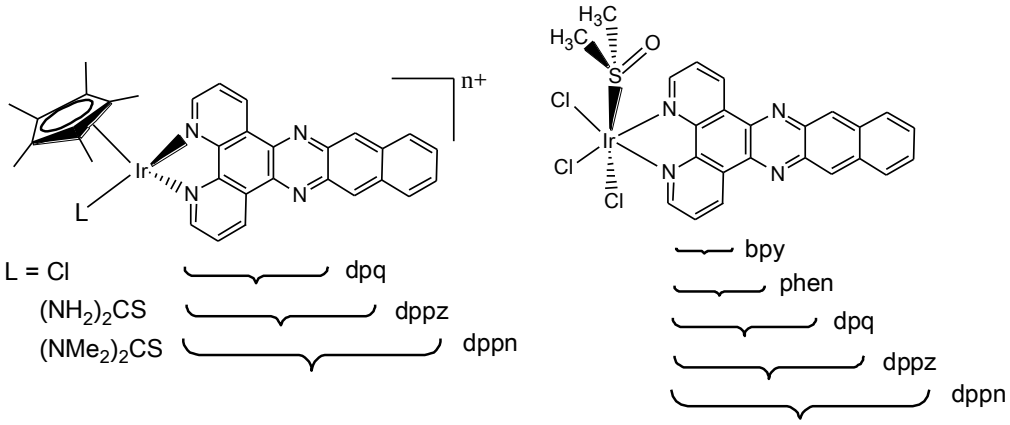

Figure 1.14. Ir^{III} anticancer complexes containing N,N-chelating polypyridyl ligands.[60,61]

Table 1.1. IC_{50} (μM) of Ir^{III} Anticancer Complexes Containing N,N-chelating Polypyridyl Ligands.[60-62]

Compound	IC_{50} (μM)	
	MCF-7	HT-29
$[(\eta^5\text{-}C_5Me_5)Ir(\mathbf{phen})Cl]^+$	>100	>100
$[(\eta^5\text{-}C_5Me_5)Ir(\mathbf{dppz})Cl]^+$	2.3(0.4)	7.4(0.9)
$[(\eta^5\text{-}C_5Me_5)Ir(\mathbf{dppn})(NMe_2)_2CS)]^{2+}$	0.17(0.02)	0.41(0.16)
fac-$[IrCl_3(DMSO)(\mathbf{bpy})]$	>100	>100
fac-$[IrCl_3(DMSO)(\mathbf{phen})]$	4.6(0.5)	4.6(0.2)
fac-$[IrCl_3(DMSO)(\mathbf{dpq})]$	5.5(0.9)	6.1(0.7)
fac-$[IrCl_3(DMSO)(\mathbf{dppz})]$	0.8(0.3)	1.5(0.2)
fac-$[IrCl_3(DMSO)(\mathbf{dppn})]$	0.21(0.11)	1.3(0.4)

In general, the antiproliferative effects of this type of N,N-bound polypyridyl Ir^{III} complexes are governed by the size of the polypyridyl ligands in the order of bpy < phen, dpq < dppz < dppn, Table 1.1. Increasing the surface area of the polypyridyl ligand generally results in a significant increase in the intercalative binding strength. A side-on intercalation mode was established by 2D NOESY for the interaction of $[(\eta^5\text{-}C_5Me_5)Ir(dppz)(H_2metOMe)]^{3+}$ (HmetOH = L-methionine) with the hexanucleotide $d(GTCGAC)_2$.[64] The polypyridyl Ir^{III} complexes interact with DNA via coordination, intercalation or a combination of both. For example, complexes $[(\eta^5\text{-}C_5Me_5)Ir(pp)Cl]^+$ (pp = dpq, dppz, dppn) interact with DNA initially through kinetically preferred intercalation, followed by thermodynamically preferred coordination to DNA after relatively slow substitution of labile chloride.[60]

Increasing the size of polypyridyl ligands also resulted in higher cellular uptake, correlated well with their cytotoxicity.[61]

Lo and co-workers have reported a series of luminescent cyclometalated Ir(III) complexes containing polypyridine as biological labels and probes.[65,66] Some of these complexes were also found to be highly cytotoxic toward HeLa cells.

The Dyson group has explored a series of pentamethylcyclopentadienyl Ir^{III} complexes containing monodentate ligands PTA (1,3,5-triaza-7-phosphatricyclo-[3.3.1.1]decane) and mPTA (1-methyl-1,3,5-triaza-7-phosphaadamantane), Figure 1.15. In contrast to Ru *p*-cymene analogue RAPTA-C, which showed effective inhibition against bovine cat B with IC_{50} value of 2.5 ± 0.5 μM,[67] all these Ir^{III} complexes were inactive *in vitro* against A2780 human ovarian cancer cell line and bovine cat B cells (IC_{50} > 300 μM).[68] Complex $[(Cp^*)Ir(PTA)Cl_2]$ is considered to undergo rapid hydrolysis in water to give mono hydroxo species, $[(Cp^*)Ir(PTA)(OH)Cl]$, similar to $[(Cp^*)Ir(PTA)_2Cl]^+$, followed by further substitution by sulphur atom of the cysteine residue in the active site of cat B. However, Ir^{III} complex forms the weakest M–S bond compared to Ru^{II} and Os^{II} analogues by DFT calculation, which may caused the inactivity against bovine cat B cells.

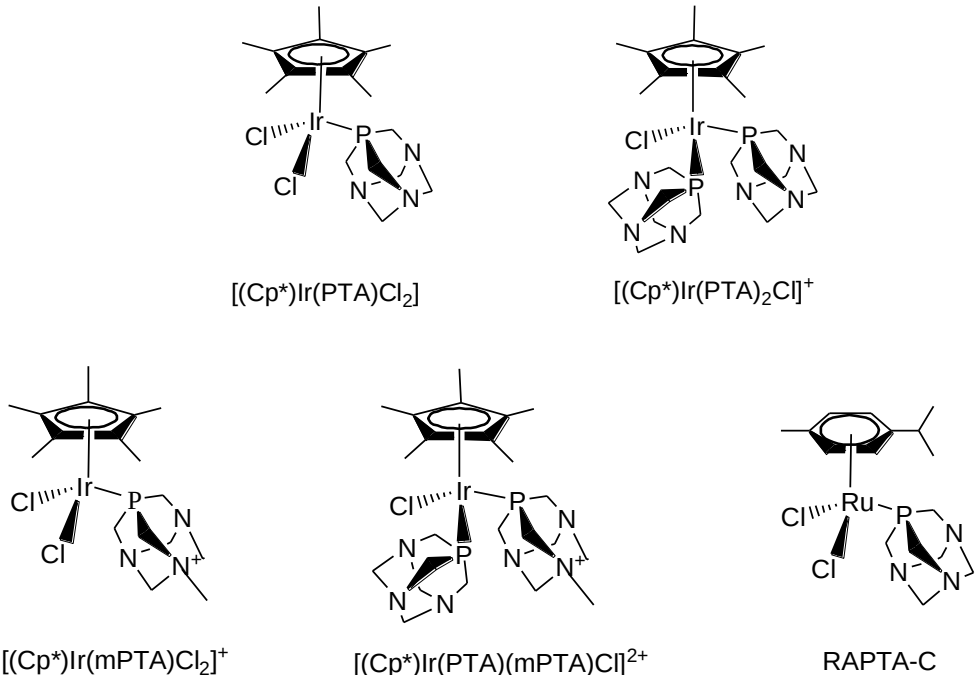

Figure 1.15. Ir^{III} and Ru^{II} monodentate PTA and mPTA complexes.

For $[(\eta^6\text{-arene})Ru(Y)(Z)(X)]^{n+}$ complexes, replacing the monodentate Y and Z ligands by a bidentate chelating group YZ generally tends to improve anticancer activity and stability in aqueous solution.[42] Several pentamethylcyclopentadienyl Ir^{III} anticancer complexes containing N,O- or N,N-chelating ligands have been studied. N,O-bound 1,2-naphthoquinone-1-oximate complex $[(\eta^5\text{-}C_5Me_5)Ir(\eta^2\text{-}C_{10}H_6N_2O)Cl]$, Figure 1.16A, exerted a more potent cytotoxicity against HeLa (cervical carcinoma) and HL60 (leukemia) cancer cells than cisplatin.[69] However, no interaction with double-stranded DNA was observed for the cytotoxic complex. Another N,O-bound quinolin-8-ol complex $[(\eta^5\text{-}C_5Me_5)Ir(qol)Cl]$, Figure 1.16B, showed reasonable effectiveness against C-32, SNB-19 and SK-Mel tumour cells.[70] Despite the anticancer activity, the mechanism of action of the complex is still

unknown. N,N-bound 2-(pyridine-2-yl)thiazole complex [(η^5-C_5Me_5)Ir(pyTz)Cl], Figure 1.16C, is inactive toward A2780 human ovarian cancer cell line and cisplatin-resistant variant (A2780cisR) with IC_{50} value > 300 μM.[71] The inactivity may be due to the absence of interaction with DNA since the complex lacks of either intercalating group or strong hydrogen bond donors on the N,N-chelating ligand.

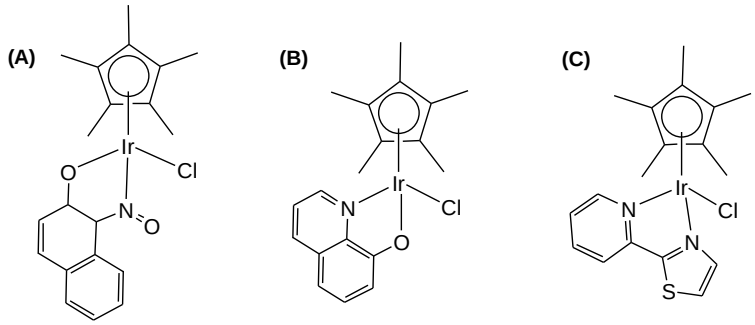

Figure 1.16. Iridium(III) anticancer complexes containing N,O- or N,N-chelating ligands.[69-71]

1.4 Ir^{III} Pentamethylcyclopentadienyl Complexes as Catalytic Agents

The global demand for iridium in 2007 was 3700 kg, out of which 750 kg was for catalysis.[72] Recently, remarkable efforts have been devoted towards the development of aqueous-phase organometallic catalysis due to the relatively easy recycling of water-soluble catalysts in aqueous-organic biphasic reaction

mixtures.[73] Iridium(III) pentamethylcyclopentadienyl (Cp*) complexes are extremely useful in synthesis due to their ability to catalyse an array of synthetic transformations, often with unique selectivity, such as in C=O hydrogenation, hydroamination, and asymmetric allylic substitutions.[74] The iridium Cp* dimer $[(Cp^*)IrCl_2]_2$ is an effective catalyst for conversion of alcohols into amides via oximes.[75] Some iridium aqua complexes are reported to catalyse CO_2 hydrogenation due to formation of active hydride complexes.[76] Ir^{III} Cp* compounds are also used as catalysts in a range of other reactions. For example, a number of Ir^{III} Cp* complexes containing C^N, or N,N-chelating ligands are highly active for water-oxidation when driven with a chemical oxidant.[77]

Transfer hydrogenation reactions provide an alternative to direct hydrogenation for the reduction of a range of substrates. Catalytic iridium complexes are the most important catalyst for transfer hydrogenation reactions.[78] In the reduction of ketones and aldehydes (one of the fundamental applications of transfer hydrogenation), iridium hydride species are often formed as actually effective agents in the reaction pathway. Typically, formic acid, formate, or alcohol can be used as the source of hydride. A water-soluble iridium hydride complex $[(Cp^*)Ir(bpy)H]^+$ (bpy = 2,2'-bipyridine) has been reported as a robust catalyst for acid-catalysed transfer hydrogenation of carbonyl compounds, Eq. 1.1.[79] HCOOH and HCOONa are used as hydrogen donors to form the hydride complex and the crystal structure is shown in Figure 1.17.

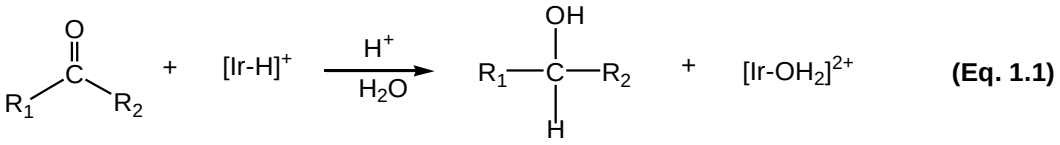

(Eq. 1.1)

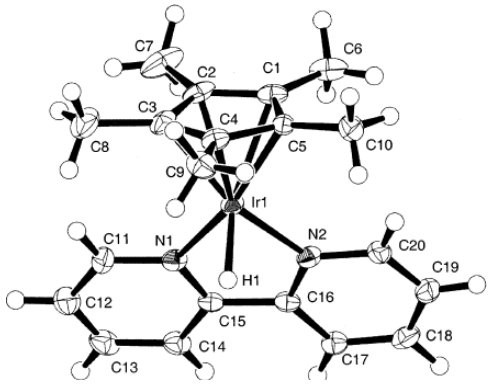

Figure 1.17. Crystal structure of hydride complex $[(Cp^*)Ir(bpy)H]^+$.[79]

For another example, a Cp* Ir^{III} catalyst containing a diamine ligand (HCOONa as hydrogen donor) showed a higher activity in transfer hydrogenation of aldehydes than its ruthenium and rhodium analogues.[80]

In numerous biological hydrogen transfer reactions, an important example is the reduction of coenzyme NAD^+ (β-nicotinamide adenine dinucleotide) to its reduced form 1,4-NADH (Figure 1.18), by accepting two electrons and a proton from a substrate in the presence of an enzyme. NAD^+/NADH have been known as classic molecules involving in energy metabolism, reductive biosynthesis and antioxidation.[81-83] Various transition metal hydrides have been studied as catalysts for the reduction of NAD^+ and NAD^+-models to the corresponding 1,4-NADH and its derivatives.[84-86] Ir^{III} Cp* complex containing 1,10-phenanthroline derivative has

shown to catalyse the reduction of NAD^+ in the presence of formate as the hydride source.[87] This reduction is regioselective, giving the biologically relevant 1,4-NADH isomer.

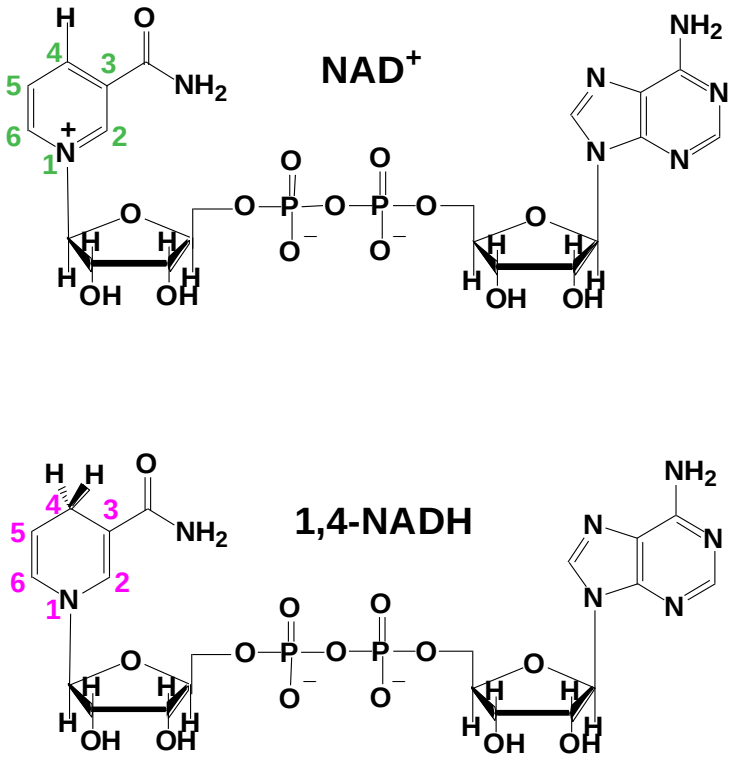

Figure 1.18. Coenzyme NAD^+ (β-nicotinamide adenine dinucleotide) and the reduced form 1,4-NADH.

1.5 Aims

The general aim of this thesis is to investigate the design and reactivity of organometallic anticancer iridium(III) complexes containing different substituted cyclopentadienyl and chelating ligands. The studies are focused on systematic variations in the design of the complexes and studying the relationships between their physical, chemical and biological properties. More specific aims are as follows.

1. To synthesise and characterise organometallic iridium(III) complexes with variations to the cyclopentadienyl and chelating ligands with a view to tune their reactivity and improve their biological properties.
2. To develop structure-activity relationships, investigate the influences of changing cyclopentadienyl ligands with different substitution and chelating ligands on their aqueous chemistry and biological activity, including rates and extent of hydrolysis, acidity of bound water, nucleobase binding, cytotoxicity, distribution in cellular fractions, cellular uptake and DNA binding.
3. To investigate the conversion between NAD^+ and NADH using organometallic iridium complexes as catalysts, explore the possibility of hydride-transfer reactions using 1,4-NADH as a hydride source.

1.6 References

(1) Jemal, A.; Bray, F.; Center, M. M.; Ferlay, J.; Ward, E.; Forman, D. *CA-Cancer J. Clin.* **2011**, *61*, 69-90.

(2) Hooning, M. J.; Aleman, B. M. P.; Hauptmann, M.; Baaijens, M. H. A.; Klijn, J. G. M.; Noyon, R.; Stovall, M.; van Leeuwen, F. E. *J. Clin. Oncol.* **2008**, *26*, 5561-5568.

(3) Albain, K. S.; Swann, R. S.; Rusch, V. W.; Turrisi Iii, A. T.; Shepherd, F. A.; Smith, C.; Chen, Y.; Livingston, R. B.; Feins, R. H.; Gandara, D. R.; Fry, W. A.; Darling, G.; Johnson, D. H.; Green, M. R.; Miller, R. C.; Ley, J.; Sause, W. T.; Cox, J. D. *The Lancet* **2009**, *374*, 379-386.

(4) *Metallotherapeutic Drugs and Metal-Based Diagnostic Agents: The Use of Metals in Medicine*; Gielen, M.; Tiekink, E. R. T., Eds.; Wiley: Chichester, 2005.

(5) Thompson, K. H.; Orvig, C. *Science* **2003**, *300*, 936-939.

(6) Orvig, C.; Abrams, M. J. *Chem. Rev.* **1999**, *99*, 2201-2204.

(7) Rosenberg, B.; Van Camp, L.; Krigas, T. *Nature* **1965**, *205*, 698-699.

(8) Rosenberg, B.; Vancamp, L.; Trosko, J. E.; Mansour, V. H. *Nature* **1969**, *222*, 385-386.

(9) Weiss, R. B.; Christian, M. C. *Drugs* **1993**, *46*, 360-377.

(10) Lebwohl, D.; Canetta, R. *Eur. J. Cancer* **1998**, *34*, 1522-1534.

(11) Dyson, P. J.; Sava, G. *Dalton Trans.* **2006**, 1929-1933.

(12) Wang, D.; Lippard, S. J. *Nat. Rev. Drug Discovery* **2005**, *4*, 307-320.

(13) Jamieson, E. R.; Lippard, S. J. *Chem. Rev.* **1999**, *99*, 2467-2498.

(14) Sherman, S.; Gibson, D.; Wang, A.; Lippard, S. *Science* **1985**, *230*, 412-417.

(15) Köpf-Maier, P. *Eur. J. Clin. Pharmacol.* **1994**, *47*, 1-16.

(16) Reedijk, J. *Platinum Met. Rev.* **2008**, *52*, 2-11.

(17) Alessio, E.; Mestroni, G.; Bergamo, A.; Sava, G. *Curr. Top. Med. Chem.* **2004**, *4*, 1525-1535.

(18) Sava, G.; Pacor, S.; Mestroni, G.; Alessio, E. *Clin. Exp. Metastasis* **1992**, *10*, 273-280.

(19) Berger, M. R.; Garzon, F. T.; Keppler, B. K.; Schmahl, D. *Anticancer Res.* **1989**, *9*, 761-766.

(20) Hartinger, C. G.; Zorbas-Seifried, S.; Jakupec, M. A.; Kynast, B.; Zorbas, H.; Keppler, B. K. *J. Inorg. Biochem.* **2006**, *100*, 891-904.

(21) Clarke, M. J.; Zhu, F.; Frasca, D. R. *Chem. Rev.* **1999**, *99*, 2511-2534.

(22) Kelman, A. D.; Clarke, M. J.; Edmonds, S. D.; Peresie, H. J. *J. Clin. Hematol. Onc.* **1977**, *7*, 274-288.

(23) Berners-Price, S. J.; Bowen, R. J.; Galettis, P.; Healy, P. C.; McKeage, M. J. *Coord. Chem. Rev.* **1999**, *185-186*, 823-836.

(24) Jakupec, M. A.; Keppler, B. K. *Curr. Top. Med. Chem.* **2004**, *4*, 1575-1583.

(25) Halpern, J. *Pure Appl. Chem.* **2001**, *73*, 209-220.

(26) Gasser, G.; Ott, I.; Metzler-Nolte, N. *J. Med. Chem.* **2011**, *54*, 3-25.

(27) Köpf-Maier, P.; Köpf, H.; Neuse, E. W. *Angew. Chem., Int. Ed. Engl.* **1984**, *23*, 456-457.

(28) Köpf-Maier, P.; Köpf, H. *Chem. Rev.* **1987**, *87*, 1137-1152.

(29) Köpf-Maier, P.; Köpf, H. In *Bioinorganic Chemistry*; Springer Berlin/Heidelberg: 1988; 70, pp 103-185.

(30) Top, S.; Vessières, A.; Leclercq, G.; Quivy, J.; Tang, J.; Vaissermann, J.; Huché, M.; Jaouen, G. *Chem.-Eur. J.* **2003**, *9*, 5223-5236.

(31) Guo, M.; Guo, Z.; Sadler, P. *J. Biol. Inorg. Chem.* **2001**, *6*, 698-707.

(32) Kröger, N.; Kleeberg, U. R.; Mross, K.; Edler, L.; Hossfeld, D. K. *Onkologie* **2000**, *23*, 60-62.

(33) Mross, K.; Robben-Bathe, P.; Edler, L.; Baumgart, J.; Berdel, W. E.; Fiebig, H.; Unger, C. *Onkologie* **2000**, *23*, 576-579.

(34) Allen, O. R.; Gott, A. L.; Hartley, J. A.; Hartley, J. M.; Knox, R. J.; McGowan, P. C. *Dalton Trans.* **2007**, 5082-5090.

(35) Oberschmidt, O.; Hanauske, A. R.; Pampillón, C.; Sweeney, N. J.; Strohfeldt, K.; Tacke, M. *Anti-Cancer Drugs* **2007**, *18*, 317-321

(36) Allen, O. R.; Croll, L.; Gott, A. L.; Knox, R. J.; McGowan, P. C. *Organometallics* **2004**, *23*, 288-292.

(37) Fricker, S. P. *Metal compounds in cancer therapy*; Chapman & Hall: London, 1994.

(38) White, C. Y., A.; Maitlis, P. M. *Inorg. Chem.* **1992**, *29*, 228-234.

(39) Amouri, H.; Moussa, J.; Renfrew, A. K.; Dyson, P. J.; Rager, M. N.; Chamoreau, L.-M. *Angew. Chem., Int. Ed.* **2010**, *49*, 7530-7533.

(40) Hartinger, C. G. *Angew. Chem., Int. Ed.* **2010**, *49*, 8304-8305.

(41) Morris, R. E.; Aird, R. E.; del Socorro Murdoch, P.; Chen, H.; Cummings, J.; Hughes, N. D.; Parsons, S.; Parkin, A.; Boyd, G.; Jodrell, D. I.; Sadler, P. J. *J. Med. Chem.* **2001**, *44*, 3616-3621.

(42) Aird, R. E.; Cummings, J.; Ritchie, A. A.; Muir, M.; Morris, R. E.; Chen, H.; Sadler, P. J.; Jodrell, D. I. *Br. J. Cancer* **2002**, *86*, 1652-1657.

(43) Wang, F.; Chen, H.; Parsons, S.; Oswald, I. D. H.; Davidson, J. E.; Sadler, P. J. *Chem.-Eur. J.* **2003**, *9*, 5810-5820.

(44) Novakova, O.; Chen, H.; Vrana, O.; Rodger, A.; Sadler, P. J.; Brabec, V. *Biochemistry* **2003**, *42*, 11544-11554.

(45) Liu, H.-K.; Wang, F.; Parkinson, J. A.; Bella, J.; Sadler, P. J. *Chem.-Eur. J.* **2006**, *12*, 6151-6165.

(46) Chen, H.; Parkinson, J. A.; Parsons, S.; Coxall, R. A.; Gould, R. O.; Sadler, P. J. *J. Am. Chem. Soc.* **2002**, *124*, 3064-3082.

(47) Peacock, A. F. A.; Habtemariam, A.; Fernández, R.; Walland, V.; Fabbiani, F. P. A.; Parsons, S.; Aird, R. E.; Jodrell, D. I.; Sadler, P. J. *J. Am. Chem. Soc.* **2006**, *128*, 1739-1748.

(48) Peacock, A. F. A.; Habtemariam, A.; Moggach, S. A.; Prescimone, A.; Parsons, S.; Sadler, P. J. *Inorg. Chem.* **2007**, *46*, 4049-4059.

(49) Peacock, A. F. A.; Melchart, M.; Deeth, R. J.; Habtemariam, A.; Parsons, S.; Sadler, P. J. *Chem.-Eur. J.* **2007**, *13*, 2601-2613.

(50) Peacock, A. F. A.; Parsons, S.; Sadler, P. J. *J. Am. Chem. Soc.* **2007**, *129*, 3348-3357.

(51) van Rijt, S. H.; Peacock, A. F. A.; Johnstone, R. D. L.; Parsons, S.; Sadler, P. J. *Inorg. Chem.* **2009**, *48*, 1753-1762.

(52) Fu, Y.; Habtemariam, A.; Pizarro, A. M.; van Rijt, S. H.; Healey, D. J.; Cooper, P. A.; Shnyder, S. D.; Clarkson, G. J.; Sadler, P. J. *J. Med. Chem.* **2010**, *53*, 8192-8196.

(53) Shnyder, S. D.; Fu, Y.; Habtemariam, A.; van Rijt, S. H.; Cooper, P. A.; Loadman, P. M.; Sadler, P. J. *Med. Chem. Comm.* **2011**, *2*, 666-668.

(54) Sava, G.; Giraldi, T.; Mestroni, G.; Zassinovich, G. *Chem. Biol. Interact.* **1983**, *45*, 1-6.

(55) Giraldi, T.; Sava, G.; Mestroni, G.; Zassinovich, G.; Stolfa, D. *Chem. Biol. Interact.* **1978**, *22*, 231-238.

(56) Messori, L.; Marcon, G.; Orioli, P.; Fontani, M.; Zanello, P.; Bergamo, A.; Sava, G.; Mura, P. *J. Inorg. Biochem.* **2003**, *95*, 37-46.

(57) Marcon, G.; Casini, A.; Mura, P.; Messori, L.; Bergamo, A.; Orioli, P. *Metal-Based Drugs* **2000**, *7*, 195-200.

(58) Sava, G.; Zorzet, S.; Perissin, L.; Mestroni, G.; Zassinovich, G.; Bontempi, A. *Inorg. Chim. Acta* **1987**, *137*, 69-71.

(59) Cleare, M. J. *Coord. Chem. Rev.* **1974**, *12*, 349-405.

(60) Schäfer, S.; Sheldrick, W. S. *J. Organomet. Chem.* **2007**, *692*, 1300-1309.

(61) Scharwitz, M. A.; Ott, I.; Gust, R.; Kromm, A.; Sheldrick, W. S. *J. Inorg. Biochem.* **2008**, *102*, 1623-1630.

(62) Schäfer, S.; Ott, I.; Gust, R.; Sheldrick, W. S. *Eur. J. Inorg. Chem.* **2007**, 3034-3046.

(63) Geldmacher, Y.; Kitanovic, I.; Alborzinia, H.; Bergerhoff, K.; Rubbiani, R.; Wefelmeier, P.; Prokop, A.; Gust, R.; Ott, I.; Wölfl, S.; Sheldrick, W. S. *Chem. Med. Chem.* **2011**, *6*, 429-439.

(64) Frodl, A.; Herebian, D.; Sheldrick, W. S. *J. Chem. Soc., Dalton Trans.* **2002**, 3664-3673.

(65) Leung, S.-K.; Liu, H.-W.; Lo, K. K.-W. *Chem. Commun.* **2011**, DOI: 10.1039/c1031cc11423a.

(66) Lo, K. K.-W.; Zhang, K. Y.; Li, S. P.-Y. *Pure Appl. Chem.* **2011**, *83*, 823-840.

(67) Casini, A.; Gabbiani, C.; Sorrentino, F.; Rigobello, M. P.; Bindoli, A.; Geldbach, T. J.; Marrone, A.; Re, N.; Hartinger, C. G.; Dyson, P. J.; Messori, L. *J. Med. Chem.* **2008**, *51*, 6773-6781.

(68) Casini, A.; Edafe, F.; Erlandsson, M.; Gonsalvi, L.; Ciancetta, A.; Re, N.; Ienco, A.; Messori, L.; Peruzzini, M.; Dyson, P. J. *Dalton Trans.* **2010**, *39*, 5556-5563.

(69) Wirth, S.; Rohbogner, C.; Cieslak, M.; Kazmierczak-Baranska, J.; Donevski, S.; Nawrot, B.; Lorenz, I.-P. *J. Biol. Inorg. Chem.* **2010**, *15*, 429-440.

(70) Sliwinska, U.; Pruchnik, F. P.; Ulaszewski, S.; Latocha, M.; Nawrocka-Musial, D. *Polyhedron* **2010**, *29*, 1653-1659.

(71) Gras, M.; Therrien, B.; Süss-Fink, G.; Casini, A.; Edafe, F.; Dyson, P. J. *J. Organomet. Chem.* **2010**, *695*, 1119-1125.

(72) Jollie, D. *Platinum 2008* **2008**, 42-43

(73) *Aqueous-Phase Organometallic Catalysis*, 2 ed.; Cornils, B.; Herrmann, W. A., Eds.; Wiley-VCH: Weinheim, Germany, 2004.

(74) *Iridium Complexes in Organic Synthesis*; Oro, L. A.; Claver, C., Eds.; WILEY-VCH: Weinheim, Germany, 2008.

(75) Owston, N. A.; Parker, A. J.; Williams, J. M. J. *Org. Lett.* **2006**, *9*, 73-75.

(76) Ogo, S.; Kabe, R.; Hayashi, H.; Harada, R.; Fukuzumi, S. *Dalton Trans.* **2006**, 4657-4663.

(77) Blakemore, J. D.; Schley, N. D.; Balcells, D.; Hull, J. F.; Olack, G. W.; Incarvito, C. D.; Eisenstein, O.; Brudvig, G. W.; Crabtree, R. H. *J. Am. Chem. Soc.* **2010**, *132*, 16017-16029.

(78) Saidi, O.; Williams, J. In *Iridium Catalysis*; Andersson, P. G., Ed.; Springer Berlin / Heidelberg: 2011; 34, pp 77-106.

(79) Abura, T.; Ogo, S.; Watanabe, Y.; Fukuzumi, S. *J. Am. Chem. Soc.* **2003**, *125*, 4149-4154.

(80) Wu, X.; Liu, J.; Li, X.; Zanotti-Gerosa, A.; Hancock, F.; Vinci, D.; Ruan, J.; Xiao, J. *Angew. Chem., Int. Ed.* **2006**, *45*, 6718-6722.

(81) Belenky, P.; Bogan, K. L.; Brenner, C. *Trends Biochem. Sci.* **2007**, *32*, 12-19.

(82) Berger, F.; Ramírez-Hernández, M. H.; Ziegler, M. *Trends Biochem. Sci.* **2004**, *29*, 111-118.

(83) Pollak, N.; Dölle, C.; Ziegler, M. *Biochem. J.* **2007**, *402*, 205-218.

(84) Lo, H. C.; Leiva, C.; Buriez, O.; Kerr, J. B.; Olmstead, M. M.; Fish, R. H. *Inorg. Chem.* **2001**, *40*, 6705-6716.

(85) Lo, H. C.; Buriez, O.; Kerr, J. B.; Fish, R. H. *Angew. Chem., Int. Ed.* **1999**, *38*, 1429-1432.

(86) Yan, Y.; Melchart, M.; Habtemariam, A.; Peacock, A.; Sadler, P. *J. Biol. Inorg. Chem.* **2006**, *11*, 483-488.

(87) Canivet, J.; Süss-Fink, G.; Štěpnička, P. *Eur. J. Inorg. Chem.* **2007**, 4736-4742.

Chapter 2

Experimental Methods and Materials

This Chapter describes the main experimental techniques used in this work. More specific methods relating to individual experiments are described in the appropriate Chapters. The synthesis and characterisation of the cyclopentadienyl ligands and dimers used for the synthesis of the iridium complexes in subsequent Chapters is also covered here.

2.1 Instrumentation and Methods

2.1.1 Nuclear Magnetic Resonance Spectroscopy (NMR)[1-3]

Nuclear magnetic resonance (NMR) spectroscopy is a powerful technique which exploits the magnetic properties of nuclei to determine physical and chemical properties of atoms or molecules. All chemical elements that possess a nuclear spin of ½ or greater are in principle observable by NMR. Most studied nuclei with NMR are ^{1}H, ^{13}C and ^{15}N. When placed in a magnetic field (B_0), nuclei with a spin ½ will distribute over two states with different energies (α and β), and process around B_0 at a characteristic frequency (Larmor frequency). The slight population difference between the α and β states results in a bulk magnetization vector (M_0) along the axes of B_0. The application of a second magnetic field (B_1) at the Larmor frequency of the nuclei will cause the nuclei to resonate. In most NMR experiments, the nuclei are irradiated with brief pulses of B_1, allowing the spins to return to their equilibrium between the pulses referred to as relaxation. The relaxation of the spins causes the NMR signal to decay with time, producing the observed Free Induction Decay or FID. The FID can be Fourier transformed to produce a NMR spectrum

where signals are plotted as a function of frequency. Depending on the local chemical environment, different nuclides in a molecule resonate at slightly different frequencies and this gives rise to the different chemical shifts observed in the NMR spectra. The chemical shift can be used to obtain structural information about the molecule by understanding the different chemical environments of the atoms in the molecule.

2D NMR spectra provide more information about a molecule than 1D NMR spectra and are especially useful in determining the structure of a molecule, particularly for molecules that are too complicated to work with using 1D NMR. In the COSY (correlation spectroscopy), TOCSY (total correlation spectroscopy) or NOESY (nuclear Overhauser effect spectroscopy) 2D NMR experiments, a second frequency domain is introduced to reveal structural connections through magnetic interactions between nuclei. In both the COSY and TOCSY experiments, two essentially identical chemical shift axes are plotted orthogonally to each other, with the 1D NMR spectra appearing on the diagonal of the plot. In a COSY experiment, all the spin-spin coupled protons are indicated by cross peaks which are symmetrically placed along the diagonal. COSY spectra typically can show two- and three-bond coupled protons, however long-range bonding can be emphasised through introducing extra delays in the pulse sequence. In TOCSY experiments, the connectivity of a whole spin system can be shown as cross peaks are found for all protons that are connected within it. 2D NOESY was used to establish structural information resulting from through-space interactions between protons that are close in spatial proximity.

2.1.1.1 Experimental

^{1}H NMR spectra were acquired in 5 mm NMR tubes at 298K (unless stated otherwise) on either Bruker AV-400, Bruker DRX 500, AVA 600 or Bruker AV II 700 NMR spectrometers. ^{1}H NMR chemical shifts were internally referenced to (C*H*D$_2$)(CD$_3$)SO (2.50 ppm) for DMSO-d_6, C*H*Cl$_3$ (7.26 ppm) for chloroform-d_1, C*H*D$_2$OD (3.33 ppm) for methanol-d_4 and to 1,4-dioxane (3.75 ppm) for aqueous solutions. The data were processed using TOPSPIN (version 2.1 Bruker UK Ltd).

2.1.1.2 Water Suppression

Many experiments in this thesis were performed on samples in aqueous solutions (99.9% D$_2$O, or 5% MeOD-d_4/95% D$_2$O, or 10% MeOD-d_4/90% H$_2$O,) so as to be of biological relevance. The use of such aqueous solutions results in a large HOD signal that can obscure the other signals in the ^{1}H spectrum. To minimize this, the HOD signal was suppressed with either presaturation or Shaka techniques.[4] Presaturation involves the saturation of the HOD peak by irradiating the frequency of water in between pulse sequences. Shaka water suppression, or Double Pulse Field Gradient Spin Echo (DPFGSE), uses pulsed field gradient spin echoes in which the refocusing pulse is the sequence soft π(x)-hard π(-x). The disadvantage of this technique is that signals close to the water peak are also reduced in intensity.

2.1.2 pH Measurements

pH values were measured at ambient temperature, using a Corning 240 pH meter equipped with a micro combination KNO_3 (chloride free) electrode calibrated with Aldrich buffer solutions of pH 4, 7 and 10. pH* values (pH meter reading) of NMR samples in D_2O were measured directly in the NMR tube, before and after recording NMR spectra using the same method.

2.1.3 Determination of pK_a Values

To generate the aqua complexes, chlorido complexes were dissolved in D_2O and 0.98 mol equiv of $AgNO_3$ were added. The solution was stirred for 24 h at 298 K, and AgCl was removed by filtration. For determinations of pK_a* values (pK_a values for solutions in D_2O) the pH* values of solutions of the aqua complexes in D_2O were varied from ca. pH* 2 to 11 by the addition of dilute NaOD and $DClO_4$, and ^{1}H NMR spectra were recorded. The chemical shifts of the chelating ligand protons and/or methyl protons of Cp^x were plotted against pH*. The pH* titration curves were fitted to the Henderson-Hasselbalch equation using ORIGIN version 8.0. These pK_a* values can be converted to pK_a values by use of the equation pK_a = 0.929pK_a* + 0.42 as suggested by Krezel and Bal[5] for comparison with related values in the literature.

2.1.4 X-ray Crystallography

X-ray diffraction (XRD) is a widely used technique for the precise determination of the position of atoms in molecules in the crystalline solid state. XRD was used in this thesis to characterise the crystal structures of several synthesised compounds. All diffraction data were obtained on an Oxford Diffraction Gemini four-circle system with a Ruby CCD area detector using Mo Kα radiation. Absorption corrections were applied using ABSPACK.[6] The crystals were mounted in oil and held at 100(2) K with the Oxford Cryosystem Cobra. The structures were solved by direct methods using SHELXS (TREF)[7] with additional light atoms found by Fourier methods. Complexes were refined against F^2 using SHELXL.[8] Data collection and solution of the structures were carried out by Dr. Guy Clarkson (Department of Chemistry, University of Warwick). Details of the acquisition and solving of the individual crystal structures are explained in the corresponding Chapters.

2.1.5 Elemental Analysis

Elemental analysis determines the percentage of C, H and N composition in a sample. Comparing the obtained C, H, N values of a sample of the complex to theoretical values provides information about the purity of the compound and was used for this purpose in this thesis. CHN elemental analyses were carried out on a CE-440 elemental analyzer by Exeter Analytical (UK) Ltd.

2.1.6 Electrospray Ionisation Mass Spectrometry (ESI-MS)[9]

Mass spectrometry (MS) is an analytical technique that measures the mass-to-charge ratios of charged particles. It is used for determining masses of particles, and for elucidating the chemical structures of molecules. The MS principle consists of ionizing chemical compounds to generate charged molecules or molecule fragments and measuring their mass-to-charge ratios. Electrospray ionization (ESI) is a technique used in mass spectrometry to produce ions. The sample must be present in the form of ions in solution and this is typically achieved by adding small amounts of acid or base to respectively protonate (ESI positive) or deprotonate (ESI negative) the solution. ESI-MS was used routinely in this work for the characterisation of the complexes.

ESI-MS were obtained on a Bruker Esquire 2000 Ion Trap Spectrometer. Samples were prepared in 50% CH_3CN and 50% H_2O (v/v). The mass spectra were recorded with a scan range of *m/z* 50–1000 for positive ions. Data were processed using Data Analysis 3.3 (Bruker Daltonics).

2.1.7 Inductively Coupled Plasma Mass Spectroscopy (ICP-MS)[9,10]

ICP-MS is a very sensitive technique that can be used to determine the elemental concentrations of solutions. More than 75 elements can be determined; most of them at detection limits of less than 1 part per billion (100 ppt–2 ppb). It is based on coupling together inductively coupled plasma as a method of producing ions

(ionization) with mass spectrometry as a method of separating and detecting the ions.

All ICP-MS analyses were carried out on an Agilent Technologies 7500 series ICP-MS instrument. The water used for ICP-MS analysis was doubly deionised (DDW) using a Millipore Milli-Q water purification system and a USF Elga UHQ water deionizer. The iridium Specpure plasma standard (Alfa Aesar, 1000 ppm in 10% HCl) was diluted with 3% HNO_3 DDW to freshly prepare calibrants at concentrations 1000, 800, 400, 200, 100, 50, 10, 1 and 0.1 ppb. The ICP-MS instrument was set to detect ^{193}Ir with typical detection limits of ca. 2 ppt using no gas mode.

2.1.8 UV-Vis Absorption Spectroscopy

UV-Vis spectroscopy is routinely used in analytical chemistry for the quantitative determination of different analytes, such as transition metal ions, highly conjugated organic compounds, and biological macromolecules.[9]

This method is used in this thesis to monitor hydrolysis of iridium chloride complexes and reactions with NADH or NAD^+. A Cary 300 UV-Vis recording spectrophotometer was used with 1 cm path-length quartz cuvettes (0.5 mL) and a PTP1 Peltier temperature controller. Spectra were processed using UVWinlab software. Experiments were carried out at 298 K unless otherwise stated.

2.1.9 Computational Methods

Calculations in Chapter 3 and 4 were performed by Dr. Luca Salassa (Department of Chemistry, University of Warwick).

The Gaussian 03 package[11] was employed for all calculations. Geometry optimization calculations for some iridium complexes were performed in the gas phase with the hybrid functional PBE1PBE.[12] The LanL2DZ basis set and effective core potential[13] were used for the Ir atom, and the 6-31G** basis set was used for all other atoms.[14] The nature of all stationary points was confirmed by performing a normal-mode analysis. Electrostatic potential surfaces (EPSs) for some iridium complexes were calculated and mapped on electron density of the molecules. The electrostatic potential is represented with a colour scale ranging from red to blue.

2.1.10 Determination of Partition Coefficient, Log *P*

The Log *P* value, or partition coefficient, is the ratio of concentrations of a compound in a mixture of two immiscible solvents at equilibrium, typically water and a hydrophobic solvent such as octanol. The partition coefficient gives a measure of how hydrophilic or hydrophobic a compound is. This is useful in estimating the distribution of drugs within the body, *e.g.* hydrophobic compounds with high partition coefficients are preferentially distributed to hydrophobic compartments such as lipid bilayers of cells while hydrophilic compounds (low partition coefficients) preferentially are found in hydrophilic compartments.

In this thesis, octanol-saturated water (OSW) and water-saturated octanol (WSO) were prepared using analytical grade octanol and 0.2 M aqueous NaCl solution (to suppress hydrolysis of the chlorido complexes). Aliquots of stock solutions of iridium complexes in OSW were added to equal volumes of WSO and shaken in an IKA Vibrax VXC basic shaker for 4 h at 500 g/min to allow partition at ambient temperature. The aqueous layer was carefully separated from the octanol layer for iridium analysis. ^{193}Ir was quantified from aliquots taken from the octanol-saturated aqueous samples before and after partition. Partition coefficients of Ir^{III} complexes were calculated using the equation $\log P = \log ([Ir]_{WSO}/[Ir]_{OSW})$, where $[Ir]_{WSO}$ was obtained by subtraction of the Ir content of the aqueous layer after partition from the Ir content of the aqueous layer before partition.

2.1.11 Cancer Cell Growth Inhibition

2.1.11.1 Cytotoxicity against A2780 Human Ovarian Cancer Cells

The cytotoxicity of iridium complexes against A2780 human ovarian cancer cells was performed by Dr. Ana M. Pizarro (Department of Chemistry, University of Warwick). The following sections outline the general cell experiments used in this thesis.

2.1.11.1.1 Materials and Maintenance

The A2780 human ovarian cancer cell line was obtained from the European Collection of Cell Cultures (ECACC, Salisbury, U.K.). The cells were maintained in RPMI 1640 medium, which was supplemented with 10% fetal calf serum, 1% glutamine and 1% penicillin/streptomycin. Experiments were performed with cells within 15 passages from each other. All cells were split two to three times a week when around 80–95% confluence was reached using 0.25% trypsin/EDTA.

2.1.11.1.2 *In Vitro* Growth Inhibition Assay

IC_{50} values (concentration at which 50% of the cell growth is inhibited) against A2780 human ovarian cancer cells were determined as part of this thesis.

Plates containing 8 rows × 12 columns, in total 96 wells with 300 μL capacity were used. The A2780 cancer cells were plated at a density of 5000 cells/well. All cells were grown for 48 h at 310 K in 5% humidified atmosphere, before addition of Ir^{III} complexes. Cisplatin (CDDP) was bought from Sigma and was included in every assay as control.

Stock solutions of the iridium complexes or CDDP were made up in 5% DMSO and saline, by initial dissolution in DMSO followed by dilution with saline. Sonication was sometimes used to facilitate complete dissolution. These stock solutions were diluted with medium to give final concentrations of 400 μM, 200 μM and 20 μM (0.5% DMSO final concentration). Aliquots of 50 μL of these solutions were added to the wells in the 96-well plate (triplicate) already containing

150 μL of media, so that the final concentrations were 100 μM, 50 μM and 5 μM (0.125% DMSO final concentration), respectively. These three concentrations were used in an initial screen for activity, and candidates were classified as either:

a) inactive <50% growth inhibition at 100 μM,

b) modest 80% to 50% growth inhibition at 50 μM,

c) potent >50% growth inhibition at 5 μM.

IC_{50} values were obtained by testing at typically six different concentrations, ranging from 0.05 μM to 100 μM. Each assay includes cisplatin which acts as a positive and comparative control as well as 16 wells free of drug solution, which acts as the 100% cell survival control. Each concentration of cisplatin or complex was tested in triplicate so that three compounds plus cisplatin could be tested per plate. Each assay was done in duplicate, so that each concentration was tested a total of six times.

After 24 h exposure (at 310 K in a 5% CO_2 humidified atmosphere), the drug containing medium was removed, the cells washed with 50 μL phosphate buffered saline (PBS) and 200 μL of fresh medium was added. The cells were left to grow for three doubling times (72 h) at 310 K in a 5% humidified atmosphere.

The remaining biomass after this time was determined using the sulforhodamine B (SRB) assay.[15] Cells were fixed to the 96-well plate by adding 50 μL 50% trichloroacetic acid (TCA) to each well (final concentration 10%) and incubating at 277 K for 1 h before washing five times with tap water. Plates were dried with the

assistance of a hairdryer until no standing moisture was visible. The TCA-fixed cells were stained by adding 50 μL of 0.4% (w/v) sulforhodamine B (SRB) dissolved in 1% acetic acid, and left to stand for 30 min at ambient temperature. The excess dye was removed with four quick rinses of 1% acetic acid and again dried with the assistance of a hairdryer until no standing moisture was visible. The cell-bound dye was solubilised by addition of 150 μL of 10 mM Tris base (tris(hydroxomethyl)aminoethane, pH 10.5) and plates were left standing at ambient temperature for 1 h to allow the solutions to become homogeneous. The optical density was then measured at 540 nm on a BioHit BP800 plate reader. IC_{50} values were obtained from plots of % cell survival against the Log of the drug concentration and fitted with a sigmoidal equation using ORIGIN 8.0.

2.1.11.2 NCI/DTP Cytotoxicity

Five iridium complexes studied in Chapters 3 and 4 were further evaluated by the National Cancer Institute Developmental Therapeutics Program (NCI/DTP, U.S.A.) for *in vitro* cytotoxic test against ca. 60 human cancer cell lines. The protocol for the determination of cytotoxicity on the 60 cell line panel can be found at http://dtp.nci.nih.gov/branches/btb/ivclsp.html. The DTP homepage can be accessed at http://dtp.cancer.gov/.

2.2 Synthesis and Characterisation of Starting Materials

The ligands tetramethyl(phenyl)cyclopentadiene ($Cp^{xph}H$) and tetramethyl(biphenyl)cyclopentadiene ($Cp^{xbiph}H$), and iridium dimers of the type $[(\eta^5\text{-}Cp^x)IrCl_2]_2$ (Cp^x = pentamethylcyclopentadienyl, Cp*; tetramethyl(phenyl)-cyclopentadienyl, Cp^{xph}; tetramethyl(biphenyl)cyclopentadienyl, Cp^{xbiph}), Figure 2.1, were synthesised and characterised, in which the ligand $Cp^{xph}H$[16] and the dimer $[(\eta^5\text{-}C_5Me_5)IrCl_2]_2$ (**1**),[17] were prepared according to literature methods.

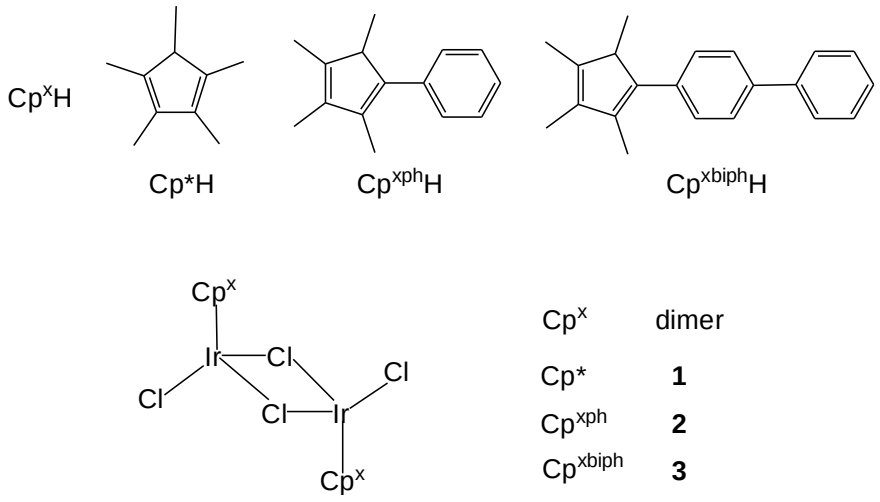

Figure 2.1. Cyclopentadiene ligands and iridium dimers studied in this work.

The derivative $Cp^{xbiph}H$, in which one of the methyls of Cp* is replaced by a biphenyl group, has not been previously reported. All the synthesised ligands and dimers were fully characterized by ^1H NMR spectroscopy and CHN elemental analysis.

2.2.1 Materials

$IrCl_3\ nH_2O$, 1,2,3,4,5-pentamethylcyclopentadiene (95%), butyllithium solution (1.6 M in hexane), 2,3,4,5-tetramethyl-2-cyclopentenone (95%), and lithium wire (99.9%), were purchased from Sigma-Aldrich.

2.2.2 Syntheses

$Cp^{xbiph}H$. A solution of 4-bromo-biphenyl (5.7 g, 24.5 mmol) in dry THF (100 mL) was treated with 1.6 M *n*-BuLi/hexane solution (15.3 mL, 24.5 mmol) at 195 K. After stirring at this temperature for 3 h, 2,3,4,5-tetramethyl-2-cyclopentenone (4.1 g, 29.4 mmol) was added. The reaction mixture was allowed to warm slowly to ambient temperature with stirring overnight. The resulting yellow solution was acidified with HCl (36%). The organic layer was separated and the aqueous layer was further extracted with diethyl ether (20 × 2 mL). The combined organic portions were dried over with anhydrous $MgSO_4$, filtered, and the solvents evaporated to dryness on a rotary evaporator to afford a light yellow powder. The product was recrystallised from chloroform and hexane (3:1). Yield: 2.7 g (40%). ^{1}H NMR ($CDCl_3$): δ = 7.64 (m, 4H), 7.44 (m, 2H), 7.33 (m, 3H), 3.25 (m, 1H), 2.08 (s, 3H), 1.95 (s, 3H), 1.88 (s, 3H), 1.00 (d, 3H, *J* = 7.5 Hz). Anal. Calcd for $C_{21}H_{22}$ (274.40): C, 91.92; H, 8.08. Found: C, 92.56; H, 7.93.

$[(\eta^5\text{-}C_5Me_4C_6H_5)IrCl_2]_2$ (2). A solution of $Cp^{xph}H$ (1.7 g, 8.5 mmol) and $IrCl_3\ nH_2O$ (1.7 g, 5.7 mmol) in MeOH (60 mL) was heated under reflux in an N_2

atmosphere for 48 h. The reaction mixture was allowed to cool to ambient temperature and the dark green precipitate was filtered off. The volume of the dark red filtrate was reduced to ca. 15 mL on a rotary evaporator. Upon cooling to ambient temperature, an orange precipitate appeared which was collected by filtration. The product was washed with methanol and diethyl ether and dried in air. Yield: 1.0 g (39%). ^{1}H NMR ($CDCl_3$): δ = 7.58 (m, 2H), 7.35 (m, 3H), 1.72 (s, 6H), 1.63 (s, 6H). Anal. Calcd for $C_{30}H_{34}Ir_2N$ (920.84): C, 39.13; H, 3.72. Found: C, 39.21; H, 3.66. Crystals suitable for X-ray diffraction were obtained by evaporation of a chloroform/hexane solution at ambient temperature.

[(η^5-$C_5Me_4C_6H_4C_6H_5$)$IrCl_2$]$_2$ (**3**). The synthesis was performed as for **2** using $Cp^{xbiph}H$ (2.7 g, 9.9 mmol) and $IrCl_3$ *n*H_2O (2.9 g, 9.9 mmol). Yield: 1.7 g (22%). ^{1}H NMR (DMSO-d_6): δ = 7.70 (m, 4H), 7.46 (m, 2H), 7.35 (m, 3H), 2.02 (s, 3H), 1.91 (s, 3H), 1.84 (s, 3H), 0.90 (s, 3H). Anal. Calcd for $C_{42}H_{42}Cl_4Ir_2$ (1073.03): C, 47.01; H, 3.95. Found: C, 47.34; H, 4.16.

2.2.3 X-ray Crystal Structure

The X-ray crystal structure of dimer [(η^5-$C_5Me_4C_6H_5$)$IrCl_2$]$_2$ (**2**) was determined. The atom numbering scheme is shown in Figure 2.2. Crystallographic data are shown in Table 2.1, and selected bond lengths and angles are listed in Table 2.2. X-ray crystallographic data for **2** have been deposited in the Cambridge Crystallographic Data Centre under the accession number CCDC 802289.

In the structure of the Cp^{xph} dimer **2**, the chlorides acts as a bridging ligand to a symmetry-related molecule across an inversion centre. The Ir−Ir bond distance is 3.7157(4) Å and the angle between mean planes through the phenyl and the cyclopentadienyl groups is 68.21 °. The phenyl group is involved in a weak π-π interaction with a symmetry-related phenyl group of a neighbouring ligand in the unit cell (Figure 2.3). The two interacting π systems are parallel, with a centroid−centroid distance of 3.956 Å. The bond distances and angles in $[(\eta^5\text{-}C_5Me_4C_6H_5)IrCl_2]_2$ (**2**) compare well to those found for the corresponding Cp* analogue $[(\eta^5\text{-}C_5Me_5)IrCl_2]_2$ (**1**).[18] The Ir–Cl(bridging)–Ir and Cl(bridging)–Ir–Cl(bridging) angles in **2** are 1.2 ° more acute and obtuse, respectively, than those of the Cp* analogue.

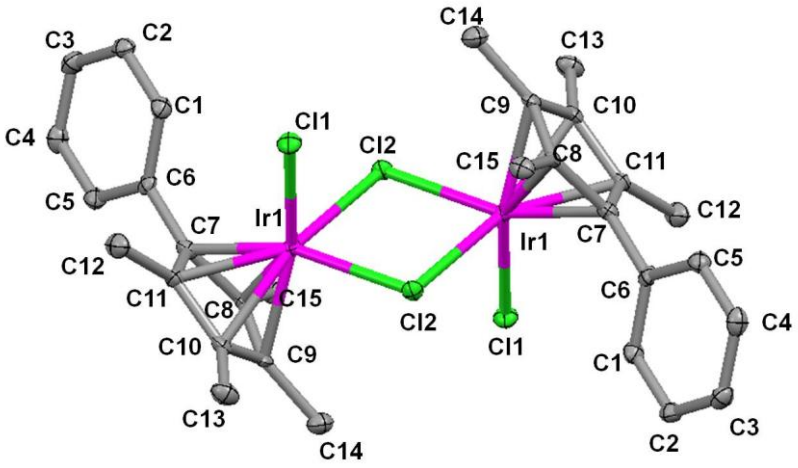

Figure 2.2. X-ray crystal structure with atom numbering scheme for [(η^5-$C_5Me_4C_6H_5$)$IrCl_2$]$_2$ (**2**), with thermal ellipsoids drawn at 50% probability. The hydrogen atoms have been omitted for clarity.

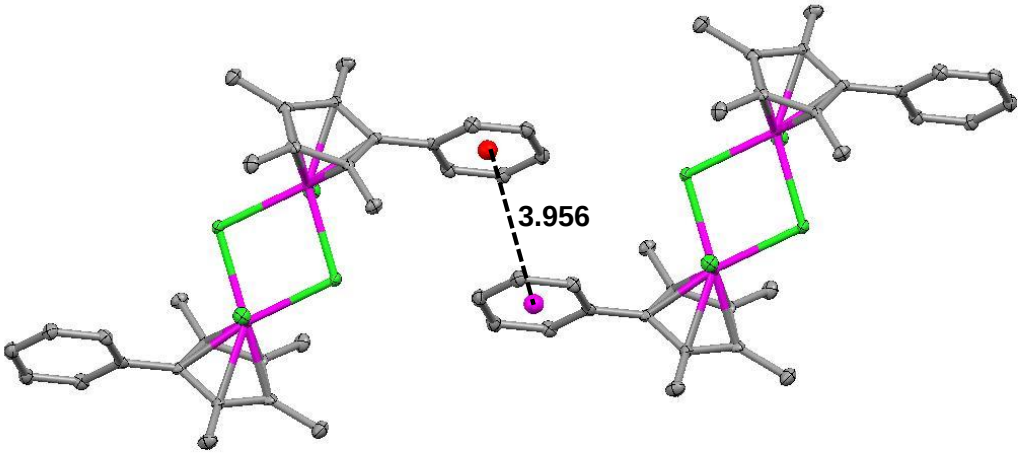

Figure 2.3. Diagram showing π-stacking between the phenyl rings of neighbouring molecules in the X-ray crystal structure of [(η^5-$C_5Me_4C_6H_5$)$IrCl_2$]$_2$ (**2**). The centroid–centroid distance between the phenyl rings of independent molecules is 3.956 Å. 50% ellipsoids. H atoms have been omitted for clarity.

Table 2.1. Crystallographic Data for the Dimer $[(\eta^5\text{-}C_5Me_4C_6H_5)IrCl_2]_2$ (**2**)

	2
formula	$C_{30}H_{34}Cl_{14}Ir_2$
MW	920.77
cryst colour	orange block
cryst size (mm)	0.20 × 0.20 × 0.06
λ (Å)	0.71073
temp(K)	100
cryst syst	monoclinic
space group	*P*2(1)/*c*
a (Å)	11.5964(5)
b (Å)	11.5025(3)
c (Å)	11.9780(5)
α (°)	90
β (°)	115.150(5)
γ (°)	90
vol(Å^3)	1446.24(9)
Z	2
R(*F*o^2)	0.0202
Rw(*F*o^2)	0.0402
GOF	0.940

Table 2.2. Selected Bond Lengths (Å) and Angles (deg) for the Dimer [(η^5-$C_5Me_4C_6H_5$)$IrCl_2$]$_2$ (**2**)

	2
Ir−C(Cp ring)	2.119(3)
	2.127(3)
	2.137(3)
	2.148(3)
	2.162(3)
Ir−C(centroid)	1.749
Ir−Cl(2)	2.4378(8)
Ir−Cl(2)	2.4411(8)
Ir−Cl(1)	2.3899(7)
Cl(2)−Ir− Cl(2)	80. 79(3)
Cl(1)−Ir−Cl(2)	86.79(3)
Cl(1)−Ir−Cl(2)	88.52(3)
Ir−Cl(2)−Ir	99.21(3)

2.3 References

(1) Claridge, T. D. W. In *High-Resolution NMR Techniques in Organic Chemistry*; Baldwin, J. E., Williams, R. M., Ed.; Pergamon: Oxford, 1999.

(2) Hore, P. J. *Nuclear Magnetic Resonance*; Oxford University Press Inc: New York, 2001.

(3) Lambert, J. B. S., H. F.; Lightner, D. A.; Cooks, R. G. *Organic Structural Spectroscopy*; Prentice-Hall, Inc: New Jersey, 1998.

(4) Hwang, T. L.; Shaka, A. J. *J. Magn. Reson.,Ser. A* **1995**, *112*, 275-279.

(5) Krezel, A.; Bal, W. *J. Inorg. Biochem.* **2004**, *98*, 161-166.

(6) *CrysAlis PRO*; Oxford Diffraction Ltd.: Abington, Oxfordshire, U. K., 2007.

(7) Sheldrick, G. M. *Acta Crystallogr.* **1990**, *A46*, 467-473.

(8) Sheldrick, G. M. *SHELXL-97*; University of Göttingen: Göttingen, Germany, 1997.

(9) Skoog, D. A.; Holler, F. J.; Crouch, S. R. *Principles of Instrumental Analysis*; 6 ed.; Brooks Cole: California, USA, 2006.

(10) Harvey, D. *Modern analytical chemistry*; McGraw-Hill: Boston, 2000.

(11) Frisch, M. J.; Trucks, G. W.; Schlegel, H. B.; Scuseria, G. E.; Robb, M. A.; Cheeseman, J. R.; Montgomery, J. A., Jr.; Vreven, T.; Kudin, K. N.; Burant, J. C.; Millam, J. M.; Iyengar, S. S.; Tomasi, J.; Barone, V.; Mennucci, B.; Cossi, M.;

Scalmani, G.; Rega, N.; Petersson, G. A.; Nakatsuji, H.; Hada, M.; Ehara, M.; Toyota, K.; Fukuda, R.; Hasegawa, J.; Ishida, M.; Nakajima, T.; Honda, Y.; Kitao, O.; Nakai, H.; Klene, M.; Li, X.; Knox, J. E.; Hratchian, H. P.; Cross, J. B.; Adamo, C.; Jaramillo, J.; Gomperts, R.; Stratmann, R. E.; Yazyev, O.; Austin, A. J.; Cammi, R.; Pomelli, C.; Ochterski, J.; Ayala, P. Y.; Morokuma, K.; Voth, G. A.; Salvador, P.; Dannenberg, J. J.; Zakrzewski, V. G.; Dapprich, S.; Daniels, A. D.; Strain, M. C.; Farkas, O.; Malick, D. K.; Rabuck, A. D.; Raghavachari, K.; Foresman, J. B.; Ortiz, J. V.; Cui, Q.; Baboul, A. G.; Clifford, S.; Cioslowski, J.; Stefanov, B. B.; Liu, G.; Liashenko, A.; Piskorz, P.; Komaromi, I.; Martin, R. L.; Fox, D. J.; Keith, T.; Al-Laham, M. A.; Peng, C. Y.; Nanayakkara, A.; Challacombe, M.; Gill, P. M. W.; Johnson, B.; Chen, W.; Wong, M. W.; Gonzalez, C.; Pople, J. A. *Gaussian 03*, revision D.01; Gaussian, Inc.: Wallingford, CT, USA, 2003.

(12) Adamo, C.; Barone, V. *J. Chem. Phys.* **1999**, *110*, 6158-6170.

(13) Hay, P. J.; Wadt, W. R. *J. Chem. Phys.* **1985**, *82*, 270-283.

(14) McLean, A. D.; Chandler, G. S. *J. Chem. Phys.* **1980**, *72*, 5639-5648.

(15) Skehan, P.; Storeng, R.; Scudiero, D.; Monks, A.; McMahon, J.; Vistica, D.; Warren, J. T.; Bokesch, H.; Kenney, S.; Boyd, M. R. *J. Natl. Cancer Inst.* **1990**, *82*, 1107-1112.

(16) Björgvinsson, M.; Halldorsson, S.; Arnason, I.; Magull, J.; Fenske, D. *J. Organomet. Chem.* **1997**, *544*, 207-215.

(17) White, C. Y., A.; Maitlis, P. M. *Inorg. Chem.* **1992**, *29*, 228-234.

(18) Churchill, M. R.; Julis, S. A. *Inorg. Chem.* **1977**, *16*, 1488-1494.

Chapter 3

Cyclopentadienyl Iridium Complexes Containing N,N- or N,O-Chelating Ligands

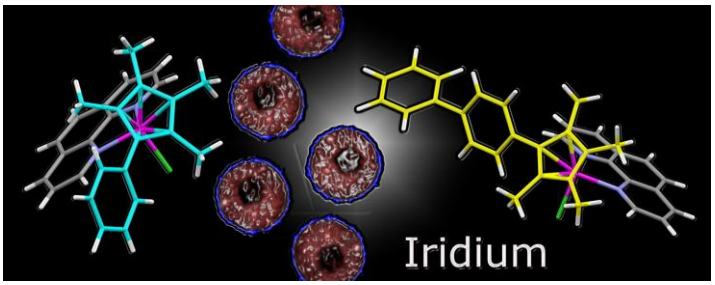

3.1 Introduction

The clinical success of cisplatin, carboplatin and oxaliplatin[1,2] has stimulated the search for other transition metal complexes which possess anticancer activity. New metal-based anticancer drugs may be able to widen the spectrum of treatable cancers, reduce toxic side-effects, and overcome platinum resistance. Interest in bio-organometallic chemistry and the design of organometallic complexes as anticancer agents is currently increasing.[3-8] Carbon-bound arenes and cyclopentadienyl ligands can provide control of the hydrophilicity and hydrophobicity of the faces of the coordination complex (which influences cell uptake and targeting).[9-11] Most metallodrugs are prodrugs and control over ligand substitution is vital if the complex is to reach and react with its target site. In this respect octahedral low-spin d^6 complexes are attractive for drug design since they are often kinetically inert. Inertness increases from 1st to 2nd to 3rd row of transition metals.[12,13] The lifetime for exchange of an aqua ligand on $[Ir(H_2O)_6]^{3+}$, for example, is about 300 years![14,15] There are only a limited number of reported studies on the biological activity of iridium complexes. Early studies were concerned with non-organometallic Ir^{I} and Ir^{III} complexes,[16-20] and more recently a few studies of organometallic Ir^{III} complexes have been reported.[21-31] Iridium(III) complexes are generally thought to be too inert to possess high reactivity. Indeed, the inertness of Ir^{III} has allowed the design of complexes which function as rigid scaffolds and inhibit kinase enzymes, for example.[32] The biological inactivity of *trans*-$[IrCl_4(DMSO)(Im)][ImH]$[33] and *trans*-$[IrCl_4(Im)_2][ImH]$ (ImH = imidazole),[34] Ir^{III} analogs of the Ru^{III} anticancer drugs NAMI-A and the imidazole analogue of the

indazole complex KP1019, respectively, has been attributed to the kinetic inertness of Ir^{III}.

Organometallic Ru^{II} and Os^{II} arene anticancer complexes of the type $[(\eta^6$-arene)(Ru/Os)(NN)Cl$]^+$, where NN is a chelating diamine ligand, can be activated by hydrolysis of the Ru/Os–Cl bond, followed by binding to DNA.[35,36] The arene is important in determining the anticancer activity and nature of the DNA distortions. In particular when the arene has an extended ring system (e.g. biphenyl or tetrahydroanthracene) direct binding to DNA bases (largely guanine) can be accompanied by arene intercalation between the bases.[37,38]

Neutral arene ligands do not stabilise Ir^{III}. In contrast, negatively-charged pentamethylcyclopentadienyl (Cp*) is an excellent stabilising ligand for Ir^{III}. In this Chapter the design concepts discovered for Ru^{II} and Os^{II} arene complexes was applied to Ir^{III} Cp* and functionalized Cp* complexes $[(\eta^5$-$Cp^x)Ir(XY)Cl]^{0/+}$ containing N,N- or N,O-bound chelating ligands. Iridium(III) Cp* complexes have attracted recent attention as catalysts, for example in hydrogen transfer reactions.[39] Only a few iridium complexes containing functionalized Cp* ligands have been reported previously.[40-43] The effect of Cp* functionalization on the rate of hydrolysis, acidity of the aqua adducts, interactions with nucleobases, hydrophobicity (octanol/water partition), cell accumulation (the net effect of uptake and efflux) and distribution, interaction with DNA, and cytotoxicity to cancer cells have been studied in this Chapter. It is found that such complexes can be thermodynamically stable and yet kinetically labile towards substitution reactions and that substituents on the cyclopentadienyl ring and chelating ligand can have a

dramatic effect on chemical and biological activity. This appears to be the first time that tetramethyl(phenyl)cyclopentadienyl (Cp^{xph}) and tetramethyl(biphenyl)cyclopentadienyl (Cp^{xbiph}) have been used as ligands in iridium complexes.

3.2 Experimental Section

3.2.1 Materials

9-Ethylguanine (9-EtG), 9-ethyladenine (9-EtA), 1,10-phenanthroline monohydrate (phen), 2,2′-bipyridine (bpy), ethylenediamine (en), 2-picolinic acid (pico), octan-1-ol (≥99%), 1,10-phenanthroline-5-amine (phen-5-amine), 2,2′-bipyridine-3,3′-diol ($bpy(OH)_2$), 4,4′-dimethyl-2,2′-bipyridine ($bpy\text{-}Me_2$), 4-(2-pyridylazo)-*N*,*N*-dimethylaniline ($azpy\text{-}NMe_2$), ammonium hexafluorophosphate and NaCl (>99.999%, used in the log *P* experiment) were purchased from Sigma-Aldrich. Cisplatin and transplatin were obtained from Sigma (Prague, Czech Republic). Ligand *p*-dimethylaminophenyliminopyridine ($impy\text{-}NMe_2$) was kindly provided by Ying Fu in our group. [Pt(dien)Cl]Cl (dien = diethylenetriamine) was a kind gift of Prof. Giovanni Natile (University of Bari, Italy). Ethylenediamine was distilled over sodium prior to use. Methanol was distilled over magnesium/iodine prior to use. The syntheses of dimer $[(\eta^5\text{-}C_5Me_4C_6H_5)IrCl_2]_2$ (**2**) and $[(\eta^5\text{-}C_5Me_4C_6H_4C_6H_5)IrCl_2]_2$ (**3**) is described in Chapter 2. Dimer $[(\eta^5\text{-}C_5Me_5)IrCl_2]_2$ (**1**),[44] ligands dipyrido[3,2-f:2′,3′-h]quinoxaline (dpq) and dipyrido[3,2-a:2′,3′-c]phenazine (dppz),[45,46] and complexes $[(\eta^5\text{-}C_5Me_5)Ir(phen)Cl]Cl$ (**4**·Cl),[47] $[(\eta^5\text{-}$

C_5Me_5)Ir(bpy)Cl]Cl (**7**·Cl),[47] and [(η^5-C_5Me_5)Ir(pico)Cl] (**12**),[48] were prepared according to literature methods.

3.2.2 Syntheses

[(η^5-$C_5Me_4C_6H_5$)Ir(phen)Cl]PF_6 (5·PF_6). A solution of [(η^5-$C_5Me_4C_6H_5$)$IrCl_2$]$_2$ (45 mg, 0.05 mmol), 1,10-phenanthroline monohydrate (24.3 mg, 0.12 mmol) in MeOH (40 mL) was heated under reflux in an N_2 atmosphere for 10 h and filtered. The volume was slowly reduced to half on a rotary evaporator and NH_4PF_6 (45 mg, 0.28 mmol) was added. After standing at 277 K, a microcrystalline product formed. This was collected by filtration, washed with diethyl ether, and recrystallised from methanol/diethyl ether. Yield: 27 mg (37%). ^{1}H NMR (DMSO-d_6): δ = 9.08 (d, 2H, *J* = 5.3 Hz), 8.99 (d, 2H, *J* = 8.5 Hz), 8.39 (s, 2H), 8.19 (dd, 2H, *J* = 5.3, 5.5 Hz), 7.56 (m, 5H), 1.84 (s, 6H), 1.73 (s, 6H). Anal. Calcd for $C_{27}H_{25}ClF_6IrN_2P$ (750.16): C, 43.23; H, 3.36; N, 3.73. Found: C, 43.01; H, 3.31; N, 3.86. Crystals suitable for X-ray diffraction were obtained by slow evaporation of a methanol/diethyl ether solution at ambient temperature.

[(η^5-$C_5Me_4C_6H_4C_6H_5$)Ir(phen)Cl]PF_6 (6·PF_6). The synthesis was performed as for **5**·PF_6 using [(η^5-$C_5Me_4C_6H_4C_6H_5$)$IrCl_2$]$_2$ (50 mg, 0.05 mmol) and 1,10-phenanthroline monohydrate (24.3 mg, 0.12 mmol). Yield: 15 mg (23%). ^{1}H NMR ($CDCl_3$): δ = 9.16 (d, 2H, *J* = 5.5 Hz), 8.78 (d, 2H, *J* = 8.3 Hz), 8.22 (s, 2H), 8.17 (dd, 2H, *J* = 5.3, 5.5 Hz), 7.76 (d, 2H, *J* = 8.3 Hz), 7.60 (d, 2H, *J* = 7.5 Hz), 7.45 (d,

2H, *J* = 8.3 Hz), 7.52 (t, 2H, *J* = 7.3 Hz), 7.44 (t, 1H, *J* = 7.3 Hz), 2.05 (s, 6H), 1.85 (s, 6H). Anal. Calcd for $C_{33}H_{29}Cl_2F_6IrN_2P$ (826.23): C, 47.97; H, 3.54; N, 3.39. Found: C, 47.61; H, 3.63; N, 3.52.

[(η^5-$C_5Me_4C_6H_5$)Ir(bpy)Cl]PF_6 (8·PF_6). A solution of [(η^5-$C_5Me_4C_6H_5$)$IrCl_2$]$_2$ (**2**) (45 mg, 0.05 mmol), 2,2′-bipyridine (18.7 mg, 0.12 mmol) in MeOH (40 mL) was heated under reflux in an N_2 atmosphere for 16 h and filtered. The volume was slowly reduced to half on a rotary evaporator and NH_4PF_6 (45 mg, 0.28 mmol) was added. After standing at 277 K, the mixture formed a microcrystalline product. This was collected by filtration, washed with diethyl ether, and recrystallised from methanol/diethyl ether. Yield: 57 mg (73%). ^{1}H NMR (DMSO-d_6): δ = 8.84 (d, 2H, *J* = 8.2 Hz), 8.71 (d, 2H, *J* = 5.4 Hz), 8.35 (t, 2H, *J* = 7.5 Hz), 7.81 (t, 2H, *J* = 7.5 Hz), 7.50 (m, 5H), 1.77 (s, 6H), 1.67 (s, 6H). Anal. Calcd for $C_{25}H_{25}ClN_2IrPF_6$ (726.10): C, 41.35; H, 3.47; N, 3.86. Found: C, 40.85; H, 3.35; N, 3.83. Crystals suitable for X-ray diffraction were obtained by slow evaporation of a methanol/diethyl ether solution at ambient temperature.

[(η^5-$C_5Me_4C_6H_4C_6H_5$)Ir(bpy)Cl]PF_6 (9·PF_6). The synthesis was performed as for **8**·PF_6 using [(η^5-$C_5Me_4C_6H_4C_6H_5$)$IrCl_2$]$_2$ (**3**) (50 mg, 0.05 mmol) and 2,2′-bipyridine (18.7 mg, 0.12 mmol). Yield: 43 mg (58%). ^{1}H NMR (DMSO-d_6): δ = 8.81 (d, 2H, *J* = 8.0 Hz), 8.74 (d, 2H, *J* = 6.0 Hz), 8.35 (t, 2H, *J* = 7.8 Hz), 7.82 (overlapped m, 4H), 7.75 (d, 2H, *J* = 8.0 Hz), 7.60 (d, 2H, *J* = 8.0 Hz), 7.50 (t, 2H, *J*

= 7.8 Hz), 7.42 (t, 1H, *J* = 7.3 Hz), 1.78 (s, 6H), 1.72 (s, 6H). Anal. Calcd for $C_{31}H_{29}ClF_6IrN_2P$ (802.21): C, 46.41; H, 3.64; N, 3.49. Found: C, 45.85; H, 3.55; N, 3.63. Crystals suitable for X-ray diffraction were obtained by slow evaporation of a methanol/diethyl ether solution at ambient temperature.

[(η^5-C_5Me_5)Ir(en)Cl]PF_6 (10·PF_6). [(η^5-C_5Me_5)$IrCl_2$]$_2$ (50 mg, 0.06 mmol) was suspended in dry methanol (15 mL), and ethylenediamine (9.0 mg, 0.15 mmol) was added in one portion. The mixture was stirred for 1 h at ambient temperature and filtered. The volume of solvent was slowly reduced to half on a rotary evaporator and NH_4PF_6 (102.2 mg, 0.63 mmol) was added. After standing at 277 K, a microcrystalline product was formed. This was collected by filtration, washed with diethyl ether, and recrystallised from methanol/diethyl ether. Yield: 39.9 mg (56%). ^{1}H NMR (DMSO-d_6): δ = 5.70 (b, 2H), 4.86 (b, 2H), 2.54 (b, 2H), 2.28 (b, 2H), 1.68 (s, 15H). Anal. Calcd for $C_{12}H_{23}ClF_6IrN_2P$ (568.08): C, 25.38; H, 4.08; N, 4.93. Found: C, 25.07; H, 3.89; N, 4.99.

[(η^5-$C_5Me_4C_6H_5$)Ir(en)Cl]BPh_4 (11·BPh_4). The synthesis was performed as for **10**·PF_6, using [(η^5-$C_5Me_4C_6H_5$)$IrCl_2$]$_2$ (45 mg, 0.05 mmol), ethylenediamine (9.0 mg, 0.15 mmol), and NH_4BPh_4 (102.3 mg, 0.30 mmol). Yield: 19.9 mg (23%). ^{1}H NMR (DMSO-d_6): δ = 7.38 (m, 2H), 7.33 (m, 3H), 7.24 (b, 8H), 6.89 (t, 8H, *J* = 7.3 Hz), 6.75 (t, 4H, *J* = 7.3 Hz), 5.75 (b, 2H), 4.64 (b, 2H), 2.64 (b, 2H), 2.35 (b, 2H), 1.77 (s, 6H), 1.65 (s, 6H). Anal. Calcd for $C_{41}H_{45}BClIrN_2$ (804.29): C, 61.65; H,

5.74; N, 3.44. Found: C, 61.76; H, 5.89; N, 3.39. Crystals suitable for X-ray diffraction were obtained by slow evaporation of a methanol/diethyl ether solution at ambient temperature.

[(η^5-$C_5Me_4C_6H_5$)Ir(pico)Cl] (13). A solution of [(η^5-$C_5Me_4C_6H_5$)$IrCl_2$]$_2$ (45 mg, 0.05 mmol), 2-picolinic acid (16.7 mg, 0.13 mmol) and sodium methoxide (7.3 mg, 0.13 mmol) in MeOH (50 mL) was refluxed under N_2 atmosphere for 3 h and filtered. The solvent was removed in vacuo, the product extracted with CH_2Cl_2 (10 mL), and the volume was reduced to ca. 0.5 mL on a rotary evaporator. A yellow precipitate formed at 253 K on addition of diethyl ether and was collected by filtration, washed with diethyl ether, and dried in air. Yield: 25.4 mg (43%). ^{1}H NMR (DMSO-d_6): δ = 8.65 (d, 1H, *J* = 4.5 Hz), 8.15 (t, 1H, *J* = 8.3 Hz), 7.93 (d, 1H, *J* = 7.8 Hz), 7.81 (t, 1H, *J* = 7.0 Hz), 7.52 (m, 5H), 1.74 (s, 6H), 1.64 (s, 6H). Anal. Calcd for $C_{21}H_{21}ClIrNO_2$ (547.09): C, 46.10; H, 3.87; N, 2.56. Found: C, 45.89; H, 3.65; N, 2.73. Crystals suitable for X-ray diffraction were obtained by slow evaporation of a methanol/diethyl ether solution at ambient temperature.

[(η^5-$C_5Me_4C_6H_4C_6H_5$)Ir(pico)Cl] (14). The synthesis was performed as for **13** using [(η^5-$C_5Me_4C_6H_4C_6H_5$)$IrCl_2$]$_2$ (50 mg, 0.05 mmol), picolinic acid (12.3 mg, 0.10 mmol) and sodium methoxide (5.4 mg, 0.10 mmol). Yield: 22 mg (37%). ^{1}H NMR (DMSO-d_6): δ = 8.70 (d, 1H, *J* = 5.7 Hz), 8.16 (t, 1H, *J* = 7.8 Hz), 7.97 (d, 1H, *J* = 8.0 Hz), 7.77 (t, 1H, *J* = 6.5 Hz), 7.72 (m, 4H), 7.64 (d, 2H, *J* = 8.3 Hz), 7.48 (t,

2H, *J* = 7.3 Hz), 7.39 (t, 1H, *J* = 7.3 Hz), 1.74 (d, 6H, *J* = 7.3 Hz), 1.69 (s, 3H), 1.65 (s, 3H). Anal. Calcd for $C_{27}H_{25}ClIrNO_2$ (623.16): C, 52.04; H, 4.04; N, 2.25. Found: C, 52.09; H, 4.15; N, 2.33.

[(η^5-C_5Me_5)Ir(phen-5-amine)Cl]PF_6 (15·PF_6). To a suspension of [(η^5-C_5Me_5)$IrCl_2$]$_2$ (50 mg, 0.06 mmol) in dry, freshly distilled methanol (25 ml), 1,10-phenanthroline-5-amine, (25.4 mg, 0.13 mmol) was added. The reaction mixture was stirred at ambient temperature overnight. The volume was slowly reduced to half on a rotary evaporator and NH_4PF_6 (45 mg, 0.28 mmol) was added. After standing at 277 K, the mixture formed a microcrystalline product. This was collected by filtration, washed with diethyl ether, and recrystallised from acetone/pertroleum ether. Yield: 55.9 mg (71.0%). ^{1}H NMR (DMSO-d_6): δ = 9.33 (d, 1H, *J* = 5.0 Hz), 8.96 (d, 1H, *J* = 8.5 Hz), 8.92 (d, 1H, *J* = 7.5 Hz), 8.33 (d, 1H, *J* = 8.5 Hz), 8.06 (dd, 1H, *J* = 5.3 Hz), 7.82 (dd, 1H, *J* = 5.0 Hz), 7.12 (s, 1H), 1.68 (s, 15H). Anal. Calcd for $C_{22}H_{24}ClF_6IrN_3P$ (703.09): C, 37.58; H, 3.44; N, 5.98. Found: C, 37.23; H, 3.50; N, 5.73.

[(η^5-C_5Me_5)Ir(bpy(Me)$_2$)Cl]PF_6 (16·PF_6). The synthesis was performed as for **5**·PF_6 using [(η^5-C_5Me_5)$IrCl_2$]$_2$ (50 mg, 0.06 mmol), 4,4′-dimethyl-2,2′-bipyridine (24.0 mg, 0.13 mmol). Yield: 58 mg (67%). ^{1}H NMR (DMSO-d_6): δ = 8. 82 (d, 2H, *J* = 5.7 Hz), 8.68 (s, 2H), 7.68 (d, 2H, *J* = 5.7 Hz), 2.62 (s, 6H), 1.64 (s, 15H). Anal.

Calcd for $C_{22}H_{27}ClN_2IrPF_6$ (688.20): C, 38.18; H, 3.93; N, 4.05. Found: C, 38.24; H, 3.95; N, 3.98.

[(η^5-$C_5Me_4C_6H_5$)Ir(bpy(Me)$_2$)Cl]PF_6 (17·PF_6). The synthesis was performed as for **5**·PF_6 using [(η^5-$C_5Me_4C_6H_5$)$IrCl_2$]$_2$ (45 mg, 0.05 mmol), 4,4′-dimethyl-2,2′-bipyridine (20.2 mg, 0.11 mmol). Yield: 45.2 mg (60%). ^{1}H NMR (DMSO-d_6): δ = 8.66 (s, 2H), 8.51 (d, 2H, J = 5.7 Hz), 7.62 (d, 2H, J = 5.7 Hz), 7.46 (m, 5H), 2.60 (s, 6H), 1.76 (s, 6H), 1.66 (s, 6H). Anal. Calcd for $C_{27}H_{29}ClN_2IrPF_6$ (754.17): C, 43.00; H, 3.88; N, 3.71. Found: C, 43.21; H, 3.95; N, 3.68. Crystals suitable for X-ray diffraction were obtained by slow evaporation of a methanol/diethyl ether solution at ambient temperature.

[(η^5-$C_5Me_4C_6H_4C_6H_5$)Ir(bpy(Me)$_2$)Cl]PF_6 (18·PF_6). The synthesis was performed as for **5**·PF_6 using [(η^5-$C_5Me_4C_6H_4C_6H_5$)$IrCl_2$]$_2$ (50 mg, 0.05 mmol), 4,4′-dimethyl-2,2′-bipyridine (18.4 mg, 0.10 mmol). Yield: 39 mg (51%). ^{1}H NMR (DMSO-d_6): δ = 8.67 (s, 2H), 8.31 (d, 2H, J = 6.0 Hz), 7.79 (d, 2H, J = 8.5 Hz), 7.75 (d, 2H, J = 6.5 Hz), 7.65 (d, 2H, J = 5.7 Hz), 7.57 (d, 2H, J = 8.3 Hz), 7.50 (t, 2H, J = 7.8 Hz), 7.42 (t, 1H, J = 7.6 Hz), 2.60 (s, 6H), 1.77 (s, 6H), 1.71 (s, 6H). Anal. Calcd for $C_{33}H_{33}ClN_2IrPF_6$ (830.26): C, 47.74; H, 4.01; N, 3.37. Found: C, 47.26; H, 4.03; N, 3.43.

[(η^5-C_5Me_5)Ir(bpy(OH)O)Cl] (19). To a suspension of [(η^5-C_5Me_5)$IrCl_2$]$_2$ (50 mg, 0.06 mmol) in dry, freshly distilled methanol (25 ml), 2,2′-bipyridine-3,3′-diol (24.5 mg, 0.13 mmol) was added. The reaction mixture was stirred at ambient temperature overnight, filtered and the volume was reduced until the onset of precipitation. It was kept at 277 K for 24 h to allow further precipitation to occur. The fine yellow solid was collected by filtration, washed with methanol followed by ether, and dried in vacuum. It was recrystallised from methanol/ether. Yield: 33.6 mg (51.0%). ^{1}H NMR (DMSO-d_6): δ = 8.06 (d, 2H, J = 5.3 Hz), 7.28 (dd, 2H, J = 8.3 Hz), 7.06 (d, 2H, J = 8.3 Hz), 1.54 (s, 15H). Anal. Calcd for $C_{20}H_{22}ClN_2O_2Ir$ (550.07): C, 43.67; H, 4.03; N, 5.09. Found: C, 42.99; H, 4.15; N, 5.33. Crystals suitable for X-ray diffraction were obtained by slow evaporation of a methanol/diethyl ether solution at ambient temperature.

[(η^5-$C_5Me_4C_6H_5$)Ir(bpy(OH)O)Cl] (20). The synthesis was performed as for **19** using [(η^5-$C_5Me_4C_6H_5$)$IrCl_2$]$_2$ (45 mg, 0.05 mmol), 2,2′-bipyridine-3,3′-diol (18.8 mg, 0.10 mmol). Yield: 34 mg (55%). ^{1}H NMR ($CDCl_3$): δ = 7.81 (d, 2H, J = 5.5 Hz), 7.46 (m, 5H), 7.15 (d, 2H, J = 8.5 Hz), 6.99 (dd, 2H, J = 8.5 Hz), 1.64 (s, 12H). Anal. Calcd for $C_{25}H_{24}ClN_2O_2Ir$ (612.12): C, 49.05; H, 3.95; N, 4.58. Found: C, 48.77; H, 4.03; N, 4.43.

[(η^5-$C_5Me_4C_6H_4C_6H_5$)Ir(bpy(OH)O)Cl] (21). The synthesis was performed as for **19** using [(η^5-$C_5Me_4C_6H_4C_6H_5$)$IrCl_2$]$_2$ (50 mg, 0.05 mmol), 2,2′-bipyridine- 3,3′-

diol (18.8 mg, 0.10 mmol). Yield: 30.7 mg (47%). ^{1}H NMR (MeOD-d_4): δ = 8.08 (d, 2H, J = 7.3 Hz), 7.73 (d, 2H, J = 7.3 Hz), 7.68 (d, 2H, J = 7.9 Hz), 7.59 (d, 2H, J = 7.9 Hz), 7.47 (t, 2H, J = 7.3 Hz), 7.41 (t, 1H, J = 7.9 Hz), 7.20 (m, 4H), 1.73 (s, 6H), 1.69 (s, 6H). Anal. Calcd for $C_{31}H_{29}ClN_2O_2Ir$ (688.20): C, 54.1; H, 4.1; N, 4.07. Found: C, 53.99; H, 4.25; N, 3.98. Crystals suitable for X-ray diffraction were obtained by slow evaporation of a methanol/diethyl ether solution at ambient temperature.

[(η^5-$C_5Me_4C_6H_5$)Ir(dpq)Cl]PF_6 (22·PF_6). A solution of [(η^5-$C_5Me_4C_6H_5$)$IrCl_2$]$_2$ (45 mg, 0.05 mmol) and ligand dipyrido[3,2-f:2′,3′-h]quinoxaline (dpq, 23 mg, 0.10 mmol) in MeOH (40 mL) was refluxed under N_2 atmosphere for 2 h and filtered. The volume was slowly reduced to half on a rotary evaporator and NH_4PF_6 (45 mg, 0.28 mmol) was added. After standing at 277 K, a microcrystalline product formed. This was collected by filtration, washed with diethyl ether, and recrystallised from methanol/diethyl ether. Yield: 44 mg (55%). ^{1}H NMR($CDCl_3$): δ = 9.68 (d, 2H, J = 8.5 Hz), 9.13 (s, 2H), 8.96 (d, 2H, J = 6.0 Hz), 8.06 (dd, 2H, J = 8.0 Hz), 7.72 (m, 2H), 7.59 (m, 3H), 1.91 (s, 6H), 1.83 (s, 6H). Anal. Calcd for $C_{29}H_{25}ClF_6IrN_4P$ (802.10): C, 43.42; H, 3.14; N, 6.98. Found: C, 43.21; H, 3.21; N, 6.86.

[(η^5-$C_5Me_4C_6H_5$)Ir(dppz)Cl]Cl (23·Cl). A solution of [(η^5-$C_5Me_4C_6H_5$)$IrCl_2$]$_2$ (45 mg, 0.05 mmol) and ligand dipyrido[3,2-a:2′,3′-c]phenazine (dppz, 28 mg, 0.10 mmol) in MeOH (40 mL) was refluxed under N_2 atmosphere for 2 h and filtered.

The volume was slowly reduced to 2 mL on a rotary evaporator. After standing at 277 K, a microcrystalline product formed. This was collected by filtration, washed with diethyl ether, and recrystallised from methanol/diethyl ether. Yield: 45 mg (60%). ^{1}H NMR(DMSO-d_6): δ = 9.79 (d, 2H, *J* = 8.3 Hz), 9.15 (d, 2H, *J* = 6.0 Hz), 8.52 (dd, 2H, *J* = 6.3 Hz), 8.31 (dd, 2H, *J* = 7.8 Hz), 8.21 (dd, 2H, *J* = 6.5 Hz), 7.54 (m, 2H), 7.51 (m, 3H), 1.87 (s, 6H), 1.76 (s, 6H). Anal. Calcd for $C_{33}H_{27}Cl_2IrN_4$ (742.12): C, 53.37; H, 3.66; N, 7.54. Found: C, 53.14; H, 3.61; N, 7.60.

[(η^5-$C_5Me_4C_6H_4C_6H_5$)Ir(dpq)Cl]Cl (24·Cl**).** The synthesis was performed as for **23** using [(η^5-$C_5Me_4C_6H_4C_6H_5$)$IrCl_2$]$_2$ (50 mg, 0.05 mmol) and ligand dipyrido[3,2-f:2′,3′-h]quinoxaline (dpq, 23 mg, 0.10 mmol). Yield: 33 mg (43%). ^{1}H NMR(MeOD-d_4): δ = 9.82 (d, 2H, *J* = 8.3 Hz), 9.30 (s, 2H), 9.24 (d, 2H, *J* = 6.0 Hz), 8.28 (dd, 2H, *J* = 8.0 Hz), 7.83 (m, 2H), 7.76 (m, 4H), 7.52 (t, 2H, *J* = 7.3 Hz), 7.44 (t, 1H, *J* = 7.3 Hz), 1.97 (s, 6H), 1.90 (s, 6H). Anal. Calcd for $C_{35}H_{29}Cl_2IrN_4$ (768.14): C, 54.68; H, 3.80; N, 7.29. Found: C, 54.29; H, 3.71; N, 7.34.

[(η^5-$C_5Me_4C_6H_4C_6H_5$)Ir(dppz)Cl]Cl (25·Cl**).** The synthesis was performed as for **23** using [(η^5-$C_5Me_4C_6H_4C_6H_5$)$IrCl_2$]$_2$ (50 mg, 0.05 mmol) and ligand dipyrido[3,2-a:2′,3′-c]phenazine (dppz, 28 mg, 0.10 mmol). Yield: 37 mg (45%). ^{1}H NMR(MeOD-d_4): δ = 9. 90 (d, 2H, *J* = 8.3 Hz), 9.19 (d, 2H, *J* = 6.0 Hz), 8.50 (dd, 2H, *J* = 6.3 Hz), 8.26 (dd, 2H, *J* = 7.6 Hz), 8.15 (dd, 2H, *J* = 6.7 Hz), 7.81 (m, 2H), 7.77 (m, 4H), 7.50 (t, 2H, *J* = 7.6 Hz), 7.41 (t, 1H, *J* = 7.6 Hz), 1.95 (s, 6H), 1.89 (s,

6H). Anal. Calcd for $C_{39}H_{21}Cl_2IrN_4$ (818.16): C, 57.21; H, 3.82; N, 6.84. Found: C, 56.86; H, 3.69; N, 6.76.

[(η^5-C_5Me_5)Ir(azpy-NMe_2)Cl]PF_6 (26·PF_6). A solution of [(η^5-C_5Me_5)$IrCl_2$]$_2$ (50 mg, 0.06 mmol), and ligand 4-(2-pyridylazo)-N,N-dimethylaniline (azpy-NMe_2, 27 mg, 0.12 mmol) in MeOH (20 mL) was stirred for 12 h at ambient temperature. The volume was slowly reduced to half on a rotary evaporator and NH_4PF_6 (45 mg, 0.28 mmol) was added. After standing at 277 K, a microcrystalline product formed. This was collected by filtration, washed with diethyl ether, and recrystallised from methanol/diethyl ether. Yield: 68 mg (77%). ^{1}H NMR (DMSO-d_6): δ = 8.82 (d, 1H, *J* = 6.0 Hz), 8.51 (d, 1H, *J* = 8.5 Hz), 8.28 (t, 1H, *J* = 7.0 Hz), 8.02 (m, 2H), 7.76 (t, 1H, *J* = 6.7 Hz), 7.02 (m, 2H), 3.31 (s, 6H), 1.55 (s, 15H). Anal. Calcd for $C_{23}H_{29}ClF_6IrN_4P$ (734.14): C, 37.63; H, 3.98; N, 7.63. Found: C, 37.41; H, 4.01; N, 7.76.

[(η^5-$C_5Me_4C_6H_5$)Ir(azpy-NMe_2)Cl]PF_6 (27·PF_6). The synthesis was performed as for **26**·PF_6 using [(η^5-$C_5Me_4C_6H_5$)$IrCl_2$]$_2$ (45 mg, 0.05 mmol), azpy-NMe_2 (23 mg, 0.10 mmol). Yield: 56 mg (70%). ^{1}H NMR ($CDCl_3$): δ = 8.34 (d, 1H, *J* = 8.0 Hz), 8.25 (d, 1H, *J* = 5.5 Hz), 8.11 (m, 2H), 8.03 (t, 1H, *J* = 8.0 Hz), 7.47 (m, 5H), 7.13 (t, 1H, *J* = 7.0 Hz), 6.65 (m, 2H), 3.31 (s, 6H), 1.75 (s, 3H), 1.69 (s, 3H), 1.65 (s, 3H), 1.49 (s, 3H). Anal. Calcd for $C_{28}H_{31}ClF_6IrN_4P$ (796.15): C, 42.24; H, 3.92; N, 7.04. Found: C, 42.32; H, 3.91; N, 7.16.

[(η^5-$C_5Me_4C_6H_5$)Ir(impy-NMe_2)Cl]PF_6 (28·PF_6). The synthesis was performed as for **26**·PF_6 using [(η^5-$C_5Me_4C_6H_5$)$IrCl_2$]$_2$ (45 mg, 0.05 mmol), *p*-dimethylaminophenyliminopyridine (impy-NMe_2, 23 mg, 0.10 mmol). Yield: 60 mg (75%). ^{1}H NMR ($CDCl_3$): δ = 8.77 (s, 1H), δ = 8.21 (dd, 2H, *J* = 10.0 Hz), 7.98 (t, 1H, *J* = 8.2 Hz), 7.68 (d, 2H, 8.5 Hz), 7.52 (m, 5H), 7.38 (t, 1H, *J* = 7.0 Hz), 6.71 (d, 2H, 8.7 Hz), 3.36 (s, 6H), 1.80 (s, 3H), 1.55 (s, 3H), 1.46 (s, 3H), 1.39 (s, 3H). Anal. Calcd for $C_{29}H_{32}ClF_6IrN_3P$ (795.22): C, 43.83; H, 4.06; N, 5.28. Found: C, 43.75; H, 3.97; N, 5.26.

3.2.3 Methods

3.2.3.1 X-ray Crystallography

The details of the diffraction instrumentation are described in Chapter 2. The structures of complexes **2**, **5**·PF_6, **8**·PF_6, **9**·PF_6, **11**·BPh_4, **13**, **17**·PF_6, **19** and **21** were solved by Dr. Guy Clarkson (Department of Chemistry, University of Warwick) using SHELXS (TREF)[49] with additional light atoms found by Fourier methods. Complexes were refined against F^2 using SHELXL,[50] and hydrogen atoms were added at calculated positions and refined riding on their parent atoms. X-ray crystallographic data for complexes **5**·PF_6, **8**·PF_6, **9**·PF_6, **11**·BPh_4 and **13** have been deposited in the Cambridge Crystallographic Data Centre under the accession numbers CCDC 802288, 802287, 802291, 802290, and 802286, respectively.

3.2.3.2 Kinetics of Hydrolysis

Solutions of complexes **4**–**10** and **12**–**14** with final concentrations of 0.2–0.7 mM in 5% MeOD-d_4/95% D_2O (v/v) were prepared by dissolution of the complexes in MeOD-d_4 followed by rapid dilution with D_2O. ^{1}H NMR spectra were recorded after various time intervals. The rates of hydrolysis were determined by fitting plots of concentrations (determined from ^{1}H NMR peak integrals) versus time to a first-order rate equation using ORIGIN version 8.0. The hydrolysis of complexes **4**, **7**, **10**, **12**, **13** and **14** was monitored by ^{1}H NMR at 278 K (to slow down the rate and avoid freezing the samples), and for complexes **5**, **6**, **8** and **9** at 278, 283, 288 and 293 K. The Arrhenius equation $\ln(k) = \ln(A) - E_a/RT$ was used to calculate the hydrolysis rate constants and half-lives of **5**, **6**, **8** and **9** at 310 K.

3.2.3.3 Determination of pK_a Values

The pK_a* and pK_a values of complexes **4A**−**10A**, and **12A**−**14A** were determined from the pH* titration curves as described in Chapter 2.

3.2.3.4 Computation

Details of computational methods are described in Chapter 2. Geometry optimization calculations for complexes **4**–**14** were performed in the gas phase with the gradient-corrected correlation functional PBE0.[51] Electrostatic potential surfaces (EPS) for chlorido complexes **4**–**6**, **12**–**14**, and aqua complexes **6A**, **14A** were

calculated and mapped on electron density (isovalue 0.004) of the molecules. The electrostatic potential is represented with a colour scale ranging from red (–0.100 au) to blue (0.150 au). This work was carried out by Dr. Luca Salassa (Department of Chemistry, University of Warwick).

3.2.3.5 Interactions with Nucleobases

The reaction of chloride complexes **4**–**14** and aqua complex **5A** (ca. 1 mM) with nucleobases typically involved addition of a solution containing one mol equiv of nucleobase in D_2O to an equilibrium solution of complexes **4**–**14** in 5% MeOD-d_4/95% D_2O (v/v), or to a solution of the aqua complex **5A** (prepared by the addition of 1 mol equiv of $AgNO_3$ to a solution of **5** and removal of AgCl by filtration). ^{1}H NMR spectra of these solutions were recorded at 310 K after various time intervals.

3.2.3.6 Cytotoxicity

Cytotoxicity assays on A2780 human ovarian cancer cell line were performed by Dr. Ana M. Pizarro (Department of Chemistry, University of Warwick) as described in Chapter 2 for complexes **4**–**14**, **16**–**24**, **26** and **27**. Complexes **5**·PF_6, **6**·PF_6 and **9**·PF_6 were further evaluated by the NCI/DTP as described in Chapter 2 for *in vitro* cytotoxic test against ca. 60 human cancer cell lines.

3.2.3.7 log *P* Determination

The partition coefficients (log *P*) were determined for complexes **4**–**6** by Dr. Ana M. Pizarro and Sally A. Fletcher (Department of Chemistry, University of Warwick) as described in Chapter 2.

3.2.3.8 Cell Accumulation, Cellular Distribution, and DNA Binding in A2780 Human Ovarian Cancer Cells

Work in this section was performed by Dr. Ana M. Pizarro and Sally A. Fletcher (Department of Chemistry, University of Warwick). A2780 cells were plated at a density of 5×10^6 cells/100 mm Petri dish in 9 mL of culture medium on day 1 (three dishes were prepared per compound tested, and three untreated control dishes, in two independent experiments). On day 2 cells were exposed to the Ir^{III} complexes **4**–**6**. Stock solutions of the iridium compounds were prepared fresh in DMSO and diluted in 0.9% saline and medium (1:1; 0.5% v/v DMSO final concentration) to a final concentration of Ir on the plates of 5 μM. After 24 h of drug exposure at 310 K on a 5% CO_2 incubator, the drug-containing medium was removed and the cells were washed, trypsinized, and counted using a haemocytometer. One-third of the cells was centrifuged, quickly washed with PBS, and stored at 253 K for determination of total cell accumulation (the net effect of uptake and efflux) of iridium. Another third of the samples was used for cytosol, nucleus, membrane/particulate and cytoskeleton fractionation, using a FractionPREP™ cell fractionation kit from BioVision (Mountain View, CA). The last third of the

samples was used for quantification of Ir bound to DNA using the Nucleon genomic DNA extraction kit (GE healthcare, Amersham, UK; BACC-1 protocol). All the cell pellets and solid cell fractions were digested in freshly distilled 72% HNO_3 in Wheaton V-Vials with a PTFE-faced rubber lined cap (Sigma-Aldrich) for 16 h at 373 K. After cooling, the samples were diluted with DDW to a maximum final concentration of 7.2% HNO_3 (suitable for ICP-MS analysis) prior quantification of iridium.

3.2.3.9 Sequence Preference of DNA Adducts

Works in this section was performed by Prof. Viktor Brabec and colleagues (Institute of Biophysics, Academy of Sciences of the Czech Republic). The primer extension footprinting assay was used to evaluate the sequence selectivity of DNA modification by complexes **4**–**6**. A fragment of pSP73KB DNA linearised by HpaI (2464 bp) was incubated with Ir^{III} complexes in 10 mM $NaClO_4$ for 24 h at 310 K to obtain r_b = 0.01 (bound Ir/base). The excess of drug was removed by ethanol precipitation. Circum VentTM Thermal Cycle Sequencing Kit with Vent(exo$^-$) DNA polymerase was used along with the protocol for thermal cycle DNA sequencing with 5′ end-labeled 20-mer SP6 primer recommended by the manufacturer with small modifications.[52] The synthesis products were separated by electrophoresis on a denaturing polyacrylamide (PAA) gel [6% polyacrylamide (PAA)/8M urea]; sequence ladders were obtained in parallel using untreated control DNA fragment.

3.2.3.10 Fluorescence Measurements

This work was performed by Prof. Viktor Brabec and colleagues (Institute of Biophysics, Academy of Sciences of the Czech Republic), using a Shimadzu RF 40 spectrofluorophotometer using a 1 cm quartz cell. Fluorescence measurements of CT DNA modified by Ir^{III} complexes, cisplatin or [Pt(dien)Cl]Cl (dien = diethylenetriamine), in the presence of EtBr, were performed at an excitation wavelength of 546 nm, and the emitted fluorescence was analyzed at 590 nm. The fluorescence intensity was measured at 298 K in 0.4 M NaCl to avoid secondary binding of EtBr to DNA.[53,54] The concentrations were 0.01 mg/mL for DNA and 0.04 mg/mL for EtBr, which corresponded to the saturation of all intercalation sites for EtBr in DNA.[53]

3.2.3.11 Viscometry

These studies were performed by Prof. Viktor Brabec and colleagues (Institute of Biophysics, Academy of Sciences of the Czech Republic). The relative viscosity of the solutions of CT DNA nonmodified or modified by complexes **4**–**6** at the concentration of 150 μg/mL was measured by microviscometry (AMVn Automated Micro Viscometer, Anton Paar GmbH, Austria) using a 1.6-mm capillary tube at 310 K. The densities of the solutions were measured using a Density Meter DMA 4500 instrument (Anton Paar GmbH, Austria).

3.2.3.12 ICP-MS Analysis

ICP analysis of all cell samples was carried out as described in Chapter 2.

3.3 Results

3.3.1 Synthesis and Characterisation

25 Ir^{III} half-sandwich complexes of the type $[(\eta^5\text{-}Cp^x)Ir(XY)Cl]^{0/+}$, where Cp^x is pentamethylcyclopentadienyl, Cp*, or its phenyl Cp^{xph} or biphenyl Cp^{xbiph} derivatives, and XY is the N,N-chelating ligand 1,10-phenanthroline (phen, **4**, **5** and **6**), 2,2'-bipyridine (bpy, **7**, **8** and **9**), ethylenediamine (en, **10** and **11**), 1,10-phenanthroline-5-amine (phen-5-amine, **15**), 4,4′-dimethyl-2,2′-bipyridine (bpy(Me_2), **16**, **17** and **18**), 2,2′-bipyridine-3,3′-diol (bpy(OH)O, **19**, **20** and **21**), dipyrido[3,2-f:2′,3′-h]quinoxaline (dpq, **22** and **24**), dipyrido[3,2-a:2′,3′-c]phenazine (dppz, **23** and **25**), 4-(2-pyridylazo)-*N*,*N*-dimethylaniline (azpy-NMe_2, **26** and **27**), *p*-dimethylaminophenyliminopyridine (impy-NMe_2, **28**) or N,O-chelating picolinate (pico, **12**, **13** and **14**), were synthesised in moderate yields by reaction of different chelating ligands with the appropriate dimer $[(\eta^5\text{-}Cp^x)IrCl_2]_2$ in methanol. Introduction of phenyl substituents on the Cp* ring decreased the reaction yields and increased difficulty to synthesise. Synthesis of the Ir^{III} complex containing Cp^{xbiph} and ethylenediamine proved to be difficult and it was not possible to study on this complex. Complexes **4**, **7**, **23**–**25** were isolated as Cl^- salts, complex **11** as a BPh_4^- salt, and complexes **5**, **6**, **8**–**10**, **15**–**18**, **22** and **26**–**28** as PF_6^- salts. All the

synthesised complexes were fully characterised by ^{1}H NMR spectroscopy and CHN elemental analysis. The cyclopentadienyl iridium(III) complexes studied in this Chapter are shown in Figure 3.1. Complexes **4**–**14** as typical complexes containing N,N- or N,O-chelating ligands are studied in more detail.

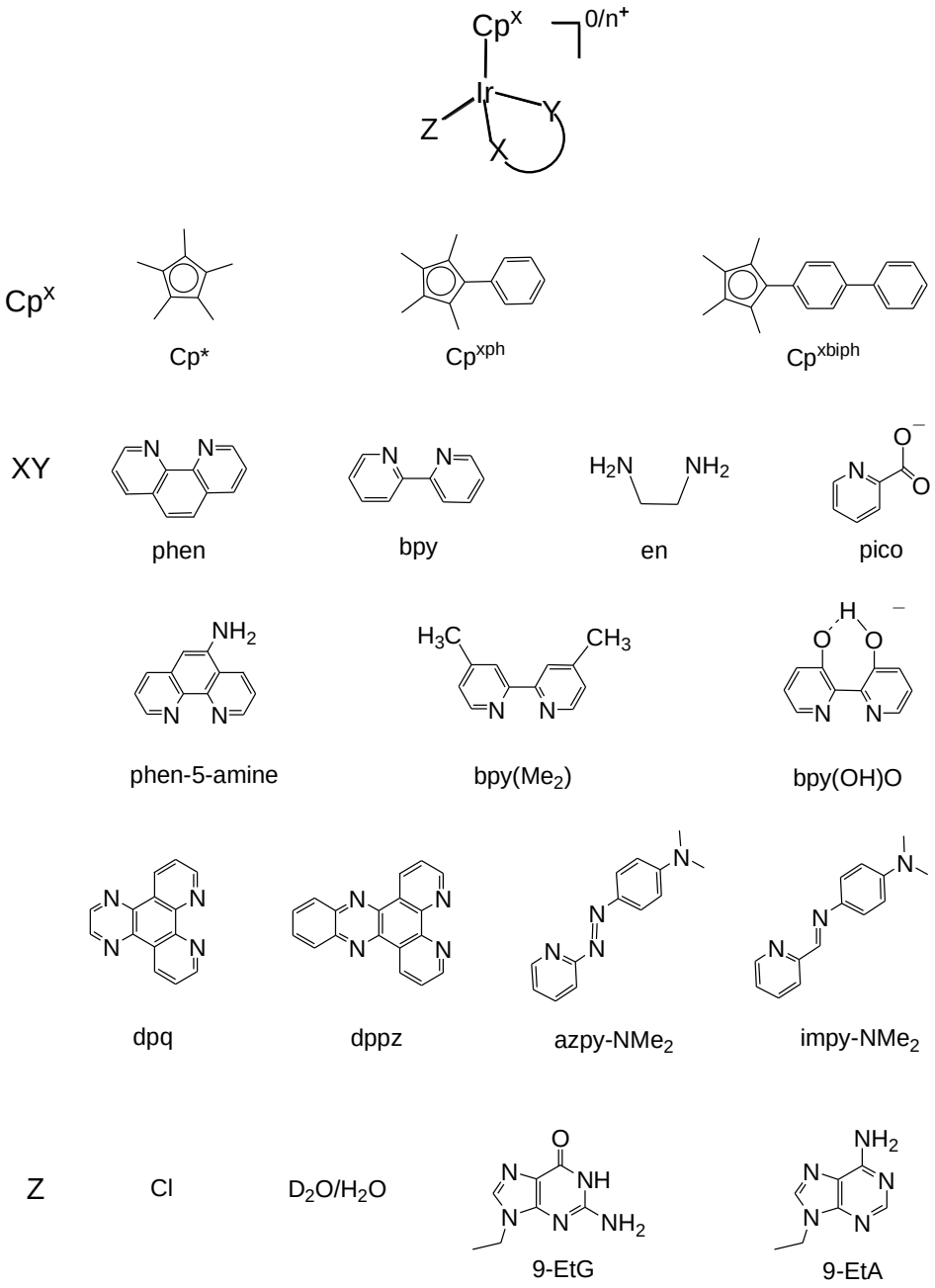

Figure 3.1. Iridium cyclopentadienyl complexes studied in this Chapter.

Z=Cl	Z=D_2O/H_2O	Z=9-EtG	Z=9-EtA	Cp^X	XY
4	**4A**	**4G**		Cp*	phen
5	**5A**	**5G**		Cp^{xph}	phen
6	**6A**	**6G**		Cp^{xbiph}	phen
7	**7A**	**7G**		Cp*	bpy
8	**8A**	**8G**		Cp^{xph}	bpy
9	**9A**	**9G**		Cp^{xbiph}	bpy
10	**10A**	**10G**		Cp*	en
11		**11G**		Cp^{xph}	en
12	**12A**	**12G**	**12Ad**	Cp*	pico
13	**13A**	**13G**	**13Ad**	Cp^{xph}	pico
14	**14A**	**14G**	**14Ad**	Cp^{xbiph}	pico
15				Cp*	phen-5-amine
16				Cp*	$bpy(Me)_2$
17				Cp^{xph}	$bpy(Me)_2$
18				Cp^{xbiph}	$bpy(Me)_2$
19				Cp*	bpy(OH)O
20				Cp^{xph}	bpy(OH)O
21				Cp^{xbiph}	bpy(OH)O
22				Cp^{xph}	dpq
23				Cp^{xph}	dppz
24				Cp^{xbiph}	dpq
25				Cp^{xbiph}	dppz
26				Cp*	azpy-NMe_2
27				Cp^{xph}	azpy-NMe_2
28				Cp^{xph}	impy-NMe_2

Figure 3.1. Iridium cyclopentadienyl complexes studied in this Chapter.

The X-ray crystal structures of complexes [(η^5-$C_5Me_4C_6H_5$)Ir(phen)Cl]PF_6 (**5**·PF_6) [(η^5-$C_5Me_4C_6H_5$)Ir(bpy)Cl]PF_6 (**8**·PF_6), [(η^5-$C_5Me_4C_6H_4C_6H_5$)Ir(bpy)Cl]PF_6 (**9**·PF_6), [(η^5-$C_5Me_4C_6H_5$)Ir(en)Cl]BPh_4 (**11**·BPh_4), [(η^5-$C_5Me_4C_6H_5$)Ir(pico)Cl] (**13**), [(η^5-$C_5Me_4C_6H_5$)Ir(bpy(Me)$_2$)Cl]PF_6 $(C_2H_5)_2O$ (**17**·PF_6 $(C_2H_5)_2O$), [(η^5-C_5Me_5)Ir-(bpy(OH)O)Cl] (**19**), and [(η^5-$C_5Me_4C_6H_4C_6H_5$)Ir(bpy(OH)O)Cl] (**21**) were determined. The complexes adopt the expected half-sandwich pseudo-octahedral "three-legged piano-stool" geometry with the iridium bound to a η^5-cyclopentadienyl ligand (Ir to ring centroid 1.760−1.793 Å), a chloride (2.384−2.415 Å) and a chelating ligand. Their structures and atom numbering schemes are shown in Figure 3.2. Crystallographic data are shown in Table 3.1, and selected bond lengths and angles are listed in Table 3.2.

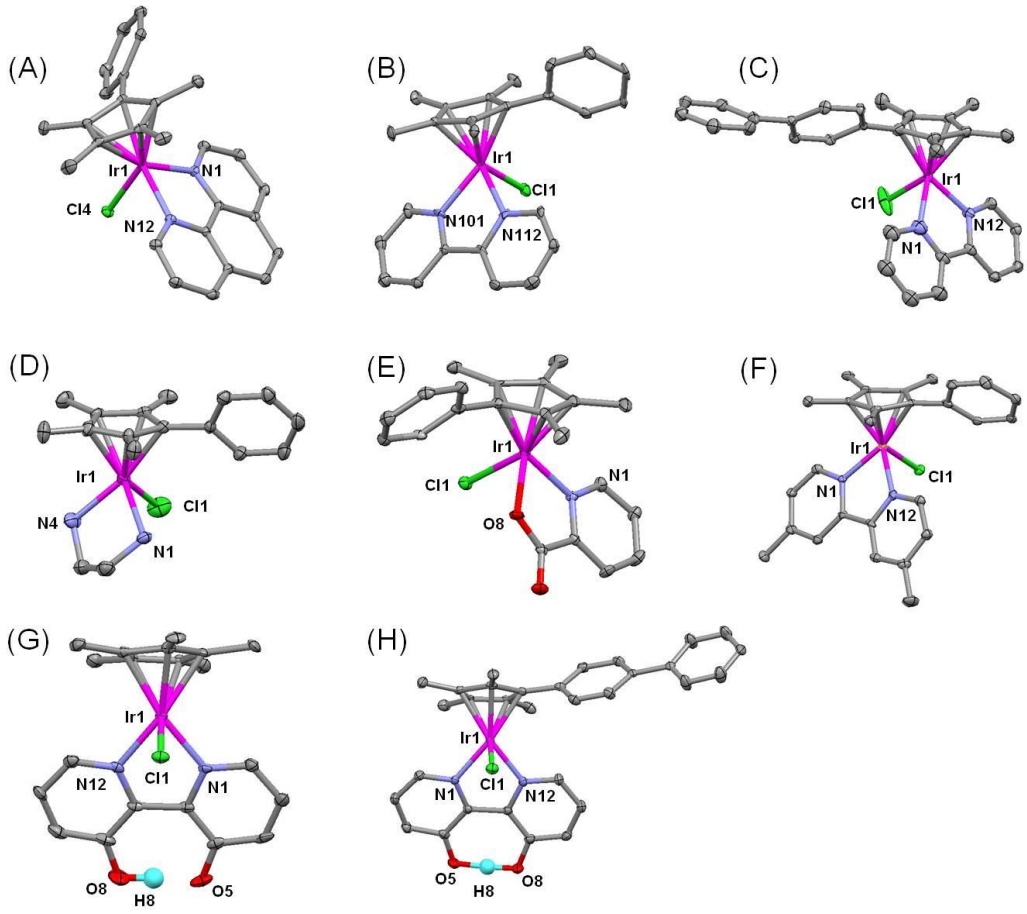

Figure 3.2. X-ray crystal structures with atom numbering schemes for (A) [(η^5-$C_5Me_4C_6H_5$)Ir(phen)Cl]PF_6 (**5**·PF_6), (B) [(η^5-$C_5Me_4C_6H_5$)Ir(bpy)Cl]PF_6 (**8**·PF_6), (C) [(η^5-$C_5Me_4C_6H_4C_6H_5$)Ir(bpy)Cl]PF_6 (**9**·PF_6), (D) [(η^5-$C_5Me_4C_6H_5$)Ir(en)Cl]BPh_4 (**11**·BPh_4), (E) [(η^5-$C_5Me_4C_6H_5$)Ir(pico)Cl] (**13**), (F) [(η^5-$C_5Me_4C_6H_5$)Ir-(bpy$(Me)_2$)Cl]PF_6 $(C_2H_5)_2O$ (**17**·PF_6 $(C_2H_5)_2O$), (G) [(η^5-C_5Me_5)Ir(bpy(OH)O)Cl] (**19**), and (H) [(η^5-$C_5Me_4C_6H_4C_6H_5$)Ir(bpy(OH)O)Cl] (**21**) with thermal ellipsoids drawn at 50% probability. The hydrogen atoms, solvent and counterions have been omitted for clarity.

Table 3.1. Crystallographic Data for Complexes $[(\eta^5\text{-}C_5Me_4C_6H_5)Ir(phen)Cl]PF_6$ (**5**·PF_6), $[(\eta^5\text{-}C_5Me_4C_6H_5)Ir(bpy)Cl]PF_6$ (**8**·PF_6), $[(\eta^5\text{-}C_5Me_4C_6H_4C_6H_5)Ir(bpy)Cl]PF_6$ (**9**·PF_6), and $[(\eta^5\text{-}C_5Me_4C_6H_5)Ir(en)Cl]BPh_4$ (**11**·BPh_4)

	5·PF_6	**8**·PF_6	**9**·PF_6	**11**·BPh_4
formula	$C_{27}H_{25}ClF_6IrN_2P$	$C_{25}H_{25}ClF_6IrN_2P$	$C_{31}H_{29}ClF_6IrN_2P$	$C_{41}H_{45}BClIrN_2$
MW	750.11	726.09	802.18	804.25
cryst colour	green block	yellow block	yellow block	yellow block
cryst size (mm)	0.10 × 0.10 × 0.05	0.40 × 0.40 × 0.04	0.18 × 0.16 × 0.12	0.32 × 0.22 × 0.20
λ (Å)	0.71073	0.71073	0.71073	0.71073
temp(K)	100	100	100	100
cryst syst	triclinic	orthorhombic	triclinic	monoclinic
space group	*P*-1	*P*na2(1)	*P*-1	*P*2(1)/*n*
a (Å)	8.3225(3)	15.0979(16)	8.3909(4)	11.93341(15)
b (Å)	12.8863(4)	38.609(3)	12.2966(5)	18.9766(3)
c (Å)	12.9181(4)	8.6693(3)	15.4848(6)	15.71286(17)
α (°)	80.375(3)	90	68.541(4)	90
β (°)	81.595(3)	90	75.835(4)	99.0672(12)
γ (°)	71.565(3)	90	81.128(4)	90
vol(Å^3)	1289.37(7)	5053.5(7)	1438.04(10)	3513.80(8)
Z	2	8	2	4
$R(Fo^2)$	0.0218	0.0445	0.0309	0.0430
$Rw(Fo^2)$	0.0555	0.0878	0.0640	0.1106
GOF	1.026	0.930	1.094	1.049

Table 3.1. Crystallographic Data for Complexes [(η^5-$C_5Me_4C_6H_5$)Ir(pico)Cl] (**13**), [(η^5-$C_5Me_4C_6H_5$)Ir(bpy(Me)$_2$)Cl]PF_6 $(C_2H_5)_2O$ (**17**·PF_6 $(C_2H_5)_2O$), [(η^5-C_5Me_5)Ir-(bpy(OH)O)Cl] (**19**), and [(η^5-$C_5Me_4C_6H_4C_6H_5$)Ir(bpy(OH)O)Cl] (**21**)

	13	**17**·PF_6 $(C_2H_5)_2O$	**19**	**21**
formula	$C_{21}H_{21}ClIrNO_2$	$C_{31}H_{39}ClF_6IrN_2OP$	$C_{20}H_{22}ClIrN_2O_2$	$C_{31}H_{28}ClIrN_2O_2$
MW	547.04	828.26	550.05	688.20
cryst colour	yellow block	yellow block	yellow block	yellow block
cryst size (mm)	0.50×0.10 ×0.05	0.18×0.18 ×0.17	0.40 ×0.20 ×0.10	0.08×0.08 ×0.06
λ (Å)	0.71073	0.71073	0.71073	0.71073
temp(K)	100	100	100	100
cryst syst	orthorhombic	orthorhombic	orthorhombic	monoclinic
space group	*P*na2(1)	*P*2(1)2(1)2(1)	*P*2(1)2(1)2(1)	*P*2(1)/*c*
a (Å)	17.6483(5)	13.7553(5)	8.4903(2)	13.4966(4)
b (Å)	9.5691(3)	15.0335(6)	13..6369(4)	11.8473(3)
c (Å)	11.0826(3)	15.2373(5)	15.7753(6)	17.1180(5)
α (°)	90	90	90	90
β (°)	90	90	90	111.367(3)
γ (°)	90	90	90	90
vol(Å^3)	1871.60(9)	3150.9(2)	1826.48(10)	2549.00(12)
Z	4	4	4	4
$R(Fo^2)$	0.0265	0.0237	0.0242	0.0201
$Rw(Fo^2)$	0.0465	0.0496	0.0541	0.0398
GOF	0.905	0.976	1.017	0.954

Table 3.2. Selected Bond Lengths (Å) and Angles (deg) for Complexes [(η^5-$C_5Me_4C_6H_5$)Ir(phen)Cl]PF_6 (**5**·PF_6), [(η^5-$C_5Me_4C_6H_5$)Ir(bpy)Cl]PF_6 (**8**·PF_6), [(η^5-$C_5Me_4C_6H_4C_6H_5$)Ir(bpy)Cl]PF_6 (**9**·PF_6), [(η^5-$C_5Me_4C_6H_5$)Ir(en)Cl]BPh_4 (**11**·BPh_4), and [(η^5-$C_5Me_4C_6H_5$)Ir(bpy(Me)$_2$)Cl]PF_6 (C_2H_5)$_2$O (**17**·PF_6 (C_2H_5)$_2$O)

	5·PF_6	**8**·PF_6	**9**·PF_6	**11**·BPh_4	**17**·PF_6 (C_2H_5)$_2$O
Ir−C(Cp ring)	2.148(2)	2.148(7)	2.151(5)	2.158(4)	2.163(4)
	2.157(2)	2.156(6)	2.155(5)	2.162(4)	2.166(4)
	2.157(2)	2.181(7)	2.161(5)	2.165(4)	2.173(3)
	2.167(2)	2.184(7)	2.172(5)	2.166(4)	2.174(4)
	2.197(2)	2.201(8)	2.184(5)	2.169(4)	2.180(3)
Ir−C(centroid)	1.783	1.789	1.787	1.789	1.790
Ir−N1	2.0916(19)	2.083(6)	2.086(4)	2.134(3)	2.079(3)
Ir−N2	2.1001(17)	2.096(6)	2.091(5)	2.136(4)	2.101(3)
Ir−Cl	2.3891(5)	2.3859(19)	2.3840(14)	2.4152(12)	2.4003(9)
N1−Ir−N2	77.58(7)	76.4(3)	76.76(16)	79.83(14)	76.82(12)
N1−Ir−Cl	84.23(5)	85.47(16)	84.84(11)	84.27(10)	84.66(8)
N2−Ir−Cl	85.05(5)	87.4(2)	86.20(14)	82.70(13)	84.61(8)

Table 3.2. Selected Bond Lengths (Å) and Angles (deg) for Complexes [(η^5-$C_5Me_4C_6H_5$)Ir(pico)Cl] (**13**), [(η^5-C_5Me_5)Ir(bpy(OH)O)Cl] (**19**), and [(η^5-$C_5Me_4C_6H_4C_6H_5$)Ir(bpy(OH)O)Cl] (**21**)

	19	**21**		**13**
Ir−C(Cp ring)	2.146(4)	2.145(2)	Ir−C(Cp ring)	2.129(4)
	2.155(4)	2.152(2)		2.135(4)
	2.166(4)	2.171(2)		2.138(4)
	2.183(4)	2.184(2)		2.154(4)
	2.184(4)	2.203(2)		2.173(4)
Ir−C(centroid)	1.791	1.793	Ir−C(centroid)	1.760
Ir−N1	2.066(3)	2.0721(19)	Ir−N	2.096(3)
Ir−N2	2.066(3)	2.0772(19)	Ir−O	2.113(3)
Ir−Cl	2.3957(11)	2.3836(6)	Ir−Cl	2.3860(10)
N1−Ir−N2	76.26(14)	76.38(7)	N−Ir−O	77.80(15)
N1−Ir−Cl	85.65(10)	87.32(5)	N−Ir−Cl	88.50(14)
N2−Ir−Cl	84.97(10)	87.4(2)	O−Ir−Cl	84.48(8)

A weak intermolecular ring stacking is observed in the crystal structures of complex **5**·PF_6, between phen ligands in neighbouring molecules. The two interacting π systems are parallel, with a centroid−centroid distance of 3.518 Å, Figure 3.3.

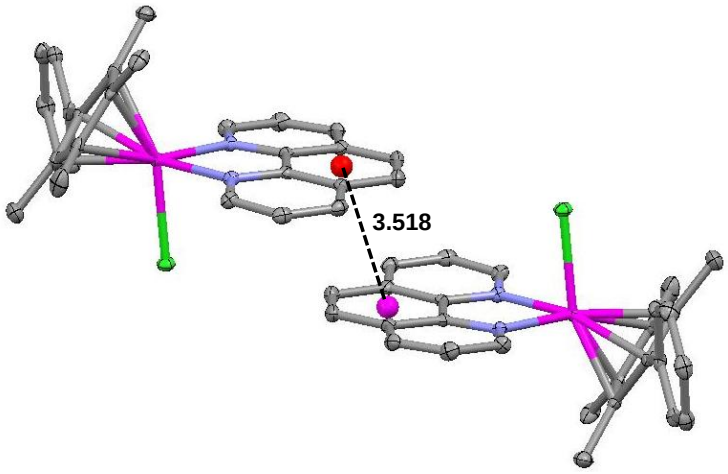

Figure 3.3. Diagram showing π-stacking between the phen ligands of neighbouring molecules in the X-ray crystal structure of $[(\eta^5\text{-}C_5Me_4C_6H_5)Ir(phen)Cl]PF_6$ (**5**·PF_6). The centroid–centroid distance between the phenyl rings of independent molecules is 3.518 Å. 50% ellipsoids. H atoms and PF_6^- counter ions have been omitted for clarity.

Stacking between the Cp^{xbiph} of neighbouring molecules is present in crystals of complex **9**·PF_6. The centroids of the three rings on independent molecules are separated by 4.447, 4.607 and 4.447 Å, at dihedral angles of 8.47, 0 and 8.47 °, respectively, Figure 3.4. The twist angle between the cyclopentadienyl and the central ring is 45.23 °, and between the central and the terminal phenyl ring is 46.34 °. In contrast, the planes of the terminal and bound rings are only twisted by 8.47 °.

The propeller twist of the phenyl-tetramethylcyclopentadienyl ligand in complex **11**·BPh_4 is 63.7°. The Ir−Cl bond length (2.4152(12) Å) is the longest of these X-ray structures.

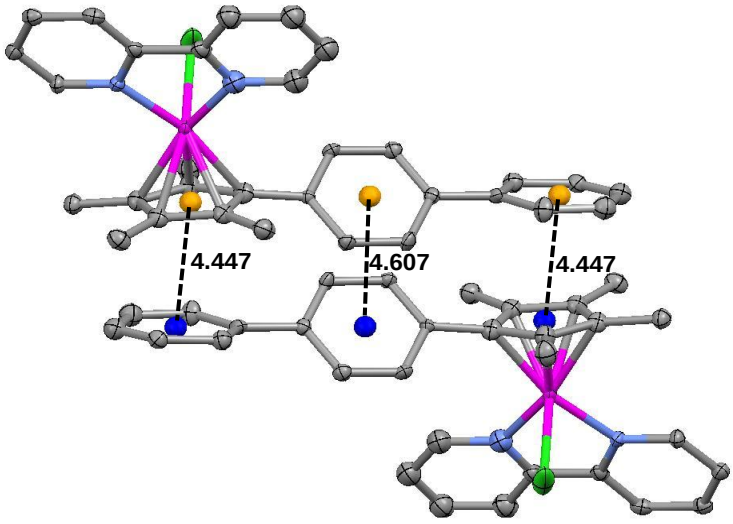

Figure 3.4. Diagram showing stacking between the planar Cp^{xbiph} of neighbouring molecules in the X-ray crystal structure of $[(\eta^5\text{-}C_5Me_4C_6H_4C_6H_5)Ir(bpy)Cl]PF_6$ (**9**·PF_6). The centroids of three rings of independent molecules are separated by 4.447, 4.607 and 4.447 Å, with dihedral angles of 8.47, 0 and 8.47 °, respectively. 50% ellipsoids. H atoms and the PF_6^- counterion have been omitted for clarity.

In the crystal structures of **19** and **21**, (Figure 3.2), one of the bipyridinediol oxygens is deprotonated, an intramolecular hydrogen bond forms (O8···H8···O5, O-O distance 2.387(5) Å and 2.396(2) Å, respectively), and the complexes are neutral.

The bond lengths of complexes **4**–**14** were also calculated by using the functional PBE1PBE. Selected calculated bond lengths are listed in Table 3.3 and are in good agreement with the experimental X-ray structures. DFT calculations show that Ir–Cl and Ir–cyclopentadienyl ring bond distances remain similar on changing Cp* to substituted Cp* groups.

Table 3.3. Selected Calculated Bond Lengths (Å) for Complexes **4**–**14**

Complex	Ir–Cl	Ir–N1	Ir–N2	Ir–Centroid
4	2.398	2.095	2.095	1.812
5	2.400	2.095	2.095	1.810
6	2.400	2.094	2.095	1.810
7	2.398	2.083	2.083	1.816
8	2.400	2.082	2.082	1.816
9	2.400	2.082	2.084	1.815
10	2.408	2.160	2.156	1.795
11	2.409	2.159	2.153	1.791
Complex	Ir–Cl	Ir–N1	Ir–O2	Ir–Centroid
12	2.468	2.078	2.071	1.783
13	2.458	2.091	2.071	1.783
14	2.458	2.089	2.070	1.783

Electrostatic potential surfaces (EPS) for phen chlorido complexes **4**−**6** and aqua adduct **6A**, and the pico chlorido complexes **12**−**14** and aqua adduct **14A** were calculated. N,N-chelating phen complexes **4**−**6** show more positive electrostatic potentials than the N,O-chelating pico complexes **12**−**14** (Figure 3.5). Moreover, higher electron density is present on the second phenyl ring of the Cp^{xbiph} ligand in complexes **6** and **14**. The same trend is observed in the electrostatic potential surfaces of the aqua derivatives $[(\eta^5\text{-}C_5Me_4C_6H_4C_6H_5)Ir(phen)(H_2O)]^{2+}$ (**6A**) and $[(\eta^5\text{-}C_5Me_4C_6H_4C_6H_5)Ir(pico)(H_2O)]^{+}$ (**14A**), which as expected show more positive surfaces compared to their chlorido analogues, **6** and **14**.

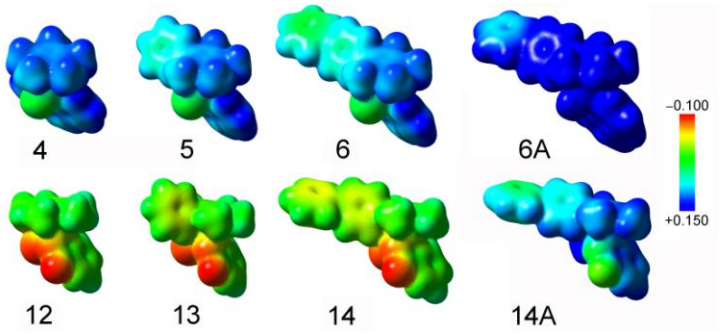

Figure 3.5. Electrostatic potential surfaces of the phen chlorido complexes **4**–**6** and aqua adduct **6A**, and the pico chlorido complexes **12**–**14** and aqua adduct **14A**. EPS surfaces are shown both in space (with positive and negative regions in blue and red, respectively) and mapped on electron density (isovalue 0.004) of the molecules. The electrostatic potential is represented with a colour scale going from red (–0.100 au) to blue (0.150 au).

3.3.2 Hydrolysis Studies

Hydrolysis of M–Cl bonds can represent an activation step for transition metal anticancer complexes.[55] M–OH_2 aqua complexes are often more reactive than the relevant chlorido complexes.[56,57] The hydrolysis of compounds **4**–**10** and **12**–**14** in 5% MeOD-d_4/95% D_2O (v/v) was monitored by ^{1}H NMR at different temperatures from 278 to 293 K. The presence of methanol ensured the solubility of the complexes.

All these Ir^{III} complexes undergo relatively rapid hydrolysis. Complexes [(η^5-C_5Me_5)Ir(phen)Cl]$^+$ (**4**), [(η^5-C_5Me_5)Ir(bpy)Cl]$^+$ (**7**), [(η^5-C_5Me_5)Ir(en)Cl]$^+$ (**10**)

containing Cp*, and [(η^5-C_5Me_5)Ir(pico)Cl] (**12**), [(η^5-$C_5Me_4C_6H_5$)Ir(pico)Cl] (**13**) and [(η^5-$C_5Me_4C_6H_4C_6H_5$)Ir(pico)Cl] (**14**) containing picolinate hydrolysed too rapidly for the rates to be determined by ^{1}H NMR spectroscopy even at 278 K: there was little change in the spectra between 5 min and 24 h, Figure 3.6. Attempts to observe hydrolysis of these complexes by UV-Vis at 288 K were also unsuccessful: equilibrium was reached before the first UV-Vis spectrum was acquired (< 1 min).

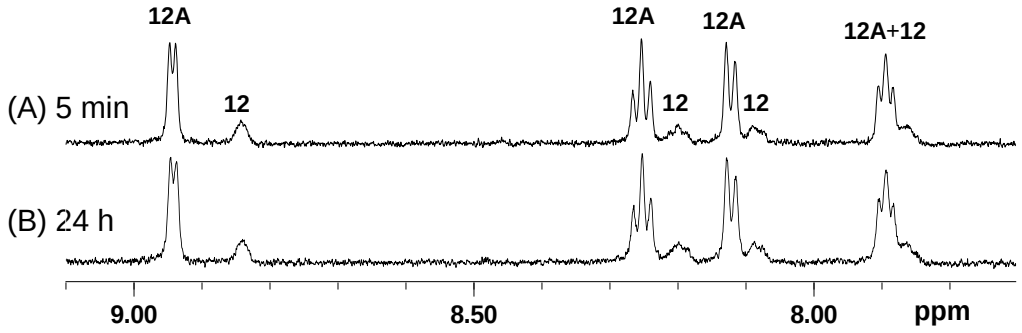

Figure 3.6. ^{1}H NMR spectra showing the hydrolysis of complex [(η^5-C_5Me_5)Ir(pico)Cl] (**12**) (1 mM) in 5% MeOD-d_4/95% D_2O at 278 K. (A) after 5 min; (B) after 24 h. Almost no difference is observed between these two spectra. Peaks labeled 12A correspond to aqua complex [(η^5-C_5Me_5)Ir(pico)(D_2O)]$^+$ (**12A**).

To confirm the hydrolysis of these complexes, NaCl (1–4 mol equiv) was added to equilibrium solutions. With increase in NaCl concentration, ^{1}H NMR peaks for the chlorido adducts increased whilst peaks for the aqua form decreased in intensity, Figure 3.7 and Figure 3.8. Similarly, addition of NaCl to an aqueous solution of the aqua complex **4A** gave rise to peaks for the chlorido complex **4**.

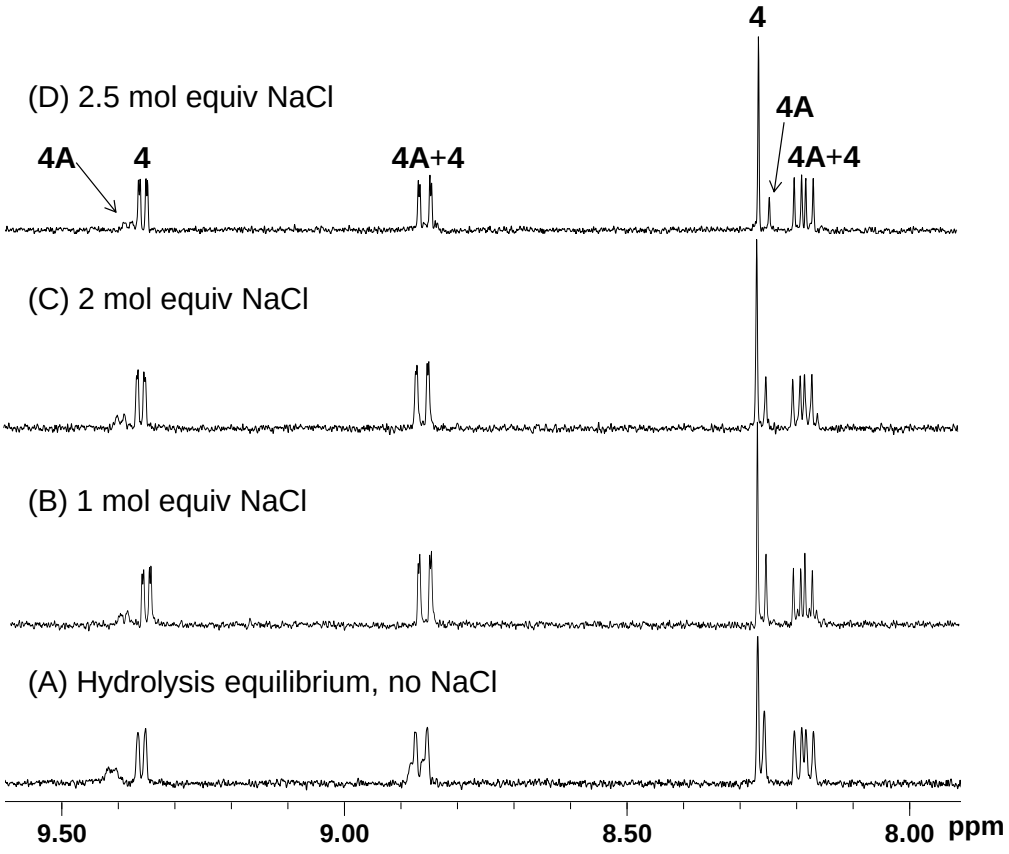

Figure 3.7. Confirmation of hydrolysis of Ir^{III} complex $[(\eta^5\text{-}C_5Me_5)Ir(phen)Cl]^+$ (**4**) by addition of various amounts of NaCl to an equilibrium solution of **4** (1 mM) in 5% MeOD-d_4/95% D_2O (v/v) at 298 K. ^1H NMR spectra recorded 10 min after addition of NaCl. The mol equiv NaCl is the total amount added. Complex **4A** corresponds to the aqua complex $[(\eta^5\text{-}C_5Me_5)Ir(phen)(D_2O)]^{2+}$. The peaks for the chlorido complex **4** increased in intensity while peaks for the aqua complex **4A** decreased on addition of NaCl.

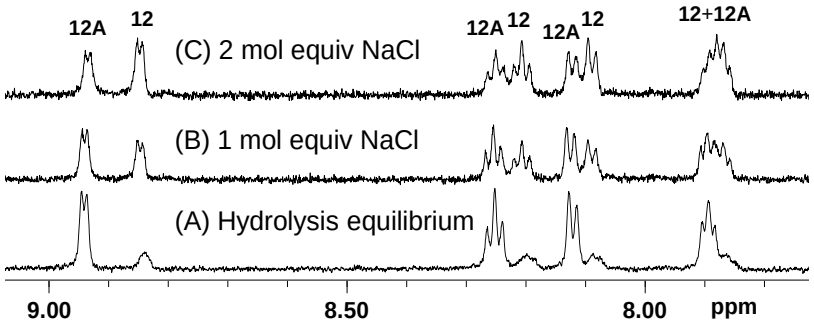

Figure 3.8. The picolinate CH region of the ^{1}H NMR spectra of [(η^5-C_5Me_5)Ir(pico)Cl] (**12**, 1 mM) in 5% MeOD-d_4/95% D_2O (v/v). (A) at equilibrium, (B) after the addition of 1 mol equiv NaCl and (C) 2 mol equiv NaCl. ^{1}H NMR spectra recorded 10 min after addition of NaCl at 298 K. The mol equiv NaCl is the total amount added. The anation reaction is evident from the decrease in intensity of the peaks for the chlorido complex **12** and increase in intensity of peaks for the aqua complex **12A** [(η^5-C_5Me_5)Ir(pico)(D_2O)]$^{+}$ on addition of NaCl.

However the hydrolysis of complexes [(η^5-$C_5Me_4C_6H_5$)Ir(phen)Cl]$^{+}$ (**5**), [(η^5-$C_5Me_4C_6H_4C_6H_5$)Ir(phen)Cl]$^{+}$ (**6**), [(η^5-$C_5Me_4C_6H_5$)Ir(bpy)Cl]$^{+}$ (**8**), and [(η^5-$C_5Me_4C_6H_4C_6H_5$)Ir(bpy)Cl]$^{+}$ (**9**), was slow enough to be studied by ^{1}H NMR at low temperature. Hydrolysis was monitored at temperatures ranging from 278 K to 293 K by observing the appearance of new ^{1}H NMR peaks over time. The time dependence for formation of the aqua adducts of **5**, **6**, **8** and **9** was fitted to pseudo first-order kinetics (Figure 3.9), and their hydrolysis rate constants, half-lives and equilibrium constants (K_{aq}) for hydrolysis were determined (Table 3.4). At 278 K, the half-life for hydrolysis of the biphenyl substituted Cp^{xbiph} complex **6** was 32 min, about 1.3 times slower than that of the phenyl-Cp* complex **5** (25 min; Table 3.4).

The half-lives and extent of hydrolysis of complexes **4**–**6** at 278 K increase with the size of the ring system in the order Cp^{xbiph} > Cp^{xph} > Cp*. This trend is also observed for complexes **7**–**9**. The hydrolysis rate constants and half-lives of **5**, **6**, **8** and **9** at 310 K (body temperature) were calculated using the Arrhenius equation and are listed in Table 3.4. These range from 1 min for complexes **5** and **8** to 4 min for complex **6**.

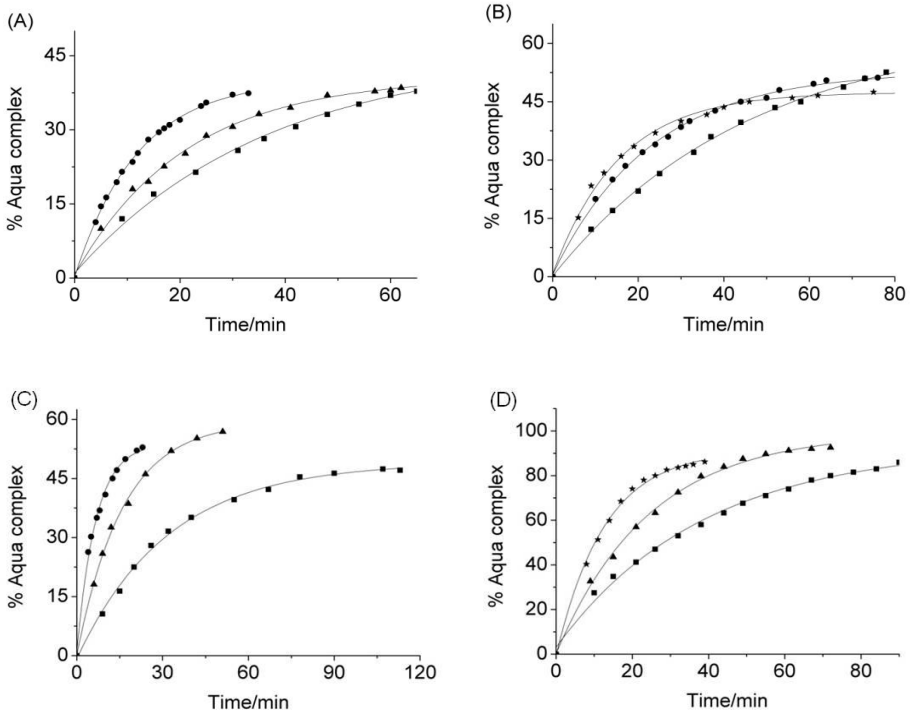

Figure 3.9. Time dependence for formation of aqua complexes (A) **5A**, (B) **6A**, (C) **8A** and (D) **9A** (based on ^{1}H NMR peak integrals) during hydrolysis of [(η^5-$C_5Me_4C_6H_5$)Ir(phen)Cl]$^+$ (**5**), [(η^5-$C_5Me_4C_6H_4C_6H_5$)Ir(phen)Cl]$^+$ (**6**), [(η^5-$C_5Me_4C_6H_5$)Ir(bpy)Cl]$^+$ (**8**), and [(η^5-$C_5Me_4C_6H_4C_6H_5$)Ir(bpy)Cl]$^+$ (**9**) in 5% MeOD-d_4/95% D_2O (v/v) at 278 K ■; 283 K ▲; 288 K ●; and 293 K ★.

Table 3.4. Hydrolysis Data for Complexes **4**−**10** and **12**−**14** at Various Temperatures

	k (min^{-1}) $t_{1/2}$ (min)					
Complex[a]	278 K	283 K	288 K	293 K	310 K[e]	K_{aq} (mM)[b]
4	–[c]					0.04
5	0.027 25.4	0.047 14.6	0.083 8.3	–[d]	0.65 1.1	0.06
6	0.022 31.8	–[d]	0.044 15.9	0.065 10.7	0.18 3.8	0.29
7	–[c]					0.05
8	0.031 22.1	0.062 11.1	0.099 7.0	–[d]	0.89 0.8	0.08
9	0.026 26.7	0.041 16.9	–[d]	0.078 8.8	0.23 3.0	1.45
10	–[c]					0.44
12	–[c]					0.78
13	–[c]					1.11
14	–[c]					2.33

[a] The course of the hydrolysis of complex **11** was difficult to interpret from NMR spectra. [b] 278 K. [c] too fast to be measured. [d] not determined. [e] obtained from Arrhenius equation.

In each series of complexes containing different N,N- or N,O-chelating ligands, the equilibrium constants (K_{aq}) for hydrolysis at 278 K increased with increasing phenyl substitution on the Cp^x ligand, Table 3.4.

3.3.3 pK_a Determination

The pK_a of coordinated water can have a significant influence on its reactivity since M−OH bonds are often much less labile than M−OH_2 bonds;[36] moreover hydroxide is a good bridging ligand and can give rise to oligomeric species.

Changes in the ^{1}H NMR chemical shifts for coordinated chelating ligands in aqua complexes **4A**−**9A**, **12A**−**14A**, and methyl groups of Cp* in aqua complex **10A**, were followed with change in pH* over a range of 2−11 (Figure 3.10). ^{1}H NMR peaks assigned to aqua complexes gradually shifted to high field with increase in pH*. The resulting pH titration curves were fitted to the Henderson-Hasselbalch equation, from which the pK_a* values of the coordinated water were determined. This gave rise to pK_a values between 6.28 and 7.99 (Table 3.5), with the bpy complexes being the most acidic (pK_a values 6.28−6.86) and the pico complexes the least acidic (pK_a values 7.52−7.99).

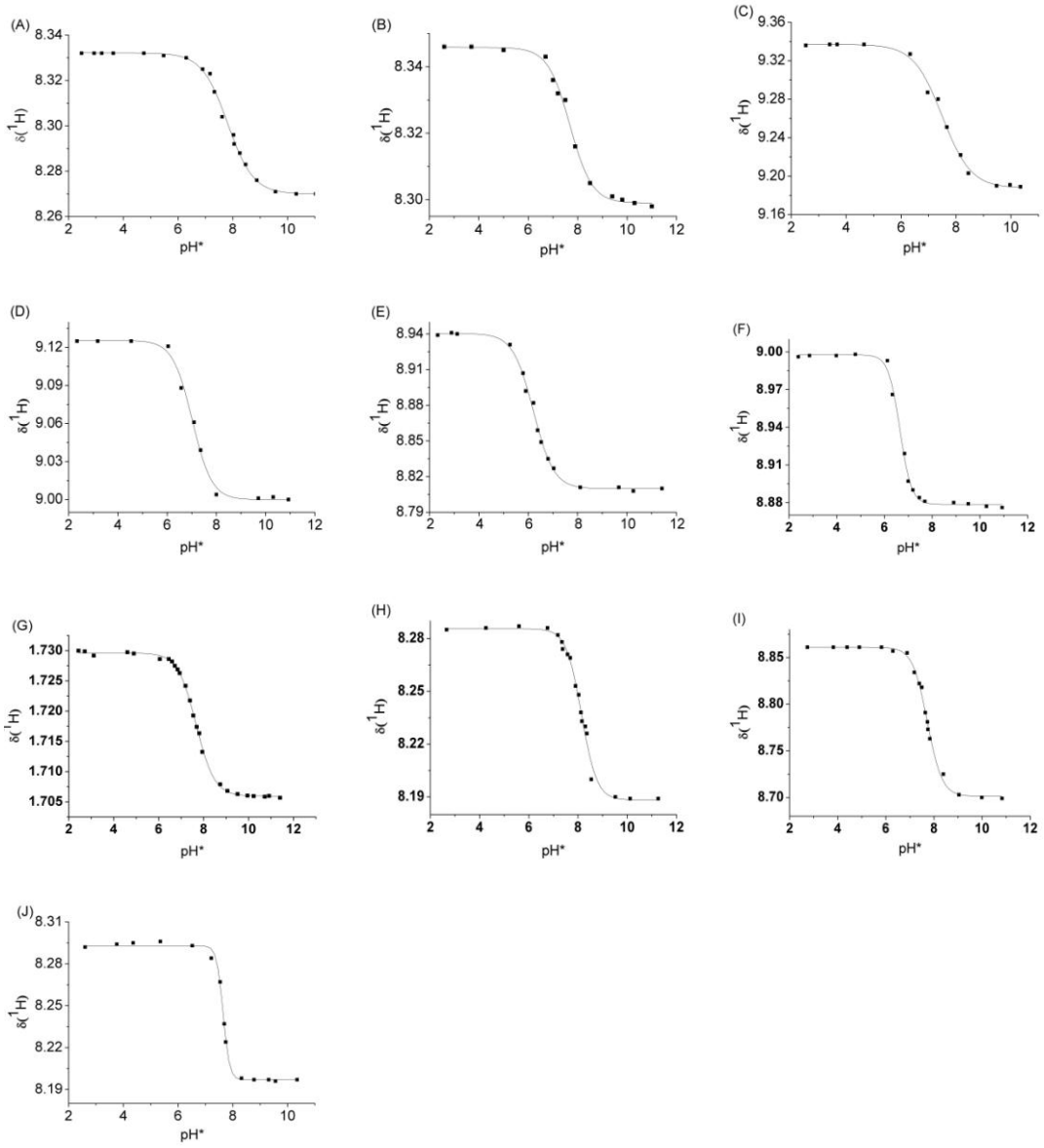

Figure 3.10. Dependence of the ^{1}H NMR chemical shifts for coordinated chelating ligands in aqua complexes **4A**−**9A**, **12A**−**14A**, and methyl group in Cp* in aqua complex **10A** on pH*. The curves are computer fits giving the pK_a* values shown in Table 3.5.

Table 3.5. pK_a* and pK_a Values[a] for the Deprotonation of the Coordinated D_2O in Complexes **4A**−**10A**, and **12A**−**14A**

Aqua Complex	pK_a*	pK_a
$[(\eta^5\text{-}C_5Me_5)Ir(phen)(D_2O)]^{2+}$ (**4A**)	7.88	7.74
$[(\eta^5\text{-}C_5Me_4C_6H_5)Ir(phen)(D_2O)]^{2+}$ (**5A**)	7.68	7.55
$[(\eta^5\text{-}C_5Me_4C_6H_4C_6H_5)Ir(phen)(D_2O)]^{2+}$ (**6A**)	7.50	7.38
$[(\eta^5\text{-}C_5Me_5)Ir(bpy)(D_2O)]^{2+}$ (**7A**)	6.94	6.86
$[(\eta^5\text{-}C_5Me_4C_6H_5)Ir(bpy)(D_2O)]^{2+}$ (**8A**)	6.31	6.28
$[(\eta^5\text{-}C_5Me_4C_6H_4C_6H_5)Ir(bpy)(D_2O)]^{2+}$ (**9A**)	6.68	6.63
$[(\eta^5\text{-}C_5Me_5)Ir(en)(D_2O)]^{2+}$ (**10A**)	7.66	7.54
$[(\eta^5\text{-}C_5Me_5)Ir(pico)(D_2O)]^{+}$ (**12A**)	8.15	7.99
$[(\eta^5\text{-}C_5Me_4C_6H_5)Ir(pico)(D_2O)]^{+}$ (**13A**)	7.75	7.62
$[(\eta^5\text{-}C_5Me_4C_6H_4C_6H_5)Ir(pico)(D_2O)]^{+}$ (**14A**)	7.65	7.52

[a] pK_a values calculated from pK_a* according to Krezel and Bal.[58]

3.3.4 Interactions with Nucleobases

Since DNA is a potential target site for transition metal anticancer complexes,[59,60] the binding of 9-ethylguanine (9-EtG) and 9-ethyladenine (9-EtA) to complexes **4**−**14**, and aqua complex **5A** were studied. The extent of nucleobase adducts formation by these complexes based on ^{1}H NMR peak integrals is shown in Table 3.6.

Table 3.6. Extent of 9-EtG and 9-EtA Adducts Formation for Complexes **4**−**14**, and **5A** (ca. 1 mM) at 310 K after 24 h

	Cp^x	XY	G adduct (%)	A adduct (%)
4	Cp*	phen(N,N-)	83	0
5	Cp^{xph}	phen(N,N-)	42	0
5A	Cp^{xph}	phen(N,N-)	74	0
6	Cp^{xbiph}	phen(N,N-)	90	0
7	Cp*	bpy(N,N-)	61	0
8	Cp^{xph}	bpy(N,N-)	47	0
9	Cp^{xbiph}	bpy(N,N-)	65	0
10	Cp*	en(N,N-)	100	0
11	Cp^{xph}	en(N,N-)	100	0
12	Cp*	pico(N,O-)	100	81
13	Cp^{xph}	pico(N,O-)	100	76
14	Cp^{xbiph}	pico(N,O-)	100	71

Addition of 1 mol equiv of 9-EtG to an equilibrium solution of complex **5**, $[(\eta^5\text{-}C_5Me_4C_6H_5)Ir(phen)Cl]^+$ (1.0 mM), in 5% MeOD-d_4/95% D_2O (v/v, pH* 7.2) at 310 K resulted in 15% of **5** reacting after 10 min, and a new 9-EtG H8 peak appearing at 7.68 ppm (species **5G**, Figure 3.11), shifted by 0.15 ppm to high field relative to that of free 9-EtG. After 24 h, 42% of **5** had reacted. The ESI-MS of an equilibrium solution (Figure 3.12) contained a major peak at *m/z* 374.6, confirming the formation of the 9-EtG adduct **5G**, $[(\eta^5\text{-}C_5Me_4C_6H_5)Ir(phen)(9\text{-EtG})]^{2+}$ (calcd *m/z* 374.5). However, 65% of aqua complex **5A** (prepared by treating a solution of **5**

with 1 mol equiv of $AgNO_3$) reacted with 9-EtG to form **5G** after 10 min and 73% after 24 h. More than 80% of complexes **4** and **6** reacted with 9-EtG under the same conditions.

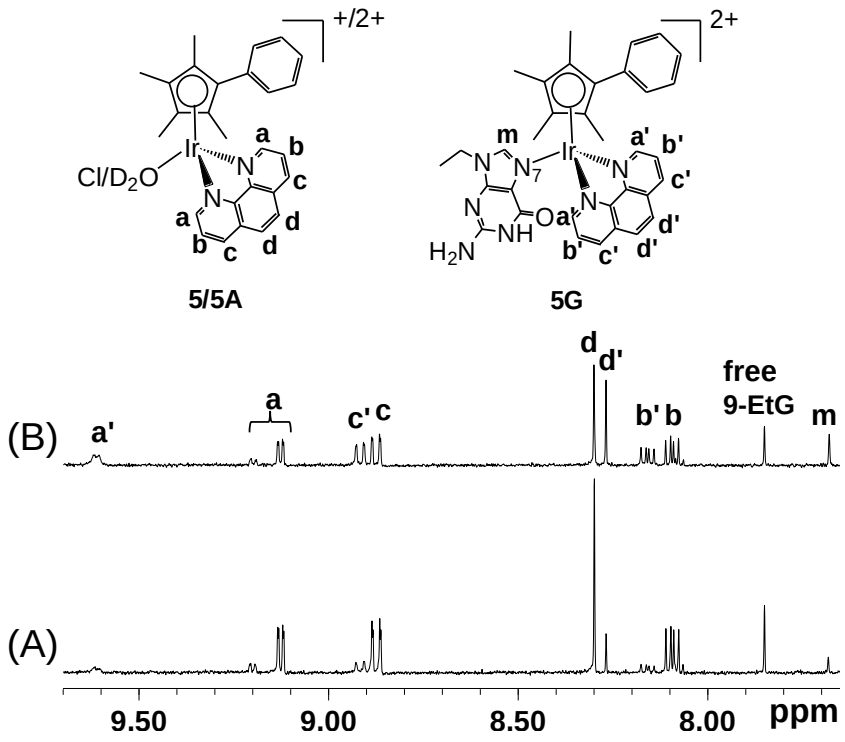

Figure 3.11. Low field region of the ^{1}H NMR spectra showing reaction of [(η^5-$C_5Me_4C_6H_5$)Ir(phen)Cl]$^+$ (**5**) with 9-ethylguanine. (A) 10 min after addition of 1 mol equiv 9-ethylguanine to an equilibrium solution of complex **5** (1.0 mM) in 5% MeOD-d_4/95% D_2O (v/v) at 310 K, pH* 7.2; and (B) after 24 h reaction. Peak assignments are indicated on the structures. After 24 h, 42% of **5** had reacted.

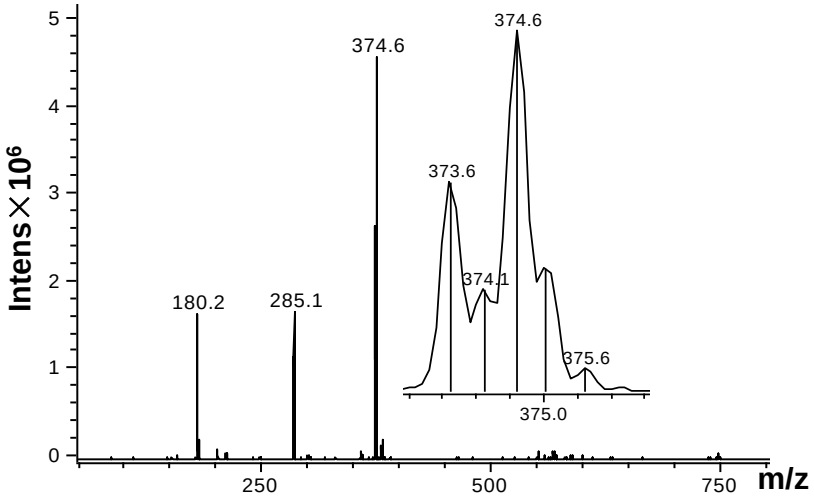

Figure 3.12. ESI-MS of an equilibrium solution (0.2 mM) of 9-EtG and complex $[(\eta^5\text{-}C_5Me_4C_6H_5)Ir(phen)Cl]^+$ (**5**) in 50% CH_3CN/50% H_2O (v/v), 298 K. The major peak at *m/z* 374.6 is assignable to the G adduct **5G**, $[(\eta^5\text{-}C_5Me_4C_6H_5)Ir(phen)(9\text{-EtG})]^{2+}$ (calcd *m/z* 374.5); The peak at *m/z* 285.1 is assignable to the fragment $[(\eta^5\text{-}C_5Me_4C_6H_5)Ir(phen)]^{2+}$ (calcd *m/z* 284.9). The peak at *m/z* 180.2 is assignable to 9-EtG (calcd *m/z* 179.2).

Complexes $[(\eta^5\text{-}C_5Me_5)Ir(en)Cl]^+$ (**10**) and $[(\eta^5\text{-}C_5Me_4C_6H_5)Ir(en)Cl]^+$ (**11**) interestingly, showed an exceptionally high affinity for 9-EtG with 100% nucleobase adduct formation within 10 min. On addition of a solution of 1 mol equiv of 9-EtG gradually to an equilibrium solution of **10** (0.9 mM) in 5% MeOD-d_4/95% D_2O (v/v) at 310 K, Figure 3.13, the methyl peak for **10** and **10A** decreased in intensity and eventually disappeared. A new Cp* methyl peak (for **10G**) appeared at 1.65 ppm. When 9-EtG was in excess, a set of new peaks assignable to free 9-EtG was clearly visible (Figure 3.13).

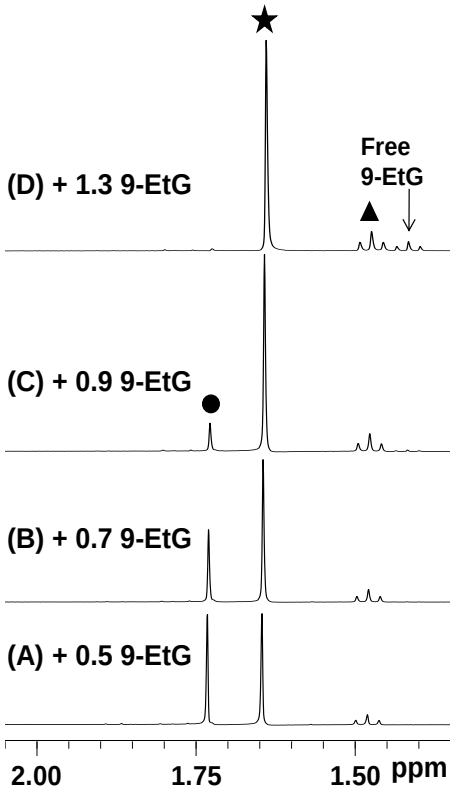

Figure 3.13. High-field region of the ^{1}H NMR spectrum of $[(\eta^5\text{-}C_5Me_5)Ir(en)Cl]^+$ (**10**, 0.9 mM) with increasing amounts of added 9-ethylguanine in 5% MeOD-d_4/95% D_2O (v/v) at 310 K. (A) 10 min after addition of 0.5 mol equiv 9-EtG; (B) 10 min after a further addition of 0.2 mol equiv 9-EtG; (C) 10 min after a further addition of 0.2 mol equiv 9-EtG; (D) 10 min after a further addition of 0.4 mol equiv 9-EtG (a total of 1.3 mol equiv of 9-EtG was added). Assignments: Peak labeled ★ represents methyl group of Cp* ring in $[(\eta^5\text{-}C_5Me_5)Ir(en)(9\text{-EtG})]^{2+}$ (**10G**); peak labeled ● represents methyl group of **10** + **10A**; peak labeled ▲ corresponds to methyl group of bound 9-EtG in $[(\eta^5\text{-}C_5Me_5)Ir(en)(9\text{-EtG})]^{2+}$ (**10G**).

Addition of 1 mol equiv of 9-EtA to an equilibrium solution of **5** (1.0 mM) in 5% MeOD-d_4/95% D_2O (v/v) at 310 K resulted in no additional ^{1}H NMR peaks over a period of 24 h. Similarly, no reaction with 9-EtA was observed for other complexes containing N,N- chelating ligands (Table 3.6).

In contrast, compounds **12**−**14** containing pico as chelating ligand formed both 9-EtG and 9-EtA adducts to the extent of 100% and more than 70% completion, respectively, after 24 h, Table 3.6. Two adenine nucleobase adducts are formed in the reaction of complexes **12**, **13** and **14** with 9-EtA, most likely through iridium binding to N1 or N7 of adenine forming 9-EtA adducts in ca. 1:3 ratio, Figure 3.14.

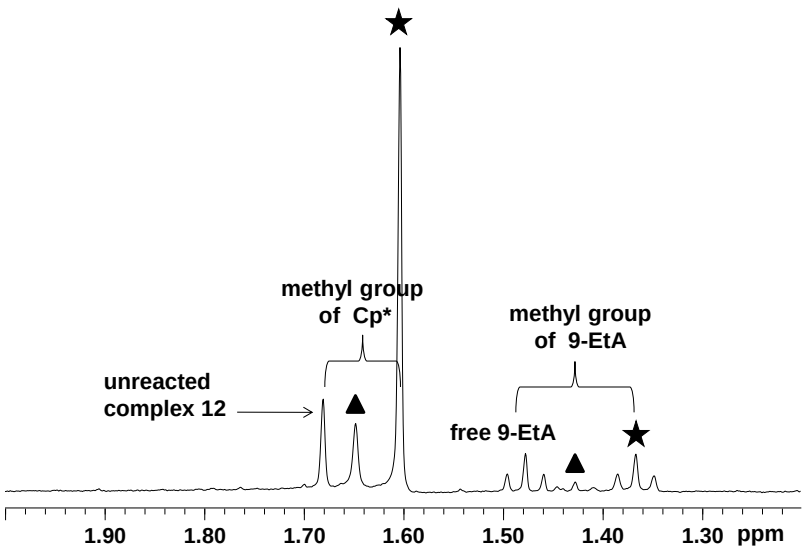

Figure 3.14. High-field region (methyl group of Cp* and 9-EtA) of the ^{1}H NMR spectrum showing the formation of two adenine adducts of [(η^5-C_5Me_5)Ir(pico)Cl] (**12**). Peaks labeled ▲ and ★ represent different adenine adducts, probably [(η^5-C_5Me_5)Ir(pico)(9-EtA-*N*7)]$^+$ and [(η^5-C_5Me_5)Ir(pico)(9-EtA-*N*1)]$^+$.

3.3.5 Cytotoxicity

The cytotoxicity of complexes **4**−**14** (studied in more details) towards A2780 human ovarian cancer cells was investigated, see Table 3.7. The IC_{50} values (concentration at which 50% of the cell growth is inhibited) for Cp* complexes **4**, **7**, **10**, **12** and the Cp^{xph} pico complex **13** were all > 100 μM and are thus deemed as inactive. However, compounds **5**, **6**, **8**, **9**, **11** and **14**, were all active. Complexes **5**, **8** and **11** containing Cp^{xph}, and **14** containing Cp^{xbiph} showed good activity, displaying IC_{50} values of 6−17 μM. Complexes **6** and **9** containing Cp^{xbiph} exhibited potent cytotoxicity with IC_{50} values of 0.7 and 0.6 μM, respectively, ca. twice as active as cisplatin in the A2780 cell line (IC_{50} 1.2 μM).

The cytotoxicity of complexes **16**−**24**, **26**, and **27** towards A2780 human ovarian cancer cells was also investigated and listed in Table 3.7.

For all series of complexes containing different chelating N,N- or N,O-chelating ligands, the trend of increasing of activity with increasing phenyl substitution was the same: Cp^{xbiph} > Cp^{xph} > Cp*.

Table 3.7. Inhibition of Growth of A2780 Human Ovarian Cancer Cells by Complexes **4**−**14**, **16**−**24**, **26**, **27** and Comparison with Cisplatin

Complex	IC_{50} [a] (μM)
[(η^5-C_5Me_5)Ir(phen)Cl]Cl (**4**·Cl)	>100
[(η^5-$C_5Me_4C_6H_5$)Ir(phen)Cl]PF_6 (**5**·PF_6)	6.70 ± 0.62
[(η^5-$C_5Me_4C_6H_4C_6H_5$)Ir(phen)Cl]PF_6 (**6**·PF_6)	0.72 ± 0.01
[(η^5-C_5Me_5)Ir(bpy)Cl]Cl (**7**·Cl)	>100
[(η^5-$C_5Me_4C_6H_5$)Ir(bpy)Cl]PF_6 (**8**·PF_6)	15.86 ± 1.49
[(η^5-$C_5Me_4C_6H_4C_6H_5$)Ir(bpy)Cl]PF_6 (**9**·PF_6)	0.57 ± 0.09
[(η^5-C_5Me_5)Ir(en)Cl]PF_6 (**10**·PF_6)	>100
[(η^5-$C_5Me_4C_6H_5$)Ir(en)Cl]BPh_4 (**11**·BPh_4)	16.97 ± 0.05
[(η^5- C_5Me_5)Ir(pico)Cl] (**12**)	>100
[(η^5-$C_5Me_4C_6H_5$)Ir(pico)Cl] (**13**)	>100
[(η^5-$C_5Me_4C_6H_4C_6H_5$)Ir(pico)Cl] (**14**)	16.30 ± 0.32
[(η^5-C_5Me_5)Ir(bpy($Me)_2$)Cl]PF_6 (**16**·PF_6)	>100
[(η^5-$C_5Me_4C_6H_5$)Ir(bpy($Me)_2$)Cl]PF_6 (**17**·PF_6)	9.22 ± 0.16
[(η^5-$C_5Me_4C_6H_4C_6H_5$)Ir(bpy($Me)_2$)Cl]PF_6 (**18**·PF_6)	0.51 ± 0.04
[(η^5-C_5Me_5)Ir(bpy(OH)O)Cl] (**19**)	17.2 ± 2.7
[(η^5-$C_5Me_4C_6H_5$)Ir(bpy(OH)O)Cl] (**20**)	7.18 ± 0.73
[(η^5-$C_5Me_4C_6H_4C_6H_5$)Ir(bpy(OH)O)Cl] (**21**)	2.79 ± 0.08
[(η^5-$C_5Me_4C_6H_5$)Ir(dpq)Cl]PF_6 (**22**·PF_6)	0.87 ± 0.12
[(η^5-$C_5Me_4C_6H_5$)Ir(dppz)Cl]Cl (**23**·Cl)	0.26 ± 0.12
[(η^5-$C_5Me_4C_6H_4C_6H_5$)Ir(dpq)Cl]Cl (**24**·Cl)	0.88 ± 0.09
[(η^5-C_5Me_5)Ir(azpy-NMe_2)Cl]PF_6 (**26**·PF_6)	1.38 ± 0.06
[(η^5-$C_5Me_4C_6H_5$)Ir(azpy-NMe_2)Cl]PF_6 (**27**·PF_6)	0.40 ± 0.00
cisplatin	1.22 ± 0.12

[a] Drug-treatment period was 24 h.

Complexes [(η^5-$C_5Me_4C_6H_5$)Ir(phen)Cl]PF_6 (**5**·PF_6), [(η^5-$C_5Me_4C_6H_4C_6H_5$)Ir-(phen)Cl]PF_6 (**6**·PF_6) and [(η^5-$C_5Me_4C_6H_4C_6H_5$)Ir(bpy)Cl]PF_6 (**9**·PF_6) were further evaluated by the National Cancer Institute Developmental Therapeutics Program (NCI/DTP, U.S.A.) *in vitro* cytotoxic tests against ca. 60 human cancer cell lines within nine tumour type subpanels.[61] The cells were treated by iridium complexes for 48 h at five concentrations ranging from 0.01 to 100 μM. Three endpoints are calculated: GI_{50} (the concentration that causes 50% cell growth inhibition), TGI (the concentration where causes 100% cell growth inhibition), and LC_{50} (the concentration that the drug decreases the original cell number by 50%).

The mean graphs for complexes **5**·PF_6, **6**·PF_6 and **9**·PF_6 are listed in Figure 3.15. Bars in the mean graphs extending to the right represent sensitivity of cell line to the test agent in excess of the average sensitivity of all tested cell lines. Bars extending to the left correspondingly imply sensitivity less than the mean. Complex **5**·PF_6, containing Cp^{xph} and 1,10-phenanthroline N,N-chelating ligand, shows high potency in wide range of cancer cell lines, selectively for leukemia, CNS cancer, melanoma, and prostate cancer (highlighted by red squares in Figure 3.15A). Complexes **6**·PF_6 and **9**·PF_6 containing Cp^{xbiph} show even higher potency with lowest GI_{50} value of 282 nM and 407 nM, respectively, and show selectivity not only towards leukemia, CNS cancer, melanoma, and prostate cancer, but also against colon cancer and breast cancer, Figures 3.15B and C.

Figure 3.15. (A) Mean graph for $[(\eta^5\text{-}C_5Me_4C_6H_5)Ir(phen)Cl]PF_6$ (**5**·PF_6) from the National Cancer Institute Developmental Therapeutic Program. The complex is particularly active towards cell lines highlighted by red squares.

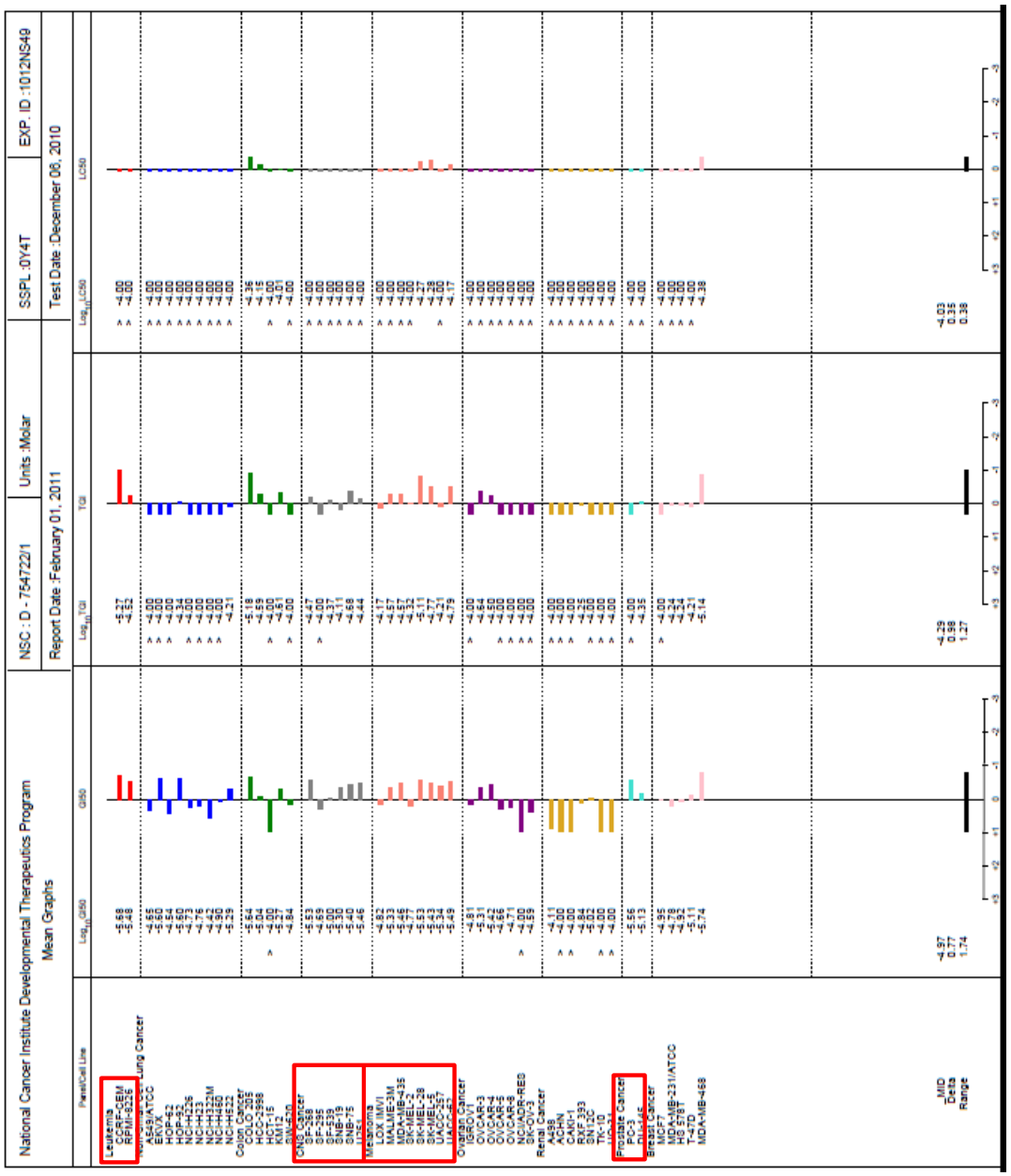

Figure 3.15. (B) Mean graph for $[(\eta^5\text{-}C_5Me_4C_6H_4C_6H_5)Ir(phen)Cl]PF_6$ (**6**·PF_6) from the National Cancer Institute Developmental Therapeutic Program. The complex is particularly active towards cell lines highlighted by red squares.

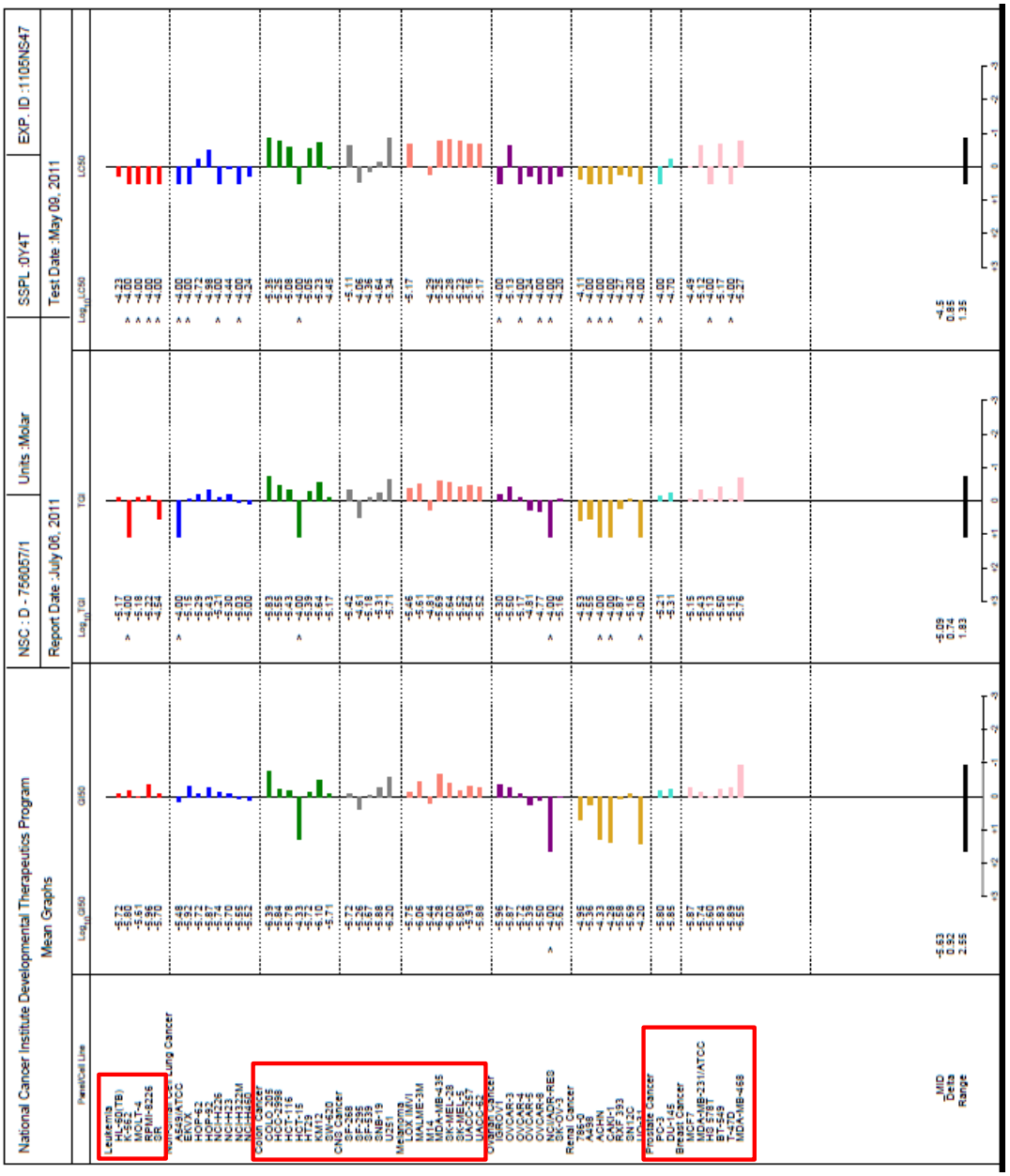

Figure 3.15. (C) Mean graph for $[(\eta^5\text{-}C_5Me_4C_6H_4C_6H_5)Ir(bpy)Cl]PF_6$ (**9**·PF_6) from the National Cancer Institute Developmental Therapeutic Program. The complex is particularly active towards cell lines highlighted by red squares.

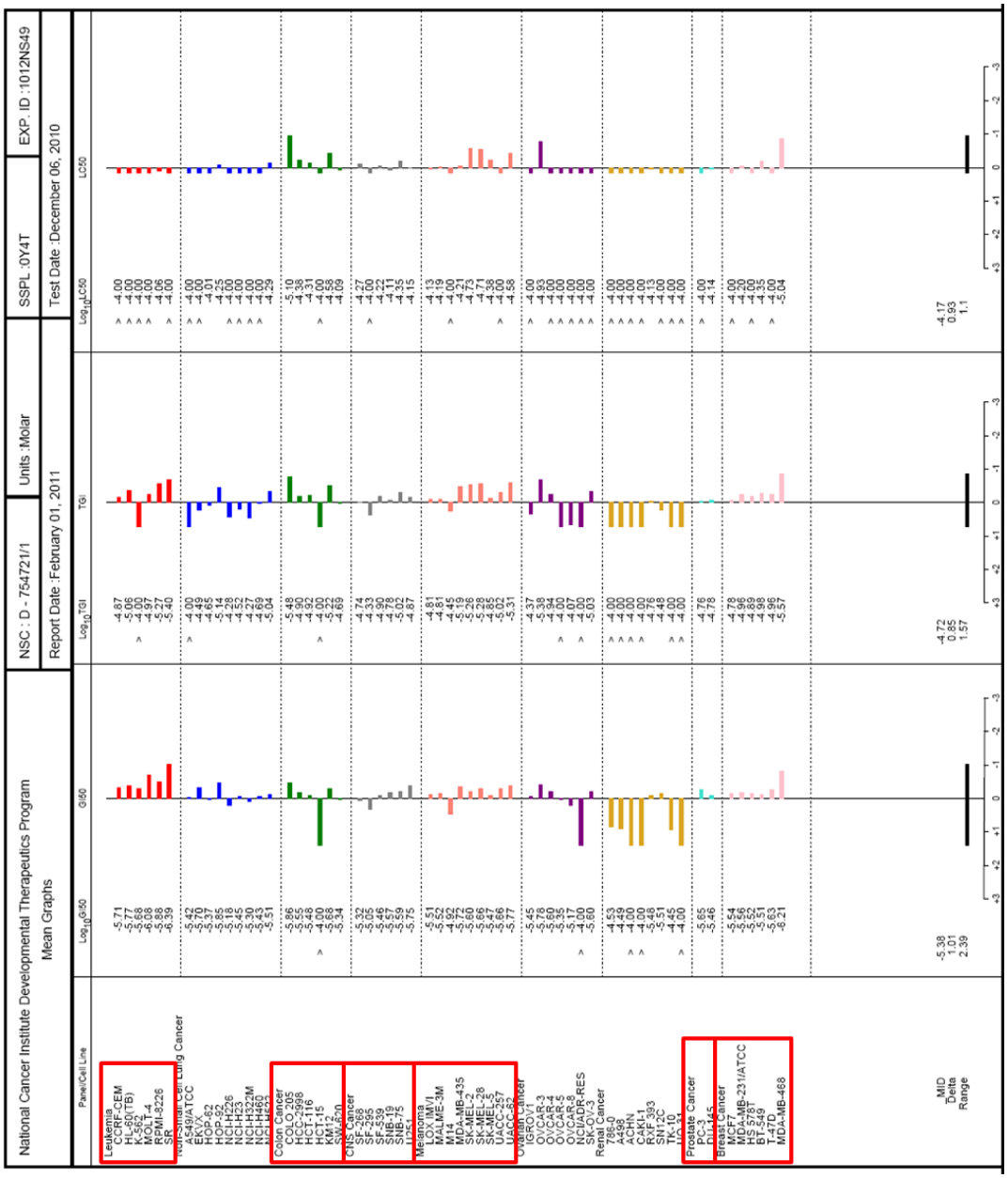

The mean GI_{50}, TGI and LC_{50} of complexes **5**·PF_6, **6**·PF_6, **9**·PF_6 and cisplatin against NCI cell lines are shown in Figure 3.16. Complex **5**·PF_6 possesses similar cytotoxic activity to that of cisplatin, whilst complex **9**·PF_6 is ca. 2.5× as potent as cisplatin toward NCI cancer cell lines. Interestingly, N,N-bound phen complex **6**·PF_6 is ca. 2 times as potent as its bpy analogue, complex **9**·PF_6. All the three iridium complexes exhibit promising cytotoxicity toward cancer cell lines.

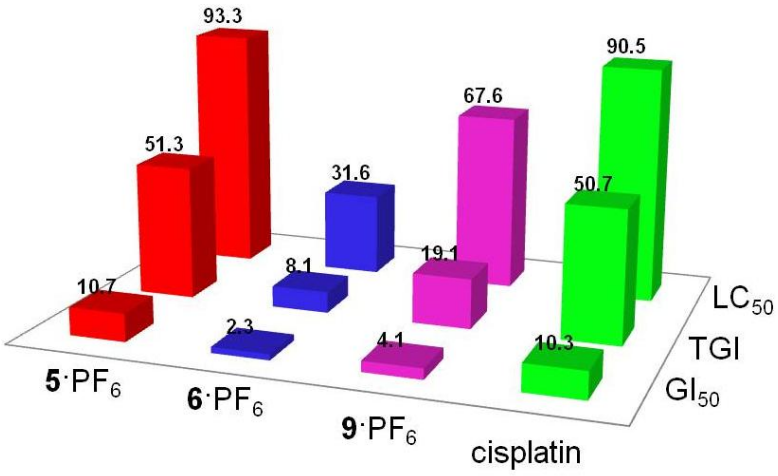

Figure 3.16. Mean graph midpoint (MG-MID) GI_{50}, TGI and LC_{50} values of complexes [(η^5-$C_5Me_4C_6H_5$)Ir(phen)Cl]PF_6 (**5**·PF_6), [(η^5-$C_5Me_4C_6H_4C_6H_5$)Ir-(phen)Cl]PF_6 (**6**·PF_6), [(η^5-$C_5Me_4C_6H_4C_6H_5$)Ir(bpy)Cl]PF_6 (**9**·PF_6), and comparison with cisplatin. Data for cisplatin are from NCI/DTP screening: October 2009, after 48 h treatment of the cells.[62]

3.3.6 Hydrophobicity (log *P*)

The octanol/water partition coefficients (log *P*) for the phen complexes [(η^5-C_5Me_5)Ir(phen)Cl]$^+$ (**4**), [(η^5-$C_5Me_4C_6H_5$)Ir(phen)Cl]$^+$ (**5**), and [(η^5-$C_5Me_4C_6H_4C_6H_5$)Ir(phen)Cl]$^+$ (**6**) were determined since lipophilicity correlates with cytotoxic potency for some reported series of metallodrugs.[63,64] The determined values are listed in Table 3.8. Addition of NaCl (200 mM) was used in order to suppress hydrolysis of the compounds, ensuring that log *P* values for the chlorido and not aqua complexes were determined. The log *P* values increase in the order **4** < **5** < **6**. Only complex **4**, containing the unsubstituted Cp* ligand, has a negative log *P* value (partitions preferentially into water, Table 3.8).

Table 3.8. log *P* Values for Complexes **4**–**6**[a]

	log *P*	
Complex	mean	SD
4	–0.82	0.01
5	0.48	0.03
6	1.11	0.17

[a]Results are the mean of three independent experiments and are expressed as mean ± SD.

3.3.7 Cell Accumulation and DNA Binding

Since increased lipophilicity has often been linked to increased cell uptake and cytotoxicity,[65,66] the accumulation and DNA binding of complexes [(η^5-C_5Me_5)Ir(phen)Cl]$^+$ (**4**), [(η^5-$C_5Me_4C_6H_5$)Ir(phen)Cl]$^+$ (**5**), and [(η^5-$C_5Me_4C_6H_4$-C_6H_5)Ir(phen)Cl]$^+$ (**6**) by A2780 ovarian cancer cells was determined after 24 h of exposure to 5 μM concentrations of the complexes. DNA from A2780 cells was isolated and the Ir content was determined. The Cp^{xbiph} complex **6** gave rise to the highest level of iridium on DNA, ca. 4× that of complex **5**, and 20× that of complex **4** (Table 3.9). Of the total Ir taken up by the cells, 7.7% for **4**, 5.5% for **5**, and 6.0% for **6** was bound to DNA.

Table 3.9. Iridium Accumulation and Binding to DNA in A2780 Human Ovarian Cancer Cells[a]

Complex	cell accumulation (ng Ir/10^6 cells)		DNA binding (ng Ir/10^6 cells)	
	mean	SD	mean	SD
4	3.9	0.2	0.3	0.04
5	23.5	3.7	1.3	0.3
6	88.8	20.0	5.3	1.6

[a] Drug-treatment period was 24 h with 5 μM Ir^{III} complexes. Each value represents the mean ± SD for two independent experiments done in triplicate.

3.3.8 Distribution of Iridium in Cell Fractions

The iridium content of the nucleus, cytosol, membrane and cytoskeleton fractions isolated from A2780 cells after 24 h of exposure to the phen complexes **4**–**6** was determined, and the results are shown in Table 3.10 and Figure 3.17. The extent of accumulation of the three complexes into the different cell fractions was similar to that observed for whole cell accumulation: **6** > **5** > **4**.

Table 3.10. Accumulation of Ir Complexes **4**–**6** into the Nucleus, Cytosol, Membrane and Cytoskeleton of A2780 Human Ovarian Cancer Cells

Complex	Accumulation (ng Ir/10^6 cells)[a]							
	nucleus		cytoskeleton		cytosol		membrane	
	mean	SD	mean	SD	mean	SD	mean	SD
4	0.4	0.04	1.1	0.3	1.1	0.2	3.8	0.4
5	1.3	0.3	1.3	0.4	3.3	0.6	16.4	3.3
6	4.8	1.6	9.9	2.7	15.7	4.3	36.4	5.0

[a] Drug-treatment period was 24 h with 5 μM Ir^{III} complexes. Each value represents the mean ± SD for six independent experiments.

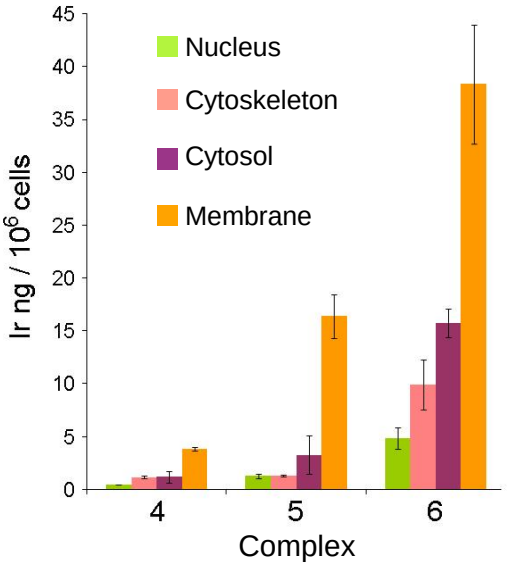

Figure 3.17. Iridium content of the nucleus, cytosol, membrane and cytoskeleton fractions (ng Ir/10^6 cells) of A2780 cells after 24 h of exposure to 5 μM **4**–**6**. Results are the mean of two independent experiments in triplicate and are expressed as mean ± SD.

The highest concentration of iridium was in the cell membrane/particulate fraction, accounting for 54% (**6**), 74% (**5**) and 59% (**4**) of the total Ir in the cell. For all complexes, the next highest concentration of Ir was in the cytosol, accounting for 24% (**6**), 15% (**5**) and 17% (**4**). For the two remaining fractions, the Ir concentration dropped significantly. For complexes **4** and **6**, the cytoskeleton was the next major compartment for Ir accumulation. The amount of Ir in the nucleus was significant and similar for all three Ir^{III} complexes: 7.2% of the total Ir for **6**, 5.8% for **5**, and 6.4% for **4**, and similar in proportion to that bound to DNA.

3.3.9 Replication Mapping of Ir−DNA Adducts

This procedure involved the extension by VentR(exo-) DNA polymerase of the 3'-end of the primer up to the metal adduct on the template strand of pSP73KB DNA linearized by HpaI restriction endonuclease. The products of the synthesis were then examined on DNA sequencing gels, and the sequence specificity of iridium adduct formation was determined to the exact base pair. *In vitro* DNA synthesis on DNA templates containing the adducts of the phen complexes **4**−**6** generated a population of DNA fragments, indicating that the adducts of these complexes effectively terminated DNA synthesis (Figure 3.18A, lanes 4−6). Complexes **4**–**6** exhibit a sequence dependence of the inhibition clearly different from that of cisplatin. The Ir compounds form more blocks on DNA for DNA polymerase than cisplatin and some of them occur at different sequences. These results are consistent with a less regular sequence specificity of complexes **4**–**6** in comparison with cisplatin. Identical patterns of blocks on DNA were observed if the template DNA was incubated with the metal complex for 8, 24 or 72 h.

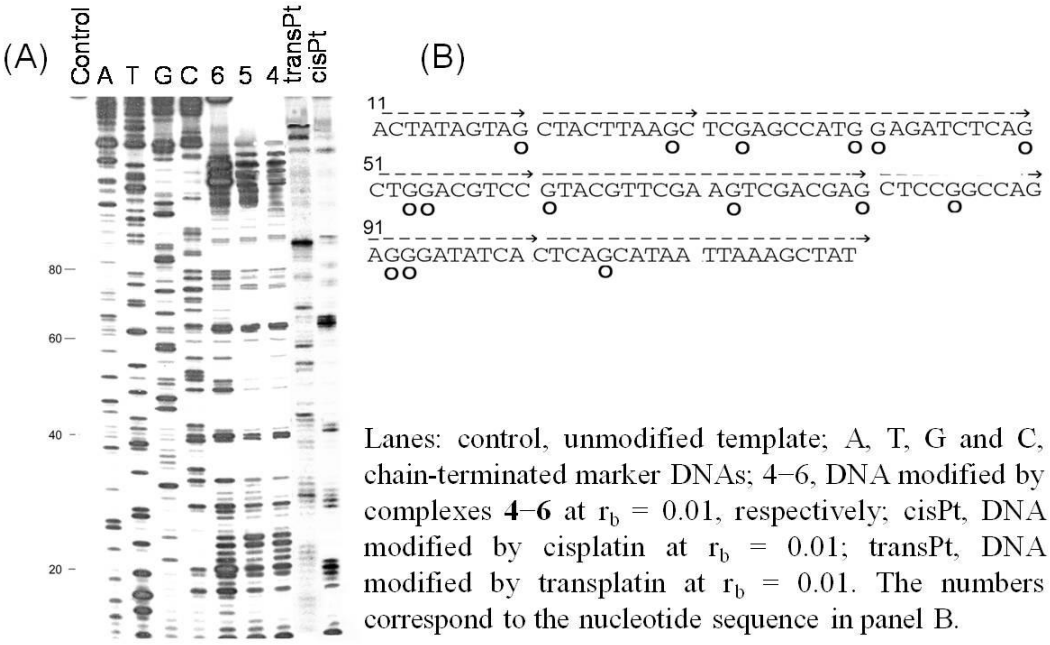

Figure 3.18. Replication mapping of Ir–DNA adducts. (A) Autoradiogram of 6% polyacrylamide/8 M urea sequencing gel showing inhibition of DNA synthesis by VentR DNA polymerase on the pSP73KB plasmid DNA linearized by HpaI restriction enzyme and subsequently modified by Ir^{III} complexes, cisplatin or transplatin. (B) Schematic diagram showing a portion of the sequence used to monitor inhibition of DNA synthesis on the template containing adducts of Ir^{III} complexes. The arrow indicates the direction of the synthesis. ○, major stop signals from panel A, lanes 4−6. The numbering of the nucleotides in this scheme corresponds to the numbering of the nucleotides in the pSP73KB nucleotide sequence map.

3.3.10 Ethidium Bromide (EtBr) Displacement

The ability of the complexes to displace the DNA intercalator EtBr from CT DNA was probed by monitoring the relative fluorescence of EtBr bound to DNA after treating the DNA with varying concentrations of **4**−**6**. Figure 3.19 shows a plot of relative fluorescence vs r_b for complexes **4**−**6**, cisplatin and monofunctional chloridobis(2-aminoethyl)amineplatinum(II) chloride ([Pt(dien)Cl]Cl).

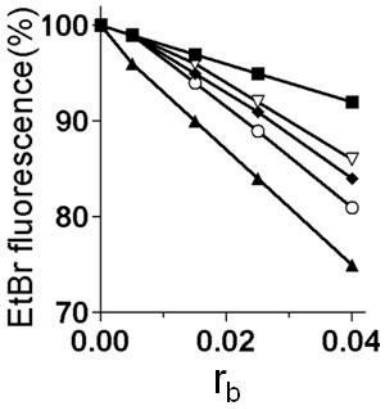

Figure 3.19. Plots showing the dependence of EtBr fluorescence on r_b for calf thymus DNA modified by Ir^{III} complexes **4**−**6**, cisplatin, and [Pt(dien)Cl]Cl in 10 mM $NaClO_4$ at 310 K for 24 h: (▽), complex **4**; (♦), complex **5**; (○), complex **6**; (▲), cisplatin; (■), [Pt(dien)Cl]Cl. Data points measured in triplicate varied on average ±3% from their mean.

The adducts of monofunctional Ir^{III} complexes competitively replaced intercalated EtBr more effectively than the adducts of monofunctional [Pt(dien)Cl]Cl, but slightly less than the adducts of bifunctional cisplatin. Notably,

the trend in ability to displace DNA intercalator EtBr from CT DNA was **6** > **5** > **4**, which correlates with their cytotoxicity (Table 3.7).

3.3.11 Viscometry

The effects of complexes **4**−**6** on the viscosity of rod-like CT DNA (0.15 mg/mL or 0.47 mM in phosphorus content) are shown in Figure 3.20. On increasing the amounts of **4**−**6** bound to DNA (in the range of r_b values of 0.005−0.04), the relative viscosity of CT DNA increased steadily; the effect follows the order **6** > **5** > **4**, which correlates with their cytotoxicity (Table 3.7) as well as with their ability to displace DNA intercalator EtBr from DNA (Figure 3.20).

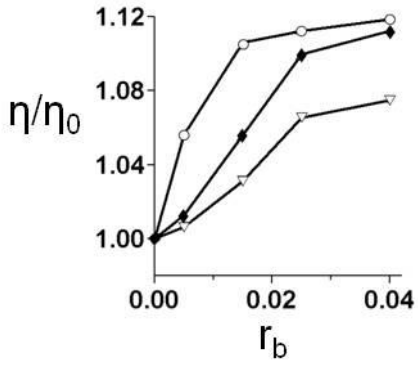

Figure 3.20. Plots showing the dependence of relative viscosity on r_b for calf thymus DNA modified by Ir^{III} complexes $[(\eta^5\text{-}C_5Me_5)Ir(phen)Cl]^+$ (**4**), $[(\eta^5\text{-}C_5Me_4C_6H_5)Ir(phen)Cl]^+$ (**5**), and $[(\eta^5\text{-}C_5Me_4C_6H_4C_6H_5)Ir(phen)Cl]^+$ (**6**). The viscosity was measured in 10 mM $NaClO_4$, pH 6 at 310 K. (▽), complex **4**; (♦), complex **5**; (○), complex **6**.

3.4 Discussion

3.4.1 X-ray Crystal Structures

A search of the Cambridge Crystallographic Database revealed that no structure of metal complexes containing the ligand Cp^{xbiph} has been reported. Complexes [(η^5-$C_5Me_4C_6H_4C_6H_5$)Ir(bpy)Cl]PF_6 (**9**·PF_6) and [(η^5-$C_5Me_4C_6H_4C_6H_5$)Ir-(bpy(OH)O)Cl] (**21**) therefore appears to be the first such structures. The crystal structures of [(η^5-$C_5Me_4C_6H_5$)Ir(phen)Cl]PF_6 (**5**·PF_6), [(η^5-$C_5Me_4C_6H_5$)Ir(bpy)Cl]-PF_6 (**8**·PF_6), [(η^5-$C_5Me_4C_6H_5$)Ir(en)Cl]BPh_4 (**11**·BPh_4), [(η^5-$C_5Me_4C_6H_5$)Ir(pico)Cl] (**13**) and [(η^5-$C_5Me_4C_6H_5$)Ir(bpy$(Me)_2$)Cl]PF_6 $(C_2H_5)_2O$ (**17**·PF_6 $(C_2H_5)_2O$) are the first examples with (η^5-$C_5Me_4C_6H_5$) (Cp^{xph}) coordinated to iridium.

The Ir–Cl bond lengths in complexes **8**·PF_6 and **9**·PF_6 (2.3859(19) and 2.3840(14) Å, respectively, Table 3.2) are almost the same, however, the Ir–Cl bond length in complex **7** is slightly longer (2.404(2) Å).[47] The twist angles in complex **9**·PF_6 are similar to those angles in Ru^{II} terphenyl arene complexes.[67] The Ir–Cl bond length in complex **13** (2.3860(10) Å) is slightly shorter than that in complex **12** [(η^5-C_5Me_5)Ir(pico)Cl] (2.3997(15) Å).[48]

The distance between Ir^{III} and the centroid of Cp ring in [(η^5-$C_5Me_4C_6H_5$)Ir(phen)Cl]PF_6 (**5**·PF_6) (1.783 Å) is similar to that in [(η^5-C_5Me_5)Ir(phen)Cl]CF_3SO_3 (1.780 Å),[68] and the Ir−Cl bond length in **5**·PF_6 (2.3891(5) Å) is similar to that in [(η^5-C_5Me_5)Ir(phen)Cl]CF_3SO_3 (2.395 Å).[68] Complexes [(η^5-C_5Me_5)Ir(bpy(OH)O)Cl] (**19**) and [(η^5-$C_5Me_4C_6H_4C_6H_5$)Ir-(bpy(OH)O)Cl] (**21**) also have similar Ir−Cl bond lengths (2.3957(11) and 2.3836(6)

Å, respectively) and similar distances from Ir^{III} to the centroid of Cp ring (1.791 and 1.793 Å, respectively). On changing Cp* to substituted Cp* ligands, no significant change is observed by DFT calculations for Ir–Cl and Ir–cyclopentadienyl ring bond distances. These results suggest that the introduction of phenyl substituent on the Cp* ring does not give rise to significant change in structure.

3.4.2 Hydrolysis and pK_a of Aqua Adducts

There are only a few previous studies of the aquation of organometallic Ir^{III} complexes.[14,69] In general, all the complexes studied in this Chapter hydrolyse rapidly. Complexes **4**, **7** and **10** containing Cp*, and **12**–**14** containing picolinate hydrolysed too rapidly to be observed by conventional UV-Vis at 288 K ($t_{1/2}$ < 1 min). Even complex $[(\eta^5\text{-}C_5Me_4C_6H_4C_6H_5)Ir(phen)Cl]^+$ (**6**), which hydrolysed the slowest of these complexes, had a calculated half life at 310 K of < 4 min (Table 3.4). These results illustrate that Ir^{III} complexes are not always inert and can be quite labile. The hydrolysis of Ir–Cl bonds in iridium complexes is strongly dependent on the coordinated ligands. These Cp^x Ir^{III} complexes undergo even faster hydrolysis than low-spin d^6 arene Ru^{II} and Os^{II} phen complexes,[35,70] more than 2 orders of magnitude faster than Os^{II} for example. The electron-donor methyl groups on the Cp ring may contribute to the fast hydrolysis. These increase the effective charge on Ir and facilitate chloride loss. This behavior is consistent with that of hexamethylbenzene Ru^{II} complexes.[71]

Previous studies on the hydrolysis rates of Os^{II} arene compounds of the type $[(\eta^6\text{-arene})Os(XY)Cl]^{n+}$ have shown that the aqueous reactivity of these complexes is highly dependent on the nature of the chelating ligand.[72,73] In particular the negatively-charged electron-donating picolinate ligand increases the rate of hydrolysis compared to complexes with diamine ligands, as seen here for complexes **12**–**14**.

The presence of bpy as a π-acceptor in complex $[(\eta^6\text{-bip})Ru(bpy)Cl]PF_6$, where bip = biphenyl, decreases the rate of hydrolysis by a factor of two compared to the en analogue.[70,74] The π-acceptor ligands bpy and phen can withdraw electron density from a metal centre, increasing the positive charge on the metal, making it less favorable for Cl^- to leave, slowing down the hydrolysis. As a result, complexes $[(\eta^5\text{-}C_5Me_4C_6H_5)Ir(phen)Cl]^+$ (**5**), $[(\eta^5\text{-}C_5Me_4C_6H_4C_6H_5)Ir(phen)Cl]^+$ (**6**), $[(\eta^5\text{-}C_5Me_4C_6H_5)Ir(bpy)Cl]^+$ (**8**), and $[(\eta^5\text{-}C_5Me_4C_6H_4C_6H_5)Ir(bpy)Cl]^+$ (**9**) containing bpy or phen as the chelating ligand hydrolysed much more slowly than the en complex **10** and pico analogues, complexes **13** and **14**. However, despite the electron withdrawing ability of bpy and phen, the hydrolysis rates of complexes $[(\eta^5\text{-}C_5Me_5)Ir(phen)Cl]^+$ (**4**) and $[(\eta^5\text{-}C_5Me_5)Ir(bpy)Cl]^+$ (**7**) are still relatively fast and appear to be controlled by the powerful electron donor Cp*.

Previous work has shown that the interaction of $[(\eta^6\text{-bip})Ru(en)Cl]^+$ with amino acids,[75] proteins,[75] peptides,[76] and DNA bases[36] involves aquation (substitution of Cl by H_2O) as the first step. The anticancer drug cisplatin also undergoes aquation prior to platination of the target site, DNA.[57,77] The equilibrium constants at 278 K for hydrolysis of complexes **4**–**6**, **7**–**9**, and **12**–**14**, decrease in the order **6** > **5** > **4**,

9 > **8** > **7**, and **14** > **12**, **13** (Table 3.4), which parallels their cytotoxicity (Table 3.7), perhaps indicating that activation by aquation is important for the mechanism of their cytotoxic action.

When the pK_a values of the aqua complexes (Table 3.5) are compared, it is evident that the presence of phenyl or biphenyl substitutent lowers the pK_a value by ca. 0.4 units consistent with withdrawal of electron density from the Ir centre. Replacement of the π-acceptor ligand bpy in aqua complex $[(\eta^5\text{-}C_5Me_5)Ir(bpy)(D_2O)]^{2+}$ (**7A**) by the chelating diamine donor en in $[(\eta^5\text{-}C_5Me_5)Ir(en)(D_2O)]^{2+}$ (**10A**), leads to a significant increase in pK_a by ca. 0.7 units, consistent with an increased electron density on the metal centre. Similarly, the replacement of the neutral chelated bpy ligand by the anionic pico ligand raises the pK_a by 1.1 units. There appears to be no correlation between the pK_a values of the aqua adducts and the cytotoxicity of these complexes. The pK_a values of the pico, en and phen aqua complexes **4A**, **6A**, **10A**, **12A**−**14A** suggest that they will be present largely as the reactive aqua adducts as opposed to the less reactive hydroxido adducts at physiological pH (7.4), whereas the pK_a values of the bpy complexes **7A**−**9A** are significantly lower, especially **8A**, and therefore most of the hydrolysed bpy complexes would be present as the hydroxo form (at pH 7.4). Despite this, complexes $[(\eta^5\text{-}C_5Me_4C_6H_5)Ir(bpy)Cl]^+$ (**8**), and $[(\eta^5\text{-}C_5Me_4C_6H_4C_6H_5)Ir(bpy)Cl]^+$ (**9**) exhibit good activity. Their reactivity would be aided by the small lowering of pH which is thought to occur in tumours.[78]

For Ru^{II} complexes which contain biphenyl as the arene and bpy as chelating ligand, loss of the arene is observed in aqueous solution.[70] In contrast, no loss of any Cp^x ligands was observed for any of the Ir^{III} complexes studied in this work.

3.4.3 Interactions with Nucleobases

DNA is often a target for cytotoxic transition metal anticancer complexes.[59,60] There is little reported work on interactions of iridium complexes with nucleobases.[79-82] In the present study, the reactions of complexes **4**−**14**, and aqua complex $[(\eta^5\text{-}C_5Me_4C_6H_5)Ir(phen)(D_2O)]^{2+}$ (**5A**) with 9-ethylguanine (9-EtG) and 9-ethyladenine (9-EtA) were investigated, Table 3.6. Complexes **4**−**11** and **5A** containing a neutral N,N- chelating ligand all bind selectively to 9-EtG compared to 9-EtA, with which no reaction was observed after 24 h. This result is consistent with the replication mapping experiments (Figure 3.18) which show that G residues are the preferential binding sites on polymeric DNA modified with complexes **4**−**6**. The selectivity in nucleobase binding can be rationalised in terms of H-bonding, non-bonding repulsive interactions between the chelating ligand and nucleobase substituents, and the electronic properties of the various nucleobase coordination sites.[72] Previous studies of Ru−N7 guanine adducts have revealed a strong H-bonding interaction between one en NH and G C6O.[36] This may explain the strong affinity of 9-EtG for the Ir^{III} en complexes **10** and **11**. A phenanthroline ligand cannot provide a donor NH group, but instead the interaction with G C6O may be stabilised by a C−H H-bond similar to that observed in a bipyridine complex of

Ru^{II}.[70] This possibility was indicated by the DFT optimized structure of the 9-EtG adduct of **6** (Figure 3.21).

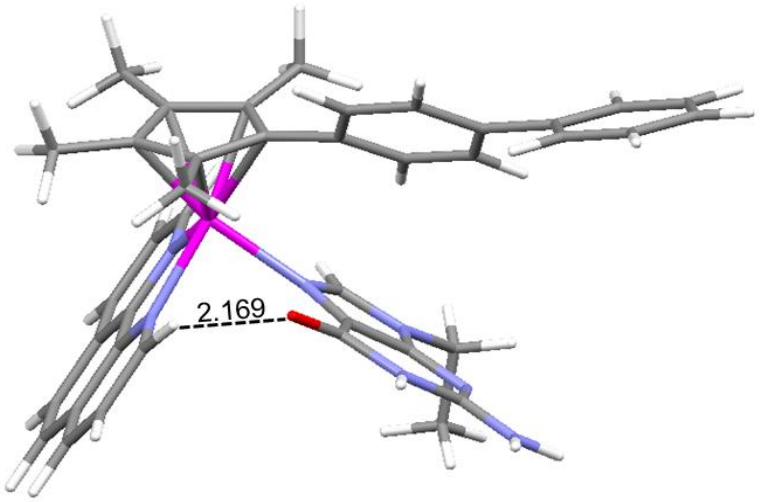

Figure 3.21. Optimized geometry of complex $[(\eta^5\text{-}C_5Me_4C_6H_4C_6H_5)Ir(phen)(9\text{-EtG})]^{2+}$ (**6G**), where phen appears to interact with 9-EtG through a C6O···H−C H-bond (2.169 Å).

Complexes **4**−**11** containing an N,N-chelating ligand did not react with 9-EtA, most likely due to the steric hindrance of the NH_2 group on the 6-position of the adenine ring. Compared to complexes containing an N,N-chelating ligand, compounds **12**−**14** which contain the N,O-chelating ligand pico, bind significantly (70−100%) to both nucleobases, see Table 3.6. These picolinate Ir^{III} adducts of complexes **12**, **13** and **14** with 9-EtA (**12Ad**, **13Ad**, and **14Ad**, respectively) can be

stabilised by hydrogen bonding between the NH_2 group of adenine and a carboxylate oxygen of the picolinate ligand.[83]

As expected, the aqua complex $[(\eta^5\text{-}C_5Me_4C_6H_5)Ir(phen)(D_2O)]^{2+}$ (**5A**) reacted to a greater extent with 9-EtG compared to the chlorido complex **5**, see Table 3.6, consistent with the increased reactivity of aqua adducts compared to their chlorido forms,[56] but the selectivity for G versus A was the same.

3.4.4 Hydrophobicity (log *P*) and Cell Accumulation

log *P* values for octanol/water partition provide a measure of hydrophobicity which is often a factor relevant for cell uptake and anticancer activity. For several classes of metallo-anticancer complexes, a correlation between increased hydrophobicity and increased cytotoxic activity has been reported.[63-66]

In this study, as expected, the log *P* values (Table 3.8) and hydrophobicity increase with increasing size of the substituted Cp* ligand. Additionally, the hydrophobicity, cancer cell activity, and cell accumulation correlate significantly, following the order **6** > **5** > **4**. Complex $[(\eta^5\text{-}C_5Me_5)Ir(phen)Cl]^+$ (**4**) is the least hydrophobic, the least cytotoxic, and the least taken up by the cells, whereas complex $[(\eta^5\text{-}C_5Me_4C_6H_4C_6H_5)Ir(phen)Cl]^+$ (**6**) displays the highest hydrophobicity, is the most cytotoxic, and the most taken up by the cells. These data suggest that in the ovarian A2780 cancer cell line, the log *P* value is a useful parameter for predicting the cytotoxicity of this class of iridium complexes. These data also show that using more extended coordinated Cp^x ligands such as tetramethyl(biphenyl)-

cyclopentadienyl (Cp^{xbiph}) gives rise to an increased hydrophobicity leading to higher cellular uptake and higher cytotoxicity.

3.4.5 Distribution of Iridium in Cells

The accumulation of the three phen complexes $[(\eta^5\text{-}C_5Me_5)Ir(phen)Cl]^+$ (**4**), $[(\eta^5\text{-}C_5Me_4C_6H_5)Ir(phen)Cl]^+$ (**5**), and $[(\eta^5\text{-}C_5Me_4C_6H_4C_6H_5)Ir(phen)Cl]^+$ (**6**) into the different cell fractions was studied. A significant proportion of the total iridium (54−74%) was in the cell membrane fraction, see Figure 3.17. This may be related not only to Ir being transported into the cytoplasm but also to Ir being exported by cells. For all complexes, the next highest concentration of iridium was found in the cytosol showing that passage through the outer membrane readily occurs.

Although the lowest proportion of iridium was found in the nucleus, especially for complexes **4** and **6**, it is notable that there is a correlation between nucleus accumulation and cytotoxicity of the complexes, both of which follow the order **6** > **5** > **4**, suggesting that penetrating the nucleus and binding to nuclear DNA may provide an important contribution to the mechanism of cytotoxicity. A similar relationship between nucleus accumulation and cytotoxicity was observed for Os^{II} arene complexes.[84]

3.4.6 DNA Binding in A2780 Human Ovarian Cancer Cells

The amount of iridium found on the DNA of A2780 cells (Table 3.9) incubated with the complexes for 24 h follows the order **6** > **5** > **4**, which correlates with their cytotoxicity, hydrophobicity (log *P*), and cellular accumulation (Table 3.9), and is similar to the total accumulation by cell nuclei. The extent of iridium binding of **4**−**6** to DNA, 5.5−7.7% of the total iridium taken up by the cells, is higher than that reported for cisplatin (~1%)[85] and Os^{II} arene complexes.[84] DNA may therefore be a potential target for these cytotoxic iridium complexes, although the possibility that nuclear DNA may not be the only target cannot be ruled out.

3.4.7 EtBr Displacement and Viscometry

The fluorescent probe EtBr can be used to distinguish between intercalating and nonintercalating ligands.[86-88] Viscosity measurements are also useful for probing the nature of DNA interactions since viscosity is sensitive to alterations in DNA length. For instance, complexes or ligands that intercalate cause an increase in overall DNA contour length due to the increase in separation of base pairs at the intercalation sites, which leads to an increase in viscosity of DNA solutions. On the other hand, drug molecules which bind in DNA grooves cause less pronounced changes in the viscosity of DNA solutions.[89]

Modification of CT DNA by complexes $[(\eta^5\text{-}C_5Me_5)Ir(phen)Cl]^+$ (**4**), $[(\eta^5\text{-}C_5Me_4C_6H_5)Ir(phen)Cl]^+$ (**5**), and $[(\eta^5\text{-}C_5Me_4C_6H_4C_6H_5)Ir(phen)Cl]^+$ (**6**) resulted in a decrease of EtBr fluorescence intensity (Figure 3.19) and an increase in the

relative viscosity of CT DNA (Figure 3.20) in the same order **6** > **5** > **4**, which correlates with their cytotoxicity. These results indicate that addition of phenyl substituents to the Cp* ring in these iridium complexes enhances the intercalative ability into DNA. Dual-mode intercalation/G N7 coordination DNA binding may therefore play an important role in the cytotoxicity of these Ir^{III} complexes. This observation parallels that of Ru^{II} and Os^{II} arene complexes for which extended arenes can also intercalate and increase the potency of the complexes.[37,90] For example, the Ru^{II} anticancer complex $[(\eta^6\text{-}p\text{-terp})Ru(en)Cl]^+$ (where *p*-terp = *para*-terphenyl, a similar arene ligand to Cp^{xbiph}) also exhibits combined intercalative and monofunctional (coordination) binding to DNA.[67]

3.4.8 Cytotoxicity

Complexes $[(\eta^5\text{-}C_5Me_5)Ir(phen)Cl]Cl$ (**4**·Cl), $[(\eta^5\text{-}C_5Me_5)Ir(bpy)Cl]Cl$ (**7**·Cl), $[(\eta^5\text{-}C_5Me_5)Ir(en)Cl]PF_6$ (**10**·PF_6), $[(\eta^5\text{-}C_5Me_5)Ir(pico)]$ (**12**) and $[(\eta^5\text{-}C_5Me_5)Ir(bpy(Me)_2)Cl]PF_6$ (**16**·PF_6) containing Cp* were non-toxic (IC_{50} > 100 μM) toward the human ovarian A2780 cancer cell line (Table 3.7). The cytotoxicity of complexes $[(\eta^5\text{-}C_5Me_4C_6H_5)Ir(phen)Cl]PF_6$ (**5**·PF_6) and $[(\eta^5\text{-}C_5Me_4C_6H_4C_6H_5)Ir(phen)Cl]PF_6$ (**6**·PF_6) containing phenyl and biphenyl substituents, respectively, on the tetramethylcyclopentadienyl ring increases dramatically compared to the parent Cp* complex **4**. Complex **6** containing Cp^{xbiph} is ca. twice as potent towards A2780 human ovarian cancer cells as the anticancer drug cisplatin (Table 3.7). In addition, complexes $[(\eta^5\text{-}C_5Me_4C_6H_5)Ir(phen)Cl]PF_6$ (**5**·PF_6), $[(\eta^5\text{-}C_5Me_4C_6H_4C_6H_5)Ir$-

(phen)Cl]PF_6 (**6**·PF_6) and [(η^5-$C_5Me_4C_6H_4C_6H_5$)Ir(bpy)Cl]PF_6 (**9**·PF_6) show potent cytotoxicity toward NCI 60 cancer cell lines and have a broad spectrum of activity (Figures 3.15 and 3.16). The introduction of phenyl and biphenyl substituents also resulted in significant increases in activity for all other complexes studied in this Chapter, suggesting that the phenyl groups play a crucial role in the mechanism of action. This is consistent with our previous observations that the cytotoxicity of η^6-arene Ru^{II} compounds increases with the size of the arene ring system in the order benzene < *p*-cymene < biphenyl < dihydroanthracene < tetrahydroanthracene.[11] The increase in potency on addition of phenyl substituents to the Cp ring, by about an order of magnitude for each of the additions (from **4** to **5** to **6**) is more dramatic than in the case of ruthenium arene ethylenediamine complexes.[67,91] For these iridium complexes, the phenyl substitutents not only enhance lipophilicity and cell accumulation, but also introduce an additional mode of DNA interaction (intercalation).

Both complexes [(η^5-$C_5Me_4C_6H_5$)Ir(bpy)Cl]$^+$ (**8**) and [(η^5-$C_5Me_4C_6H_5$)Ir(pico)Cl] (**13**) contain Cp^{xph}, however, **8** exhibits activity towards A2780 cancer cells whereas **13** is inactive, which suggests that the chelating ligand also plays a role. Replacement of neutral bpy by anionic pico as the chelating ligand increases the rate and extent of hydrolysis, the pK_a of the aqua complex (from 6.31 to 7.75 for ring = Cp^{xph}, Table 3.5), and changes the nucleobase specificity. For complexes **7**−**9** containing neutral bpy, there is exclusive binding to 9-EtG. In contrast, complexes **12**−**14** containing anionic pico bind strongly to both 9-EtG and 9-EtA. However the picolinate complexes have lower cytotoxicity than the N,N-bound phen or bpy

complexes. The reasons for the low cytotoxicity are not clear. These complexes may be too reactive with components of the cell culture medium and/or the cells before they reach target sites, thus effectively being deactivated. For example, the amino acids (methionine or cysteine) or tripeptides can form S-bound adducts with Ir^{III} Cp* complexes.[79]

The inactivity of Cp* complexes [(η^5-C_5Me_5)Ir(phen)Cl]Cl (**4**·Cl) and [(η^5-C_5Me_5)Ir(bpy)Cl]Cl (**7**·Cl), may be correlated with poor cellular accumulation and lack of intercalation into DNA. These factors may also explain the inactivity of [(η^5-C_5Me_5)Ir(en)Cl]PF_6 (**10**·PF_6). Interestingly some ruthenium[92] and osmium[35] arene complexes containing phen or bpy derivatives also show poor or no activity against A2780 cells.

Unlike [(η^5-C_5Me_5)Ir(bpy)Cl]Cl (**7**·Cl), which is inactive toward the human ovarian A2780 cancer cell line, Cp* complex [(η^5-C_5Me_5)Ir(bpy(OH)O)Cl] (**19**) showed moderate activity toward A2780 cell line (Table 3.7). This result is consistent with previous reports on bipyridine and bipyridinediol Ru^{II} arene complexes.[70] Complexes **22**−**24** containing dpq or dppz chelating ligand showed potent cytotoxicity toward A2780 cancer cell line, which may benefit from the strong intercalation of the chelating ligands.[26] The potent cytotoxicity of complexes [(η^5-C_5Me_5)Ir(azpy-NMe_2)Cl]PF_6 (**26**·PF_6) and [(η^5-$C_5Me_4C_6H_5$)Ir(azpy-NMe_2)Cl]-PF_6 (**27**·PF_6) containing azpy-NMe_2 chelating ligand may be related to redox mechanisms.[93]

3.5 Conclusions

The goal of the present study was to explore the rational design of organometallic half-sandwich Ir^{III} anticancer complexes based on knowledge of the features which contribute to the activity of half-sandwich Ru^{II} and Os^{II} arene complexes.[3-8,94-96] The biological and medicinal chemistry of iridium complexes has been little explored previously,[16-28] perhaps because it is often assumed that low-spin $5d^6$ Ir^{III} complexes are highly kinetically inert.[14,15,33,34] The study in this Chapter shows that this is not always the case. Cyclopentadienyl ligands, whilst stabilising Ir^{III}, can confer kinetic lability on trans monodentate ligands such as chloride. Moreover phenyl substituents on the Cp* ring as in Cp^{xph} and Cp^{xbiph} can have a major effect on the chemical and biological behaviour of $[(\eta^5\text{-}Cp^x)Ir(XY)Cl]^{0/+}$ complexes. This appears to be the first time that Cp^{xph} and Cp^{xbiph} ligands have been used in iridium complexes.

The introduction of a phenyl substituent into the Cp* ring switches on cancer cell cytotoxicity. For example, complex $[(\eta^5\text{-}C_5Me_4C_6H_5)Ir(phen)Cl]^+$ (**5**) is more than one order of magnitude more potent than the Cp* complex $[(\eta^5\text{-}C_5Me_5)Ir(phen)Cl]^+$ (**4**), and the biphenyl complex $[(\eta^5\text{-}C_5Me_4C_6H_4C_6H_5)Ir(phen)Cl]^+$ (**6**) is more than 2 orders of magnitude more potent than complex **4**, and twice as potent as cisplatin in the same cell line. This increase in activity parallels the increase in hydrophobicity, increase in cell accumulation and DNA binding. Complexes **5** and **6** can exhibit dual mode binding to DNA: iridium binding to G N7 accompanied by intercalation of the phenyl substituents on the Cp* ring. On the other hand, the chelating ligand

can also play an important role in the anticancer activity. For example, the pico complex [(η^5-$C_5Me_4C_6H_5$)Ir(pico)Cl] (**13**) shows no activity toward the A2780 cell line while the bpy analogue complex **8** [(η^5-$C_5Me_4C_6H_5$)Ir(bpy)Cl]$^+$, shows good activity, and the bpy complex [(η^5-$C_5Me_4C_6H_4C_6H_5$)Ir(bpy)Cl]$^+$ (**9**) is more than one order of magnitude more potent than the pico analogue, complex **14** [(η^5-$C_5Me_4C_6H_4C_6H_5$)Ir(pico)Cl].

Figure 3.22A provides an overview of the relationships between cancer cell cytotoxicity, intercalative ability, cellular accumulation, hydrophobicity, and rates and extents of hydrolysis for the phen complexes **4**–**6**. Figure 3.22B shows how the chelating and Cp^x ligands affect the anticancer activity, nucleobase binding, and aqueous chemistry of the bpy complexes **7**–**9** and pico complexes **12**–**14**. These [(η^5-Cp^x)Ir(XY)Cl]$^{0/+}$ complexes hydrolyse rapidly (the slowest half-life < 4 min at 310 K), and the nature of the cyclopentadienyl and chelating ligands significantly influence their aqueous chemistry. In general, the introduction of phenyl and biphenyl Cp* ring substituents slows down the hydrolysis rate, increases the extent of hydrolysis, and increases the acidity of the respective aqua species. The chelating ligand appears to determine the selectivity of nucleobase binding. The complexes containing N,N-chelating ligands discriminate strongly between the purine nucleobases guanine and adenine, showing little binding to the latter for either for Cp*, Cp^{xph} or Cp^{xbiph} complexes. In contrast, complexes **12**−**14** containing the N,O-chelating ligand picolinate bind both to 9-EtG and 9-EtA.

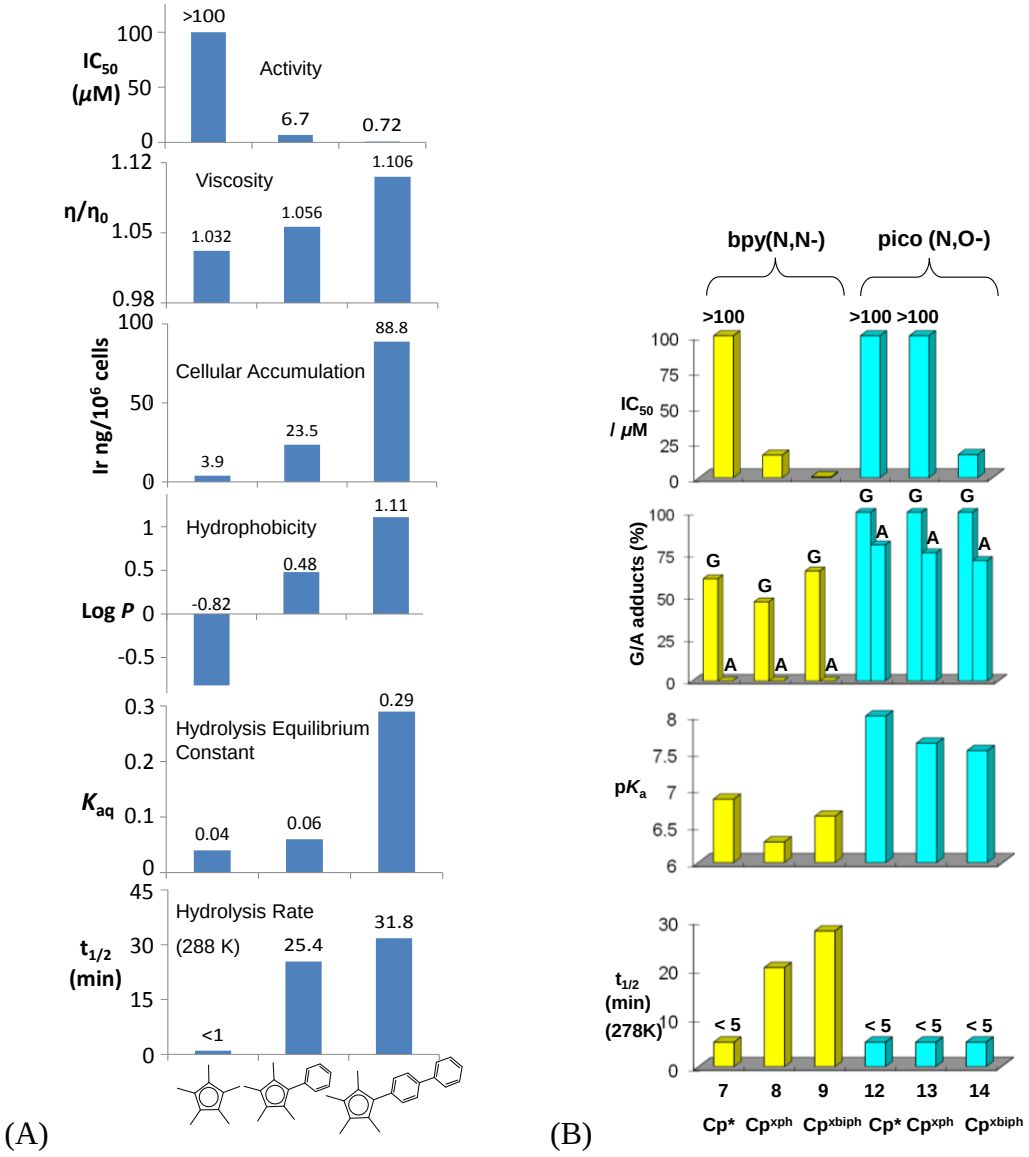

Figure 3.22. (A) Bar charts illustrating the relationship between cytotoxicity toward human cancer cells, intercalative ability, cellular accumulation, hydrophobicity, and rates (288 K) and equilibrium constants (278 K) of hydrolysis for iridium complexes $[(\eta^5\text{-Cp}^x)\text{Ir(phen)Cl}]^+$ containing Cp^x = Cp* (**4**), Cp^{xph} (**5**), and Cp^{xbiph} (**6**). (B) Bar charts illustrating the influence of N,N-, N,O-chelating ligands and Cp^x ligands on the cytotoxicity, nucleobase binding, hydrolysis and pK_a of the aqua adducts of the bpy complexes **7**–**9**, and pico complexes **12**–**14**.

The work in this Chapter demonstrates that rational chemical design can be applied to Ir^{III} complexes to achieve potent cancer cell cytotoxicity. It is notable that Cp ring substituents can also play a major role in controlling the chemical and biological properties of ferrocenyl and titanocenyl anticancer complexes.[97,98] In general, organometallic complexes offer much promise for the design of novel therapeutic agents.[3-8,94,95]

3.6 References

(1) Kelland, L. *Nat. Rev. Cancer* **2007**, *7*, 573-584.

(2) Wang, D.; Lippard, S. J. *Nat. Rev. Drug Discovery* **2005**, *4*, 307-320.

(3) Halpern, J. *Pure Appl. Chem.* **2001**, *73*, 209-220.

(4) Fish, R. H.; Jaouen, G. *Organometallics* **2003**, *22*, 2166-2177.

(5) *Medicinal Organometallic Chemistry (Topics in Organometallic Chemistry)*, 1st ed.; Jaouen, G.; Metzler-Nolte, N., Eds.; Springer-Verlag: Heidelberg, Germany, 2010; Vol. 32.

(6) Hartinger, C. G.; Dyson, P. J. *Chem. Soc. Rev.* **2009**, *38*, 391-401.

(7) Yan, Y. K.; Melchart, M.; Habtemariam, A.; Sadler, P. J. *Chem. Commun.* **2005**, 4764-4776.

(8) Suss-Fink, G. *Dalton Trans.* **2010**, *39*, 1673-1688.

(9) Mendoza-Ferri, M. G.; Hartinger, C. G.; Mendoza, M. A.; Groessl, M.; Egger, A. E.; Eichinger, R. E.; Mangrum, J. B.; Farrell, N. P.; Maruszak, M.; Bednarski, P. J.; Klein, F.; Jakupec, M. A.; Nazarov, A. A.; Severin, K.; Keppler, B. K. *J. Med. Chem.* **2009**, *52*, 916-925.

(10) Loughrey, B. T.; Healy, P. C.; Parsons, P. G.; Williams, M. L. *Inorg. Chem.* **2008**, *47*, 8589-8591.

(11) Aird, R. E.; Cummings, J.; Ritchie, A. A.; Muir, M.; Morris, R. E.; Chen, H.; Sadler, P. J.; Jodrell, D. I. *Br. J. Cancer* **2002**, *86*, 1652-1657.

(12) Tobe, M. L.; Burgess, J. *Inorganic Reaction Mechanisms*; Addison Wesley Longman Inc.: Essex, 1999.

(13) Lay, P. A.; Harman, W. D. In *Advances in Inorganic Chemistry*; Sykes, A. G., Ed.; Academic Press: 1991; 37, pp 219-379.

(14) Helm, L.; Merbach, A. E. *Coord. Chem. Rev.* **1999**, *187*, 151-181.

(15) Richens, D. T. *Chem. Rev.* **2005**, *105*, 1961-2002.

(16) Cleare, M. J. *Coord. Chem. Rev.* **1974**, *12*, 349-405.

(17) Sava, G.; Giraldi, T.; Mestroni, G.; Zassinovich, G. *Chem. Biol. Interact.* **1983**, *45*, 1-6.

(18) Sava, G.; Zorzet, S.; Perissin, L.; Mestroni, G.; Zassinovich, G.; Bontempi, A. *Inorg. Chim. Acta* **1987**, *137*, 69-71.

(19) Giraldi, T.; Sava, G.; Mestroni, G.; Zassinovich, G.; Stolfa, D. *Chem. Biol. Interact.* **1978**, *22*, 231-238.

(20) Köpf-Maier, P. *Eur. J. Clin. Pharmacol.* **1994**, *47*, 1-16.

(21) Casini, A.; Edafe, F.; Erlandsson, M.; Gonsalvi, L.; Ciancetta, A.; Re, N.; Ienco, A.; Messori, L.; Peruzzini, M.; Dyson, P. J. *Dalton Trans.* **2010**, *39*, 5556-5563.

(22) Amouri, H.; Moussa, J.; Renfrew, A. K.; Dyson, P. J.; Rager, M. N.; Chamoreau, L.-M. *Angew. Chem., Int. Ed.* **2010**, *49*, 7530-7533.

(23) Ali Nazif, M.; Bangert, J.-A.; Ott, I.; Gust, R.; Stoll, R.; Sheldrick, W. S. *J. Inorg. Biochem.* **2009**, *103*, 1405-1414.

(24) Wirth, S.; Rohbogner, C.; Cieslak, M.; Kazmierczak-Baranska, J.; Donevski, S.; Nawrot, B.; Lorenz, I.-P. *J. Biol. Inorg. Chem.* **2010**, *15*, 429-440.

(25) Gras, M.; Therrien, B.; Süss-Fink, G.; Casini, A.; Edafe, F.; Dyson, P. J. *J. Organomet. Chem.* **2010**, *695*, 1119-1125.

(26) Schäfer, S.; Sheldrick, W. S. *J. Organomet. Chem.* **2007**, *692*, 1300-1309.

(27) Kokoschka, M.; Bangert, J. A.; Stoll, R.; Sheldrick, W. S. *Eur. J. Inorg. Chem.* **2010**, 1507-1515.

(28) Hartinger, C. G. *Angew. Chem., Int. Ed.* **2010**, *49*, 8304-8305.

(29) Leung, S.-K.; Kwok, K. Y.; Zhang, K. Y.; Lo, K. K.-W. *Inorg. Chem.* **2010**, *49*, 4984-4995.

(30) Shao, F.; Barton, J. K. *J. Am. Chem. Soc.* **2007**, *129*, 14733-14738.

(31) Sliwinska, U.; Pruchnik, F. P.; Ulaszewski, S.; Latocha, M.; Nawrocka-Musial, D. *Polyhedron* **2010**, *29*, 1653-1659.

(32) Wilbuer, A.; Vlecken, D. H.; Schmitz, D. J.; Kräling, K.; Harms, K.; Bagowski, C. P.; Meggers, E. *Angew. Chem., Int. Ed.* **2010**, *49*, 3839-3842.

(33) Messori, L.; Marcon, G.; Orioli, P.; Fontani, M.; Zanello, P.; Bergamo, A.; Sava, G.; Mura, P. *J. Inorg. Biochem.* **2003**, *95*, 37-46.

(34) Marcon, G.; Casini, A.; Mura, P.; Messori, L.; Bergamo, A.; Orioli, P. *Metal-Based Drugs* **2000**, *7*, 195-200.

(35) Peacock, A. F. A.; Habtemariam, A.; Moggach, S. A.; Prescimone, A.; Parsons, S.; Sadler, P. J. *Inorg. Chem.* **2007**, *46*, 4049-4059.

(36) Chen, H.; Parkinson, J. A.; Morris, R. E.; Sadler, P. J. *J. Am. Chem. Soc.* **2003**, *125*, 173-186.

(37) Liu, H.-K.; Berners-Price, S. J.; Wang, F.; Parkinson, J. A.; Xu, J.; Bella, J.; Sadler, P. J. *Angew. Chem., Int. Ed.* **2006**, *45*, 8153-8156.

(38) Liu, H.-K.; Parkinson, J. A.; Bella, J.; Wang, F.; Sadler, P. J. *Chem. Sci.*, **2010**, 258-270.

(39) Liu, S.; Rebros, M.; Stephens, G.; Marr, A. C. *Chem. Commun.* **2009**, 2308-2310.

(40) Hanasaka, F.; Fujita, K.-i.; Yamaguchi, R. *Organometallics* **2006**, *25*, 4643-4647.

(41) Ito, M.; Endo, Y.; Tejima, N.; Ikariya, T. *Organometallics* **2010**, *29*, 2397-2399.

(42) Kohl, G.; Pritzkow, H.; Enders, M. *Eur. J. Inorg. Chem.* **2008**, 4230-4235.

(43) Pontes da Costa, A.; Viciano, M.; Sanaú, M.; Merino, S.; Tejeda, J.; Peris, E.; Royo, B. *Organometallics* **2008**, *27*, 1305-1309.

(44) White, C. Y., A.; Maitlis, P. M. *Inorg. Chem.* **1992**, *29*, 228-234.

(45) Delgadillo, A.; Romo, P.; Leiva, A. M.; Loeb, B. *Helv. Chim. Acta* **2003**, *86*, 2110-2120.

(46) Dickeson, J.; Summers, L. *Aust. J. Chem.* **1970**, *23*, 1023-1027.

(47) Youinou, M.-T.; Ziessel, R. *J. Organomet. Chem.* **1989**, *363*, 197-208.

(48) Gorol, M.; Roesky, H. W.; Noltemeyer, M.; Schmidt, H.-G. *Eur. J. Inorg. Chem.* **2005**, 4840-4844.

(49) Sheldrick, G. M. *Acta Crystallogr.* **1990**, *A46*, 467-473.

(50) Sheldrick, G. M. *SHELXL-97*; University of Göttingen: Göttingen, Germany, 1997.

(51) Adamo, C.; Barone, V. *J. Chem. Phys.* **1999**, *110*, 6158-6170.

(52) Novakova, O.; Kasparkova, J.; Vrana, O.; van Vliet, P. M.; Reedijk, J.; Brabec, V. *Biochemistry* **1995**, *34*, 12369-12378.

(53) Butour, J.-L.; Macquet, J.-P. *Eur. J. Biochem.* **1977**, *78*, 455-463.

(54) Butour, J.-L.; Alvinerie, P.; Souchard, J.-P.; Colson, P.; Houssier, C.; Johnson, N. P. *Eur. J. Biochem.* **1991**, *202*, 975-980.

(55) Pizarro, A. M.; Habtemariam, A.; Sadler, P. J. In *Medicinal Organometallic Chemistry (Topics in Organometallic Chemistry)*, 1st ed.; Jaouen, G., Metzler-Nolte, N., Ed.; Springer-Verlag: Heidelberg, Germany, 2010; 32, pp 21-56.

(56) Hohmann, H.; Hellquist, B.; van Eldik, R. *Inorg. Chem.* **1992**, *31*, 345-351.

(57) Martin, R. B. In *Cisplatin: Chemistry and Biochemistry of a Leading Anticancer Drug*; Lippert, B., Ed.; VHCA & Wiley-VCH: Zürich, Switzerland, 1999, pp 181-205.

(58) Krezel, A.; Bal, W. *J. Inorg. Biochem.* **2004**, *98*, 161-166.

(59) Zhang, C. X.; Lippard, S. J. *Curr. Opin. Chem. Biol.* **2003**, *7*, 481-489.

(60) Deubel, D. V.; Lau, J. K.-C. *Chem. Commun.* **2006**, 2451-2453.

(61) http://dtp.nci.nih.gov/branches/btb/ivclsp.html (accessed on 16 September 2011)

(62) Görmen, M.; Pigeon, P.; Top, S.; Hillard, E. A.; Huché, M.; Hartinger, C. G.; de Montigny, F.; Plamont, M.-A.; Vessières, A.; Jaouen, G. *Chem. Med. Chem.* **2010**, *5*, 2039-2050.

(63) Mendoza-Ferri, M.-G.; Hartinger, C. G.; Eichinger, R. E.; Stolyarova, N.; Severin, K.; Jakupec, M. A.; Nazarov, A. A.; Keppler, B. K. *Organometallics* **2008**, *27*, 2405-2407.

(64) Gramatica, P.; Papa, E.; Luini, M.; Monti, E.; Gariboldi, M.; Ravera, M.; Gabano, E.; Gaviglio, L.; Osella, D. *J. Biol. Inorg. Chem.* **2010**, *15*, 1157-1169.

(65) Loh, S. Y.; Mistry, P.; Kelland, L. R.; Abel, G.; Harrap, K. R. *Br. J. Cancer* **1992**, *66*, 1109-1115.

(66) Oldfield, S. P.; Hall, M. D.; Platts, J. A. *J. Med. Chem.* **2007**, *50*, 5227-5237.

(67) Bugarcic, T.; Nováková, O.; Halámiková, A.; Zerzánková, L.; Vrána, O. i.; Kašpárková, J.; Habtemariam, A.; Parsons, S.; Sadler, P. J.; Brabec, V. *J. Med. Chem.* **2008**, *51*, 5310-5319.

(68) Scharwitz, M.; Schäfer, S.; Almsick, T. v.; Sheldrick, W. S. *Acta Crystallogr.* **2007**, *E63*, m1111-m1113.

(69) Koelle, U. *Coord. Chem. Rev.* **1994**, *135-136*, 623-650.

(70) Bugarcic, T.; Habtemariam, A.; Stepankova, J.; Heringova, P.; Kasparkova, J.; Deeth, R. J.; Johnstone, R. D. L.; Prescimone, A.; Parkin, A.; Parsons, S.; Brabec, V.; Sadler, P. J. *Inorg. Chem.* **2008**, *47*, 11470-11486.

(71) Wang, F.; Habtemariam, A.; van der Geer, E. P. L.; Fernández, R.; Melchart, M.; Deeth, R. J.; Aird, R.; Guichard, S.; Fabbiani, F. P. A.; Lozano-Casal, P.; Oswald, I. D. H.; Jodrell, D. I.; Parsons, S.; Sadler, P. J. *Proc. Natl. Acad. Sci. U. S. A.* **2005**, *102*, 18269-18274.

(72) Peacock, A. F. A.; Habtemariam, A.; Fernández, R.; Walland, V.; Fabbiani, F. P. A.; Parsons, S.; Aird, R. E.; Jodrell, D. I.; Sadler, P. J. *J. Am. Chem. Soc.* **2006**, *128*, 1739-1748.

(73) Peacock, A. F. A.; Parsons, S.; Sadler, P. J. *J. Am. Chem. Soc.* **2007**, *129*, 3348-3357.

(74) Wang, F.; Chen, H.; Parsons, S.; Oswald, I. D. H.; Davidson, J. E.; Sadler, P. J. *Chem.-Eur. J.* **2003**, *9*, 5810-5820.

(75) Wang, F.; Bella, J.; Parkinson, J. A.; Sadler, P. J. *J. Biol. Inorg. Chem.* **2005**, *10*, 147-155.

(76) Wang, F.; Xu, J.; Habtemariam, A.; Bella, J.; Sadler, P. J. *J. Am. Chem. Soc.* **2005**, *127*, 17734-17743.

(77) Reedijk, J. *Proc. Natl. Acad. Sci. U. S. A.* **2003**, *100*, 3611-3616.

(78) Fukamachi, T.; Chiba, Y.; Wang, X.; Saito, H.; Tagawa, M.; Kobayashi, H. *Cancer Lett.* **2010**, *297*, 182-189.

(79) Herebian, D.; Sheldrick, W. S. *J. Chem. Soc., Dalton Trans.* **2002**, 966-974.

(80) Annen, P.; Schildberg, S.; Sheldrick, W. S. *Inorg. Chim. Acta* **2000**, *307*, 115-124.

(81) Yamanari, K.; Ito, R.; Yamamoto, S.; Konno, T.; Fuyuhiro, A.; Kobayashi, M.; Arakawa, R. *Dalton Trans.* **2003**, 380-386.

(82) Yamanari, K.; Ito, R.; Yamamoto, S.; Konno, T.; Fuyuhiro, A.; Fujioka, K.; Arakawa, R. *Inorg. Chem.* **2002**, *41*, 6824-6830.

(83) van Rijt, S. H.; Peacock, A. F. A.; Johnstone, R. D. L.; Parsons, S.; Sadler, P. J. *Inorg. Chem.* **2009**, *48*, 1753-1762.

(84) van Rijt, S. H.; Mukherjee, A.; Pizarro, A. M.; Sadler, P. J. *J. Med. Chem.* **2010**, *53*, 840-849.

(85) Jung, Y.; Lippard, S. J. *Chem. Rev.* **2007**, *107*, 1387-1407.

(86) Novakova, O.; Chen, H.; Vrana, O.; Rodger, A.; Sadler, P. J.; Brabec, V. *Biochemistry* **2003**, *42*, 11544-11554.

(87) Keck, M. V.; Lippard, S. J. *J. Am. Chem. Soc.* **1992**, *114*, 3386-3390.

(88) Kasparkova, J.; Marini, V.; Najajreh, Y.; Gibson, D.; Brabec, V. *Biochemistry* **2003**, *42*, 6321-6332.

(89) Satyanarayana, S.; Dabrowiak, J. C.; Chaires, J. B. *Biochemistry* **1992**, *31*, 9319-9324.

(90) Kostrhunova, H.; Florian, J.; Novakova, O.; Peacock, A. F. A.; Sadler, P. J.; Brabec, V. *J. Med. Chem.* **2008**, *51*, 3635-3643.

(91) Morris, R. E.; Aird, R. E.; del Socorro Murdoch, P.; Chen, H.; Cummings, J.; Hughes, N. D.; Parsons, S.; Parkin, A.; Boyd, G.; Jodrell, D. I.; Sadler, P. J. *J. Med. Chem.* **2001**, *44*, 3616-3621.

(92) Habtemariam, A.; Melchart, M.; Fernández, R.; Parsons, S.; Oswald, I. D. H.; Parkin, A.; Fabbiani, F. P. A.; Davidson, J. E.; Dawson, A.; Aird, R. E.; Jodrell, D. I.; Sadler, P. J. *J. Med. Chem.* **2006**, *49*, 6858-6868.

(93) Fu, Y.; Habtemariam, A.; Pizarro, A. M.; van Rijt, S. H.; Healey, D. J.; Cooper, P. A.; Shnyder, S. D.; Clarkson, G. J.; Sadler, P. J. *J. Med. Chem.* **2010**, *53*, 8192-8196.

(94) *Bioorganometallics: Biomolecules, Labeling, Medicine*; Jaouen, G., Ed.; Wiley-VCH: Weinheim, Germany, 2006.

(95) Barry, N. P. E.; Edafe, F.; Dyson, P. J.; Therrien, B. *Dalton Trans.* **2010**, *39*, 2816-2820.

(96) Peacock, A. F. A.; Sadler, P. J. *Chem. Asian J.* **2008**, *3*, 1890-1899.

(97) Allen, O. R.; Gott, A. L.; Hartley, J. A.; Hartley, J. M.; Knox, R. J.; McGowan, P. C. *Dalton Trans.* **2007**, 5082-5090.

(98) Tan, Y. L. K.; Pigeon, P.; Hillard, E. A.; Top, S.; Plamont, M.-A.; Vessieres, A.; McGlinchey, M. J.; Muller-Bunz, H.; Jaouen, G. *Dalton Trans.* **2009**, 10871-10881.

Chapter 4

Cyclopentadienyl Iridium Complexes Containing C^N-Chelating Ligands

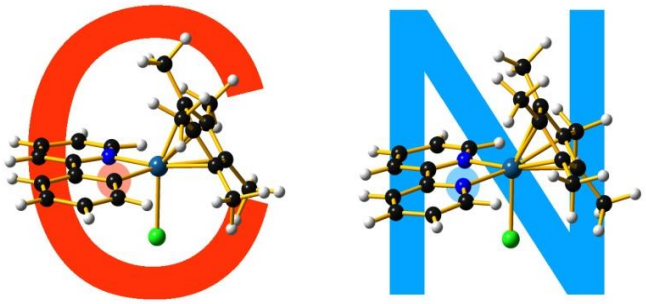

4.1 Introduction

Organometallic complexes offer enormous scope for the design of anticancer candidates due to their versatile structures, potential redox features and wide range of ligand substitution rates.[1-6] Iridium complexes are best known for their inertness,[7,8] and indeed inert organometallic Ir^{III} scaffolds are finding use as potent enzyme inhibitors.[9] The half-sandwich fragment {Cp*Ir^{III}} (Cp* = pentamethylcyclopentadienyl) has been used as a stabilising entity in many organometallic iridium complexes.[10,11] However, in Chapter 3 it was shown that Cp* Ir^{III} complexes with N,N-bound ethylenediamine (en), 2,2′-bipyridine (bpy), 1,10-phenanthroline (phen), and N,O-bound picolinate (pico), are all inactive towards A2780 human ovarian cancer cells with IC_{50} values > 100 μM. Also Cp* Ir^{III} PTA complexes (PTA = 1,3,5-triaza-7-phosphatricyclo-[3.3.1.1]decane),[12] and Cp* Ir^{III} pyTz complexes (pyTz = 2-(pyridine-2-yl)thiazole),[13] are reported to be noncytotoxic against A2780 cells (IC_{50} values > 300 μM). It has been demonstrated in Chapter 3 that introduction of phenyl or biphenyl substituents on Cp* can switch on cancer cell cytotoxicity of N,N- or N,O-chelated Cp* Ir^{III} complexes. Chelating ligands are already known to have a major influence on the DNA base specificity and cytotoxicity of organometallic half-sandwich complexes of the type [(η^6-arene)Ru/Os(XY)Z].[14-16] In this Chapter, a different switch involving a single atom change (C^- for N) in chelating ligand to afford a neutral complex is introduced.

The Cyclometallated organometallic complexes incorporating C^N-chelating ligands have attracted much attention because of their wide applications in both catalysis and luminescence.[17,18] However, few such previous studies have involved their anticancer activity.[19-21]

In this Chapter, the aqueous chemistry (hydrolysis, acidity of the resultant aqua adducts), nucleobase binding and cancer cell toxicity of Ir^{III} complexes containing C^N-chelating ligands based on 2-phenylpyridine (phpy) with electron-donating or electron-withdrawing substituents, and with Cp* and substituted Cp* ligands, Figure 4.1, is studied. The differences between C^N-bound complex [(η^5-C_5Me_5)Ir(phpy)Cl] (**32**) and N,N-bound complex [(η^5-C_5Me_5)Ir(bpy)Cl]$^+$ (**7**) in the structure, reactivity and cancer cell cytotoxicity are also compared. The results suggest that this new class of organometalic Ir(III) complexes is well suited for development as anticancer agents.

Figure 4.1 C^N-chelated iridium cyclopentadienyl complexes studied in this Chapter.

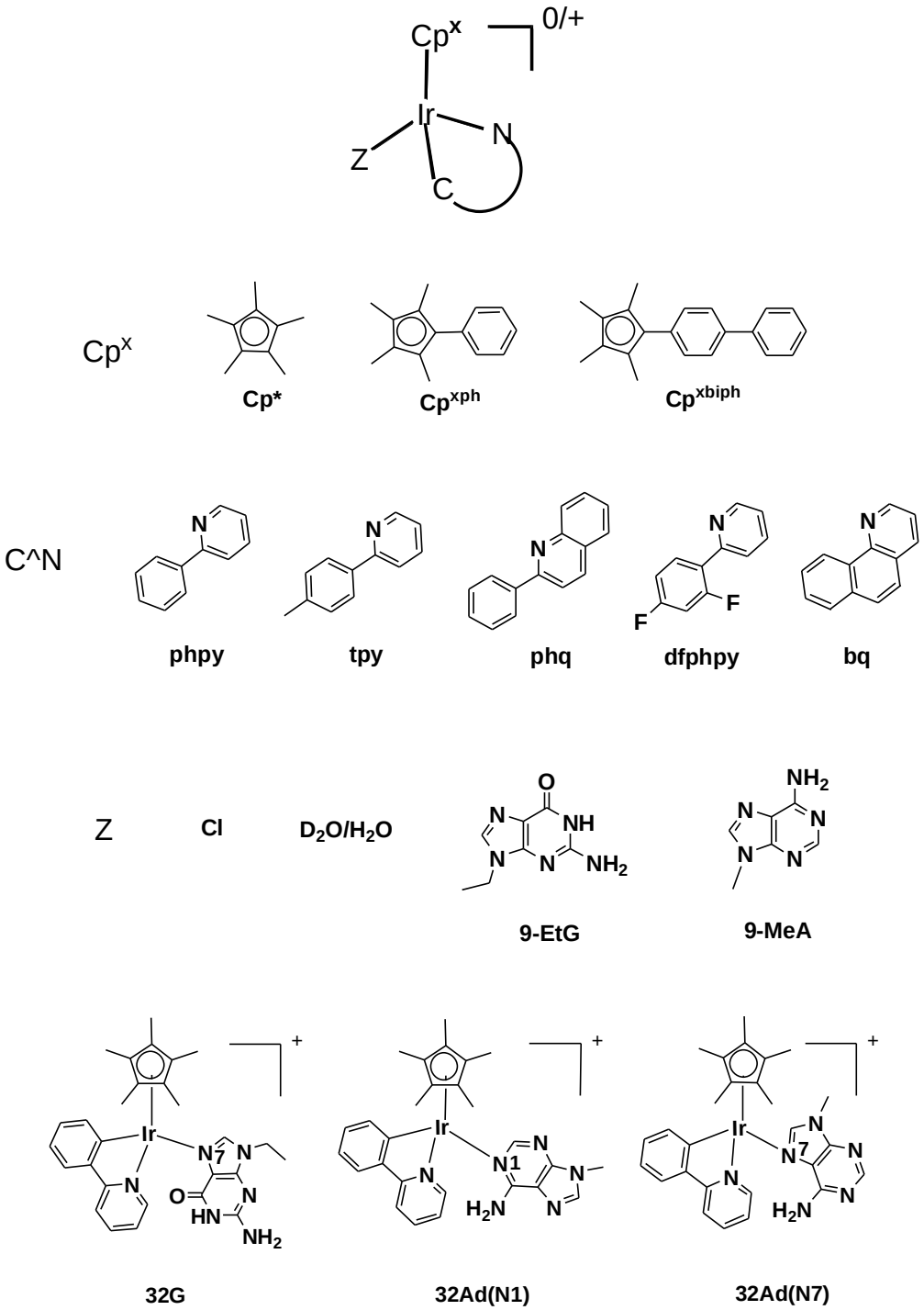

Z=Cl	Z=D_2O/H_2O	Z=9-EtG	Z=9-MeA	Cp^x	C^N
29	**29A**	**29G**	**29Ad**	Cp*	tpy
30	**30A**	**30G**	**30Ad**	Cp*	phq
31	**31A**	**31G**	**31Ad**	Cp*	dfphpy
32	**32A**	**32G**	**32Ad**	Cp*	phpy
33	**33A**	**33G**	**33Ad**	Cp^{xph}	phpy
34	**34A**	**34G**	**34Ad**	Cp^{xbiph}	phpy
35				Cp*	bq
36				Cp^{xph}	bq
37				Cp^{xbiph}	dfphpy

dimer	Cp^x
38	**Cp***
39	**Cp^{xph}**
40	**Cp^{xbiph}**

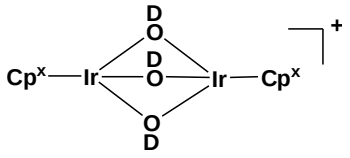

Figure 4.1 C^N-chelated iridium cyclopentadienyl complexes studied in this Chapter.

4.2 Experimental Section

4.2.1 Materials

2-Phenylpyridine (phpy), 2-(2,4-difluorophenyl)pyridine (dfphpy), 2-(*p*-tolyl)-pyridine (tpy), 2-phenylquinoline (phq), benzo[*h*]quinoline (bq), 9-ethylguanine (9-EtG), 9-methyladenine (9-MeA), octan-1-ol (≥ 99%), and NaCl (> 99.999%) were purchased from Sigma-Aldrich. Nitric acid (72%) from Sigma Aldrich was double distilled and diluted using double de-ionized water. Methanol was distilled

over magnesium/iodine prior to use. The syntheses of the dimer $[(\eta^5\text{-}C_5Me_4C_6H_5)IrCl_2]_2$ (**2**) and $[(\eta^5\text{-}C_5Me_4C_6H_4C_6H_5)IrCl_2]_2$ (**3**) is described in Chapter 2. Dimer $[(\eta^5\text{-}C_5Me_5)IrCl_2]_2$ (**1**),[22] complexes $[(\eta^5\text{-}C_5Me_5)Ir(phpy)Cl]$ (**32**)[23] and $[(\eta^5\text{-}C_5Me_5)Ir(bq)Cl]$ (**35**)[23] were prepared according to reported methods.

4.2.2 Syntheses

$[(\eta^5\text{-}C_5Me_5)Ir(tpy)Cl]$ (29). A solution of $[(\eta^5\text{-}C_5Me_5)IrCl_2]_2$ (48 mg, 0.06 mmol), 2-(*p*-tolyl)pyridine (20 mg, 0.12 mmol) and sodium acetate (20 mg, 0.24 mmol) in CH_2Cl_2 (15 mL) was stirred for 2 h at ambient temperature. The solution was filtered through celite. The filtrate was evaporated to dryness on a rotary evaporator, and washed with diethyl ether. The product was recrystallised from $CHCl_3$/hexane. Yield: 45 mg (70%). ^{1}H NMR ($CDCl_3$): δ = 8.65 (d, 1H, *J* = 5.7 Hz), 7.75 (d, 1H, *J* = 8.3 Hz), 7.62 (m, 2H), 7.57 (d, 1H, *J* = 8.0 Hz), 7.03 (t, 1H, *J* = 6.3 Hz), 6.86 (d, 1H, *J* = 7.8 Hz), 1.68 (s, 15H). Anal. Calcd. for $C_{22}H_{25}ClNIr$ (531.14): C, 49.75; H, 4.74; N, 2.64. Found: C, 49.66; H, 4.65; N, 2.68.

$[(\eta^5\text{-}C_5Me_5)Ir(phq)Cl]$ (30). The synthesis was performed as for **29** using $[(\eta^5\text{-}C_5Me_5)IrCl_2]_2$ (48 mg, 0.06 mmol), 2-phenylquinoline (25 mg, 0.12 mmol), and

sodium acetate (20 mg, 0.24 mmol). Yield: 43 mg (75%). ^{1}H NMR ($CDCl_3$): δ = 8.71 (d, 1H, *J* = 8.8 Hz), 8.02 (d, 1H, *J* = 8.7 Hz), 7.93 (d, 2H, *J* = 8.8 Hz), 7.77 (m, 2H), 7.69 (t, 1H, *J* = 8.1 Hz), 7.53 (t, 1H, *J* = 6.7 Hz), 7.24 (t, 1H, *J* = 7.8 Hz), 7.07 (t, 1H, *J* = 7.7 Hz), 1.57 (s, 15H). Anal. Calcd. for $C_{25}H_{25}ClNIr$ (567.13): C, 52.94; H, 4.44; N, 2.47. Found: C, 53.06; H, 4.41; N, 2.42. Crystals suitable for X-ray diffraction were obtained by slow evaporation of a methanol/diethyl ether solution at ambient temperature.

[(η^5-C_5Me_5)Ir(dfphpy)Cl] (31). The synthesis was performed as for **29** using [(η^5-C_5Me_5)$IrCl_2$]$_2$ (48 mg, 0.06 mmol), 2-(2,4-difluorophenyl)pyridine (23 mg, 0.12 mmol), and sodium acetate (20 mg, 0.24 mmol). Yield: 46 mg (70%). ^{1}H NMR ($CDCl_3$): δ = 8.71 (d, 1H, *J* = 6.0 Hz), 8.19 (d, 1H, *J* = 8.8 Hz), 7.69 (t, 1H, *J* = 8.0 Hz), 7.31 (d, 1H, *J* = 8.8 Hz), 7.10 (t, 1H, *J* = 6.3 Hz), 6.49 (t, 1H, *J* = 9.5 Hz), 1.67 (s, 15H). Anal. Calcd. for $C_{21}H_{21}ClF_2NIr$ (553.10): C, 45.60; H, 3.83; N, 2.53. Found: C, 45.76; H, 3.71; N, 2.46.

[(η^5-C_5Me_5)Ir(phpy)(9-EtG-*N*7)]NO_3 (32G·NO_3). A solution of [(η^5-C_5Me_5)Ir(phpy)Cl] (**32**) (52 mg, 0.1 mmol) and $AgNO_3$ (17 mg, 0.1 mmol) in MeOH (10 mL) and water (20 mL) was stirred at ambient temperature for 24 h. The

precipitate (AgCl) was removed by filtration through a glass wool plug, and 9-ethylguanine (19 mg, 1.1 mol equiv) was added to the filtrate. The solution was stirred at ambient temperature for 12 h, and evaporated to dryness on a rotary evaporator. The residue was extracted with CH_2Cl_2 (10 mL), and the volume reduced to ca. 2 mL on a rotary evaporator. A yellow precipitate formed at 253 K on addition of hexane and was collected by filtration, washed with diethyl ether and dried in air. Yield: 23 mg (32%). ^{1}H NMR (MeOD-d_4): δ = 9.35 (d, 1H, *J* = 5.8 Hz), 8.10 (d, 1H, *J* = 7.5 Hz), 7.84 (d, 1H, *J* = 8.0 Hz), 7.79 (t, 1H, *J* = 7.0 Hz), δ = 7.72 (d, 1H, *J* = 7.5 Hz), 7.44 (t, 1H, *J* = 7.8 Hz), 7.42 (s, 1H), 7.26 (t, 1H, *J* = 6.3 Hz), 7.21 (t, 1H, *J* = 8.0 Hz), 3.82 (q, 2H, *J* = 7.3 Hz), 1.62 (s, 15H), 1.12 (t, 3H, *J* = 7.3 Hz). Anal. Calcd for $C_{28}H_{32}IrN_7O_4$ (722.82): C, 46.53; H, 4.46; N, 13.56. Found: C, 46.74; H, 4.21; N, 13.23%. Crystals suitable for X-ray diffraction were obtained as **32G**·NO_3·$1.5CH_2Cl_2$ by slow evaporation of a CH_2Cl_2/hexane solution at ambient temperature.

[(η^5-$C_5Me_4C_6H_5$)Ir(phpy)Cl] (33). A solution of [(η^5-$C_5Me_4C_6H_5$)$IrCl_2$]$_2$ (46 mg, 0.05 mmol), 2-phenylpyridine (15 mg, 0.10 mmol) and sodium acetate (16 mg, 0.20 mmol) in CH_2Cl_2 (15 mL) was heated under reflux in an N_2 atmosphere for 24 h. The solution was filtered through celite. The filtrate was evaporated to dryness on a rotary evaporator and washed with diethyl ether. The product was recrystallised

from $CHCl_3$/hexane. Yield: 37 mg (57%). ^{1}H NMR (MeOD-d_4): δ = 8.60 (d, 1H, J = 5.3 Hz), 8.04 (d, 1H, J = 8.3 Hz), 7.84 (m, 2H), 7.65 (d, 1H, J = 7.8 Hz), 7.38 (m, 3H), 7.33 (m, 2H), 7.16 (t, 1H, J = 6.1 Hz), 7.13 (t, 1H, J = 7.2 Hz), 7.09 (t, 1H, J = 7.3 Hz), 1.85 (s, 3H), 1.74 (s, 3H),1.72 (s, 3H), 1.56 (s, 3H). Anal. Calcd. for $C_{26}H_{25}ClNIr$ (579.16): C, 53.92; H, 4.35; N, 2.42. Found: C, 53.77; H, 4.31; N, 2.41.

[(η^5-$C_5Me_4C_6H_4C_6H_5$)Ir(phpy)Cl] (34). The synthesis was performed as for **33** using [(η^5-$C_5Me_4C_6H_4C_6H_5$)$IrCl_2$]$_2$ (53 mg, 0.05 mmol), 2-phenylpyridine (15 mg, 0.10 mmol) and sodium acetate (16 mg, 0.20 mmol). Yield: 37 mg (57%). ^{1}H NMR ($CDCl_3$): δ = 8.51 (d, 1H, J = 5.3 Hz), 7.81 (d, 1H, J = 7.3 Hz), 7.72 (m, 2H), 7.64 (m, 5H), 7.51 (m, 4H), 7.37 (d, 1H, J = 7.6 Hz), 7.16 (t, 1H, J = 7.3 Hz), 7.05 (t, 1H, J = 6.0 Hz), 6.94 (t, 1H, J = 7.3 Hz), 1.92 (s, 3H), 1.82 (s, 3H),1.79 (s, 3H), 1.67 (s, 3H). Anal. Calcd. for $C_{32}H_{29}ClNIr$ (655.25): C, 58.66; H, 4.46; N, 2.14. Found: C, 58.46; H, 4.35; N, 2.18. Crystals suitable for X-ray diffraction were obtained by slow evaporation of a methanol/diethyl ether solution at ambient temperature.

[(η^5-$C_5Me_4C_6H_5$)Ir(bq)Cl] (36). The synthesis was performed as for **33** using [(η^5-$C_5Me_4C_6H_5$)$IrCl_2$]$_2$ (46 mg, 0.05 mmol), benzo[*h*]quinoline (18 mg, 0.10 mmol)

and sodium acetate (16 mg, 0.20 mmol). Yield: 28 mg (46%). ^{1}H NMR ($CDCl_3$): δ = 8.68 (d, 1H, *J* = 5.5 Hz), 8.09 (d, 1H, *J* = 7.5 Hz), 7.93 (dd, 1H, *J* = 5.3 Hz), 7.81 (d, 1H, *J* = 9.0 Hz), 7.56 (m, 5H), 7.39 (m, 3H), 7.31 (dd, 1H, *J* = 7.5 Hz), 1.83 (s, 3H), 1.81 (s, 3H),1.55 (s, 3H), 1.53 (s, 3H). Anal. Calcd for $C_{28}H_{25}ClNIr$ (603.13): C, 55.75; H, 4.18; N, 2.32. Found: C, 55.05; H, 3.16; N, 2.27. Crystals suitable for X-ray diffraction were obtained by slow evaporation of a methanol/diethyl ether solution at ambient temperature.

[(η^5-$C_5Me_4C_6H_4C_6H_5$)Ir(dfphpy)Cl] (37). The synthesis was performed as for **33** using [(η^5-$C_5Me_4C_6H_4C_6H_5$)$IrCl_2$]$_2$ (53 mg, 0.05 mmol), 2-(2,4-difluorophenyl)pyridine (19 mg, 0.10 mmol), and sodium acetate (16 mg, 0.20 mmol). Yield: 25 mg (37%). ^{1}H NMR ($CDCl_3$): δ = 8.53 (d, 1H, *J* = 5.5 Hz), 8.19 (d, 1H, *J* = 8.5 Hz), 7.64 (m, 5H), 7.50 (m, 4H), 7.38 (t, 1H, *J* = 7.3 Hz), 7.22 (d, 1H, *J* = 8.3 Hz), 6.96 (t, 1H, *J* = 6.5 Hz), 6.51 (t, 1H, *J* = 10.3 Hz), 1.81 (s, 3H), 1.77 (s, 3H), 1.75 (s, 3H), 1.59 (s, 3H). Anal. Calcd for $C_{32}H_{27}ClF_2NIr$ (691.23): C, 55.60; H, 3.94; N, 2.03. Found: C, 55.96; H, 3.95; N, 2.08. Crystals suitable for X-ray diffraction were obtained by slow evaporation of a methanol/diethyl ether solution at ambient temperature.

4.2.3 Methods

4.2.3.1 X-ray Crystallography

The details of the diffraction instrumentation are described in Chapter 2. The structures of complexes **30**, **32G**·NO_3·$1.5CH_2Cl_2$, **34**, **36** and **37** were solved by Dr. Guy Clarkson (Department of Chemistry, University of Warwick) using SHELXS (TREF)[24] with additional light atoms found by Fourier methods. Complexes were refined against F^2 using SHELXL,[25] and hydrogen atoms were added at calculated positions and refined riding on their parent atoms. There is one CH_2Cl_2 molecule in a general position in the cell and one CH_2Cl_2 molecule that straddles a cell face in **32G**·NO_3·$1.5CH_2Cl_2$. X-ray crystallographic data for complexes **30**, **32G**·NO_3·$1.5CH_2Cl_2$ and **34** have been deposited in the Cambridge Crystallographic Data Centre under the accession numbers CCDC 829525, 816981, and 829524, respectively.

4.2.3.2 Determination of pK_a Values

The pK_a* and pK_a values of complexes **29A**–**34A** were determined as described in Chapter 2.

4.2.3.3 Computation

Details of computational methods are described in Chapter 2. Geometry optimization calculations for complexes [(η^5-C_5Me_5)Ir(phpy)Cl] (**32**), [(η^5-C_5Me_5)Ir(bpy)Cl]$^+$ (**7**), and their aqua derivatives were performed in the gas phase with the gradient-corrected correlation functional PBE0.[26] 9-EtA was chosen instead of 9-MeA (used in experimental work) for the sake of comparison in the DFT work. Electrostatic potential surfaces (EPSs) for complexes **32**, **7**, and their aqua derivatives were calculated and mapped on electron density (isovalue 0.04) of the molecules. The electrostatic potential is represented with a colour scale ranging from red (–0.500 au) to blue (0.500 au). This work was carried out by Dr. Luca Salassa (Department of Chemistry, University of Warwick).

4.2.3.4 Interactions with Nucleobases

The reaction of complexes **29**–**34** (ca. 1 mM) with nucleobases typically involved addition of a solution containing 1 mol equiv of nucleobase in D_2O to an equilibrium solution of complexes **29**–**34** in 20% MeOD-d_4/80% D_2O (v/v). ^{1}H NMR spectra of these solutions were recorded at 310 K after various time intervals.

4.2.3.5 log *P* Determination

The partition coefficients (log *P*) were determined for complexes **32** and **7** as described in Chapter 2.

4.2.3.6 Cytotoxicity

Cytotoxicity assays on A2780 human ovarian cancer cell line was performed by Dr. Ana M. Pizarro (Department of Chemistry, University of Warwick) as described in Chapter 2 for complexes **29**–**34** and **37**. Complexes **32** and **34** were further evaluated by the NCI/DTP as described in Chapter 2 for *in vitro* cytotoxic test against ca. 60 human cancer cell lines.

4.2.3.7 ICP-MS Analysis

ICP analysis for the determination of the partition coefficients (log *P*) was performed as described in Chapter 2.

4.3 Results

4.3.1 Synthesis and Characterisation

Nine Ir^{III} half-sandwich complexes of the type [(η^5-Cp^x)Ir(C^N)Cl], where Cp^x is pentamethylcyclopentadienyl Cp*, or its phenyl (Cp^{xph}) or biphenyl (Cp^{xbiph}) derivatives, and the C^N-chelating ligands are 2-(*p*-tolyl)pyridine (tpy, **29**), 2-phenylquinoline (phq, **30**), 2-(2,4-difluorophenyl)pyridine (dfphpy, **31** and **37**), 2-phenylpyridine (phpy, **32**–**34**), or benzo[*h*]quinoline (bq, **35** and **36**) were synthesised in moderate yields by reaction of the chelating ligand with the appropriate dimer [(η^5-Cp^x)$IrCl_2$]$_2$ in CH_2Cl_2. All the synthesised complexes were fully characterised by ^{1}H NMR and CHN elemental analysis. All the complexes in this study are chiral, but no attempt was made to resolve them and racemates are used in the following studies. Complexes **29**–**34** as typical complexes containing C^N-chelating ligands are studied in more detail.

The X-ray crystal structures of [(η^5-C_5Me_5)Ir(phq)Cl] (**30**), [(η^5-$C_5Me_4C_6H_4C_6H_5$)Ir(phpy)Cl] (**34**), [(η^5-$C_5Me_4C_6H_4C_6H_5$)Ir(bq)Cl] (**36**) and [(η^5-$C_5Me_4C_6H_4C_6H_5$)Ir(dfphpy)Cl] (**37**) were determined. The structures and atom numbering schemes are shown in Figure 4.2. Crystallographic data are shown in Table 4.1, and selected bond lengths and angles are listed in Table 4.2. All complexes adopt the expected half-sandwich pseudo-octahedral "three-legged piano-stool" geometry with the iridium bound to a η^5-cyclopentadienyl ligand (Ir to

ring centroid 1.817−1.829 Å). The Ir−Cl bond distances range from 2.3886(8) to 2.4013(8) Å. In general, the Ir−C(chelating ligand) bond lengths are significantly shorter than the Ir−N bond lengths, except in **36**. For complex **34**, the twist angle between the bound cyclopentadienyl ring and the central phenyl ring is 48.93°, while that between the bound ring and the terminal phenyl ring is 28.50°. The phenyl rings are twisted by 21.55°. No intermolecular π-ring stacking in the unit cell is observed in the two crystal structures.

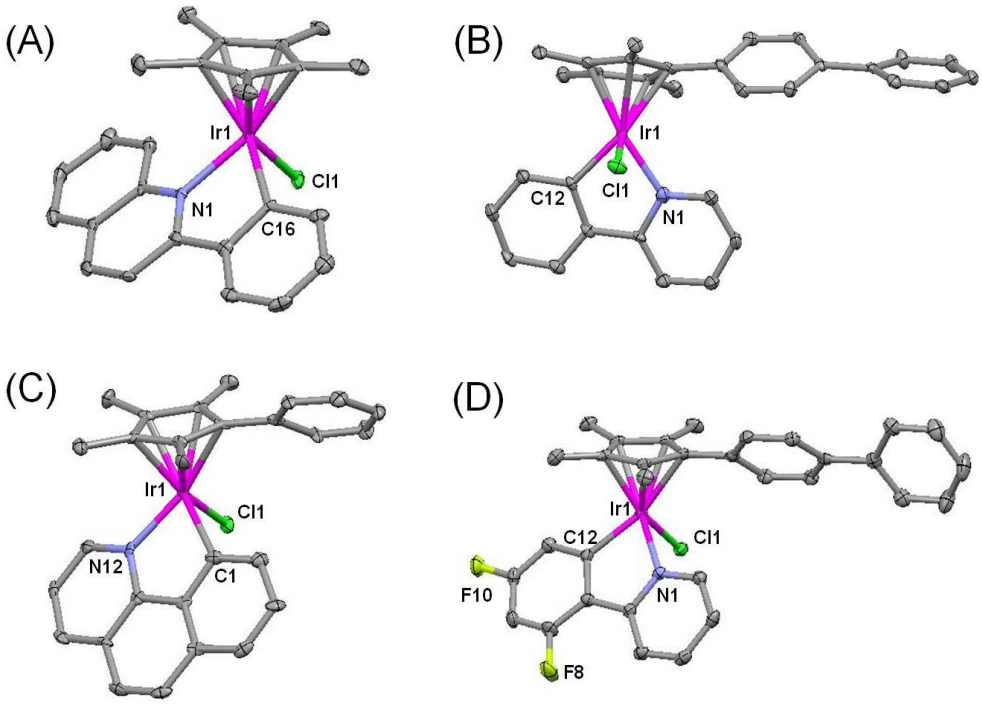

Figure 4.2. X-ray crystal structures and atom numbering schemes for complexes [(η^5-C_5Me_5)Ir(phq)Cl] (**30**), [(η^5-$C_5Me_4C_6H_4C_6H_5$)Ir(phpy)Cl] (**34**), [(η^5-C_5Me_4-C_6H_5)Ir(bq)Cl] (**36**) and [(η^5-$C_5Me_4C_6H_4C_6H_5$)Ir(dfphpy)Cl] (**37**).

Table 4.1. Crystallographic Data for Complexes [(η^5-C_5Me_5)Ir(phq)Cl] (**30**), [(η^5-C_5Me_5)Ir(phpy)(9-EtG-*N*7)]NO_3·1.5CH_2Cl_2 (**32G**·NO_3·1.5CH_2Cl_2), [(η^5-$C_5Me_4C_6H_4C_6H_5$)Ir(phpy)Cl] (**34**), [(η^5-$C_5Me_4C_6H_4C_6H_5$)Ir(bq)Cl] (**36**) and [(η^5-$C_5Me_4C_6H_4C_6H_5$)Ir(dfphpy)Cl] (**37**)

	30	**34**	**36**	**37**	**32G**·NO_3·1.5CH_2Cl_2
formula	$C_{25}H_{25}ClIrN$	$C_{32}H_{29}ClIrN$	$C_{28}H_{25}ClIrN$	$C_{32}H_{27}ClF_2IrN$	$C_{29.50}H_{35}Cl_3IrN_7O_4$
MW	567.11	655.21	603.14	691.20	850.20
cryst colour	orange block	orange block	orange block	yellow block	yellow block
cryst size	0.40 ×0.40	0.22 ×0.18	0.28 ×0.20	0.16 ×0.14	0.40×0.40
(mm)	×0.10	×0.12	×0.06	×0.12	×0.10
λ (Å)	0.71073	0.71073	0.71073	0.71073	0.71073
temp (K)	100	100	100	100	100
cryst syst	orthorhombic	monoclinic	triclinic	monoclinic	triclinic
space group	*P*2(1)2(1)2(1)	*P*2(1)/*n*	*P*1	*P*2(1)/*c*	*P*-1
a (Å)	8.05090(13)	10.0094(4)	8.4631(3)	14.8865(3)	11.00314(16)
b (Å)	15.9169(3)	22.9497(6)	16.1135(4)	9.09997(18)	12.2976(2)
c (Å)	16.0586(3)	11.2128(4)	8.4706(3)	19.9316(5)	13.3976(2)
α (°)	90	90	90	90	76.7310(14)
β (°)	90	103.473(3)	107.513(3)	103.267(2)	67.6432(14)
γ (°)	90	90	90	90	88.3673(13)
vol(Å^3)	2057.84(6)	2504.84(14)	1101.61(6)	2628.00(10)	1628.35(5)
Z	4	4	2	4	2
R(*F*o^2)	0.0370	0.0293	0.0321	0.0314	0.0218
Rw(*F*o^2)	0.0890	0.0699	0.0774	0.0559	0.0555
GOF	1.053	0.999	1.069	1.019	1.070

Table 4.2. Selected Bond Lengths (Å) and Angles (deg) for [(η^5-C_5Me_5)Ir(phq)Cl] (**30**), [(η^5-C_5Me_5)Ir(phpy)(9-EtG-*N*7)]$NO_3 \cdot 1.5CH_2Cl_2$ (**32G** $\cdot NO_3 \cdot 1.5CH_2Cl_2$), [($\eta^5$-$C_5Me_4C_6H_4C_6H_5$)Ir(phpy)Cl] (**34**), [(η^5-$C_5Me_4C_6H_4C_6H_5$)Ir(bq)Cl] (**36**) and [(η^5-$C_5Me_4C_6H_4C_6H_5$)Ir(dfphpy)Cl] (**37**)

Bond(s)	**30**	**34**	**36**	**37**	Bond(s)	**32G** $\cdot NO_3 \cdot 1.5CH_2Cl_2$
Ir−C	2.139(6)	2.151(3)	2.134(7)	2.150(3)	Ir(1)−C(Cp*)	2.156(2)
(Cp^x)	2.157(6)	2.163(3)	2.160(5)	2.156(4)		2.166(2)
	2.167(5)	2.183(3)	2.203(7)	2.185(3)		2.166(2)
	2.243(6)	2.240(3)	2.216(7)	2.235(3)		2.233(2)
	2.304(6)	2.243(3)	2.235(8)	2.236(3)		2.277(3)
Ir−C	1.829	1.825	1.817	1.819	Ir−C	1.827
(centroid)					(centroid)	
Ir−C	2.045(6)	2.057(3)	2.073(7)	2.035(3)	Ir(1)−C(12)	2.048(2)
Ir−N	2.128(5)	2.080(3)	2.051(7)	2.078(3)	Ir(1)−N(1)	2.097(2)
Ir−Cl	2.3989(16)	2.3886(8)	2.3952(16)	2.4013(8)	Ir(1)−N(23)	2.114(2)
C−Ir−N	77.4(2)	78.27(13)	78.9(3)	78.40(12)	C(12)−Ir(1)−N(1)	77.92(9)
C−Ir−Cl	89.66(17)	88.20(9)	86.12(18)	89.64(10)	C(12)−Ir(1)−N(23)	86.32(8)
N−Ir−Cl	87.23(13)	86.34(8)	86.47(19)	84.85(8)	N(1)−Ir(1)−N(23)	91.56(8)

4.3.2 Structural and Electronic Differences between Complexes 32 and 7

There is a change in the overall charge on the complex from positive for complex **7**, where the chelating ligand is N,N-bound 2,2′-bipyridine, to neutral for complex

32 which contains C^N-bound 2-phenylpyridine. Geometry optimization calculations for complexes **7** and **32** were performed using the PBE0 functional. Selected bond distances for $[(\eta^5\text{-}C_5Me_5)Ir(bpy)Cl]^+$ (**7**) and $[(\eta^5\text{-}C_5Me_5)Ir(phpy)Cl]$ (**32**) are listed in Table 4.3. In complex **32**, the chelating ligand is closer to the Ir^{III} centre than in complex **7**; a short Ir–C(phenyl) distance causes elongation of the Ir–Cl bond as well as the Ir–Cp*(centroid) distance (Table 4.3).

Table 4.3. Selected Bond Distances for $[(\eta^5\text{-}C_5Me_5)Ir(bpy)Cl]^+$ (**7**) and $[(\eta^5\text{-}C_5Me_5)Ir(phpy)Cl]$ (**32**) Calculated at the PBE1PBE/LANLD2Z/6-31G** Level

Complex	Ir–Cl	Ir–N1/C1	Ir–N2	Ir–Centroid
7	2.398	2.083	2.083	1.816
32	2.411	2.009	2.077	1.863

Electrostatic potential surfaces (EPS) for complexes **7**, **32**, and their aqua adducts were calculated. The N,N-chelating bpy complex **7** shows more positive electrostatic potentials than the C^N-chelating phpy complex **32** (Table 4.4). The same trend is observed in the electrostatic potential surfaces of the aqua derivatives $[(\eta^5\text{-}C_5Me_5)Ir(bpy)(H_2O)]^{2+}$ (**7A**) and $[(\eta^5\text{-}C_5Me_5)Ir(phpy)(H_2O)]^+$ (**32A**), which as

expected show more positive surfaces compared to their chlorido analogues, **7** and **32**.

Table 4.4. Electrostatic Potential Surfaces (EPSs) for Chlorido Complexes **7**, **32**, and Their Aqua Adducts **7A** and **32A**.

Complex	Structure	EPS (isovalue = 0.04) -0.500 +0.500
7	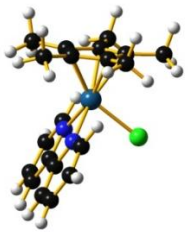	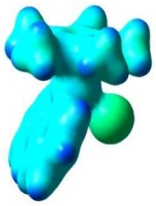
32	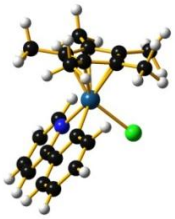	
7A	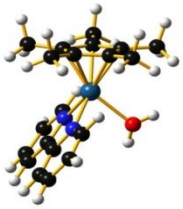	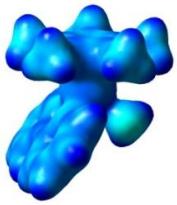
32A	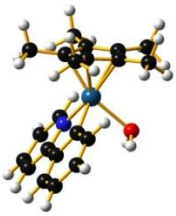	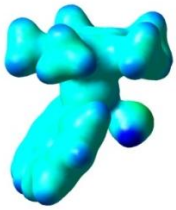

4.3.3 Hydrolysis Studies

The hydrolysis of complexes **29**–**34** in 20% MeOD-d_4/80% D_2O (v/v) was monitored by ^{1}H NMR spectroscopy at different temperatures. The presence of methanol ensured the solubility of the complexes. All these Ir^{III} complexes undergo rapid hydrolysis. Equilibrium was reached by the time the first ^{1}H NMR spectrum was acquired (~5 min) even at 278 K. At equilibrium 20%–50% of complex **29**–**34** was in the hydrolysed form, based on ^{1}H NMR peak integrals.

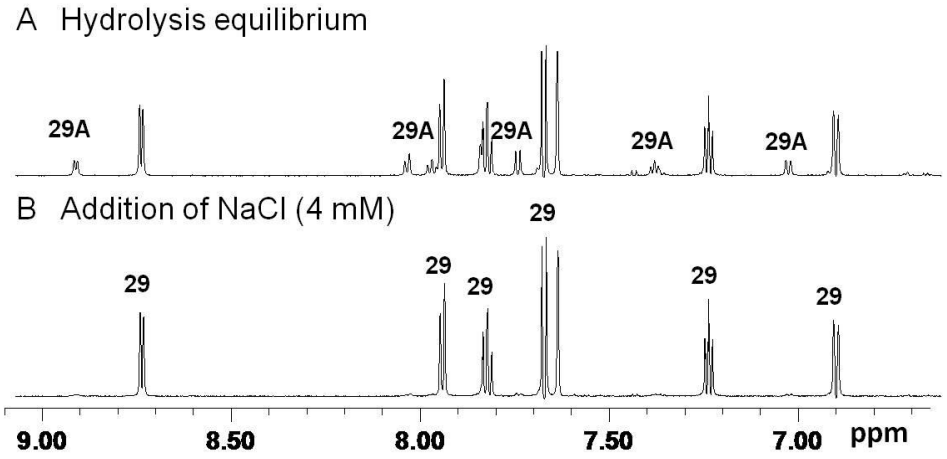

Figure 4.3. Confirmation of hydrolysis of Ir^{III} complex [(η^5-C_5Me_5)Ir(tpy)Cl] (**29**). (A) ^{1}H NMR spectrum of an equilibrium solution of **29** (1 mM) in 20% MeOD-d_4/80% D_2O (v/v) at 298 K. (B) ^{1}H NMR spectrum recorded 10 min after addition of NaCl (final concentration, 4 mM) to the equilibrium solution of **29**. Complex **29A** corresponds to the aqua complex [(η^5-C_5Me_5)Ir(tpy)(D_2O)]$^+$.

To confirm the hydrolysis of the complexes, 4 mol equiv of NaCl was added to equilibrium solutions containing the chlorido complexes and their aqua adducts. ^{1}H NMR spectra were then recorded within 10 min of the Cl^{-} additions at 298 K. Upon addition of NaCl, the ^{1}H NMR peaks corresponding to the chlorido complexes increased in intensity whilst peaks for the aqua adducts decreased, Figure 4.3. These data confirm the formation of the aqua adducts and the reversibility of the process.

4.3.4 pK_a Determination

Changes in the ^{1}H NMR chemical shifts of the methyl protons of Cp* or protons of the coordinated chelating ligands in aqua complexes **29A**−**34A**, were followed with change in pH* over a range of 2−10 (Figure 4.4). ^{1}H NMR peaks assigned to aqua complexes gradually shifted to high field with increase in pH*. The resulting pH titration curves were fitted to the Henderson-Hasselbalch equation, from which the pK_a* values of the coordinated water were determined. This gave pK_a values between 8.31 and 8.87 (Table 4.5), with the Cp^{xbiph} aqua complex **34A** and fluoro-substituted phenylpyridine Cp* complex **31A** having the lowest pK_a values (8.31 and 8.32, respectively) and the methyl-substituted phenylpyridine complex **29A** having the highest (8.87).

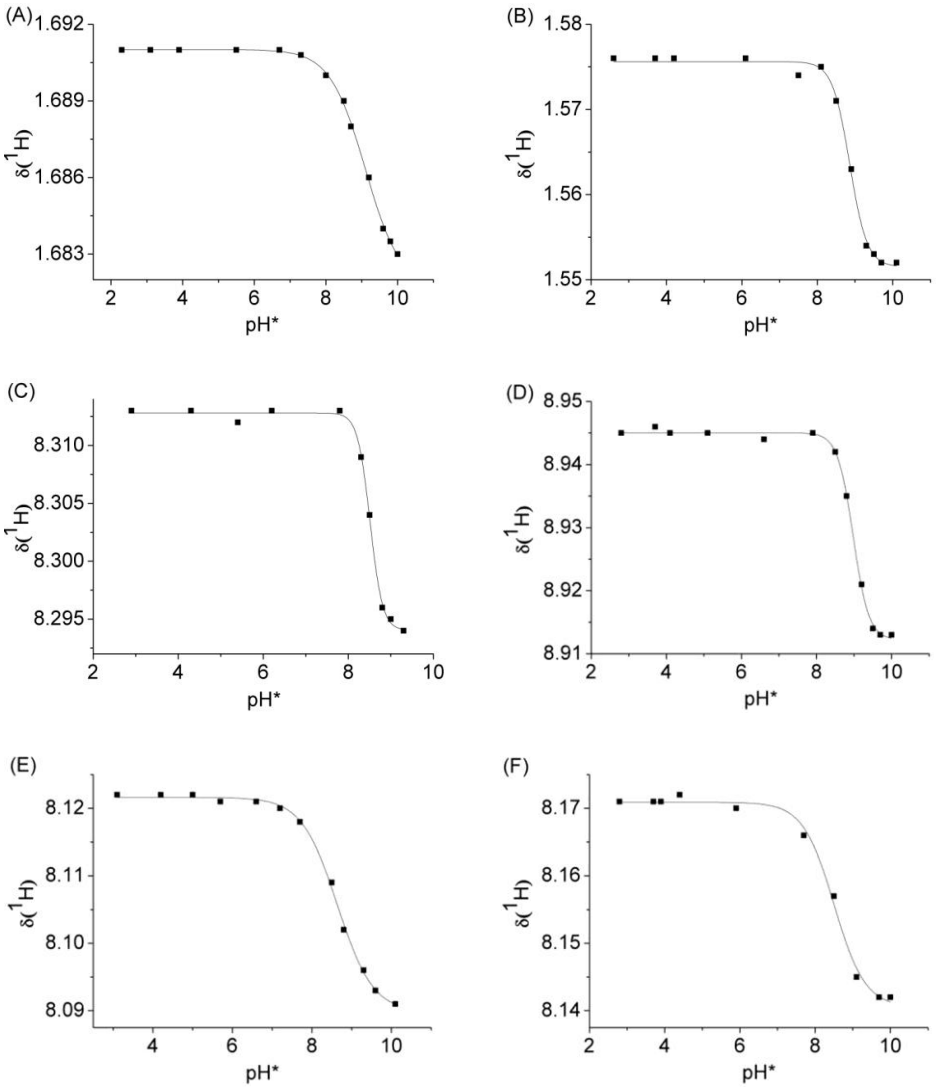

Figure 4.4. Dependence of the ^{1}H NMR chemical shifts for Cp* methyl groups in aqua complexes **29A** and **30A**, and for coordinated chelating ligands in aqua complexes **31A**−**34A** on pH* for complexes (A) $[(\eta^5\text{-}C_5Me_5)Ir(tpy)(D_2O)]^+$ (**29A**), (B) $[(\eta^5\text{-}C_5Me_5)Ir(phq)(D_2O)]^+$ (**30A**), (C) $[(\eta^5\text{-}C_5Me_5)Ir(dfphpy)(D_2O)]^+$ (**31A**), (D) $[(\eta^5\text{-}C_5Me_5)Ir(phpy)(D_2O)]^+$ (**32A**), (E) $[(\eta^5\text{-}C_5Me_4C_6H_5)Ir(phpy)(D_2O)]^+$ (**33A**), and (F) $[(\eta^5\text{-}C_5Me_4C_6H_4C_6H_5)Ir(phpy)(D_2O)]^+$ (**34A**). The curves are computer fits giving the pK_a* values shown in Table 4.5.

Table 4.5. pK_a* and pK_a Values[a] for the Deprotonation of the Coordinated D_2O in Complexes **29A**−**34A**

Aqua Complex	pK_a*	pK_a
$[(\eta^5\text{-}C_5Me_5)Ir(tpy)(D_2O)]^+$ (**29A**)	9.10	8.87
$[(\eta^5\text{-}C_5Me_5)Ir(phq)(D_2O)]^+$ (**30A**)	8.86	8.65
$[(\eta^5\text{-}C_5Me_5)Ir(dfphpy)(D_2O)]^+$ (**31A**)	8.51	8.32
$[(\eta^5\text{-}C_5Me_5)Ir(phpy)(D_2O)]^+$ (**32A**)	8.97	8.75
$[(\eta^5\text{-}C_5Me_4C_6H_5)Ir(phpy)(D_2O)]^+$ (**33A**)	8.64	8.45
$[(\eta^5\text{-}C_5Me_4C_6H_4C_6H_5)Ir(phpy)(D_2O)]^+$ **(34A**)	8.50	8.31

[a] pK_a values calculated from pK_a* according to Krezel and Bal.[27]

During the pH titrations for aqua complexes **29A**−**34A**, the appearance of a new set of peaks was detected with increasing pH* (>8.7). The new peaks are attributable to the free C^N-chelating ligands and to the hydroxo-bridged dimers $\{[(\eta^5\text{-}Cp^x)Ir]_2(\mu\text{-}OD)_3\}^+$ (Cp^x = Cp*, **38**; Cp^{xph}, **39**; Cp^{xbiph}, **40**, see Figure 4.1). The ^{1}H NMR peaks for hydroxo-bridged dimers **38**−**40** increased in intensity with increase in pH*. For complex $[(\eta^5\text{-}C_5Me_5)Ir(dfphpy)(D_2O)]^+$ (**31A**), the amount of dimer **38** increased from 23% at pH* 9.0 to 50% at pH* 9.6, Figure 4.5. ESI-MS studies on the diluted sample (0.2 mM) gave a major peak at *m*/*z* 709.2, consistent with the presence of $\{[(\eta^5\text{-}C_5Me_5)Ir]_2(\mu\text{-}OD)_3\}^+$ (calcd *m/z* 710.2).

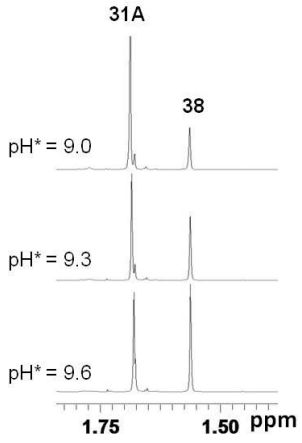

Figure 4.5. Methyl region of ^{1}H NMR spectra from the pH titration of the aqua complex $[(\eta^5\text{-}C_5Me_5)Ir(dfphpy)(D_2O)]^+$ (**31A**), showing an increase in intensity of the peak for the hydroxo-bridged dimer $\{[(\eta^5\text{-}C_5Me_5)Ir]_2(\mu\text{-}OD)_3\}^+$ (**38**) with increase in pH*.

4.3.5 Interactions with Nucleobases

Since DNA is a potential target for transition metal anticancer drugs,[28,29] nucleobase binding reactions of complexes $[(\eta^5\text{-}C_5Me_5)Ir(tpy)Cl]$ (**29**), $[(\eta^5\text{-}C_5Me_5)Ir(phq)Cl]$ (**30**), $[(\eta^5\text{-}C_5Me_5)Ir(dfphpy)Cl]$ (**31**), $[(\eta^5\text{-}C_5Me_5)Ir(phpy)Cl]$ (**32**), $[(\eta^5\text{-}C_5Me_4C_6H_5)Ir(phpy)Cl]$ (**33**) and $[(\eta^5\text{-}C_5Me_4C_6H_4C_6H_5)Ir(phpy)Cl]$ (**34**), with 9-ethylguanine (9-EtG) and 9-methyladenine (9-MeA) were investigated. Solutions of **29**−**34** (ca. 1 mM, containing an equilibrium mixture of **29**−**34** and their respective aqua adducts **29A**−**34A**) and 1 mol equivalent of 9-EtG or 9-MeA in 20% MeOD-d_4/80% D_2O (v/v) were prepared, and ^{1}H NMR spectra were

recorded at different time intervals at 310 K. The percentages of nucleobase adducts formed by the complexes after 24 h reaction, based on ^{1}H NMR peak integrals, are shown in Table 4.6 and Figure 4.6.

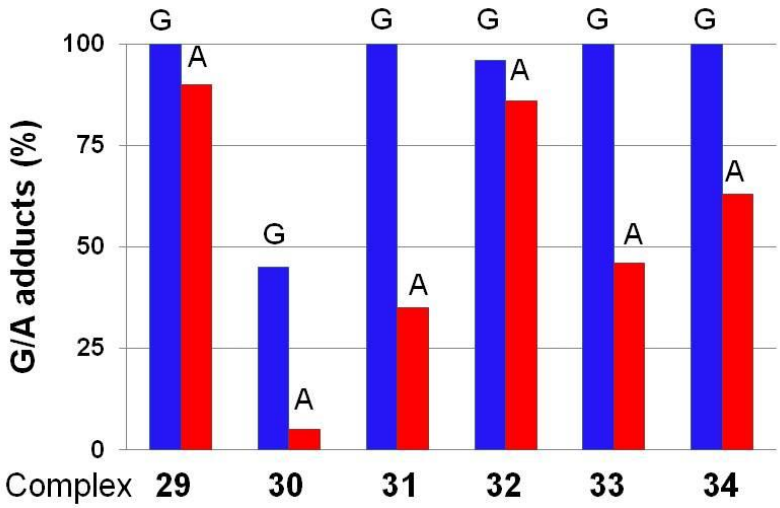

Figure 4.6. Bar chart showing the extent of binding of complexes **29**−**34** (ca. 1 mM in 20% MeOD-d_4/80% D_2O) to the nucleobases 9-EtG and 9-MeA at equilibrium (24 h), based on ^{1}H NMR peak integrals.

Table 4.6. Extent of 9-EtG and 9-MeA Adduct Formation for Complexes **29**–**34** (ca. 1 mM) at 310 K after 24 h.

	9-EtG adduct	9-MeA adduct	9-EtG/9-MeA competition	
Complex	(%)	(%)	G adduct (%)	A adduct (%)
29	100	90	80	20
30	45	<5	-[a]	-[a]
31	100	35	100	0
32	96	86	85	15
33	100	46	100	0
34	100	63	100	0

[a] Not determined.

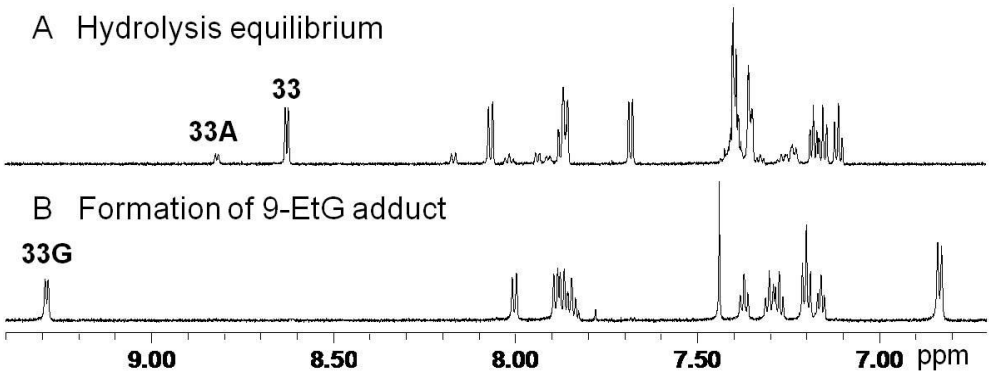

Figure 4.7. Low field region of ^{1}H NMR spectra showing reaction of [(η^5-$C_5Me_4C_6H_5$)Ir(phpy)Cl] (**33**) with 9-ethylguanine. (A) Equilibrium solution of **33** (0.8 mM) in 20% MeOD-d_4/80% D_2O (v/v, pH* 7.4) at 310 K, containing an equilibrium mixture of **33** and its aqua adduct **33A**. (B) 10 min after addition of 1 mol equiv 9-ethylguanine, showing the complete formation of the 9-EtG adduct **33G**.

In the ^{1}H NMR spectrum of a solution containing [(η^5-$C_5Me_4C_6H_5$)Ir(phpy)Cl] (**33**) (0.8 mM) and 1 mol equiv 9-ethylguanine (20% MeOD-d_4/80% D_2O, pH* 7.4, 310 K), one set of new peaks assignable to the 9-EtG adduct **33G** appeared, showing that 100% of **33** had reacted after 10 min (Figure 4.7). A significant change in chemical shift from 8.62 ppm for the chlorido complex **33** to 9.28 ppm for 9-EtG adduct **33G** for the CH=N (phpy ligand) proton was observed. A new 9-EtG H8 peak appeared at 7.44 ppm (singlet), shifted by 0.34 ppm to high field relative to that of free 9-EtG. After 24 h, no further change was observed. The ESI-MS of an equilibrium solution contained a major peak at *m/z* 723.2, confirming the formation of the 9-EtG adduct **33G**, [(η^5-$C_5Me_4C_6H_5$)Ir(phpy)(9-EtG)]$^+$ (calcd *m/z* 722.9). Similarly, complexes **29**, **31**, **32** and **34** also formed 9-EtG adducts to the extent of 96%−100% after 24 h. Only complex **30** containing 2-phenylquinoline showed less strong binding to 9-EtG (45%, Table 4.6 and Figure 4.6).

The 9-EtG adduct of complex **32**, [(η^5-C_5Me_5)Ir(phpy)(9-EtG)]NO_3 (**32G**·NO_3) was isolated and the X-ray crystal structure confirmed that 9-EtG is bound through N7 (Figure 4.8A). Crystallographic data are shown in Table 4.1, and selected bond lengths and angles are listed in Table 4.2. The nitrate counter ion shows H-bonding to a 9-EtG ligand, with distances of 1.987(19) Å (O12···H26) and 1.975(19) Å (O10···H27A), Figure 4.8B and Table 4.7. The H-bonded chains are linked by two

hydrogen bonds N27−H27B···N28 (2.105(19) Å) between two symmetrical guanines.

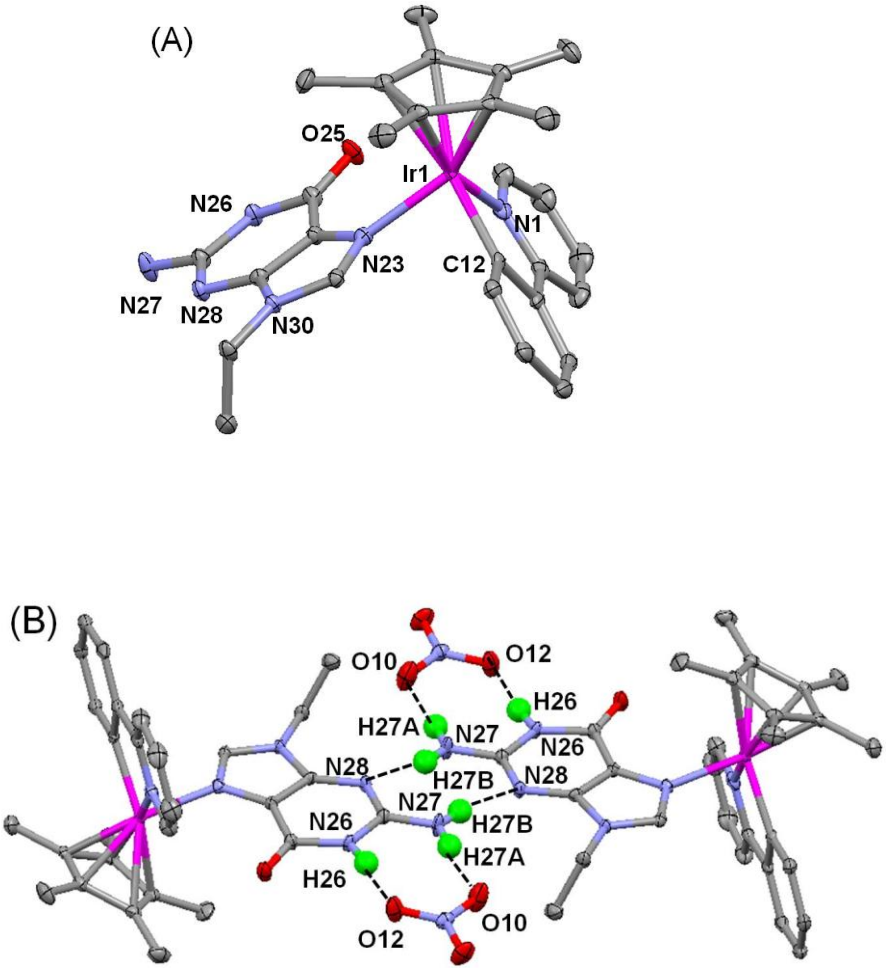

Figure 4.8. X-ray crystal structure of [(η^5-C_5Me_5)Ir(phpy)(9-EtG-*N*7)] NO_3·1.5CH_2Cl_2 (**32G**·NO_3·1.5CH_2Cl_2). (A) Atom numbering scheme. Only the cation is shown for clarity. (B) Formation of dimers linked by N27−H27B···N28 hydrogen bonds of 9-EtG (2.105(19) Å). The NO_3^- counter anions form H-bonds with N26H and N27H (O12···H26 1.987(19) Å and O10···H27A 1.975(19) Å).

Table 4.7. H-bond Interactions between Nitrate Counter Ion and Guanine in the X-ray Crystal Structure of $[(\eta^5\text{-}C_5Me_5)Ir(phpy)(9\text{-}EtG\text{-}N7)]NO_3 \cdot 1.5CH_2Cl_2$ (**32G**·NO_3·1.5 CH_2Cl_2)

D–H···A	D–H (Å)	H···A (Å)	D···A (Å)	∠D–H···A(°)
N27–H27A···O10	0.888(18)	1.987(19)	2.871(3)	174(3)
N26–H26···O12	0.877(18)	1.975(19)	2.850(3)	175(3)
N27–H27B···N28	0.910(18)	2.105(19)	3.004(3)	169(3)

Complexes $[(\eta^5\text{-}C_5Me_5)Ir(dfphpy)Cl]$ (**31**), $[(\eta^5\text{-}C_5Me_4C_6H_5)Ir(phpy)Cl]$ (**33**) and $[(\eta^5\text{-}C_5Me_4C_6H_4C_6H_5)Ir(phpy)Cl]$ (**34**), formed moderately strong 9-MeA adducts (35−63% at equilibrium after 24 h, Table 4.6 and Figure 4.6). Only complex **29** $[(\eta^5\text{-}C_5Me_5)Ir(tpy)Cl]$ and **32** $[(\eta^5\text{-}C_5Me_5)Ir(phpy)Cl]$ showed an exceptionally high affinity for 9-MeA, with 90% and 86% adduct formation after 24 h, respectively. Complex $[(\eta^5\text{-}C_5Me_5)Ir(phq)Cl]$ (**30**) containing 2-phenylquinoline formed almost no 9-MeA adduct (<5%). Except for **30**, two adenine nucleobase adducts were formed in the reactions between complexes **29**, **31**−**34** with 9-MeA, most likely through iridium binding to N1 or N7 of adenine in a ratio typically of 1:5.

To understand the mode of binding to adenine, 1:1 mol equiv of 9-MeA and complex **32** were dissolved in MeOD-d_4 (7 mM), and 2D ^1H–^1H TOCSY (Figure 4.9) and NOESY spectra were recorded (Figure 4.10). Only 40% of complex **32**

reacted with 9-MeA in MeOD-d_4 at 310 K after 24 h. Complex **32** also formed two 9-MeA adducts in a 6.6:1 ratio in MeOD-d_4 based on the integration of the Cp* ^{1}H NMR peaks. The ^{1}H NMR peaks of the minor adduct in the low field region are weak and overlapped by the peaks of the major adduct, Figure 4.9.

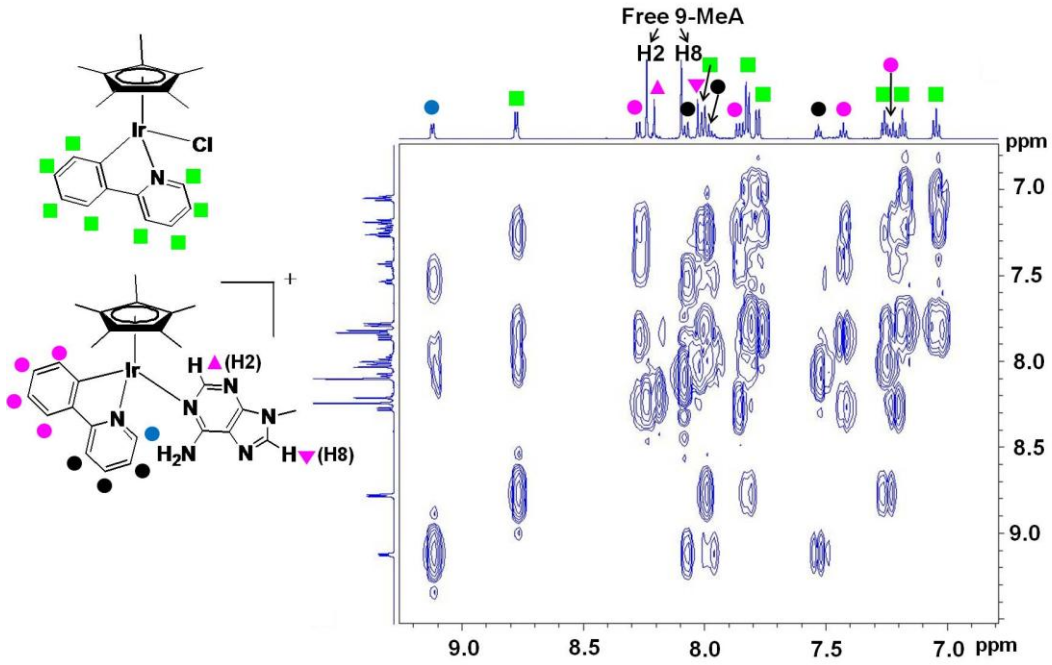

Figure 4.9. ^{1}H–^{1}H TOCSY 2D NMR spectrum of an equimolar equilibrium solution of 9-MeA and complex **32** [(η^5-C_5Me_5)Ir(phpy)Cl] (7 mM) in MeOD-d_4. Peak assignments are indicated on the structures.

An NOE cross-peak between H2 of 9-MeA and the HC=N proton of phpy was observed (Figure 4.10), suggesting that coordination of 9-MeA through N1 is the

major binding mode. This result is consistent with the DFT calculations which show that $[(\eta^5\text{-}C_5Me_5)Ir(phpy)(9\text{-}EtA\text{-}N1)]^+$ is more stable than $[(\eta^5\text{-}C_5Me_5)Ir(phpy)(9\text{-}EtA\text{-}N7)]^+$ by 18.36 kJ/mol.

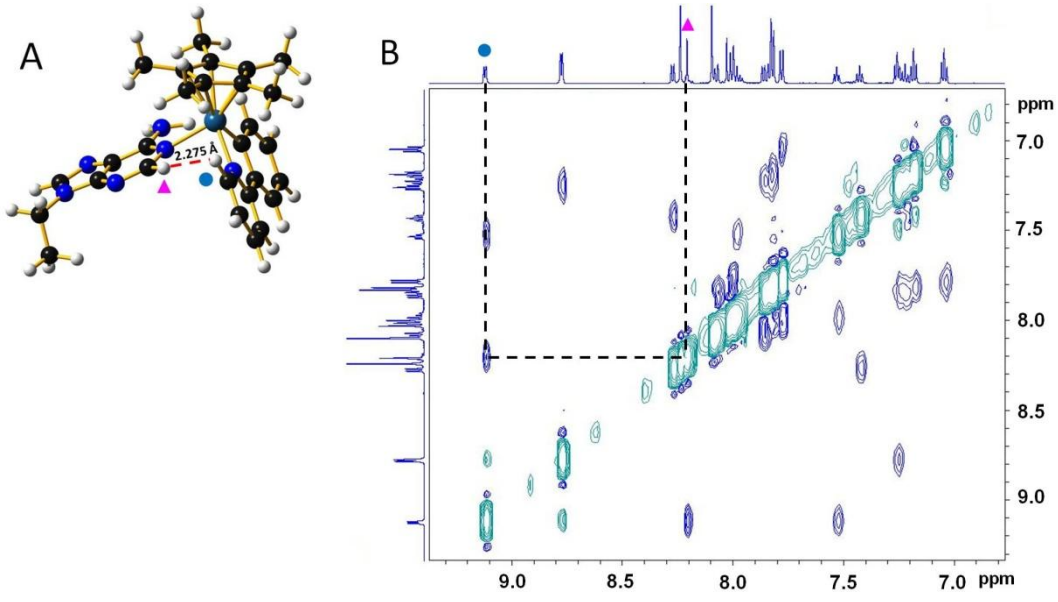

Figure 4.10. (A) Optimized geometry of $[(\eta^5\text{-}C_5Me_5)Ir(phpy)(9\text{-}EtA\text{-}N1)]^+$ showing a short distance of 2.275 Å between the HC=N proton of phpy (●) and H2 of bound 9-EtA (▲); (B) ^1H–^1H NOESY 2D NMR spectrum of adduct in the reaction mixture of complex **32** $[(\eta^5\text{-}C_5Me_5)Ir(phpy)Cl]$ with 1 mol equiv of 9-MeA (7 mM, MeOD-d_4), which confirms coordination of 9-MeA through N1 as the major binding mode.

The calculations suggest that there is a π orbital interaction between N(NH_2 of adenine) and C1 and C2(phpy) for the DFT-optimized complex $[(\eta^5\text{-}C_5Me_5)Ir(phpy)(9\text{-}EtA\text{-}N1)]^+$, Figure 4.11. This may explain the formation of adenine adducts $[(\eta^5\text{-}C_5Me_5)Ir(phpy)(9\text{-}MeA)]^+$ by complex **32**. These negatively-charged carbons on the phenyl ring appear to be favoured for such interactions compared with the analogous atoms in the pyridine ring where C1 is positively charged and C2 is slightly negative.

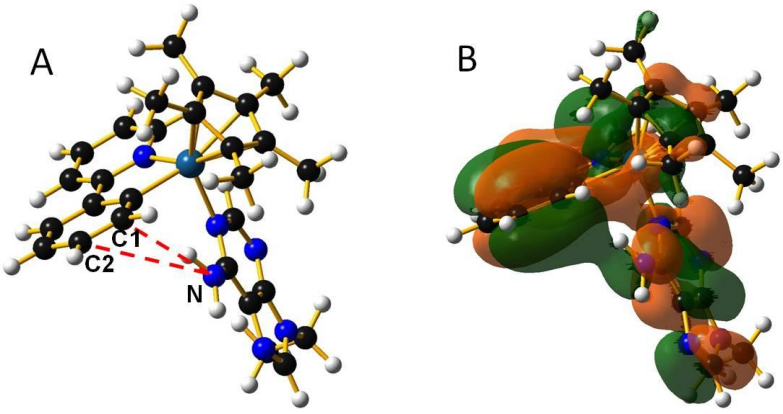

Figure 4.11. (A) DFT optimized structure of complex $[(\eta^5\text{-}C_5Me_5)Ir(phpy)(9\text{-}EtA\text{-}N1)]^+$. (B) HOMO–2 orbital for the DFT-optimized complex $[(\eta^5\text{-}C_5Me_5)Ir(phpy)(9\text{-}EtA\text{-}N1)]^+$ showing the N(NH_2 of 9-EtA)···C1/C2 (phpy) interactions.

Competition reactions between equi-molar amounts of 9-EtG and 9-MeA and complexes **29**, and **31**−**34** (ca. 1 mM) in 20% MeOD-d_4/80% D_2O (v/v, pH* ca. 7.4) at 310 K were investigated. In the competitive experiment, 9-EtG adducts **31G**, **33G** or **34G** were observed as the only product for complexes **31**, **33** or **34**, and as ca. 80% 9-EtG adduct for complex **29** and **32** (20% 9-MeA adduct), Table 4.6. The ^{1}H NMR spectra for the competition reaction for **31** are shown in Figure 4.12.

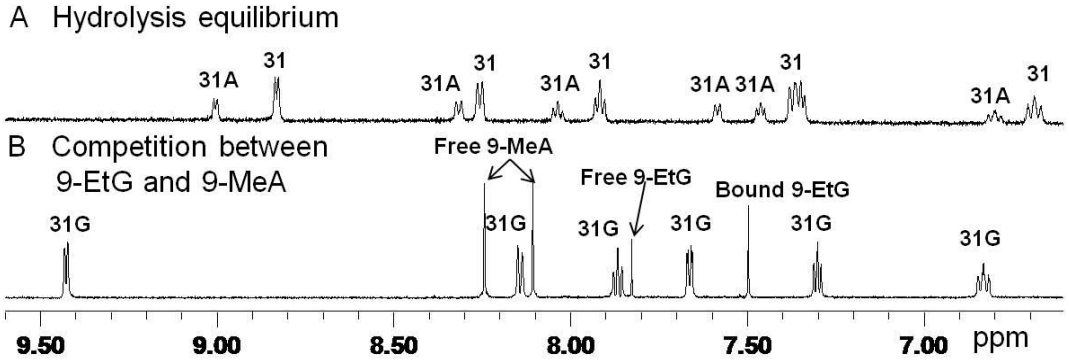

Figure 4.12. Low field region of the ^{1}H NMR spectra for the competitive reaction between 9-EtG and 9-MeA and complex **31** [(η^5-C_5Me_5)Ir(dfphpy)Cl]. (A) Equilibrium solution of **31** (1.0 mM) in 20% MeOD-d_4/80% D_2O (v/v, pH* 7.4) at 310 K, containing both the chlorido complex **31** and its aqua adduct **31A**. (B) 10 min after addition of equimolar amounts of 9-EtG and 9-MeA, showing the complete formation of 9-EtG adduct **31G**.

4.3.6 Cytotoxicity

The cytotoxicity of complexes **29**−**34**, and **37** towards A2780 human ovarian cancer cells was investigated, Table 4.8. The IC_{50} value (concentration at which 50% of the cell growth is inhibited) for Cp* Ir^{III} complexes **29**−**32** is comparable with that of cisplatin. Complexes **33**, **34** and **37** containing Cp^{xph} or Cp^{xbiph} were even more potent, especially complexes **34** and **37** with an IC_{50} value of 0.7 μM (ca. twice as active as cisplatin). Overall, the cytotoxic potency increases with phenyl substitution on Cp*: Cp^{xbiph} > Cp^{xph} > Cp*, Table 4.8.

Table 4.8. Inhibition of Growth of A2780 Human Ovarian Cancer Cells by Complexes **29**−**34**, **37** and Comparison with Cisplatin

Complex	IC_{50} [a] (μM)
[(η^5-C_5Me_5)Ir(tpy)Cl] (**29**)	3.28 ±0.14
[(η^5-C_5Me_5)Ir(phq)Cl] (**30**)	2.55 ±0.03
[(η^5-C_5Me_5)Ir(dfphpy)Cl] (**31**)	6.53 ±0.50
[(η^5-C_5Me_5)Ir(phpy)Cl] (**32**)	10.78 ±1.72
[(η^5-$C_5Me_4C_6H_5$)Ir(phpy)Cl] (**33**)	2.14 ±0.50
[(η^5-$C_5Me_4C_6H_4C_6H_5$)Ir(phpy)Cl] (**34**)	0.70 ±0.04
[(η^5-$C_5Me_4C_6H_4C_6H_5$)Ir(dfphpy)Cl] (**37**)	0.67 ±0.11
cisplatin	1.19 ±0.12

[a] Drug-treatment period was 24 h.

Complexes [(η^5-C_5Me_5)Ir(phpy)Cl] (**32**) and [(η^5-$C_5Me_4C_6H_4C_6H_5$)Ir(phpy)Cl] (**34**) were further evaluated by the National Cancer Institute Developmental Therapeutics Program (NCI/DTP, U.S.A.) for *in vitro* cytotoxic test against ca. 60 human cancer cell lines within nine tumour type subpanels.[30] The cells were treated by iridium complexes for 48 h at five concentrations ranging from 0.01 to 100 μM. Three endpoints are calculated: GI_{50} (the concentration that causes 50% cell growth inhibition), TGI (the concentration where causes 100% cell growth inhibition), and LC_{50} (the concentration that the drug decreases the original cell number by 50%).

The mean graphs for complexes **32** and **34** are listed in Figure 4.13. Complex **32** containing Cp* shows high potency in wide range of cancer cell lines, selectively for leukemia, non-small cell lung cancer and CNS cancer (highlighted by red squares in Figure 4.13A). Complex **34** containing Cp^{xbiph} ligand is selective for leukemia, colon cancer, and melanoma (Figure 4.13B), particularly active towards colon COLO 205, melanoma SK-MEL-5, and breast MDA-MB-468, with GI_{50} values less than 0.2 μM. The mean GI_{50}, TGI and LC_{50} of complexes **32**, **34** and cisplatin against ca. 60 cell lines are shown in Figure 4.14. Complex **32** is ca. 2.5× as potent as cisplatin toward NCI cancer cell lines, whilst complex **34** is ca. 15× as potent as cisplatin.

Figure 4.13. (A) Mean graph for complex [(η^5-C_5Me_5)Ir(phpy)Cl] (**32**) from the National Cancer Institute Developmental Therapeutic Program. The complex is particularly active towards cell lines highlighted by red squares.

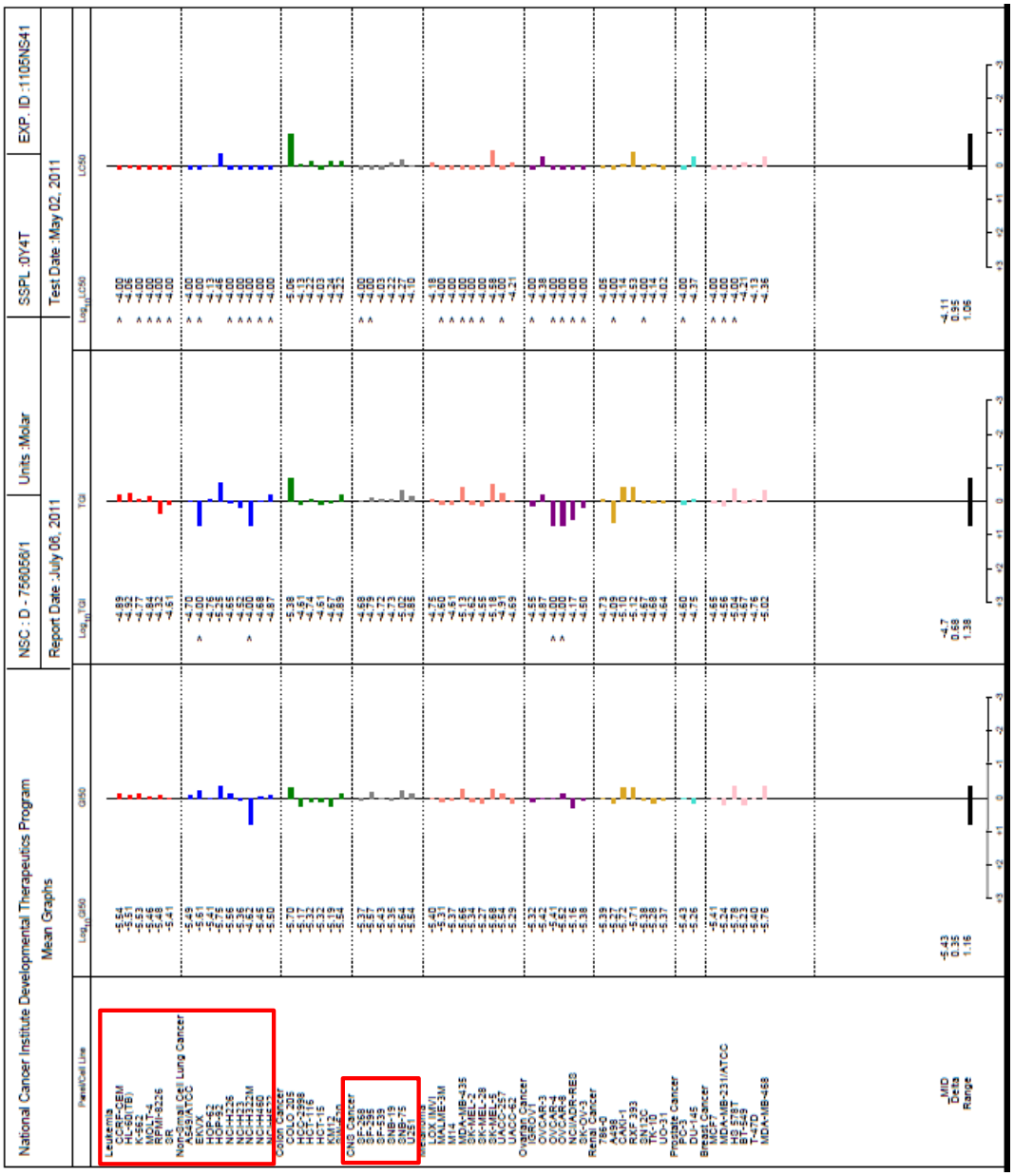

Figure 4.13. (B) Mean graph for complex [(η^5-$C_5Me_4C_6H_4C_6H_5$)Ir(phpy)Cl] (**34**) from the National Cancer Institute Developmental Therapeutic Program. The complex is particularly active towards cell lines highlighted by red squares.

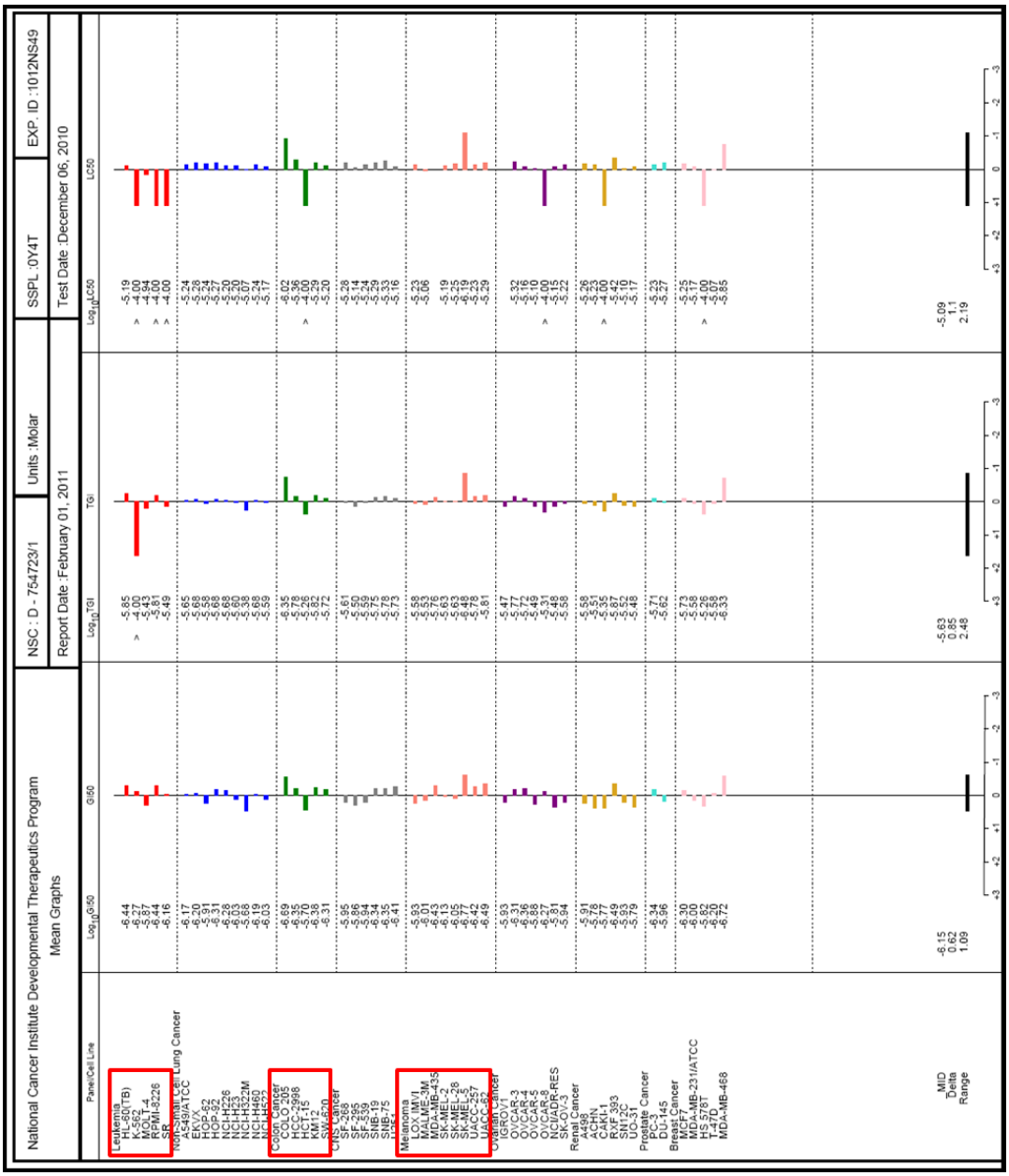

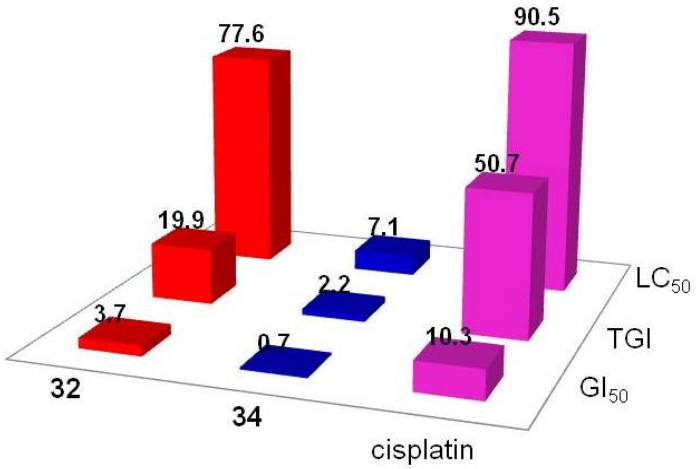

Figure 4.14. Mean graph midpoint (MG-MID) GI_{50}, TGI and LC_{50} values of complexes [(η^5-C_5Me_5)Ir(phpy)Cl] (**32**), [(η^5-$C_5Me_4C_6H_4C_6H_5$)Ir(phpy)Cl] (**34**), and comparison with cisplatin. Data for cisplatin are from NCI/DTP screening: October 2009, after 48 h treatment of the cells.[31]

4.3.7 Hydrophobicity (log *P*)

Lipophilicity often correlates with cytotoxic potency and has therefore been used extensively in structure-activity correlations.[32-38] The octanol-water partition coefficients (log *P*) for complex [(η^5-C_5Me_5)Ir(bpy)Cl]Cl (**7**·Cl) containing N,N-chelating 2'2-bipyridine and [(η^5-C_5Me_5)Ir(phpy)Cl] (**32**) containing C^N-chelating 2-phenylpyridine were determined. Instead of water alone, 0.2 M NaCl was used to suppress hydrolysis of the complexes. Complex **7** is positively-charged and shows a negative log *P* value of –0.95 (partitions

preferentially into water ca. 10-fold), whilst the neutral complex **32** is much more hydrophobic with log *P* value of 1.57 (partitions preferentially into octanol ca. 30-fold). The difference in partition coefficients between complexes **7** and **32** is thus directly related to the difference in their charges.

4.4 Discussion

4.4.1 X-ray Crystal Structures

A search of the Cambridge Crystallographic Database showed that the crystal structure of complexes [(η^5-$C_5Me_4C_6H_4C_6H_5$)Ir(phpy)Cl] (**34**) and [(η^5-$C_5Me_4C_6H_4C_6H_5$)Ir(dfphpy)Cl] (**37**) in this Chapter, with complexes [(η^5-$C_5Me_4C_6H_4C_6H_5$)Ir(bpy)Cl]PF_6 (**9**·PF_6) and [(η^5-$C_5Me_4C_6H_4C_6H_5$)Ir-(bpy(OH)O)Cl] (**21**) in Chapter 3 are the only examples containing the Cp^{xbiph} ligand. Complexes **9**·PF_6 containing N,N-bound 2,2'-bipyridine and **34** containing C^N-bound 2-phenylpyridine are structurally very similar. In complex **34**, the chelating ligand is closer to the Ir^{III} centre than in **9**·PF_6 since the Ir−C bond length [2.057(3) Å] in complex **34** is significantly shorter than the Ir−N bond length [2.091(5) Å] in the latter complex. The short Ir–C(phenylpyridine) distance causes a slight elongation of the Ir–cyclopentadienyl (centroid) bond with distance of 1.825 Å in complex **34** (Table 4.2), compared to 1.787 Å in complex **9**·PF_6. The Ir–Cl

bond lengths are similar in the two complexes, with distances of 2.3886(8) Å (Table 4.2) and 2.3840(14) Å, respectively. This behavior is similar to that observed for the C^N-chelated complex [(η^5-C_5Me_5)Ir(phpy)Cl][23] (**32**) when compared to the N,N-chelated complex [(η^5-C_5Me_5)Ir(bpy)Cl]Cl (**7**·Cl), and [(η^5-$C_5Me_4C_6H_5$)Ir-(bq)Cl] (**36**) compared to [(η^5-$C_5Me_4C_6H_5$)Ir(phen)Cl]PF_6 (**5**·PF_6), Tables 4.2 and 3.1.

The bond lengths and bond angles in complexes [(η^5-C_5Me_5)Ir(phq)Cl] (**30**) and [(η^5-C_5Me_5)Ir(phpy)Cl] (**32**)[23] are similar, except that the Ir−N bond for **30** [2.128(5) Å] is longer than that of [(η^5-C_5Me_5)Ir(phpy)Cl] [2.080(2) Å], implying weaker σ donation from N to the iridium centre due to the electron-withdrawing phenyl ring in the quinoline moiety.

From a search of the Cambridge Database, [(η^5-C_5Me_5)Ir(phpy)(9-EtG)]NO_3 (**32G**·NO_3) appears to be the first example of an X-ray structure of a guanine adduct containing a chiral iridium centre.

4.4.2 Hydrolysis and pK_a of Aqua Adducts

Since M–OH_2 (M = metal) aqua complexes are often more reactive than the equivalent chlorido complexes,[39,40] hydrolysis of the M–Cl bonds can represent an activation step for transition metal anticancer complexes.[41] There are only a few

previous studies of the aquation (substitution of Cl by H_2O) of organometallic Ir^{III} complexes.[42,43] In this Chapter, all the [(η^5-Cp^x)Ir(C^N)Cl] complexes **29**–**34** hydrolysed too rapidly for determination of their hydrolysis rates by NMR, even for the biphenyl substituted Cp^{xbiph} complex **34** [(η^5-$C_5Me_4C_6H_4C_6H_5$)Ir(phpy)Cl]. In Chapter 3, half-lives for the hydrolysis of some Cp^{xph} or Cp^{xbiph} Ir^{III} complexes containing N,N-bound 2,2′-bipyridine (bpy) or 1,10-phenanthroline (phen) chelating ligands of ca. 4 min at 310 K were determined. The electron-donor methyl groups on the Cp ring and the negatively-charged C^N-chelating ligands may together contribute to the fast hydrolysis observed for the complexes studied here since the increased effective charge on the Ir centre may facilitate chloride loss. Fast hydrolysis rates have been reported for some hexamethylbenzene Ru^{II} complexes,[44] acetylacetonate Ru^{II} and Os^{II} complexes,[16,45] and picolinate Ir^{III} complexes **12**–**14**. These results illustrate that Ir^{III} complexes are not always inert and that Ir−Cl bonds can be labile.

The aqua complexes [(η^5-C_5Me_5)Ir(tpy)(D_2O)]$^+$ (**29A**), [(η^5-C_5Me_5)Ir(phq)-(D_2O)]$^+$ (**30A**), [(η^5-C_5Me_5)Ir(dfphpy)(D_2O)]$^+$ (**31A**), [(η^5-C_5Me_5)Ir(phpy)(D_2O)]$^+$ (**32A**), [(η^5-$C_5Me_4C_6H_5$)Ir(phpy)(D_2O)]$^+$ (**33A**), and [(η^5-$C_5Me_4C_6H_4C_6H_5$)Ir-(phpy)(D_2O)]$^+$ (**34A)**, have similar pK_a values, ranging from 8.31 to 8.87 (Table 4.5). Although the substituents on the Cp* ring and the 2-phenylpyridine chelating ligand do not significantly affect the acidity of the bound water, the observed trend

caused by these substituents is clear, following the order **29A** > **32A** > **30A** > **33A** > **34A** ≈ **31A**. The presence of phenyl and biphenyl substituents on the Cp* ring lower the pK_a value by ca. 0.3 to 0.4 units, consistent with the electron-withdrawing properties of these groups. Substitution of cyclometalated 2-phenylpyridine by the fluorinated chelating ligand 2-(2,4-difluorophenyl)pyridine leads to a decrease in pK_a by 0.4 units. However, replacing cyclometalated 2-phenylpyridine by 2-(p-tolyl)pyridine or by the more π-delocalized 2-phenylquinoline, has little effect on the pK_a value (ca. 0.1 unit).

However, the aqua complexes $[(\eta^5\text{-}C_5Me_5)Ir(phpy)(D_2O)]^+$ (**32A**), $[(\eta^5\text{-}C_5Me_4C_6H_5)Ir(phpy)(D_2O)]^+$ (**33A**) and $[(\eta^5\text{-}C_5Me_4C_6H_4C_6H_5)Ir(phpy)(D_2O)]^+$ (**34A**) containing the C^N-chelated 2-phenylpyridine ligand, have significantly higher pK_a values (average 1.9 units higher) than those for the structurally similar Ir^{III} Cp^x analogues **7**−**9** bearing the N,N-bound 2,2'-bipyridine (bpy) ligand. Therefore, the replacement of the neutral bpy ligand by the anionic phpy ligand plays a significant role in decreasing the acidity of the aqua complexes, consistent with previous reports.[16] The high pK_a values of **29A**−**34A** thus ensure that most of the hydrolysed complexes would be present in the active aqua form at physiological pH.

The pH titration also showed that additional species were formed for all complexes studied here above pH 8.7 (Figure 4.5), indicating the formation of the

hydroxo-bridged dimers $\{[(\eta^5\text{-}Cp^x)Ir]_2(\mu\text{-}OD)_3\}^+$ (**38**−**40**, Figure 4.1). However, this does not occur when the chelating ligand is N,N-chelated bipyridine ligand. Clearly the Ir−C bond shows less stability with respect to the formation of dimers **38**−**40** than the Ir−N bond. It seems likely that the mechanism of formation of **38**−**40** involves initial cleavage of the Ir−C bond, followed by Ir−N bond breakage. Some Os^{II} and Ru^{II} complexes containing N,O-bound or O,O-bound ligands have been reported to form hydroxo-bridged dimers readily during their hydrolysis, resulting in their inactivity toward cancer cell lines.[46-48] In this Chapter, no hydroxo-bridged dimers of **38**−**40** were observed during hydrolysis, and all the complexes are active toward A2780 human ovarian cancer cells. This indicates that the C^N-chelated Ir^{III} complexes are stable in aqueous solution and the dimers **38**−**40** formed only appear at high pH and have no negative effect on their cytotoxicity at physiological pH.

4.4.3 Interaction with Nucleobases

Interaction with DNA is often associated with the cytotoxicity of metal anticancer drugs.[28,29] In this study, the interactions of model nucloebases, 9-EtG and 9-MeA, with complexes $[(\eta^5\text{-}C_5Me_5)Ir(tpy)Cl]$ (**29**), $[(\eta^5\text{-}C_5Me_5)Ir(phq)Cl]$ (**30**), $[(\eta^5\text{-}C_5Me_5)Ir(dfphpy)Cl]$ (**31**), $[(\eta^5\text{-}C_5Me_5)Ir(phpy)Cl]$ (**32**), $[(\eta^5\text{-}C_5Me_4C_6H_5)Ir(phpy)Cl]$ (**33**) and $[(\eta^5\text{-}C_5Me_4C_6H_4C_6H_5)Ir(phpy)Cl]$ (**34**), were investigated

(Figure 4.6 and Table 4.6). All C^N-chelated Ir^{III} complexes, except **30**, showed an exceptionally high nucleobase affinity with ca. 100% guanine adduct formation for 9-EtG, which may contribute to their high cytotoxicity. Compared with N,N-chelated Ir^{III} complexes in Chapter 3, complexes containing a C^N-bound chelating ligand bind more significantly to 9-EtG, which may be due to their inherent advantage of having higher pK_a values. Under similar pH conditions, hydrolysed C^N- complexes are more likely to be present as the reactive aqua form compared to the N,N-chelated complexes.

Complexes **29**−**34** bind more weakly to adenine compared to guanine. The competition between 9-EtG and 9-MeA for the C^N-bound Ir^{III} complexes give rise to 9-EtG adducts as the only product for complexes [(η^5-C_5Me_5)Ir(dfphpy)Cl] (**31**), [(η^5-$C_5Me_4C_6H_5$)Ir(phpy)Cl] (**33**) and [(η^5-$C_5Me_4C_6H_4C_6H_5$)Ir(phpy)Cl] (**34**), and as major product for [(η^5-C_5Me_5)Ir(tpy)Cl] (**29**) and [(η^5-C_5Me_5)Ir(phpy)Cl] (**32**), Table 4.6, confirming that binding to guanine is stronger than to adenine. This may be due to the steric hindrance caused by the NH_2 group at the 6-position of the adenine ring. In addition, guanine is usually considered to be a stronger electron donor than adenine.[49] The widely used anticancer drug in clinical, cisplatin, also prefers guanine over adenine.[50] Organometallic Ru^{II}, Os^{II} and Ir^{III} complexes containing N,O-chelating ligands or O,O-chelating ligands such as picolinate and

acetylacetonate, which possess oxygen as an H-bond acceptor for adenine C6NH_2, also bind to both guanine and adenine residues.[16,47,51]

Ir^{III} cyclopentadienyl complexes in Chapter 3 containing a neutral N,N-chelating ligand (phen, bpy, or ethylenediamine) bind selectively to 9-EtG, but not to adenine. The formation of adenine adducts in this Chapter may be due to the interaction between NH_2 of 9-MeA and negatively-charged carbons on the C^N-chelating ligand, Figure 4.11. Thus complexes **29**−**31** containing different substituents on the phenylpyridine bind to 9-MeA differently. The electron donating methyl group on the phenyl ring in complex [(η^5-C_5Me_5)Ir(tpy)Cl] (**29**) increases electron density and may facilitate the interaction with 9-MeA (>90%). In contrast, only 35% of complex [(η^5-C_5Me_5)Ir(dfphpy)Cl] (**31**) formed 9-MeA adducts which may be due to the presence of the electron-withdrawing fluoro group. Complex **30** [(η^5-C_5Me_5)Ir(phq)Cl] has the lowest affinity for both model nucleobases among the five complexes, with 45% and <5% binding to 9-EtG and 9-MeA, respectively. The weaker binding is most likely due to the steric hindrance caused by the quinoline ligand.

2D NMR spectra (Figures 4.9 and 4.10) show that complex **32** binds to adenine mainly through N1, which is consistent with DFT calculations. The N7 atoms of guanine and adenine are accessible to metal ions, such as Pt in cisplatin,[52] for coordination in the major groove of DNA, whereas N1 of A is involved in

Watson-Crick base-pairing. Complex **32** reacted with guanine via N7 (as confirmed by X-ray crystal structure of **32G** $\cdot NO_3$), and formed adenine adducts mainly via N1. In addition, complex **32** has a higher affinity for guanine compared to adenine. Binding to guanine may therefore play a more significant role in its cytotoxicity.

4.4.4 Hydrophobicity (log *P*)

The log *P* value as a measure for hydrophobicity, has been investigated as a factor relevant to anticancer activity of metal-based drugs for many years. Neutral complex [(η^5-C_5Me_5)Ir(phpy)Cl] (**32**) is more hydrophobic than negatively charged complex [(η^5-C_5Me_5)Ir(bpy)Cl]$^+$ (**7**), with log *P* values of 1.57 and –0.95, respectively. The difference in partition coefficients between complexes **32** and **7** is thus related to the difference in their charges.

The hydrophobicity and cancer cell activity correlate significantly in this study. Complex **7** is less hydrophobic and inactive. Complex **32** displays much higher hydrophobicity, and is cytotoxic. This hydrophobicity difference is likely to result in higher cancer cell uptake and contribute to the higher cytotoxicity of complex **32**. For compounds in the Comprehensive Medicinal Chemistry (CMC) database, which is often used to validate new pharmacophores, log *P* values range between –0.4 and 5.6, with an average value of 2.52.[53] The log *P* value of 1.57 for complex **32** is

within this range, whilst the log *P* of –0.95 for complex **7** is more negative, i.e. the complex **7** may be too hydrophilic for optimum drug-like properties.

4.4.5 Cytotoxicity

Some Cp* Ir^{III} complexes studied in Chapter 3 containing N,N-, or N,O-chelating ligands are inactive toward A2780 human ovarian cancer cells. However, all Cp* complexes [(η^5-C_5Me_5)Ir(tpy)Cl] (**29**), [(η^5-C_5Me_5)Ir(phq)Cl] (**30**), [(η^5-C_5Me_5)Ir(dfphpy)Cl] (**31**), and [(η^5-C_5Me_5)Ir(phpy)Cl] (**32**) studied here showed promising activity toward the human ovarian A2780 cancer cell line with IC_{50} values ranging from 2.5−10.8 μM (Table 4.8). Thus the introduction of C^N-chelating ligands is an effective method for switching on the cancer cell cytotoxicity of Cp* Ir^{III} complexes. The Cp* complex [(η^5-C_5Me_5)Ir(phpy)Cl] (**32**) containing C^N-chelating ligand is even as potent as the Cp^{xbiph} complex [(η^5-$C_5Me_4C_6H_4C_6H_5$)Ir(bpy)Cl]PF_6 (**9**·PF_6) against NCI 60 cancer cell lines, Figures 3.16 and 4.14. The strong binding of Ir to nucleobases, especially to guanine bases, may provide an important contribution towards the cytotoxicity. Also the neutral C^N- complexes display more hydrophobic character than the positively-charged N,N- complexes and therefore possess enhanced cellular uptake which may also contribute to the cytotoxicity. The introduction of substituents on

the phenylpyridine ring enhanced the cytotoxicity of **32** [(η^5-C_5Me_5)Ir(phpy)Cl], Table 4.8. Particularly active is the complex [(η^5-C_5Me_5)Ir(phq)Cl] (**30**), which is 4 times more potent than **32**. The ability of the phq ligand to intercalate into DNA may contribute to this enhanced potency.[54,55]

Compared to the parent Cp* complex [(η^5-C_5Me_5)Ir(phpy)Cl] (**32**), the introduction of phenyl or biphenyl substituents onto the tetramethylcyclopenta-dienyl ring to give complexes [(η^5-$C_5Me_4C_6H_5$)Ir(phpy)Cl] (**33**) and [(η^5-$C_5Me_4C_6H_4C_6H_5$)Ir(phpy)Cl] (**34**), results in a dramatic increase in cytotoxicity, Table 4.8. Complex **34** is more than 5 times more potent than complex **32** against NCI 60 cancer cell lines, Figure 4.14. The Cp^{xbiph} complex [(η^5-$C_5Me_4C_6H_4C_6H_5$)Ir(dfphpy)Cl] (**37**) is one order of magnitude more potent than Cp* complex [(η^5-C_5Me_5)Ir(dfphpy)Cl] (**31**). The activity of Ru^{II} arene complexes also increases with the size of the coordinated arene.[56,57] This suggests that phenyl groups may play a crucial role in the mechanism of action of these phenylpyridine complexes. First, the phenyl or biphenyl ring increases the hydrophobicity of the molecule, which may assist with passage across cell membranes. In addition, the extended phenyl rings can intercalate into DNA, thus causing distortion of DNA structure. It was shown in Chapter 3 that the intercalative ability of 1,10-phenanthroline Ir^{III} chlorido complexes increases in the order of Cp^{xbiph} > Cp^{xph} > Cp*. Complexes [(η^5-$C_5Me_4C_6H_5$)Ir(phpy)Cl] (**33**),

[(η^5-$C_5Me_4C_6H_4C_6H_5$)Ir(phpy)Cl] (**34**) and [(η^5-$C_5Me_4C_6H_4C_6H_5$)Ir(dfphpy)Cl] (**37**) containing phenyl or biphenyl substitutions may interact with DNA by a dual mode: nucleobase binding to iridium accompanied by intercalation of the phenyl groups, which is a different mechanism of action from that of cisplatin.

4.5 Conclusions

Iridium-based anticancer agents, including organometallic iridium complexes, are currently attracting attention as potential anticancer agents with novel mechanisms of action. The effects of changing the Cp^x ligand and negatively-charged C^N-chelating ligand of Ir^{III} cyclopentadienyl complexes of the type [(η^5-Cp^x)Ir(C^N)Cl] on the hydrolysis of the chlorido complexes, acidity of the aqua adducts, nucleobase binding, and cancer cell cytotoxicity have been studied in this Chapter.

All the studied complexes undergo rapid hydrolysis (<5 min at 278 K) due to the strongly electron-donating methyl groups on Cp ring and negatively-charged C^N-chelating ligand. Generally, the aqua adducts of the C^N- complexes studied here possess low acidity, with pK_a values 1.9 units higher than N,N- analogues, which ensures that the active aqua adduct is the major form after hydrolysis at physiological pH, and may contribute to the strong binding to guanine. The

substituents on both the Cp* ring and on 2-phenylpyridine can fine-tune the acidity of aqua adducts according to their electronic effects. Hydroxo-bridged dimers $\{[(\eta^5\text{-}Cp^x)Ir]_2(\mu\text{-}OD)_3\}^+$ (**38**–**40**) are observed at high pH (>8.7), indicating the stability of C^N- complexes is not as high as N,N- analogues under strongly basic conditions.

Complexes **29** and **31**–**34** show strong binding to the nucleobase guanine. Unlike the Ir^{III} complexes containing N,N-chelating ligands, the C^N- complexes can also bind to adenine. However, they show a strong preference for binding to guanine over adenine. Complex **30** displayed the lowest extent of nucleobase binding among the complexes studied due to steric hindrance from the chelating ligand 2-phenylquinoline.

The C^N- complexes showed very promising anticancer activity toward A2780 human ovarian cancer cells and NCI 60 cancer cell lines. The Cp* complexes possess more potent activity than cisplatin. The introduction of phenyl or biphenyl substituent significantly improved their cytotoxicity, especially for the Cp^{xbiph} complexes **34** and **37** which have submicromolar activity against 60 cancer cells. The strong binding to guanine bases and hydrophobicity may contribute to their high activity. This study shows that desirable features can be introduced into this class of complexes to optimize their design as anticancer agents.

4.6 References

(1) *Medicinal Organometallic Chemistry (Topics in Organometallic Chemistry)*, 1st ed.; Jaouen, G.; Metzler-Nolte, N., Eds.; Springer-Verlag: Heidelberg, Germany, 2010; Vol. 32.

(2) Gasser, G.; Ott, I.; Metzler-Nolte, N. *J. Med. Chem.* **2011**, *54*, 3-25.

(3) Fish, R. H. *Aust. J. Chem.* **2010**, *63*, 1505-1513.

(4) Suss-Fink, G. *Dalton Trans.* **2010**, *39*, 1673-1688.

(5) Dyson, P. J.; Sava, G. *Dalton Trans.* **2006**, 1929-1933.

(6) Bruijnincx, P. C. A.; Sadler, P. J. In *Advances in Inorganic Chemistry*; Rudi van, E., Hubbard, C. D., Eds.; Academic Press: New York, 2009; 61, pp 1-62.

(7) Marcon, G.; Casini, A.; Mura, P.; Messori, L.; Bergamo, A.; Orioli, P. *Metal-Based Drugs* **2000**, *7*, 195-200.

(8) Messori, L.; Marcon, G.; Orioli, P.; Fontani, M.; Zanello, P.; Bergamo, A.; Sava, G.; Mura, P. *J. Inorg. Biochem.* **2003**, *95*, 37-46.

(9) Wilbuer, A.; Vlecken, D. H.; Schmitz, D. J.; Kräling, K.; Harms, K.; Bagowski, C. P.; Meggers, E. *Angew. Chem., Int. Ed.* **2010**, *49*, 3839-3842.

(10) Youinou, M.-T.; Ziessel, R. *J. Organomet. Chem.* **1989**, *363*, 197-208.

(11) Amouri, H.; Moussa, J.; Renfrew, A. K.; Dyson, P. J.; Rager, M. N.; Chamoreau, L.-M. *Angew. Chem., Int. Ed.* **2010**, *49*, 7530-7533.

(12) Casini, A.; Edafe, F.; Erlandsson, M.; Gonsalvi, L.; Ciancetta, A.; Re, N.; Ienco, A.; Messori, L.; Peruzzini, M.; Dyson, P. J. *Dalton Trans.* **2010**, *39*, 5556-5563.

(13) Gras, M.; Therrien, B.; Süss-Fink, G.; Casini, A.; Edafe, F.; Dyson, P. J. *J. Organomet. Chem.* **2010**, *695*, 1119-1125.

(14) van Rijt, S. H.; Sadler, P. J. *Drug Discovery Today* **2009**, *14*, 1089-1097.

(15) Peacock, A. F. A.; Sadler, P. J. *Chem. Asian J.* **2008**, *3*, 1890-1899.

(16) Fernández, R.; Melchart, M.; Habtemariam, A.; Parsons, S.; Sadler, P. J. *Chem.-Eur. J.* **2004**, *10*, 5173-5179.

(17) Hull, J. F.; Balcells, D.; Blakemore, J. D.; Incarvito, C. D.; Eisenstein, O.; Brudvig, G. W.; Crabtree, R. H. *J. Am. Chem. Soc.* **2009**, *131*, 8730-8731.

(18) Lo, K. K.-W.; Louie, M.-W.; Zhang, K. Y. *Coord. Chem. Rev.* **2010**, *254*, 2603-2622.

(19) Fan, D.; Yang, C.-T.; Ranford, J. D.; Vittal, J. J.; Foo Lee, P. *Dalton Trans.* **2003**, 3376-3381.

(20) Ruiz, J.; Vicente, C.; de Haro, C.; Bautista, D. *Dalton Trans.* **2009**, 5071-5073.

(21) Leung, S.-K.; Kwok, K. Y.; Zhang, K. Y.; Lo, K. K.-W. *Inorg. Chem.* **2010**, *49*, 4984-4995.

(22) White, C. Y., A.; Maitlis, P. M. *Inorg. Chem.* **1992**, *29*, 228-234.

(23) Li, L.; Brennessel, W. W.; Jones, W. D. *J. Am. Chem. Soc.* **2008**, *130*, 12414-12419.

(24) Sheldrick, G. M. *Acta Crystallogr.* **1990**, *A46*, 467-473.

(25) Sheldrick, G. M. *SHELXL-97*; University of Göttingen: Göttingen, Germany, 1997.

(26) Adamo, C.; Barone, V. *J. Chem. Phys.* **1999**, *110*, 6158-6170.

(27) Krezel, A.; Bal, W. *J. Inorg. Biochem.* **2004**, *98*, 161-166.

(28) Zhang, C. X.; Lippard, S. J. *Curr. Opin. Chem. Biol.* **2003**, *7*, 481-489.

(29) Deubel, D. V.; Lau, J. K.-C. *Chem. Commun.* **2006**, 2451-2453.

(30) http://dtp.nci.nih.gov/branches/btb/ivclsp.html (accessed on 16 September 2011)

(31) Görmen, M.; Pigeon, P.; Top, S.; Hillard, E. A.; Huché, M.; Hartinger, C. G.; de Montigny, F.; Plamont, M.-A.; Vessières, A.; Jaouen, G. *Chem. Med. Chem.* **2010**, *5*, 2039-2050.

(32) Loh, S. Y.; Mistry, P.; Kelland, L. R.; Abel, G.; Harrap, K. R. *Br. J. Cancer* **1992**, *66*, 1109-1115.

(33) Barbieri, R. *Inorg. Chim. Acta* **1992**, *191*, 253-259.

(34) Mendoza-Ferri, M.-G.; Hartinger, C. G.; Eichinger, R. E.; Stolyarova, N.; Severin, K.; Jakupec, M. A.; Nazarov, A. A.; Keppler, B. K. *Organometallics* **2008**, *27*, 2405-2407.

(35) Song, R.; Park, S. Y.; Kim, Y.-S.; Kim, Y.; Kim, S.-J.; Ahn, B. T.; Sohn, Y. S. *J. Inorg. Biochem.* **2003**, *96*, 339-345.

(36) Gramatica, P.; Papa, E.; Luini, M.; Monti, E.; Gariboldi, M.; Ravera, M.; Gabano, E.; Gaviglio, L.; Osella, D. *J. Biol. Inorg. Chem.* **2010**, *15*, 1157-1169.

(37) Leo, A. J. *Chem. Rev.* **1993**, *93*, 1281-1306.

(38) Reithofer, M. R.; Bytzek, A. K.; Valiahdi, S. M.; Kowol, C. R.; Groessl, M.; Hartinger, C. G.; Jakupec, M. A.; Galanski, M.; Keppler, B. K. *J. Inorg. Biochem.* **2011**, *105*, 46-51.

(39) Hohmann, H.; Hellquist, B.; van Eldik, R. *Inorg. Chem.* **1992**, *31*, 345-351.

(40) Martin, R. B. In *Cisplatin: Chemistry and Biochemistry of a Leading Anticancer Drug*; Lippert, B., Ed.; VHCA & Wiley-VCH: Zürich, Switzerland, 1999, pp 181-205.

(41) Pizarro, A. M.; Habtemariam, A.; Sadler, P. J. In *Medicinal Organometallic Chemistry (Topics in Organometallic Chemistry)*, 1st ed.; Jaouen, G., Metzler-Nolte, N., Ed.; Springer-Verlag: Heidelberg, Germany, 2010; 32, pp 21-56.

(42) Helm, L.; Merbach, A. E. *Coord. Chem. Rev.* **1999**, *187*, 151-181.

(43) Koelle, U. *Coord. Chem. Rev.* **1994**, *135-136*, 623-650.

(44) Wang, F.; Habtemariam, A.; van der Geer, E. P. L.; Fernández, R.; Melchart, M.; Deeth, R. J.; Aird, R.; Guichard, S.; Fabbiani, F. P. A.; Lozano-Casal, P.; Oswald, I. D. H.; Jodrell, D. I.; Parsons, S.; Sadler, P. J. *Proc. Natl. Acad. Sci. U. S. A.* **2005**, *102*, 18269-18274.

(45) Peacock, A. F. A.; Melchart, M.; Deeth, R. J.; Habtemariam, A.; Parsons, S.; Sadler, P. J. *Chem.-Eur. J.* **2007**, *13*, 2601-2613.

(46) Peacock, A. F. A.; Habtemariam, A.; Fernández, R.; Walland, V.; Fabbiani, F. P. A.; Parsons, S.; Aird, R. E.; Jodrell, D. I.; Sadler, P. J. *J. Am. Chem. Soc.* **2006**, *128*, 1739-1748.

(47) Peacock, A. F. A.; Parsons, S.; Sadler, P. J. *J. Am. Chem. Soc.* **2007**, *129*, 3348-3357.

(48) Kljun, J.; Bytzek, A. K.; Kandioller, W.; Bartel, C.; Jakupec, M. A.; Hartinger, C. G.; Keppler, B. K.; Turel, I. *Organometallics* **2011**, *30*, 2506-2512.

(49) Pullman, B.; Pullman, A. *Biochim. Biophys. Acta* **1959**, *36*, 343-350.

(50) Baik, M.-H.; Friesner, R. A.; Lippard, S. J. *J. Am. Chem. Soc.* **2003**, *125*, 14082-14092.

(51) Melchart, M.; Habtemariam, A.; Parsons, S.; Sadler, P. *J. Inorg. Biochem.* **2007**, *101*, 1903-1912.

(52) Jung, Y.; Lippard, S. J. *Chem. Rev.* **2007**, *107*, 1387-1407.

(53) Ghose, A. K.; Viswanadhan, V. N.; Wendoloski, J. J. *J. Comb. Chem.* **1999**, *1*, 55-68.

(54) Atwell, G. J.; Bos, C. D.; Baguley, B. C.; Denny, W. A. *J. Med. Chem.* **1988**, *31*, 1048-1052.

(55) Atwell, G. J.; Baguley, B. C.; Denny, W. A. *J. Med. Chem.* **1989**, *32*, 396-401.

(56) Morris, R. E.; Aird, R. E.; del Socorro Murdoch, P.; Chen, H.; Cummings, J.; Hughes, N. D.; Parsons, S.; Parkin, A.; Boyd, G.; Jodrell, D. I.; Sadler, P. J. *J. Med. Chem.* **2001**, *44*, 3616-3621.

(57) Aird, R. E.; Cummings, J.; Ritchie, A. A.; Muir, M.; Morris, R. E.; Chen, H.; Sadler, P. J.; Jodrell, D. I. *Br. J. Cancer* **2002**, *86*, 1652-1657.

Chapter 5

Hydride-Transfer Reactions of Cyclopentadienyl Iridium Aqua Complexes

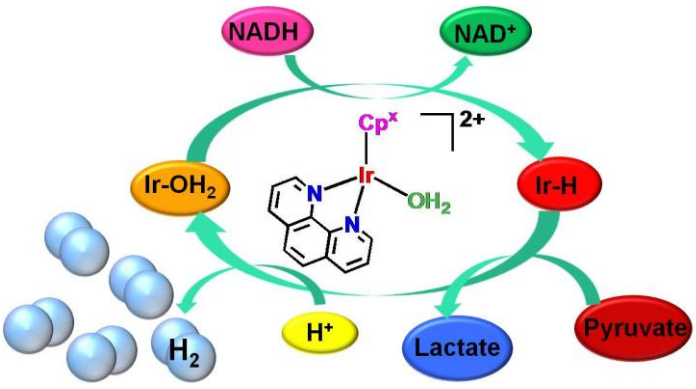

5.1 Introduction

Coenzymes are small organic molecules that link to enzymes and whose presence is essential to the activity of those enzymes. NAD^+ (β-nicotinamide adenine dinucleotide) is an important coenzyme found in all living cells. In metabolism, NAD^+ and its reduced form 1,4-NADH (Figure 5.1) are involved in redox reactions, carrying electrons from one reaction to another. Both NAD^+ and 1,4-NADH play important roles as cofactors in numerous biocatalysed processes, including energy metabolism, antioxidation and oxidative stress, immunological functions and cell death.[1]

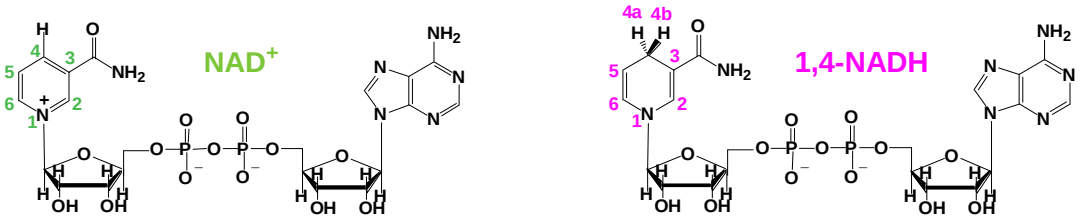

Figure 5.1. Structures and numbering schemes for NAD^+ and 1,4-NADH.

There is an increasing demand for regeneration of the coenzyme 1,4-NADH in biocatalysis.[2,3] Conversion of NAD^+ to 1,4-NADH by enzymatic, chemical, photochemical or electrochemical methods has been extensively studied.[4-7] For example, Ir^{III} and Rh^{III} pentamethylcyclopentadienyl complexes have been shown to catalyse the regioselective reduction of NAD^+ to 1,4-NADH with formate as the

hydride source.[8,9] However, the reverse reaction, i.e. conversion from 1,4-NADH to NAD^+, has little been reported.[10]

In our group, it was shown that $[(\eta^6\text{-arene})Ru(en)Cl)]^+$ complexes (where arene = hexamethylbenzene (hmb), *p*-cymene (*p*-cym), indane (ind), and en = ethylenediamine) can convert NAD^+ to 1,4-NADH using formate as hydride source.[11] Such reactions might be feasible in cells which can tolerate millimolar levels of formate, a potential basis for the design of catalytic drugs. In an attempt to improve the efficiency of the Ru^{II} arene catalyst, the effect of replacing en by π-acceptor ligands has been investigated.[12] It has been discovered that not only can these complexes convert NAD^+ to 1,4-NADH using formate as the hydride source, but also that the reverse reaction, hydride donation from 1,4-NADH to a metal centre, is facile, the first observation of such a transfer.

In this Chapter, hydride-transfer reactions of cyclopentadienyl Ir^{III} aqua complex to regioselectively reduce NAD^+ in the presence of formate under biologically relevant conditions are described. The reverse reaction, i.e. hydride-transfer reaction from 1,4-NADH to the iridium complexes and formation of NAD^+, was also investigated. Moreover it is shown that these organometallic Ir^{III} complexes can act as robust hydrogenation catalysts using 1,4-NADH as a source of hydride, including the production of H_2. A preliminary elucidation of the mechanisms involved is proposed.

5.2 Experimental Section

5.2.1 Materials

β-Nicotinamide adenine dinucleotide hydrate (NAD^+), *β*-nicotinamide adenine dinucleotide reduced dipotassium salt (1,4-NADH), alcohol dehydrogenase from saccharomyces cerevisiae (ADH), sodium formate ($NaHCO_2$), silver nitrate ($AgNO_3$), and sodium pyruvate were obtained from Sigma-Aldrich.

The Ir^{III} precursor [(η^5-C_5Me_5)Ir(phen)Cl]Cl (**4**) was synthesised according to literature methods.[13] The synthesis of the Ir^{III} precursor [(η^5-$C_5Me_4C_6H_5$)Ir(phen)Cl]PF_6 (**5**) was described in Chapter 3. To generate the aqua complexes [(η^5-C_5Me_5)Ir(phen)(H_2O)]$^{2+}$ (**4A**) and [(η^5-$C_5Me_4C_6H_5$)Ir(phen)-(H_2O)]$^{2+}$ (**5A**), their respective chlorido complexes **4** and **5** were dissolved in 10% MeOD-d_4/90% H_2O (v/v), then 1.96 and 0.98 mol equiv of $AgNO_3$ were added. The solution was stirred for 24 h at 298 K, and AgCl was removed by filtration.

The solvent used for UV-Vis absorption spectroscopy was deionised water. The solvents used for ^{1}H NMR spectroscopy were methanol-d_4 from Aldrich, and deionised water.

5.2.2 Methods

5.2.2.1 NMR Spectroscopy

^{1}H and ^{1}H–^{1}H TOCSY 2D NMR spectra were acquired in 5 mm NMR tubes at 298 K (unless otherwise stated) on either Bruker DRX 500, Bruker AV III 600 or Bruker AV II 700 NMR spectrometers. For NMR experiments using 90% H_2O/10% MeOD-d_4, the water peak was suppressed as described in Chapter 2.

5.2.2.2 UV-Vis Absorption Spectroscopy

Reactions of Ir^{III} complex **5A** with 1,4-NADH produced from reaction of the enzyme alcohol dehydrogenase (ADH) and NAD^+, and catalytic conversion of 1,4-NADH to NAD^+ by Ir^{III} complex **5A** were studied by UV-Vis spectroscopy. UV-Vis absorption spectra were recorded at different temperatures ranging from 298 K to 315 K, from 220 to 500 nm as described in Chapter 2. The concentrations of 1,4-NADH, NAD^+, enzyme ADH and complex $[(\eta^5\text{-}C_5Me_4C_6H_5)Ir(phen)(H_2O)]^{2+}$ (**5A**) in UV-Vis spectroscopy studies were obtained using the Beer–Lambert law and extinction coefficients: 259 nm $\varepsilon_{(NAD^+)}$ = 16900 $M^{-1}cm^{-1}$;[14] 339 nm $\varepsilon_{(1,4\text{-NADH})}$ = 6220 $M^{-1}cm^{-1}$;[15] 280 nm $\varepsilon^{1\%}_{(ADH)}$ = 14.6;[16] 274 nm $\varepsilon_{(\mathbf{5A})}$ = 8900 $M^{-1}cm^{-1}$.

5.2.2.3 pH Measurements

pH values were measured at ambient temperature using a Corning 240 pH meter as described in Chapter 2.

5.2.2.4 Reduction of NAD^+ by 4A Using Formate as a Hydride Source

NAD^+ (1.5 mol equiv) was added to an NMR tube containing a 1 mM solution of the $[(\eta^5\text{-}C_5Me_5)Ir(phen)(H_2O)]^{2+}$ (**4A**) and an excess of $NaHCO_2$ (25 mol equiv) in 10% MeOD-d_4/90% H_2O at ambient temperature. The ^1H NMR spectra of the resulting solutions were recorded at 298 K at various time intervals for 3 h.

5.2.2.5 NMR Spectroscopy Studied Reactions with 1,4-NADH

Two or 3 mol equiv of 1,4-NADH were added to an NMR tube containing a 1 mM solution of $[(\eta^5\text{-}C_5Me_5)Ir(phen)(H_2O)]^{2+}$ (**4A**) or $[(\eta^5\text{-}C_5Me_4C_6H_5)Ir\text{-}(phen)(H_2O)]^{2+}$ (**5A**) in 10% MeOD-d_4/90% H_2O at ambient temperature. The ^1H NMR spectra of the resulting solutions were recorded at 298 K at various time intervals for 33 h. A $^1H–^1H$ TOCSY 2D NMR spectrum was recorded for the reaction of **5A** with 1,4-NADH after 22 h.

5.2.2.6 Detection of H_2 by Gas Chromatography

A solution containing complex $[(\eta^5\text{-}C_5Me_4C_6H_5)Ir(phen)(H_2O)]^{2+}$ (**5A**, 0.9 mM) and 1,4-NADH (1.3 mM), was prepared in 5 mM phosphate buffer, pH 7.2 in a 5 mm NMR tube equipped with a suba seal from stock solutions of the reactants which had been thoroughly purged with N_2 before mixing. Aliquots of the head space (100 uL) were sampled by using a gas-tight syringe immediately, after 40 min,

80 min, 130 min, 160 min, 5 h, and 23 h of incubation at 298 K, and analysed on an Agilent GC 7890A instrument equipped with a thermal conductivity detector, a 5-Å molecular sieve column, using N_2 as the carrier gas. Under these conditions different amounts of H_2 were detected with a retention time of 0.39 min.

5.2.2.7 Hydrogenation of Pyruvate

Three mol equiv of 1,4-NADH were added to an NMR tube containing a 1 mM solution of **5A** in 10% MeOD-d_4/90% H_2O (v/v) at ambient temperature, followed by the addition of 3 mol equiv of sodium pyruvate. The ^{1}H NMR spectra of the resulting solutions were recorded at 298 K at various time intervals for 24 h.

5.2.2.8 Catalytic Conversion of 1,4-NADH to NAD^+ by 5A

Kinetic experiments were performed with changes in concentration of 1,4-NADH at 70, 110, 156 and 173 μM, while keeping concentration of the catalyst [(η^5-$C_5Me_4C_6H_5$)Ir(phen)(H_2O)]$^{2+}$ (**5A**) constant at 1.5 μM (ca. pH 7.4), or with changes in concentration of **5A** at 1.0, 1.5 and 3.0 μM in water (pH 7.5) at different temperatures, while keeping concentration of 1,4-NADH at 160 μM. UV-Vis spectra were recorded after different time intervals to monitor the course of reaction at 310 K from 220 nm to 500 nm. The absorbance at 339 nm, assignable to 1,4-NADH, was used to analyse data.

5.3 Results

Two cyclopentadienyl Ir^{III} aqua complexes $[(\eta^5\text{-}C_5Me_5)Ir(phen)(H_2O)]^{2+}$ (**4A**) and $[(\eta^5\text{-}C_5Me_4C_6H_5)Ir(phen)(H_2O)]^{2+}$ (**5A**) (where phen = 1,10-phenanthroline, Figure 5.2), generated from their respective chlorido complexes using Ag^+ to remove Cl^-, were exploited in this Chapter.

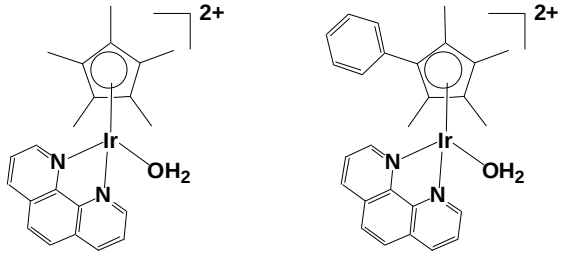

4A **5A**

Figure 5.2. Iridium cyclopentadienyl complexes studied in this Chapter.

5.3.1 Reduction of NAD^+ Using Formate as a Hydride Source

The possibility that Ir^{III} aqua complex $[(\eta^5\text{-}C_5Me_5)Ir(phen)(H_2O)]^{2+}$ (**4A**) could react directly with sodium formate to generate hydride species (Ir–H) was investigated. Addition of 25 mol equiv of $NaHCO_2$ to 1 mM solution of **4A** in 10% MeOD-d_4/90% H_2O at 298 K formed a set of new peaks immediately, which was attributed to the formation of a formato adduct (Ir–O_2CH), Figure 5.3B. Peak assigned to the bound formate are high-field shifted ca. 0.9 ppm in comparison to those of free formate (8.43 ppm). The ^{1}H NMR peaks of the formato adduct

decreased in intensity rapidly and a second set of new peaks was observed over time and was assigned to formation of hydride adduct $[(\eta^5\text{-}C_5Me_5)Ir(phen)(H)]^+$ (Ir–H, –11.1 ppm), Figures 5.3C and 5.3D.

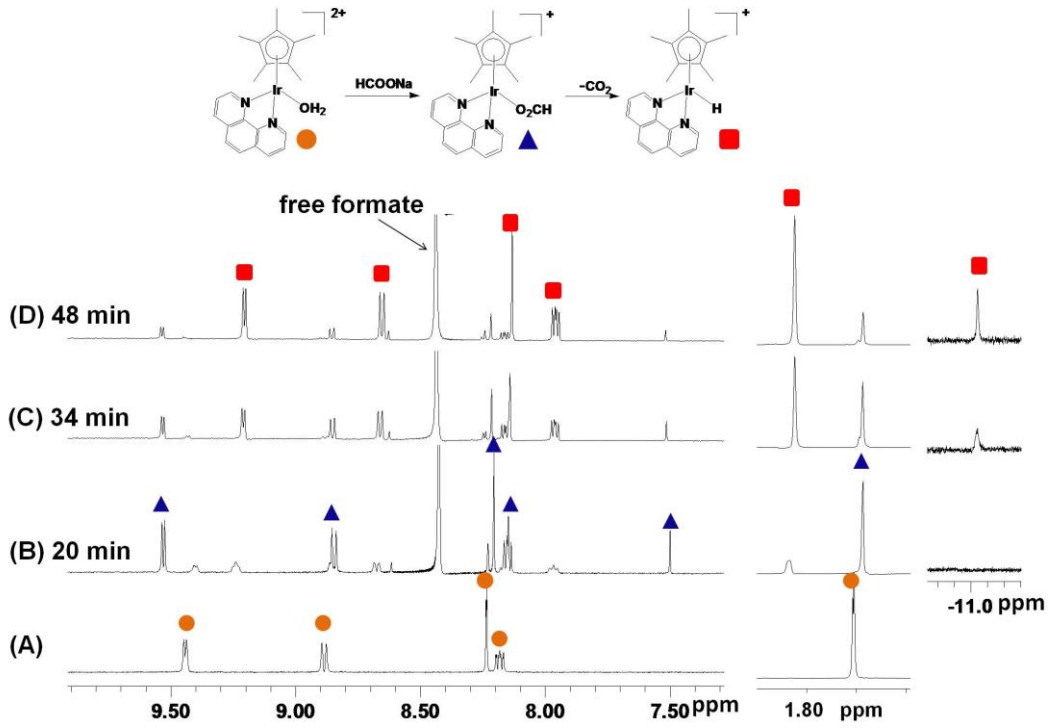

Figure 5.3. ^{1}H NMR spectra of a 1 mM solution of $[(\eta^5\text{-}C_5Me_5)Ir(phen)(H_2O)]^{2+}$ (**4A**, spectrum A) with sodium formate (molar ratio 1:25) in 10% MeOD-d_4/90% H_2O at 298 K at various time intervals. Peak assignments are indicated on the structures. The 3 sections from left to right show the low-field region, methyl groups on Cp* ring (×0.25), and Ir−H hydride peak (×4), respectively.

Next the hydride-transfer reaction from Ir^{III} aqua complex $[(\eta^5\text{-}C_5Me_5)Ir(phen)(H_2O)]^{2+}$ (**4A**) to NAD^+ using sodium formate as a source of hydride

was studied. The ^{1}H NMR spectra of $[(\eta^5\text{-}C_5Me_5)Ir(phen)(H_2O)]^{2+}$ (**4A**) (1 mM) with NAD^+ and sodium formate (molar ratios 1:1.5:25) in 10% MeOD-d_4/90% H_2O at 298 K at various time intervals shown the fast reduction of NAD^+ to 1,4-NADH as indicated by a decrease on the intensity of the signals of free NAD^+ (H2 at 9.45 ppm) and the new peaks assignable to 1,4-NADH (H2 at 7.05 ppm and H4a/H4b at 2.80 ppm), Figure 5.4. The results show that complex **4A** can convert NAD^+ to 1,4-NADH through hydride-transfer using formate as a hydride source.

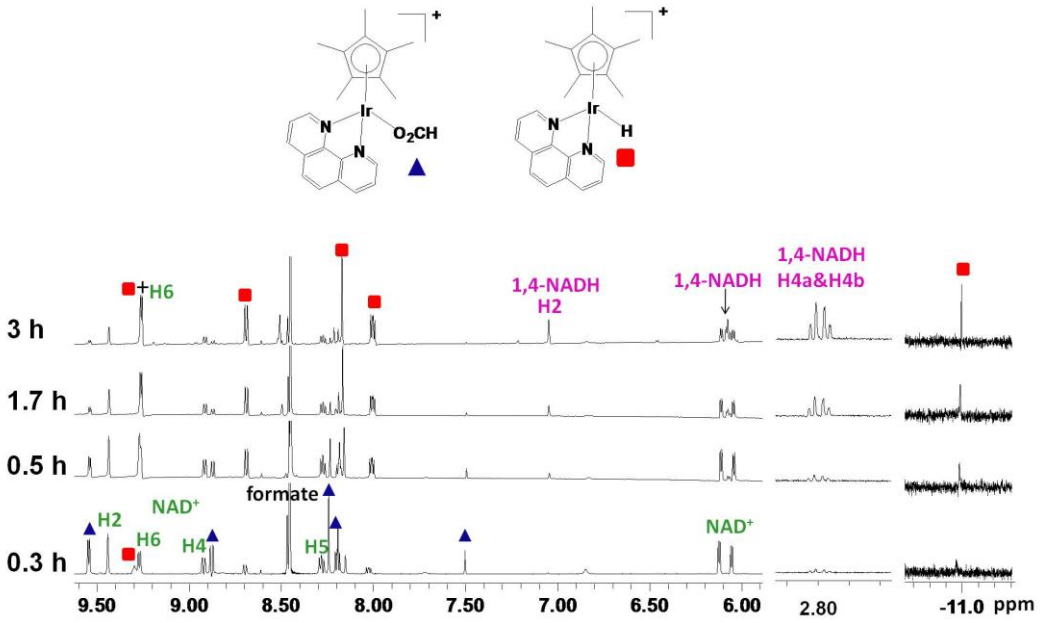

Figure 5.4. ^{1}H NMR spectra of a 1 mM $[(\eta^5\text{-}C_5Me_5)Ir(phen)(H_2O)]^{2+}$ (**4A**) with NAD^+ and sodium formate (molar ratios 1:1.5:25) in 10% MeOD-d_4/90% H_2O at 298 K at various time intervals. Peak assignments are indicated on the structures. The 3 sections show the low-field region, H4a & H4b peaks (×2) of 1,4-NADH, and Ir−H hydride region (×8), respectively.

5.3.2 NMR Spectroscopy of Reactions with 1,4-NADH

When two mol equiv of 1,4-NADH were added to a 1 mM solution of [(η^5-C_5Me_5)Ir(phen)(H_2O)]$^{2+}$ (**4A**), the colour of solution changed from light to dark yellow immediately. ^{1}H NMR spectra of the resulting solution recorded at 298 K after various time intervals (Figure 5.5) contained a sharp singlet at –11.3 ppm within the first 10 min of the reaction corresponding to an iridium(III) hydride adduct together with a new set of signals attributable to NAD^+. Over the next 33 h, the signal for the hydride adduct decreased in intensity and the major signals present were those for NAD^+ and aqua complex **4A**. During that time the pH of the solution increased significantly from 6.8 to 8.9. Addition of 2 further mol equiv of 1,4-NADH again rapidly gave rise to an Ir–H peak (top spectrum in Figure 5.5). Similar results were obtained for reactions of [(η^5-$C_5Me_4C_6H_5$)Ir(phen)(H_2O)]$^{2+}$ (**5A**) (Figure 5.6).

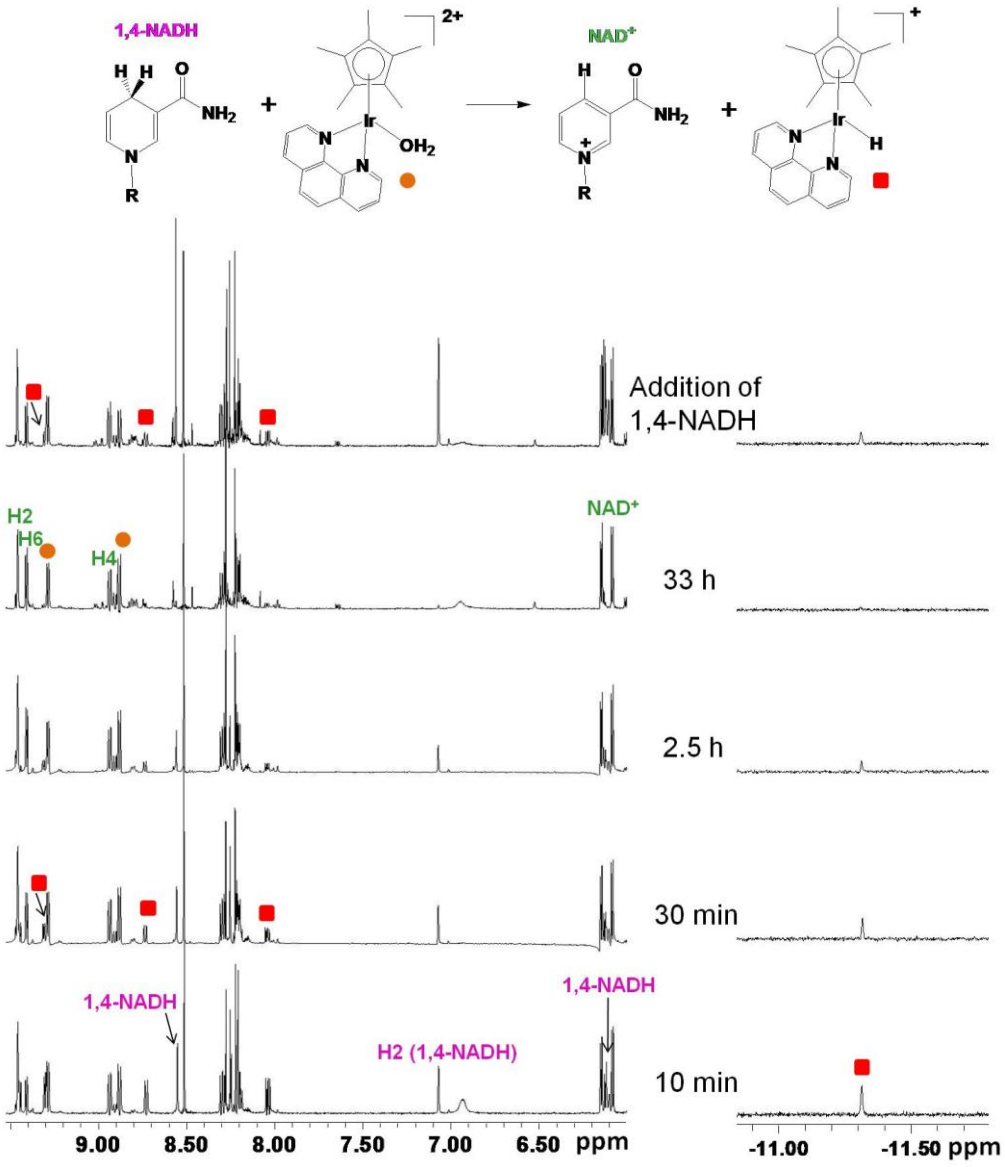

Figure 5.5. Conversion of 1,4-NADH to NAD^+ in the presence of complex $[(\eta^5\text{-}C_5Me_5)Ir(phen)(H_2O)]^{2+}$ (**4A**). ^1H NMR spectra of a 1 mM **4A** with 1,4-NADH (molar ratio 1:2) in 10% MeOD-d_4/90% H_2O at 298 K at various time intervals during 33 h. After 33 h, a further 2 mol equiv of 1,4-NADH were added to the solution and the resulting ^1H NMR spectrum was recorded after 10 min (top spectrum). Peak assignments are indicated on the structures. Left: low-field region; right: Ir−H hydride region (×2).

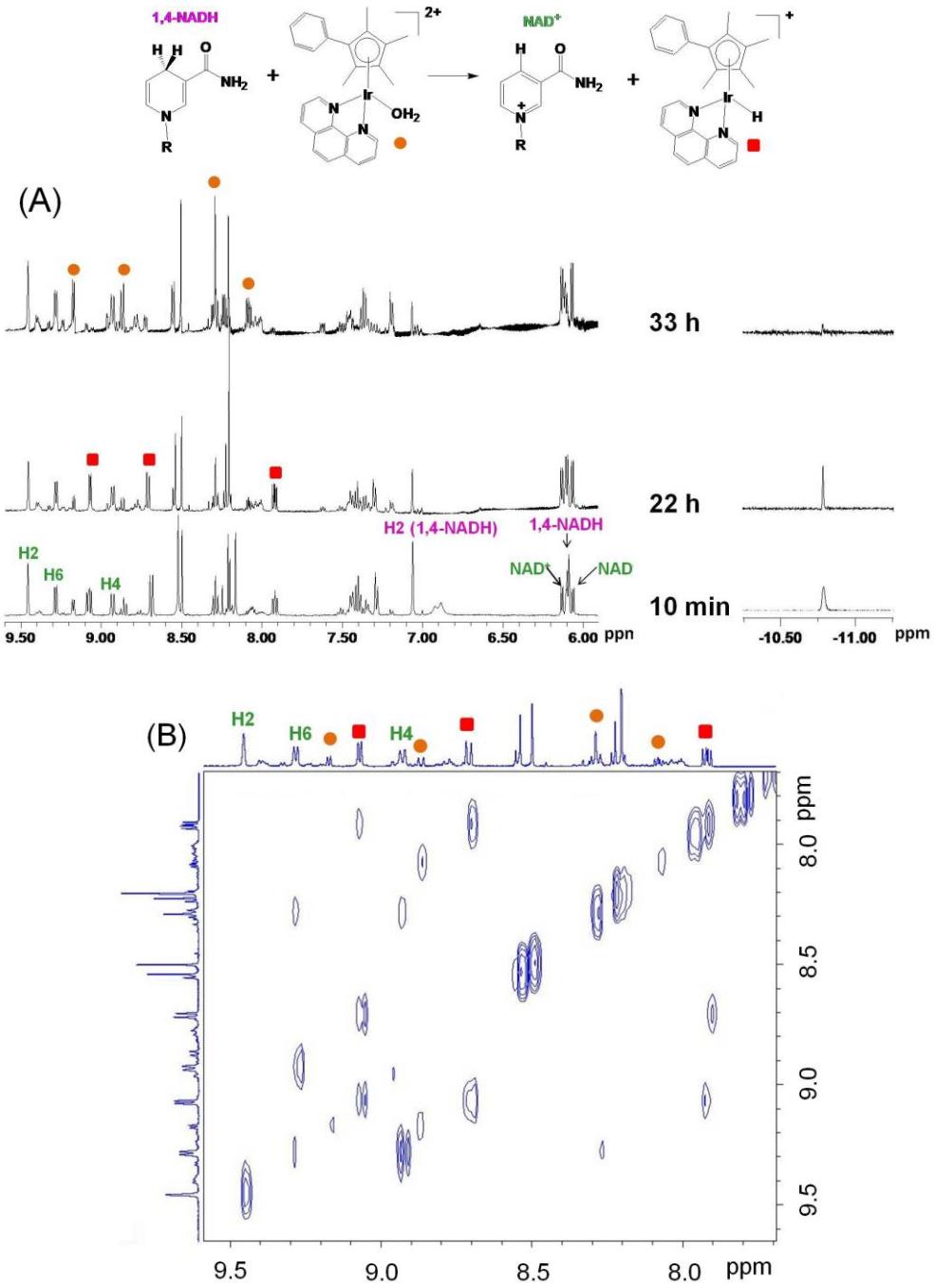

Figure 5.6. Reactions of $[(\eta^5\text{-}C_5Me_4C_6H_5)Ir(phen)(H_2O)]^{2+}$ (**5A**) and 1,4-NADH. (A) ^{1}H NMR spectra of 1 mM of **5A** with 3 mol equiv of 1,4-NADH in 10% MeOD-d_4/90% H_2O at 298 K at various time intervals during 33 h. Left: low-field region; right: region of Ir−H hydride peak (×2). (B) ^{1}H–^{1}H TOCSY 2D NMR spectrum recorded after 22 h. Peak assignments are indicated on the structures.

5.3.3 Hydrogenation of Pyruvate

Next it was shown that hydride-transfer from 1,4-NADH to Ir^{III} complexes can be coupled to the reduction of biologically relevant substrates. The conversion of pyruvate to lactate was studied, a reduction carried out *in vivo* by 1,4-NADH as cofactor for the enzyme lactate dehydrogenase (LDH), Eq. 5.1.[17]

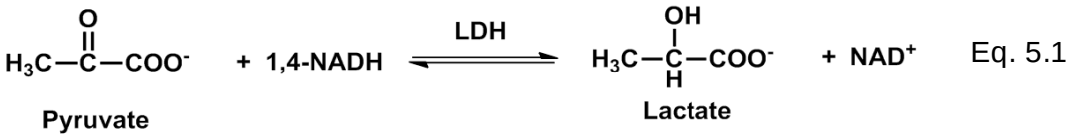

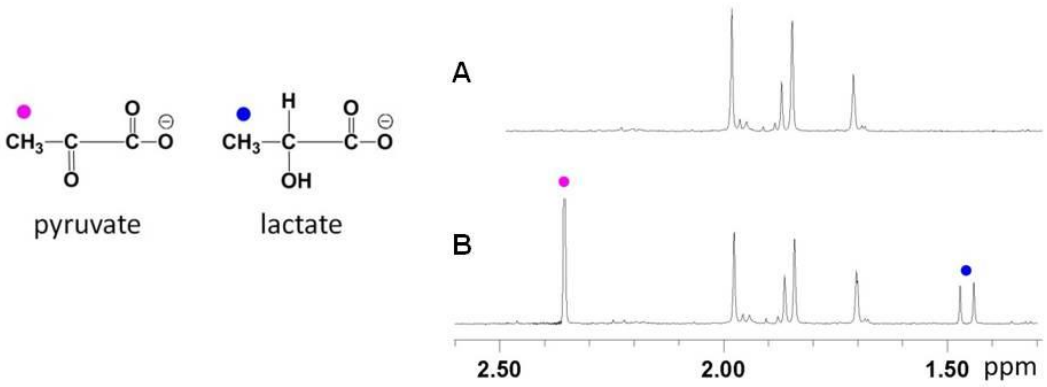

Figure 5.7. ^{1}H NMR spectra showing conversion of pyruvate to lactate in the presence of $[(\eta^5\text{-}C_5Me_4C_6H_5)Ir(phen)(H_2O)]^{2+}$ (**5A**). (A) ^{1}H NMR spectrum recorded 10 min after addition of 3 mol equiv of 1,4-NADH to a 1 mM solution of **5A** in 10% MeOD-d_4/90% H_2O (v/v) at 298 K. (B) ^{1}H NMR spectrum recorded 10 min after addition of 3 mol equiv of sodium pyruvate to the solution in (A). Peak assignments are indicated on the structures.

Addition of 3 mol equiv of sodium pyruvate to a solution containing 3 mol equiv of 1,4-NADH and 1 mM $[(\eta^5\text{-}C_5Me_4C_6H_5)Ir(phen)(H_2O)]^{2+}$ (**5A**) in 10% MeOD-d_4/90% H_2O (v/v), resulted in a doublet at ca 1.45 ppm corresponding to protons of methyl group of lactate, suggested conversion of ca. 30% of the pyruvate to lactate after 10 min at 298 K (Figure 5.7). However, no further pyruvate was converted after 24 h.

5.3.4 Reaction with Enzymatically Produced 1,4-NADH

Then it was shown that Ir–H generation can be coupled to the enzymatic production of 1,4-NADH, Eq. 5.2. Complex **5A** (final concentration 72 μM) was added to a solution containing 1,4-NADH (final concentration 33 μM) generated from NAD^+ by enzymatic oxidation of ethanol by alcohol dehydrogenase (ADH, in 6 mM Na_2HPO_4/NaH_2PO_4 buffer, 3.4 M ethanol, pH 7.2). UV-Vis spectroscopy indicated that all the 1,4-NADH produced was immediately consumed after addition of complex **5A**, as judged by the decrease in absorption at 339 nm (Figure 5.8). This reaction was also studied by ^{1}H NMR spectroscopy, with similar results (Figure 5.9).

$$\mathbf{CH_3CH_2OH + NAD^+} \xrightarrow{\mathbf{ADH}} \mathbf{CH_3CHO + 1,4\text{-}NADH} \xrightarrow{\mathbf{Ir\text{-}OH_2}} \mathbf{Ir\text{-}H + NAD^+} \quad \text{Eq.5.2}$$

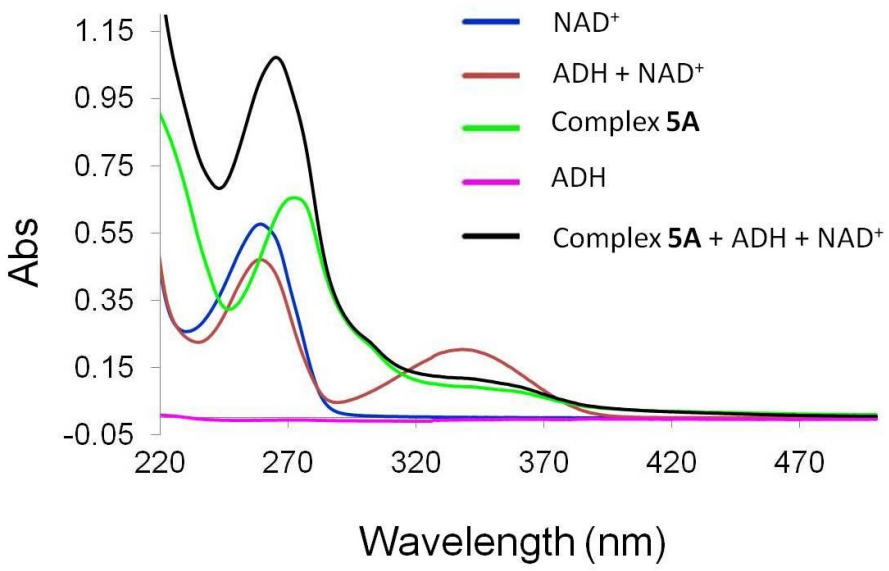

Figure 5.8. UV-Vis spectra showing reaction of 1,4-NADH (produced as a result of an enzymatic reaction) with $[(\eta^5\text{-}C_5Me_4C_6H_5)Ir(phen)(H_2O)]^{2+}$ (**5A**) in 6 mM Na_2HPO_4/NaH_2PO_4 buffer, 3.4 M ethanol, pH 7.2, at 298 K. Spectra of NAD^+ (blue line), complex **5A** (green line), and ADH (pink line) were recorded separately as controls before mixing, with final concentrations of 34 μM, 72 μM and 3.8×10^{-3} mg/ml, respectively. After mixing NAD^+ and ADH, the UV-Vis spectrum was recorded after 10 min (dark red line). No change was observed after 30 min. An absorption band at 339 nm was observed, suggesting the generation of 1,4-NADH (33 μM). Then to this solution, complex **5A** (final concentration 72 μM) was added and the resulting UV-Vis spectrum (black line) was recorded immediately. The decrease of absorption at 339 nm suggested that 1,4-NADH was oxidised (to NAD^+) in the presence of aqua complex **5A**.

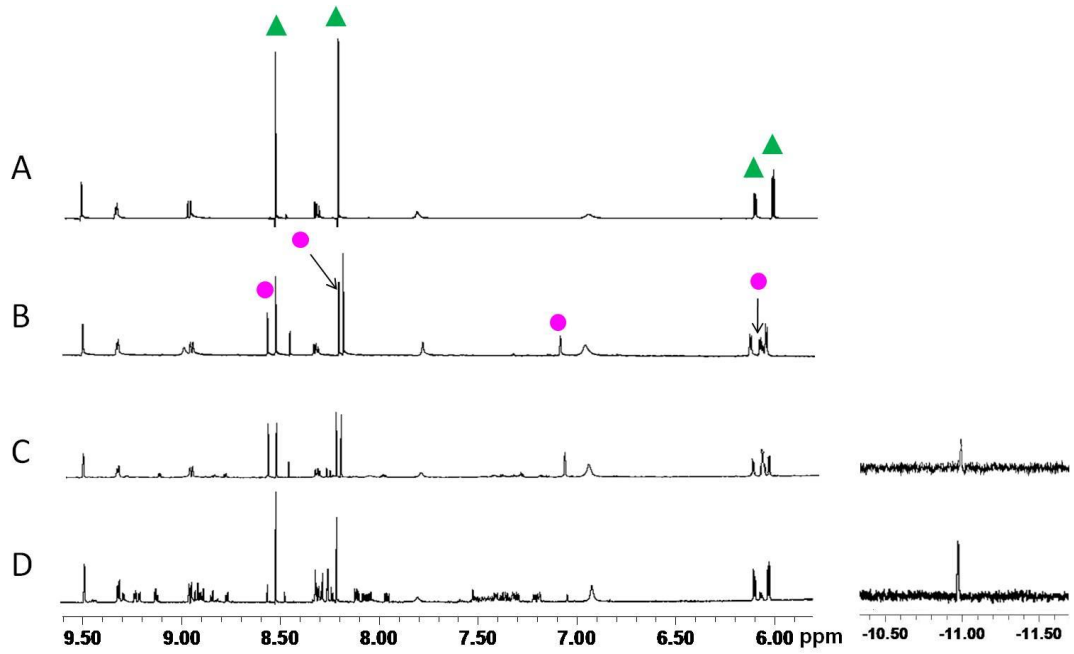

Figure 5.9. ^{1}H NMR spectra showing the rapid reaction of 1,4-NADH (produced as a result of the enzymatic reaction) with $[(\eta^5\text{-}C_5Me_4C_6H_5)Ir(phen)(H_2O)]^{2+}$ (**5A**). (A) NAD^+ (3 mM, ▲) in 6 mM Na_2HPO_4/NaH_2PO_4 buffer, 3.4 M ethanol, and 4% (v/v) of MeOD-d_4 (as NMR lock signal), pH = 7.2, 298 K. (B) Addition of enzyme ADH (ca. 0.03 mM) resulted the formation of 1,4-NADH (●) after 10 min. (C) Formation of more 1,4-NADH and addition of 0.3 mol equiv of complex **5A**. (D) Addition of a further 0.3 mol equiv of **5A** decreased the intensity of 1,4-NADH. Left: low-field region; right: Ir−H hydride peak region (×4).

5.3.5 Detection of H_2

Strikingly, these initial data showing the turnover of more than one mol equiv of NAD^+ per Ir^{III} suggested that the Ir complex might act as a catalyst and be recycled via Ir–H protonation and formation of H_2, Eq. 5.3. The possible production of H_2

was investigated by gas chromatography for solutions containing $[(\eta^5\text{-}C_5Me_4C_6H_5)Ir(phen)(H_2O)]^{2+}$ (**5A**, 0.9 mM) and 1,4-NADH (1.3 mM in 5 mM phosphate buffer pH 7.2). The time dependence of H_2 evolution was monitored from the peak with retention time of ca. 0.39 min (Figure 5.10). The sum of H_2 detected in the headspace and H_2 dissolved in solution (1.6×10^{-2} mL), was in good agreement with the amount of H_2 which would be produced if all the available hydride from 1,4-NADH is converted to H_2 (1.8×10^{-2} mL).

$$\text{Ir-OH}_2 \xrightarrow{\text{1,4-NADH}} \text{Ir-H} \xrightarrow{\text{H}^+,\ \text{H}_2\text{O}} \text{Ir-OH}_2 + \text{H}_2 \qquad \text{Eq.5.3}$$

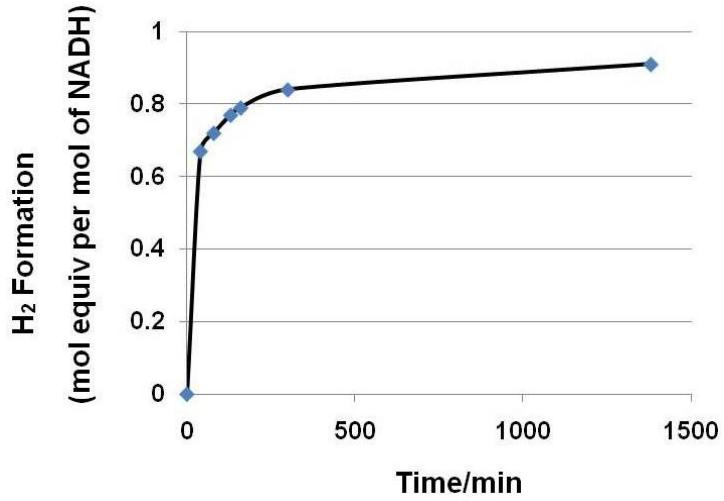

Figure 5.10. H_2 formation with time during reaction of $[(\eta^5\text{-}C_5Me_4C_6H_5)Ir(phen)(H_2O)]^{2+}$ (**5A**, 0.9 mM) with 1,4-NADH (1.3 mM) in phosphate buffer (5 mM, pH 7.2) at 298 K as detected by gas chromatography.

5.3.6 Catalytic Studies on Reactions with 1,4-NADH

The turnover of 1,4-NADH using $[(\eta^5\text{-}C_5Me_4C_6H_5)Ir(phen)(H_2O)]^{2+}$ (**5A**) as catalyst was investigated in more detail.

5.3.6.1 Effect of 1,4-NADH on the Catalytic Reaction

Kinetic experiments on aqueous solutions (ca. pH 7.4) with 1,4-NADH concentrations of 70, 110, 156 and 173 μM, and a constant catalyst **5A** concentration of 1.5 μM were monitored by UV-Vis absorption spectroscopy at 310 K. Typical UV-Vis spectra recorded are shown in Figure 5.11, in which the absorption band at 339 nm decreased with time while the band at ca. 259 nm increased,[14,15] suggested the conversion of 1,4-NADH to NAD^+ in the presence of **5A** as catalyst. Figure 5.12 shows the time dependence of 1,4-NADH absorption at 339 nm, and plots of lnA (A = absorbance of 1,4-NADH at 339 nm) against time, indicating reactions are first-order with respect to 1,4-NADH. From the slop of these lines an average rate constant k of 6.14×10^{-4} min^{-1} and half life 403 min were determined.

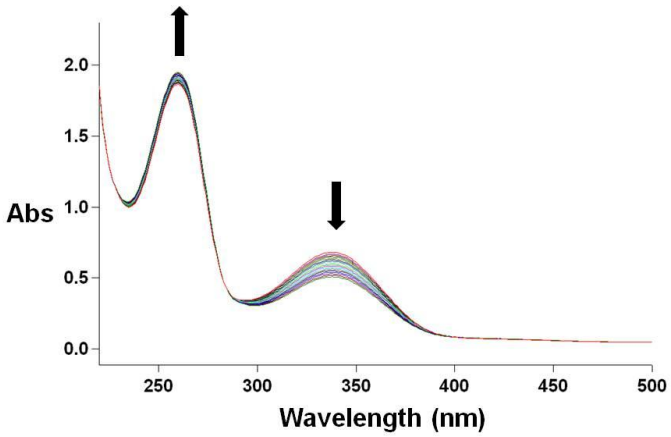

Figure 5.11. Typical UV-Vis spectra in kinetic experiments, showing degeneration of 1,4-NADH (initial concentration 110 μM) catalysed by [(η^5-$C_5Me_4C_6H_5$)Ir-(phen)(H_2O)]$^{2+}$ (**5A**, 1.5 μM) in water (pH = 7.4) at 310 K.

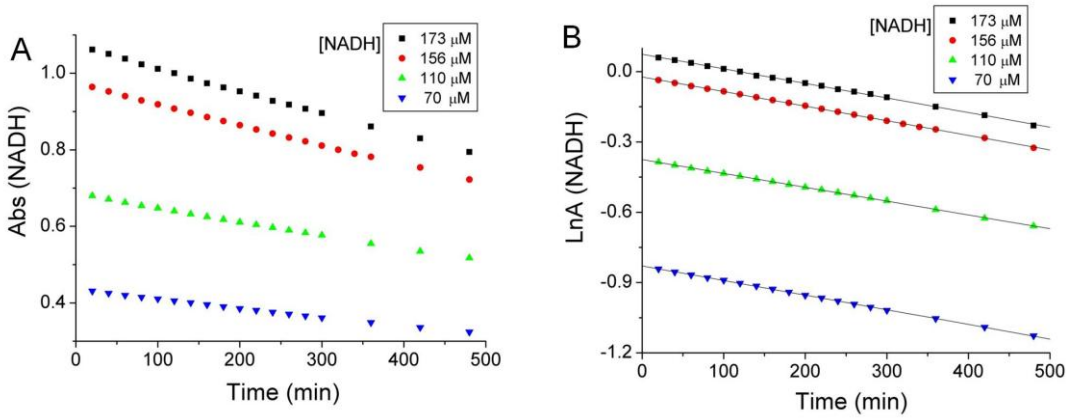

Figure 5.12. [(η^5-$C_5Me_4C_6H_5$)Ir(phen)(H_2O)]$^{2+}$ (**5A**) catalysed decomposition of 1,4-NADH studied detected by UV-Vis spectroscopy. (A) Time dependence of 1,4-NADH absorption at 339 nm, showing degeneration of 1,4-NADH catalysed by **5A** (1.5 μM) in water (ca. pH 7.4) at 310 K. (B) Plots of lnA (A = absorbance of 1,4-NADH at 339 nm) against time, suggest that conversion of 1,4-NADH is first-order reaction with respect to 1,4-NADH.

The turnover numbers (TON) of these reactions increased with time and 1,4-NADH concentration (Figure 5.13A). The maximum TON reached 75 after 24 h for 173 μM 1,4-NADH. Initial turnover frequencies (TOF) expressed as the number of moles of consumed 1,4-NADH per mole of catalyst after an initial 1 h of the reaction, increased with [1,4-NADH] (Figure 5.13B), 4.3 h^{-1} for 173 μM 1,4-NADH and double that for 70 μM 1,4-NADH.

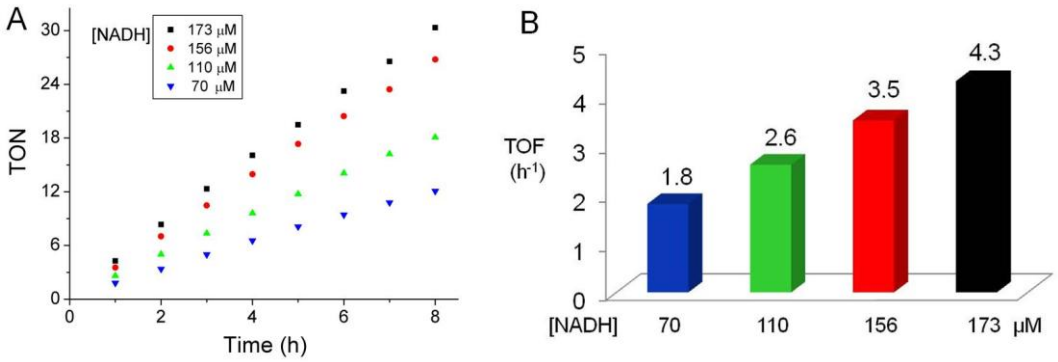

Figure 5.13. Turnover number (TON) and initial turnover frequencies (TOF) for the oxidation of 1,4-NADH catalysed by $[(\eta^5\text{-}C_5Me_4C_6H_5)Ir(phen)(H_2O)]^{2+}$ (**5A**) at 310 K in aqueous solution (ca. pH 7.4). (A) Plots of TON against time. (B) 1,4-NADH concentration dependence of TOF. The concentration of **5A** in each case was 1.5 μM.

5.3.6.2 Effect of 5A and Temperature on the Catalytic Reaction

Kinetic experiments on aqueous solutions (pH 7.5) with $[(\eta^5\text{-}C_5Me_4C_6H_5)Ir(phen)(H_2O)]^{2+}$ (**5A**) concentrations of 1.0, 1.5 and 3.0 μM, and a constant 1,4-NADH concentration of 160 μM were monitored by UV-Vis absorption spectroscopy at different temperatures ranging from 300 K to 315 K. Rate constant *k* of these reactions increased with **5A** concentration and temperature, Table 5.1. An Arrhenius plot (ln*k* vs. 1/T) of these reactions yielded straight lines between 300 K and 315K, Figure 5.14, with activation energies E_a listed in Table 5.1. The increase of concentration of **5A** from 1.0 μM to 3.0 μM resulted in the decrease of E_a of ca. 9.1 kJ·mol^{-1}, and then increased the rate of reaction.

Table 5.1. Rate Constant *k* and Activation Energy Data for **5A** Catalysed Conversion of 1,4-NADH

[**5A**]	$k \times 10^{-4}$ (min^{-1})				E_a
(μM)	300 K	305 K	310 K	315 K	(kJ·mol^{-1})
1.0	2.3	3.4	5.2	8.2	66.4
1.5	2.9	4.1	6.1	9.6	62.6
3.0	4.0	5.6	8.0	12.0	57.3

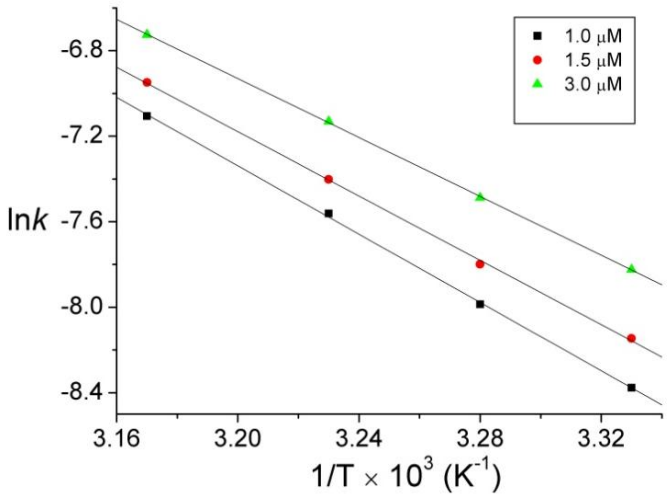

Figure 5.14. Arrhenius plots of ln*k* against 1/T for the oxidation of 1,4-NADH (160 μM) catalysed by $[(\eta^5\text{-}C_5Me_4C_6H_5)Ir(phen)(H_2O)]^{2+}$ (**5A**, 1.0, 1.5 and 3.0 μM, respectively) in water (pH 7.5) at various temperatures from 300 K to 315 K.

5.4 Discussion

5.4.1 Reduction of NAD^+ Using Formate as a Hydride Source

Most studies of Ru^{II}, Rh^{III} or Ir^{III} complexes as transfer hydrogenation catalysts for the reduction of ketones and aldehydes have been carried out in non-aqueous solvents such as glycerol, 2-propanol or formic acid/triethylamine,[18-20] although recently it has been discovered that some hydrogenations can also be carried out efficiently in water.[21] Applications of these organometallic complexes to biocatalysis have so far mainly been concerned with the conversion of the coenzyme NAD^+ to its reduced form 1,4-NADH using formate as the hydride source.[8,11,22]

In this study, the interaction of cyclopentadienyl Ir^{III} aqua complex **4A** $[(\eta^5\text{-}C_5Me_5)Ir(phen)(H_2O)]^{2+}$ with an excess of sodium formate in aqueous solution resulted in the formation of formato adduct ($Ir–O_2CH$), Figure 5.3B. A significant high-field chemical shift (0.9 ppm) was observed between free and bound formate, consistent with previous report for Ru^{II} arene formato complex.[23] The formato adduct ($Ir–O_2CH$) degenerated rapidly, and was followed by the formation of hydride adduct $[(\eta^5\text{-}C_5Me_5)Ir(phen)(H)]^+$ (Ir–H, –11.1 ppm). A signal at –11.8 ppm corresponding to hydrido ligand of $[(\eta^5\text{-}C_5Me_5)Ir(bpy)(H)]^+$ (bpy = 2'2-bipyridine) has been reported.[24] The observation of stable hydride complex in aqueous solution using formate as the hydride donor provides a basis for following hydride-transfer from $[(\eta^5\text{-}C_5Me_5)Ir(phen)(H)]^+$ to NAD^+, confirmed by the reduction of ^1H NMR signal of NAD^+ and the observation of 1,4-NADH peaks (H2 at 7.05 ppm and H4a/H4b at 2.80 ppm, Figure 5.4).

The mechanism in Figure 5.15 can be proposed for hydride-transfer from the formato adduct of the cyclopentadienyl Ir^{III} aqua complex **4A** to NAD^+, based on the data obtained here and reported studies of hydride-transfer from formate.[8,22]

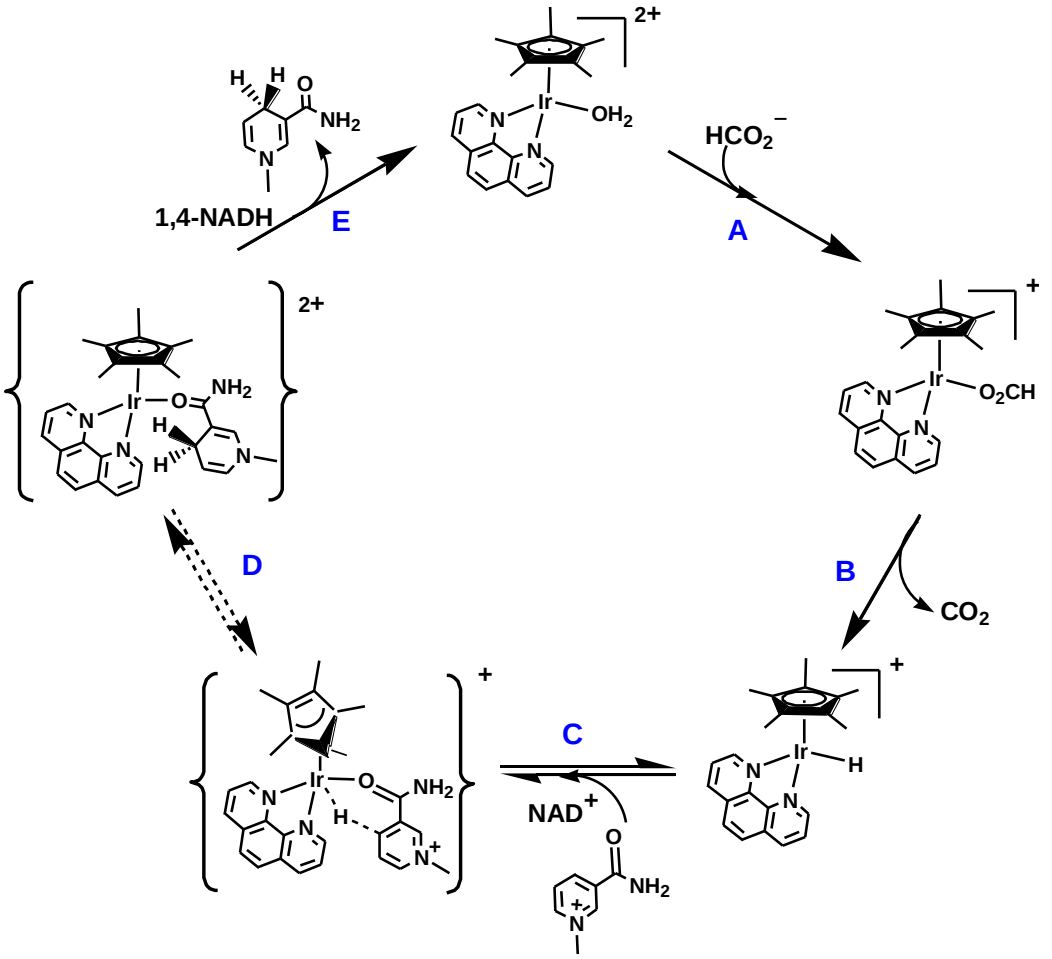

Figure 5.15. Proposed mechanism for the regioselective reduction of NAD^+ to 1,4-NADH by the Ir^{III} complex $[(\eta^5\text{-}C_5Me_5)Ir(phen)(H_2O)]^{2+}$ (**4A**) using formate as a hydride source.

The first step of the reaction shown in Figure 5.15(A) proceeds *via* a rapid binding of formate to the Ir^{III} centre in the $Ir–OH_2$ complex. In the followed step (B), hydride adduct $[(\eta^5\text{-}C_5Me_5)Ir(phen)(H)]^+$ formed after a β-hydrogen elimination reaction to produce CO_2. In Figure 5.15(C), an open coordination site made available by the well documented ring-slippage mechanism[25,26] of the Cp* ring by a

change from η^5 to η^3 coordination. It is believed that NAD^+ can coordinate to Ir^{III} via its amide oxygen, and ring-slippage then allows formation of a kinetically-favoured six-membered-ring transition state. This intermediate further provides the driving force for regioselective hydride-transfer to C4 of NAD^+, Figure 5.15(D); by an induced electronic effect of the bound carbonyl group, the C4 position might become a more electrophilic site towards hydride-transfer. This step also includes the reversion of the η^3 to η^5 coordination of the Cp* ring, along with binding and hydride-transfer. Finally, displacement of the 1,4-NADH by H_2O recycles the Ir^{III} aqua complex, completing the catalytic cycle, Figure 5.15(E).

5.4.2 Hydride-Transfer from 1,4-NADH

The interactions of the cyclopentadienyl Ir^{III} aqua complexes $[(\eta^5\text{-}C_5Me_5)Ir(phen)(H_2O)]^{2+}$ (**4A**) and $[(\eta^5\text{-}C_5Me_4C_6H_5)Ir(phen)(H_2O)]^{2+}$ (**5A**) with 1,4-NADH were followed by ^1H NMR spectroscopy and UV-Vis spectroscopy. The ^1H NMR spectra of the reaction suggest that 1,4-NADH could be transferring a hydride anion to the corresponding $Ir–OH_2$ adducts to generate a detectable Ir–H species (sharp singlet ca. –11.1 ppm) and the observed accumulation of NAD^+. In addition, complex **5A** can convert 1,4-NADH produced from enzymatic reaction between ADH and ethanol, Figures 5.8 and 5.9. Hence 1,4-NADH produced by various biochemical pathways might readily react with iridium complexes such as this in cells. This study appears to be the first report of the catalytic transfer of hydride from 1,4-NADH to organometallic iridium complexes, although the conversion of

1,4-NADH to NAD^+ catalysed by Ru^{II} arene complexes[12] and Pd-Au nanoparticles[10] has recently been achieved.

Interestingly, the reduction of pyruvate to lactate, a reaction catalysed by the enzyme lactate dehydrogenase, can be achieved by Ir^{III} complexes via hydride-transfer from 1,4-NADH, Figure 5.7. Organometallic Ir^{III} complexes offer the prospect of carrying out such reactions without the presence of an enzyme.

The transient appearance of ^1H NMR signals for Ir–H species at high field together with rises in pH during the course of the reactions with 1,4-NADH, suggested that the protonation of the Ir–H adducts might be facile with the generation of H_2. Gas chromatography experiments for the Ir complex **5A** showed that this was indeed the case, Figure 5.10. This may provide a new route to produce H_2. A total H_2 yield of 1.33 mol per mol glucose has been reported by using an NAD^+-dependent formate dehydrogenase in enterobacter aerogenes.[29] Molecular hydrogen has recently reported to be an efficient antioxidant, such as quenching injurious reactive oxygen species (ROS) and suppressing oxidative stress-induced injury.[30,31]

A possible mechanism for the oxidative conversion of 1,4-NADH to NAD^+ by Ir^{III} aqua complexes $[(\eta^5\text{-}C_5Me_4C_6H_5)Ir(phen)(H_2O)]^{2+}$ (**5A**) is shown in Figure 5.16.

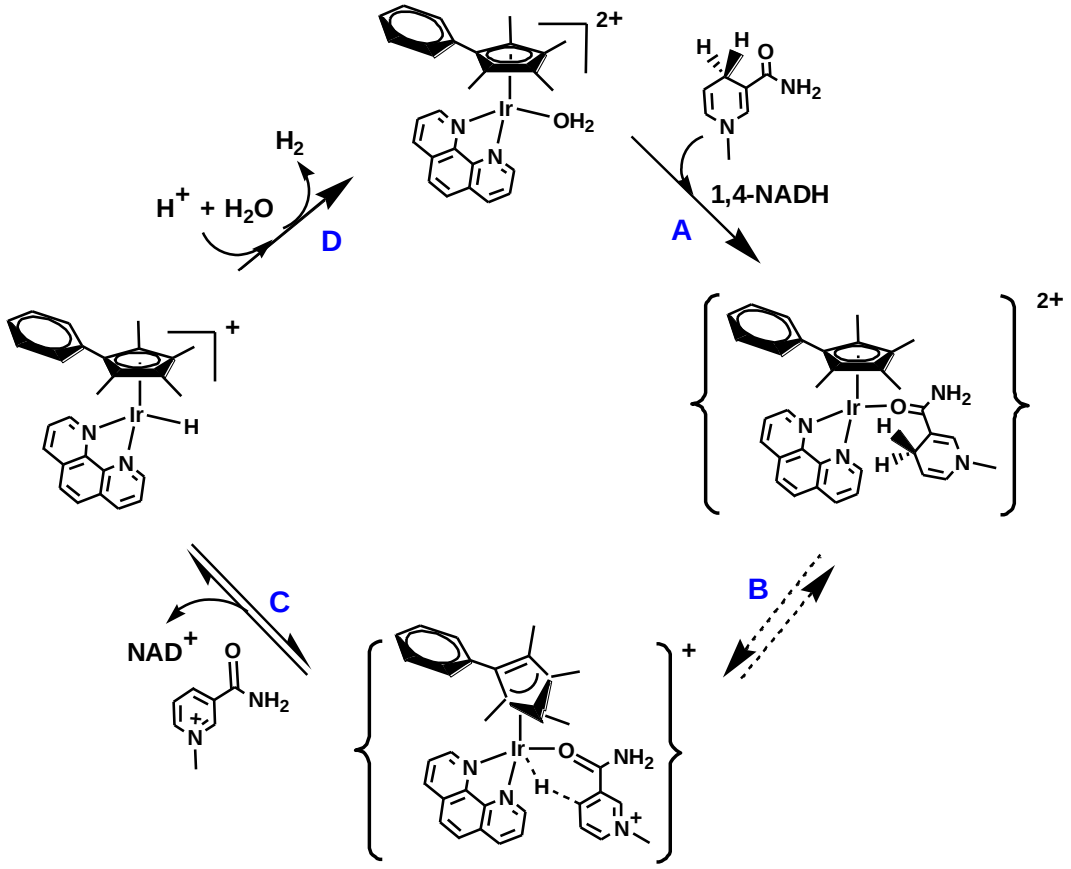

Figure 5.16. Proposed mechanism for hydride-transfer from 1,4-NADH to complex $[(\eta^5\text{-}C_5Me_4C_6H_5)Ir(phen)(H_2O)]^{2+}$ (**5A**), followed by protonation to give H_2 and regenerate the reactive aqua adduct.

The first step, Figure 5.16(A), proceeds *via* plausible coordination of the amide functionality in 1,4-NADH to iridium centre, most probably through direct displacement of the bound water. Figure 5.16(B) involves direct hydride-transfer from 1,4-NADH to **5A** *via* the formation of a kinetically-favoured six-membered-ring transition state, through a coordination site which becomes available by a ring-slippage mechanism (suggested previously for other hydride-transfer reactions).

Figure 5.16(C) includes the reversal of the η^3 to η^5 coordination of the Cp ring, and finally the release of the NAD^+ product and generation of the Ir–H complex. Protonation of bound hydride can then give rise to H_2 release which is detectable by gas chromatography. Coordination of water then completes the cycle, Figure 5.16(D).

It is shown here for the first time that the Ir^{III} catalyst **5A** is efficient in the course of conversion 1,4-NADH to NAD^+, with turnover number (TON) of 75 in a 173 μM solution of 1,4-NADH within 24 h when present at 0.9 mol %. TOF values up to 4.3 h^{-1} have been obtained at 310 K and pH 7.4. In addition, **5A** catalysed conversion of 1,4-NADH showed first-order behaviour with respect to 1,4-NADH, which is consistent with study using Pd-Au nanoparticles.[10] Both temperature and the concentration of 1,4-NADH and **5A** have significant influences on the oxidation of 1,4-NADH. Increasing the concentration of **5A** can significantly decrease the activation energy of the reactions and increase the rate of reaction.

5.5 Conclusions

In summary, cyclopentadienyl Ir^{III} aqua complexes $[(\eta^5\text{-}C_5Me_5)Ir(phen)(H_2O)]^{2+}$ (**4A**) and $[(\eta^5\text{-}C_5Me_4C_6H_5)Ir(phen)(H_2O)]^{2+}$ (**5A**) mediate the interconversion of 1,4-NADH and NAD^+ through hydride-transfer reactions. It is shown that the Ir^{III} aqua complexes can not only convert NAD^+ to 1,4-NADH using formate as the hydride source, but also catalyse the reverse reaction with hydride donation from 1,4-NADH to a iridium centre, recovered by protonation of bound hydride with

generation of H_2. Possible mechanisms for the two types of hydride-transfer reactions are also proposed. This appears to be the first report that organometallic Ir^{III} complexes can use 1,4-NADH as a hydride source for hydrogenation reactions, converting pyruvate to lactate in the absence of an enzyme. The iridium complex **5A** appears to be a robust catalyst for the oxidation of 1,4-NADH with high TON of 75 after 24 h and TOF values up to 4.3 h^{-1} under physiologically relevant conditions (pH 7.4, 310 K, in water). These new findings open up wide possibilities for the coupling of hydrogenations to biological processes, including control of the redox status of cells.

5.6 References

(1) Ying, W. *Antioxid. Redox Signal.* **2008**, *10*, 179-206.

(2) Chenault, H.; Whitesides, G. *Appl. Biochem. Biotech.* **1987**, *14*, 147-197.

(3) Held, M.; Schmid, A.; van Beilen, J. B.; Witholt, B. *Pure Appl. Chem.* **2000**, *72*, 1337-1343.

(4) Liese, A. In *Technology Transfer in Biotechnology: From Lab to Industry to Production*; Kragl, U., Ed.; Springer-Verlag Berlin Heidelberg: New York, 2005; 92, pp 197-224.

(5) Zhao, H.; van der Donk, W. A. *Curr. Opin. Biotechnol.* **2003**, *14*, 583-589.

(6) Hollmann, F.; Schmid, A. *Biocatal. Biotransform.* **2004**, *22*, 63-88.

(7) Vuorilehto, K.; Lütz, S.; Wandrey, C. *Bioelectrochemistry* **2004**, *65*, 1-7.

(8) Canivet, J.; Süss-Fink, G.; Štěpnička, P. *Eur. J. Inorg. Chem.* **2007**, 4736-4742.

(9) Fish, R. H. *Aust. J. Chem.* **2010**, *63*, 1505-1513.

(10) Gopalan, A.; Ragupathy, D.; Kim, H. T.; Manesh, K. M.; Lee, K. P. *Spectrochim. Acta, Part A* **2009**, *74*, 678-684.

(11) Yan, Y.; Melchart, M.; Habtemariam, A.; Peacock, A.; Sadler, P. *J. Biol. Inorg. Chem.* **2006**, *11*, 483-488.

(12) Betanzos Lara, S. *Design, synthesis and activation of ruthenium arene anticancer complexes.* PhD thesis, University of Warwick, 2010, pp 202-250.

(13) Youinou, M.-T.; Ziessel, R. *J. Organomet. Chem.* **1989**, *363*, 197-208.

(14) Dawson, R. B. *Data for biochemical research*; 3rd ed.; Clarendon Press: Oxford, 1985.

(15) Smeets, E. H. J.; Muller, H.; De Wael, J. *Clin. Chim. Acta* **1971**, *33*, 379-386.

(16) Bühner, M.; Sund, H. *Eur. J. Biochem.* **1969**, *11*, 73-79.

(17) Buhl, S.; Jackson, K. *Clin. Chem.* **1978**, *24*, 828-831.

(18) Wolfson, A.; Dlugy, C.; Shotland, Y.; Tavor, D. *Tetrahedron Lett.* **2009**, *50*, 5951-5953.

(19) Tan, D.-M.; Chan, K. S. *Tetrahedron Lett.* **2005**, *46*, 503-505.

(20) Kawasaki, I.; Tsunoda, K.; Tsuji, T.; Yamaguchi, T.; Shibuta, H.; Uchida, N.; Yamashita, M.; Ohta, S. *Chem. Commun.* **2005**, 2134-2136.

(21) Wu, X.; Wang, C.; Xiao, J. *Platinum Met. Rev.* **2010**, *54*, 3-19.

(22) Lo, H. C.; Buriez, O.; Kerr, J. B.; Fish, R. H. *Angew. Chem., Int. Ed.* **1999**, *38*, 1429-1432.

(23) Koike, T.; Ikariya, T. *Adv. Synth. Catal.* **2004**, *346*, 37-41.

(24) Abura, T.; Ogo, S.; Watanabe, Y.; Fukuzumi, S. *J. Am. Chem. Soc.* **2003**, *125*, 4149-4154.

(25) O'Connor, J. M.; Casey, C. P. *Chem. Rev.* **1987**, *87*, 307-318.

(26) Jones, W. D.; Kuykendall, V. L.; Selmeczy, A. D. *Organometallics* **1991**, *10*, 1577-1586.

(27) Fukuzumi, S.; Fujioka, N.; Kotani, H.; Ohkubo, K.; Lee, Y.-M.; Nam, W. *J. Am. Chem. Soc.* **2009**, *131*, 17127-17134.

(28) Fukuzumi, S.; Kotani, H.; Lee, Y.-M.; Nam, W. *J. Am. Chem. Soc.* **2008**, *130*, 15134-15142.

(29) Lu, Y.; Zhao, H.; Zhang, C.; Lai, Q.; Wu, X.; Xing, X.-H. *Biotechnol. Lett.* **2009**, *31*, 1525-1530.

(30) Ohsawa, I.; Ishikawa, M.; Takahashi, K.; Watanabe, M.; Nishimaki, K.; Yamagata, K.; Katsura, K.-i.; Katayama, Y.; Asoh, S.; Ohta, S. *Nat. Med.* **2007**, *13*, 688-694.

(31) Hayashida, K.; Sano, M.; Ohsawa, I.; Shinmura, K.; Tamaki, K.; Kimura, K.; Endo, J.; Katayama, T.; Kawamura, A.; Kohsaka, S.; Makino, S.; Ohta, S.; Ogawa, S.; Fukuda, K. *Biochem. Biophys. Res. Commun.* **2008**, *373*, 30-35.

Chapter 6

Future Work

This Chapter explores possible areas of future work for this project. In some cases this is based on preliminary results obtained in this thesis.

6.1 Cyclopentadienyl Ligand, Chelating Ligand and Leaving Group

It was shown that the iridium complexes of the type $[(\eta^5\text{-}Cp^x)Ir(XY)Cl]^{0/+}$, where Cp^x is pentamethylcyclopentadienyl, Cp*, or its phenyl Cp^{xph} or biphenyl Cp^{xbiph} derivatives, and XY is the N,N-, NO-, or C^N-chelating ligand discussed in this thesis can lead not only to significant changes in the chemical reactivity in relation to hydrolysis and acidity of aqua adducts but also in the interaction with biologically relevant molecules such as nucleobases and DNA. Furthermore, some of the complexes show potent cytotoxicity against the A2780 human ovarian cancer cell line and against the NCI panel of ca. 60 human cancer cell lines that is comparable to clinically used chemotherapeutics, cisplatin and carboplatin.

However, the complexes studied in this thesis make up only a small section of half-sandwich cyclopentadienyl Ir^{III} complexes that can be envisaged. There are still large numbers of active cyclopentadienyl Ir^{III} complexes that can be designed and synthesised by changing the cyclopentadienyl ligand, chelating ligand or leaving group. The use of functionalised cyclopentadienyl ligands and other kinds of chelating ligands with hetero atoms such as sulphur, selenium or phosphorus may result in more potent iridium complexes which would be interesting to investigate for future work.[1-7]

In addition, the effect of the leaving group (chloride was used in this thesis) has also been largely unexplored for these organometallic iridium complexes. For Ru^{II} and Os^{II} arene complexes, it was reported that substituting the chloride by iodide can increase the potency for some classes of these complexes.[8,9] Also the complex [(η^5-$C_5Me_4C_6H_4C_6H_5$)Ir(phpy)(py)]PF_6 (**ZL105**, where py = pyridine) showed more potent activity than complex [(η^5-$C_5Me_4C_6H_4C_6H_5$)Ir(phpy)Cl] (**34**) toward A2780 human ovarian cancer cells, with IC_{50} values of 0.12 μM and 0.70 μM, respectively. For future work it would be interesting to investigate the influence of leaving groups (idodide, bromide, pyridine, thiophenolate) on the cytotoxicity of the several classes of iridium cyclopentadienyl compounds.

There is no report yet for an organometallic half-sandwich iridium complex which shows activity *in vivo*. Improving the potency of the iridium complexes even more (nanomolar) and investigating the anticancer efficacy *in vivo* are also included in the future.

6.2 Intercalation into DNA

It was shown in Chapter 3 that addition of phenyl substituents to the Cp* ring in organometallic iridium complexes enhances the intercalative ability into DNA by EtBr displacement and viscometry experiments. For future work, it would be useful to study further the intercalation of the extended phenyl rings into DNA with more experimental methods and instrumentation, such as UV-Vis spectroscopy, circular dichroism (CD), linear dichroism (LD), DNA melting.[10,11]

Interaction with small oligonucleotides is also a useful method to study the intercalation of iridium complexes with DNA, defining more fully the structural changes induced by intercalating ligands. Interactions of Ru^{II} complex [(η^6-biphenyl)Ru(en)Cl][PF_6] (en = ethylenediamine) with the single-stranded (ss) DNA hexamer d(CGGCCG) and the duplex $d(CGGCCG)_2$ have been reported, Figure 6.1.[12,13]

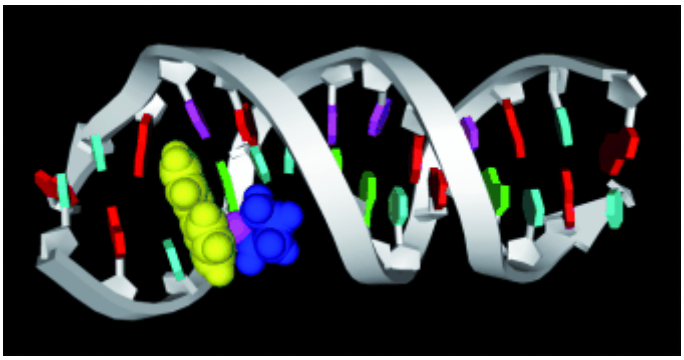

Figure 6.1. Model showing intercalation of a Ru^{II} arene complex into DNA.[12]

6.3 Enantiomer Separation

In Chapter 4, Ir^{III} cyclopentadienyl complexes of the type [(η^5-Cp^x)Ir(C^N)Cl] show strong binding to the nucleobases and low IC_{50} values towards cancer cells. This new class of organometalic Ir(III) complexes has potential for development as potent anticancer agents. However, the C^N-bound complexes are chiral, and no attempt was made to resolve them here.

Normally, the enantiomers of a molecule behave identically to each other. For example, they will migrate with identical R_f in thin layer chromatography. Their NMR and IR spectra are identical. However, enantiomers behave differently in the presence of other chiral molecules or objects. For example, enantiomers do not migrate identically on chiral HPLC column.[14] Chiral counterions, such as trisphat (Figure 6.2), are also used to separate enantiomers by addition of other chiral centre in the molecules.[15] Sometimes crystallisation is also effective in separation of enantiomers.[16]

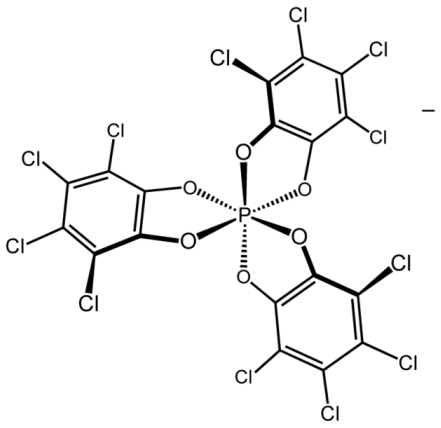

Figure 6.2. The chemical structure of trisphat.

Can the chiral anticancer iridium enantiomers be separated? Are the separated enantiomers stable? Do the enantiomers exhibit different cytotoxicity toward the same cancer cells? All the questions need to be answered in the future.

6.4 Other Biological Targets

Organometallic Ir^{III} complexes containing N,N-, N,O-, or C^N-chelating ligands studied in Chapters 3 and 4 can bind moderately or strongly with nucleobases guanine and adenine, suggesting DNA may be a target for these complexes. However, DNA may not be the only biological target. In other word, the iridium complexes may also react with other biological targets. In addition, a drawback of traditional anticancer drugs which target DNA is the fact that healthy cells are affected as well when malignant cells are inhibited or killed, causing severe toxic side-effects. Previous studies have shown that other biological targets, such as proteins,[17] enzymes,[18] mitochondria,[19] and peptides[20] can be a relevant target for organometallic transition metal complexes. For future work it would be interesting to explore more potential targets for the organometallic iridium complexes.

6.5 Bio-inspired Hydride-Transfer Reactions

In Chapter 5, it was shown that 1,4-NADH can readily donate hydride to iridium in organometallic complexes, forming Ir−H species and NAD^+. This reaction is of importance since it mimics the function of NADH in cells. The bio-inspired hydride-transfer is currently being explored in our laboratory towards the reduction of biologically relevant substrates. It was shown that it is possible to mimic enzyme reactions by coupling hydride donation from an iridium half-sandwich centre to substrates such as pyruvate. In addition, iridium complexes at micromolar concentrations can also catalyse the generation of hydrogen. The results imply that

these organometallic iridium complexes should be able to mediate the redox states of cells, since the NAD^+/NADH couple plays a central role in controlling cellular redox potentials. It would be interesting in the future to evaluate the effect of iridium complexes on the cellular redox state. Future work can also involve the use of other important biologically substrates and improvements in the design of the catalytic iridium complexes.

6.6 References

(1) Field, L. D.; Lindall, C. M.; Masters, A. F.; Clentsmith, G. K. B. *Coord. Chem. Rev.* **2011**, *255*, 1733-1790.

(2) Pontes da Costa, A.; Viciano, M.; Sanaú, M.; Merino, S.; Tejeda, J.; Peris, E.; Royo, B. *Organometallics* **2008**, *27*, 1305-1309.

(3) Allen, O. R.; Knox, R. J.; McGowan, P. C. *Dalton Trans.* **2008**, 5293-5295.

(4) Kandioller, W.; Hartinger, C. G.; Nazarov, A. A.; Bartel, C.; Skocic, M.; Jakupec, M. A.; Arion, V. B.; Keppler, B. K. *Chem.-Eur. J* **2009**, *15*, 12283-12291.

(5) Parr, J.; Smith, M. B.; Elsegood, M. R. J. *J. Organomet. Chem.* **2002**, *664*, 85-93.

(6) García-Yebra, C.; Janssen, J. P.; Rominger, F.; Helmchen, G. *Organometallics* **2004**, *23*, 5459-5470.

(7) Gasser, G.; Sosniak, A. M.; Metzler-Nolte, N. *Dalton Trans.* **2011**, *40*, 7061-7076.

(8) Dougan, S. J.; Habtemariam, A.; McHale, S. E.; Parsons, S.; Sadler, P. J. *Proc. Natl. Acad. Sci. U. S. A.* **2008**, *105*, 11628-11633.

(9) Fu, Y.; Habtemariam, A.; Basri, A. M. B. H.; Braddick, D.; Clarkson, G. J.; Sadler, P. J. *Dalton Trans.* **2011**, DOI: 10.1039/c1031dt10937e.

(10) Schäfer, S.; Sheldrick, W. S. *J. Organomet. Chem.* **2007**, *692*, 1300-1309.

(11) Bugarcic, T.; Nováková, O.; Halámiková, A.; Zerzánková, L.; Vrána, O. i.; Kašpárková, J.; Habtemariam, A.; Parsons, S.; Sadler, P. J.; Brabec, V. *J. Med. Chem.* **2008**, *51*, 5310-5319.

(12) Liu, H.-K.; Berners-Price, S. J.; Wang, F.; Parkinson, J. A.; Xu, J.; Bella, J.; Sadler, P. J. *Angew. Chem., Int. Ed.* **2006**, *45*, 8153-8156.

(13) Liu, H.-K.; Wang, F.; Parkinson, J. A.; Bella, J.; Sadler, P. J. *Chem.-Eur. J* **2006**, *12*, 6151-6165.

(14) Davankov, V. *Chromatographia* **1989**, *27*, 475-482.

(15) Damas, A.; Moussa, J.; Rager, M. N.; Amouri, H. *Chirality* **2010**, *22*, 889-895.

(16) Schmid, W. F.; John, R. O.; Mühlgassner, G.; Heffeter, P.; Jakupec, M. A.; Galanski, M.; Berger, W.; Arion, V. B.; Keppler, B. K. *J. Med. Chem.* **2007**, *50*, 6343-6355.

(17) Casini, A.; Gabbiani, C.; Sorrentino, F.; Rigobello, M. P.; Bindoli, A.; Geldbach, T. J.; Marrone, A.; Re, N.; Hartinger, C. G.; Dyson, P. J.; Messori, L. *J. Med. Chem.* **2008**, *51*, 6773-6781.

(18) Urig, S.; Becker, K. *Semin. Cancer Biol.* **2006**, *16*, 452-465.

(19) Wang, Y.; He, Q.-Y.; Che, C.-M.; Chiu, J.-F. *Proteomics* **2006**, *6*, 131-142.

(20) Noor, F.; Wüstholz, A.; Kinscherf, R.; Metzler-Nolte, N. *Angew. Chem., Int. Ed.* **2005**, *44*, 2429-2432.

Chemical Structures of Iridium Complexes Studied in This Thesis

Chapter 2

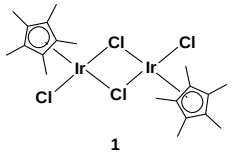

1

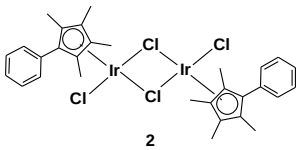

2

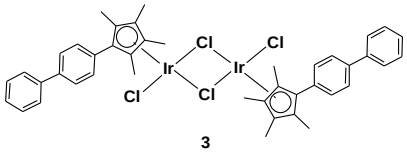

3

Chapter 3

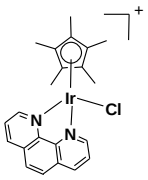

4

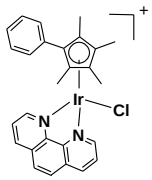

5

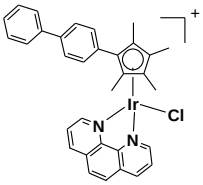

6

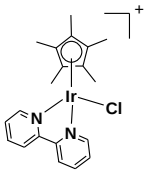

7

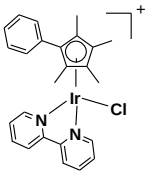

8

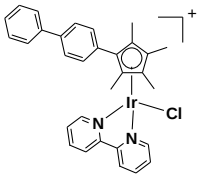

9

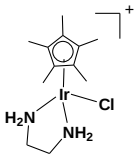

10

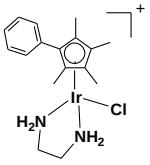

11

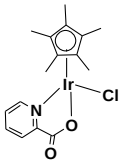

12

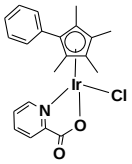

13

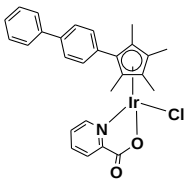

14

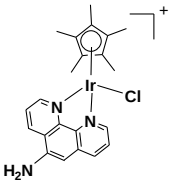

15

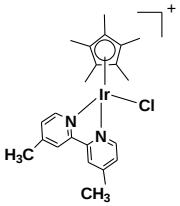

16

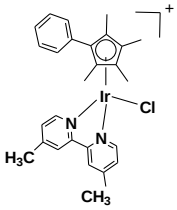

17

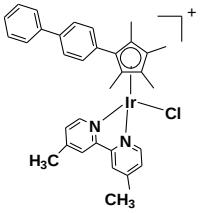

18

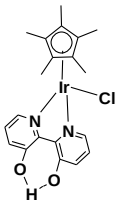

19

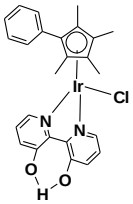

20

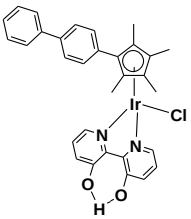

21

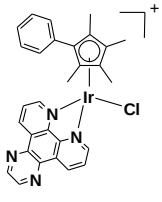

22

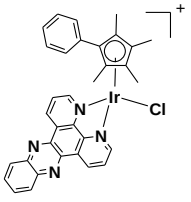

23

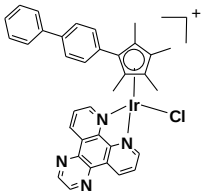

24

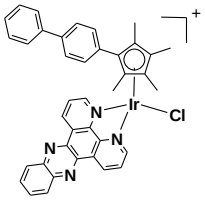

25

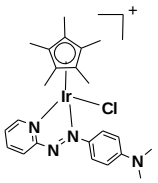

26

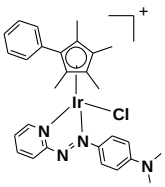

27

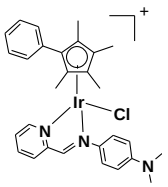

28

Chapter 4

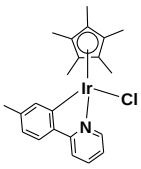

29

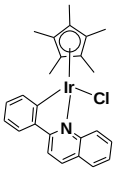

30

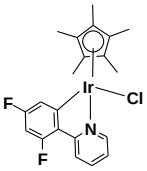

31

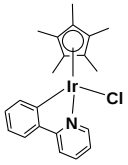

32

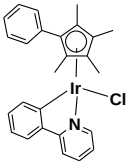

33

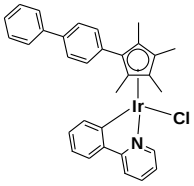

34

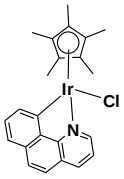

35

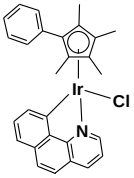

36

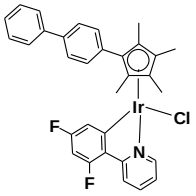

37

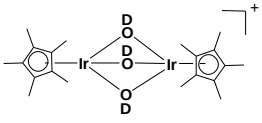

38

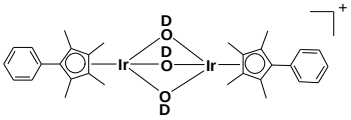

39

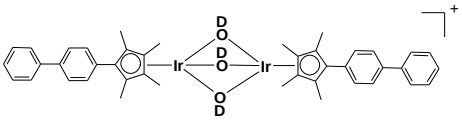

40

Chapter 5

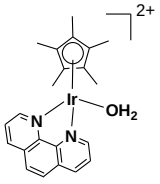

4A

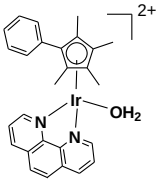

5A

Courses Attended

1. Postgraduate teaching courses at University of Warwick, **2008**.
2. Graduate School Skills Programme, University of Warwick training sessions, **2008**–**2010**.
    - Team Development and Networking Module
    - Project Management
    - Academic Scientific Writing
3. RSC (Royal Society of Chemistry) Research Lectures held at the University of Warwick, **2008**–**2011**.
4. Weekly chemical biology section seminars during term time, **2008**–**2011**.

Conferences and Meetings Attended

1. University of Warwick Chemistry Postgraduate Symposium, June **2010**. *Poster presentation.*

2. 5th International Symposium on Bioorganometallic Chemistry, Ruhr-Universität Bochum, Germany, July **2010**. *Poster presentation.*

3. COST D39 working group meeting: "Analysis of DNA Damage by Metal-Based Compounds", Brno, Czech Republic, May **2011**. *Oral presentation.*

4. University of Warwick Chemistry Postgraduate Symposium, June **2011**. *Oral presentation.*